Out of equilibrium dynamics of complex systems

Cours de 3ème cycle de la Suisse Romande

Leticia F. Cugliandolo
Université Pierre et Marie Curie - Paris VI
Laboratoire de Physique Théorique et Hautes Energies

December 15, 2011

Contents

1 Introduction

1.1 Falling out of equilibrium

In standard condensed matter or statistical physics focus is set on **equilibrium** systems. Microcanonical, canonical or grand canonical ensembles are used depending on the conditions one is interested in. The relaxation of a tiny perturbation away from equilibrium is also sometimes described in textbooks and undergraduate courses.

More recently, attention has turned to the study of the evolution of similar macroscopic systems in **far from equilibrium** conditions. These can be achieved by changing the properties of the environment (e.g. the temperature) in a canonical setting or by changing a parameter in the system's Hamiltonian in a microcanonical one. The procedure of rapidly (ideally instantaneously) changing a parameter is called a **quench**. Right after both types of quenches the initial configuration is not one of equilibrium at the new conditions and the systems subsequently evolve in an out of equilibrium fashion. The relaxation towards the new equilibrium (if possible) could be fast (and not interesting for our purposes) or it could be very slow (and thus the object of our study). There are plenty of examples of the latter. Dissipative ones include systems quenched through a phase transition and later undergoing domain growth, and problems with competing interactions that behave as glasses. Energy conserving ones are of great interest at present due to the rapid growth of activity in cold-atom systems.

Out of equilibrium situations can also be established by **driving** a system, that otherwise would reach equilibrium in observable time-scales, with an external perturbation. In the context of macroscopic systems an interesting example is the one of sheared complex liquids. Yet another interesting case is the one of powders that stay in static metastable states unless externally perturbed by tapping, vibration or shear that drives them out of equilibrium and makes them slowly evolve towards more compact configurations. Such situations are usually called non-equilibrium steady states (NESS). Small systems can also be driven out of equilibrium with external perturbations. Transport in nano-structures is the quantum (small) counterpart phenomenon of these cases, also of special interest at present.

Our interest is, therefore, in **macroscopic complex**[1] **systems**:

- With out of equilibrium initial condition. These include
  - open dissipative systems;
  - closed systems with energy conserving dynamics.
- with external driving forces.

[1] Complex simply means here 'not easy to understand'.

A number of questions one would like to give an answer to naturally arise. Among these are:

- Is the (instantaneous) **structure** out of equilibrium similar to the one in equilibrium (at some temperature, pressure, etc.)?
- What **microscopic/mesoscopic relaxation mechanism** takes place after the quench?
- Does the system quickly settle into a stationary state? In more technical terms, is there a **finite relaxation time** to reach a steady state and which are the properties of the system on which it depends?
- What is the **microscopic/mesoscopic** dynamics in non-equilibrium steady states when these are reached?
- Can one describe the states of the system sometime after the quench with some kind of **effective equilibrium-like measure**?
- Are there **thermodynamic concepts**, such as temperature, entropy, free-energy, playing a rôle in the non-equilibrium relaxation? Under which conditions?

One notices that some of these questions apply to the free as well as to the driven dynamics.

In the last 20 years or so a rather complete theory of the dynamics of **classical macroscopic systems evolving slowly in a small entropy production limit** (asymptotic regime after a quench, small drives), that encompasses the situations described above has been developed [1, 2]. This is a **mean-field theory** type in the sense that it applies strictly to models with long-range interactions or in the infinite dimensional limit. It is, however, expected that many aspects of it also apply to systems with short-range interactions although with some caveats. A number of finite dimensional problems have been solved demonstrating this fact.

In several cases of practical interest, **quantum effects** play an important rôle. For instance, glassy phases at very low temperatures have been identified in a large variety of materials (spin-glass like systems, interacting electrons with disorder, materials undergoing super-conductor transitions, metallic glasses, etc.). Clearly, the driven case is also very important in systems with quantum fluctuations. Take for instance a molecule or an interacting electronic system driven by an external current applied via the coupling to leads at different chemical potential. It is then necessary to settle whether the approach developed and the results obtained for the classical dynamics in a limit of small entropy production carry through when quantum fluctuations are included.

In these notes we start by exposing some examples of the **phenomenology** of out of equilibrium dynamics we are interested in. We focus on classical problems and their precise setting. We introduce nucleation [3], phase ordering kinetics [4], critical dynamics [5] structural glasses [6] and disordered systems [7, 8]. We also discuss

some interdisciplinary problems that have many points in common with glassy physics including optimization problems [9], neural networks [10] and active matter [11].

Next we go into the **formalism** used to deal with these problems. The basic techniques used to study classical glassy models with or without disorder are relatively well documented in the literature (the replica trick, scaling arguments and droplet theories, the dynamic functional method used to derive macroscopic equations from the microscopic Langevin dynamics, functional renormalization, Monte Carlo and molecular dynamic numerical methods). On the contrary, the techniques needed to deal with the statics and dynamics of quantum macroscopic systems are much less known in general. I shall briefly discuss the role played by the environment in a quantum system and introduce and compare the equilibrium and dynamic approaches.

Concretely, we recall some features of the Langevin formalism and its generating function. We dwell initially with some emblematic aspects of classical macroscopic systems slowly evolving out of equilibrium. Concerning models, we focus on two, that are intimately related: the $O(N)$ **model in the large** N **limit** that is used to describe **coarsening phenomena**, and the **random manifold**, that finds applications to many physical problems like charge density waves, high-Tc superconductors, etc. Both problems are of **field-theoretical** type and can be treated both **classically and quantum mechanically**. These two models are ideal for the purpose of introducing and discussing formalism and some basic ideas we would wish to convey in these lectures. Before entering the technical part we explain the two-fold meaning of the word **disorder** by introducing the glass problem and some of the numerous questions it raises.

1.2 Nucleation

When a system with a **first order phase transition** is taken to a region in the phase diagram in which it is still locally stable but metastable with respect to the new absolute minimum of the free-energy, its evolution towards the new equilibrium state occurs by nucleation of the stable phase. The theory of simple nucleation [3] is well established and the time needed for one bubble of the stable state to conquer the sample grows as an exponential of the free-energy difference between the metastable and the stable states over the thermal energy available, $k_B T$. Once the bubble has reached a critical size that also depends on this free-energy difference it very rapidly conquers the full sample and the system reaches the stable state. The textbook example is the one of a magnetic system, *e.g.* an Ising model, in equilibrium under a magnetic field that is suddenly reversed. The sample has to reverse its magnetization but this involves a nucleation process of the kind just explained. Simple nucleation is therefore not very interesting to us but one should notice that as soon as multiple nucleation and competition between different states intervenes the problem becomes rapidly hard to describe quantitatively and it becomes very relevant to the mean-field theory of fragile structural glasses that we shall discuss.

1.3 Phase ordering kinetics

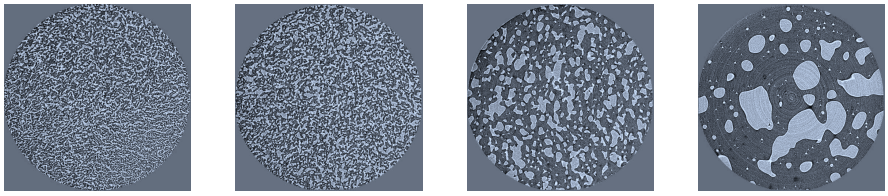

Figure 1: Four images after a quench of a two species mixture (of glasses!) that tends to demix under the new working conditions. Images courtesy of E. Gouillart (St. Gobain), D. Bouttes and D. Vandembroucq (ESPCI).

Choose a system with a well-understood equilibrium phase transition and take it across the critical point (second order phase transition) very quickly by tuning a control parameter. If the system is taken from its disordered (mixed) phase to its ordered (demixed) phase the sample will tend to phase separate in the course of time to approach the ideal equilibrium configuration under the new conditions. Such an example of **phase ordering kinetics** [4], i.e. **phase separation**, is shown in Fig. 1. None of the two species disappears, they just separate. This is such a slow process that the time needed to fully separate the mixture diverges with the size of the sample, as we shall see later on.

Another example of phase ordering kinetics is given by the **crystal grain growth** sketched in the left-most panel in Fig. 2. Grains are formed by pieces of the lattice with the same orientation. Boundaries between these grains are drawn with lines in the figure. The other panels show snapshots of a $2d$ isotropic ferromagnetic Potts model

$$H_J[\{s_i\}] = -J \sum_{\langle ij \rangle} \delta_{s_i s_j} \tag{1.1}$$

with $s_i = 1, \ \ldots, \ q = 8$ quenched below its first order phase transition at the initial time $t = 0$ from a configuration in equilibrium at infinite temperature. The quench is done well below the region of metastability and the dynamics are the ones of **domain growth**. Indeed, domains of neighboring spin ordered in the same direction grow in the course of time. This is clear from the subsequent snapshots taken at $t = 128$ MCs and $t = 1024$ MCs. This model has been used to mimic this kind of physical process when the number of spin components becomes very large, $q \gg 1$. Note that the number of spins of each kind is not conserved along the system's evolution.

These problems are simple in that the systems try to order in configurations that are easy to visualize and to characterize. It is also quite clear from the figures that two kinds of processes coexist: what happens within the domains, far from the interfaces,

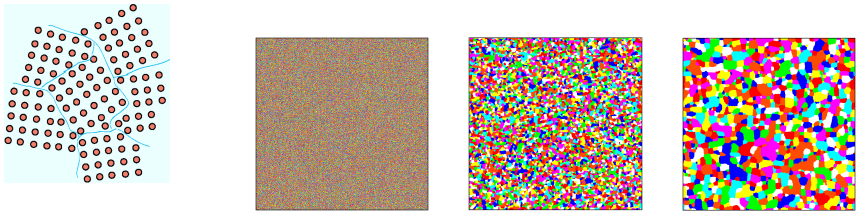

Figure 2: Grain boudaries in crystal growth. Three snapshots of the $2d$ ferromagnetic Potts model with $q = 8$ quenched below its (first order) phase transition to $T = T_c/2$. The times at which the images were taken are $t = 0,\ 128, 1024$ MCs. Data from M. P. Loureiro, J. J. Arenzon, and LFC

and what the interfaces do. We shall come back to this very important issue. To conclude phase ordering kinetics are rather well understood qualitatively although a full quantitative description is hard to develop as the problem is set into the form of a non-linear field theory with no small parameter.

1.4 Critical dynamics

In **critical quenches** [5], patches with equilibrium critical fluctuations grow in time but their linear extent never reaches the equilibrium correlation length that diverges. Clusters of neighboring spins pointing in the same direction of many sizes are visible in the figures and the structure is quite intricate with clusters within clusters and so on and so forth. The interfaces look pretty rough too. A comparison between critical and sub-critical coarsening are shown in Figs. 23 and 24.

Critical slowing down implies that the relaxation time diverges close to the phase transition as a power law of the distance to criticality

$$\tau \sim (T - T_c)^{-\nu z} \tag{1.2}$$

with ν the exponent that controls the divergence of the correlation length and z the dynamic critical exponent.

1.5 Structural disorder: glassy physics

While the understanding of equilibrium phases, the existence of phase transitions as well as the characterization of critical phenomena are well understood in clean systems, as soon as **competing interactions** or **geometric frustration** are included one faces the possibility of destroying this simple picture by giving way to novel phenomena like **glassy** behavior [6].

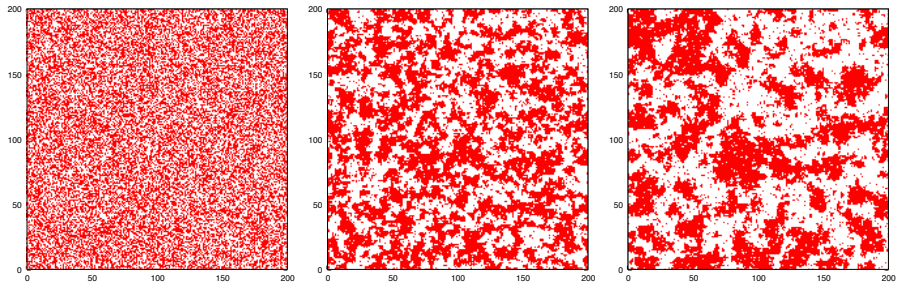

Figure 3: Monte Carlo simulations of a $2d$ Ising model. Three snapshots at $t = 1,\ 3 \times 10^5,\ 3 \times 10^6$ MCs after a quench to T_c. Data from T. Blanchard, LFC and M. Picco.

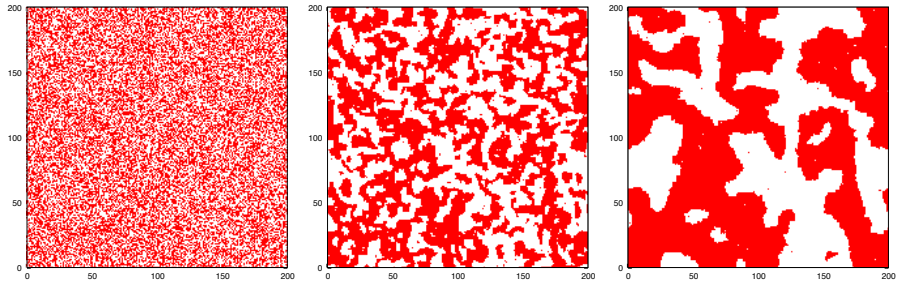

Figure 4: Monte Carlo simulations of a $2d$ Ising model. Three snapshots at $t = 1,\ 3 \times 10^5,\ 3 \times 10^6$ MCs after a quench to $0.5\ T_c$. Thermal fluctuations within the domains are visible. Data from T. Blanchard, LFC and M. Picco.

Glassy systems are usually **dissipative**, that is to say in contact with a much larger environment, that has a well defined temperature and with which the systems in question can exchange heat. We deal with open dissipative systems here.

Competing interactions in physical systems can be dynamic, also called **annealed**, or **quenched**. A simple example illustrates the former: the Lennard-Jones potential,

$$V(r) = V_0\ [(r_0/r)^a - (r_0/r)^b] \tag{1.3}$$

with usually, $a = 12$ and $b = 6$ [2] (see Fig. 7-left) that gives an effective interaction between soft[3] particles in a liquid has a repulsive and an attractive part, depending

[2] The first term is chosen to take care of a quantum effect due to Pauli repulsion in a phenomenological way, the asymptotically leading attractive term is the van der Waals contribution when $b = 6$.

[3] Soft means that the particles can overlap at the price of an energy cost. In the case this is forbidden one works with hard particles.

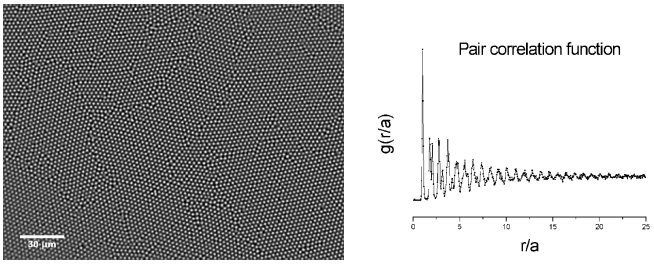

Figure 5: A crystal in a $2d$ colloidal suspension of hard spheres

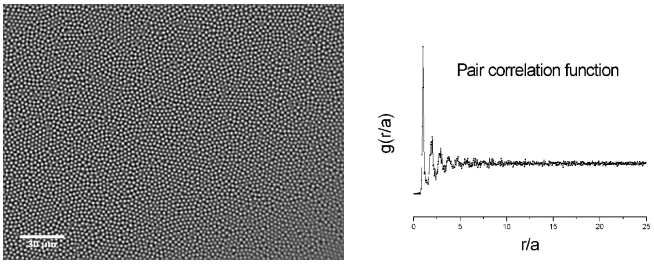

Figure 6: A liquid or a glass in a $2d$ colloidal suspension of hard spheres.

on the distance between the particles, a set of dynamic variables. In this example, the interactions depend on the positions of the particles and evolve with them.

When competing interactions are present the low-temperature configurations may look disordered but still have macroscopic properties of a kind of crystalline state. Again, cooling down a liquid to obtain a glass is helpful to exemplify what we mean here: the liquid cannot support stress and flows while the glass has solid-like properties as crystals, it can support stress and does not easily flow in reasonable time-scales (this is why glasses can be made of glass!) However, when looked at a microscopic scale, one does not identify any important structural difference between the liquid and the glass: no simple long-range structural order has been identified for glasses. Moreover, there is no clear evidence for a phase transition between the liquid and the glass. At present one can only talk about a dynamic crossover. The glassy regime is however usually called a **glassy phase** and it is sometimes said to be a **disordered phase** due to the lack of a clear structural order – this does not mean that there is no order whatsoever (see Fig. 6 for an example of a system with a liquid, a crystal and glassy phase). Lennard-Jones binary mixtures are prototypical examples of systems that undergo a glass transition (or crossover) when cooled across the glass temperature T_g

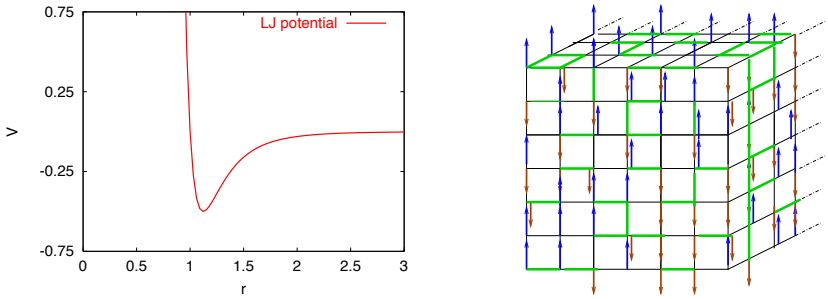

Figure 7: Left: The Lennard-Jones potential. Right: the Edwards-Anderson $3d$ spin-glass.

or when compressed across a density n_g [6].

There are many types of glasses and they occur over an astounding range of scales from macroscopic to microscopic. See Fig. 8 for some images. Macroscopic examples include **granular media** like sand and powders. Unless fluidized by shaking or during flow these quickly settle into jammed, amorphous configurations. Jamming can also be caused by applying stress, in response to which the material may effectively convert from a fluid to a solid, refusing further flow. Temperature (and of course quantum fluctuations as well) is totally irrelevant for these systems since the grains are typically big, say, of $1mm$ radius. **Colloidal suspensions** contain smaller (typically micrometre-sized) particles suspended in a liquid and form the basis of many paints and coatings. Again, at high density such materials tend to become glassy unless crystallization is specifically encouraged (and can even form arrested gels at low densities if attractive forces are also present). On smaller scales still, there are atomic and **molecular glasses**: window glass is formed by quick cooling of a silica melt, and of obvious everyday importance. The plastics in drink bottles and the like are also glasses produced by cooling, the constituent particles being long polymer molecules. Critical temperatures are of the order of 80C for, say, PVC and these systems are glassy at room temperature. Finally, on the nanoscale, glasses are also formed by vortex lines in type-II superconductors. **Atomic glasses** with very low critical temperature, of the order of 10 mK, have also been studied in great detail.

A set of experiments explore the macroscopic **macroscopic** properties of glass formers. In a series of usual measurements one estimates de entropy of the sample by using calorimetric measurements and the thermodynamic relation

$$S(T_2) - S(T_1) = \int_{T_1}^{T_2} dT \, \frac{C_p(T)}{T} \, . \tag{1.4}$$

In some cases the specific volume of the sample is shown as function of temperature. In numerical simulations the potential energy density can be equally used. Figure 9

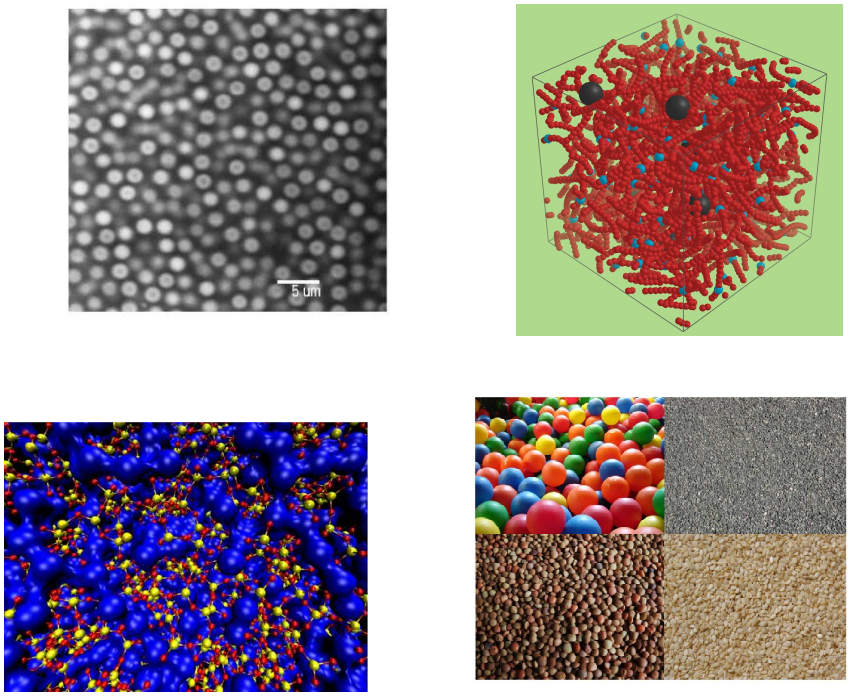

Figure 8: Several kinds of glasses. A colloidal suspension observed with confocal microscopy. A polymer melt configuration obtained with molecular dynamics. A simulation box of a Lennard-Jones mixture. A series of photograph of granular matter.

shows the entropy of the equilibrium liquid, $S(T) \simeq cT$ and the jump to the entropy of the equilibrium crystal at the melting temperature T_m, a first order phase transition. The figure also shows that when the cooling rate is sufficiently fast, and how fast is fast depends on the sample, the entropy follows the curve of the liquid below T_m, entering a metastable phase that is called a super-cooled liquid. The curves obtained with different cooling rates are reproducible in this range of temperatures. However, below a characteristic temperature T_g the curves start to deviate from the liquid-like behavior, they become flatter and, moreover, they depend on the cooling rate (red, orange and yellow curves in the figure). The slower the cooling rate the lower the entropy and the closer it comes to the one of the crystal. Typical cooling rates used in the laboratory are $0.1 - 100$ K/min. Within these experiments T_g is defined as the temperature at which the shoulder appears.

The extrapolation of the entropy of the liquid below T_g crosses the entropy of the

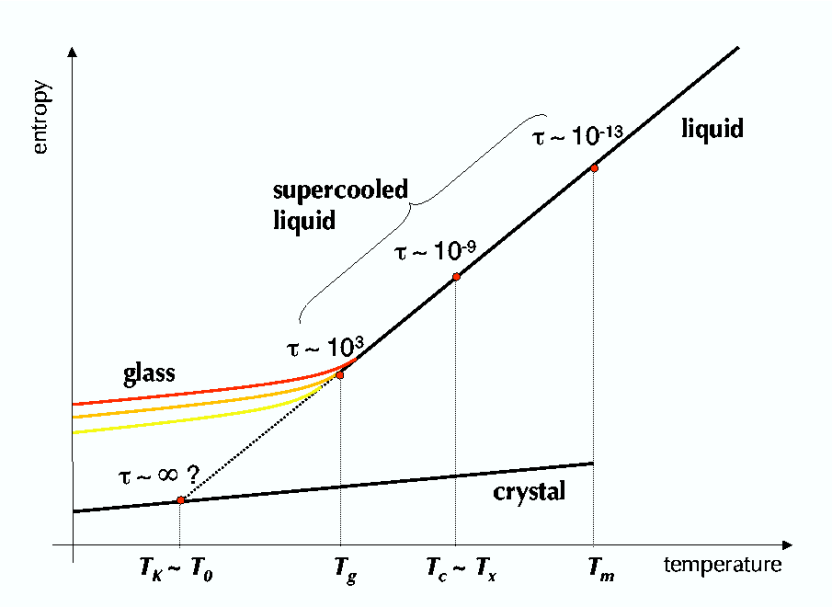

Figure 9: The typical plot showing the four 'phases' observed in a cooling experiment: liquid, supercooled liquid, glass and crystal. The characteristic temperatures T_m (a first order phase transition), T_g and the Kauzmann temperature T_K are shown as well as the typical relaxation times in the liquid and super-cooled liquid phases.

crystal at a value of the temperature that was conjectured by Kauzmann to correspond to an actual phase transition. Indeed at T_K the entropy of the 'glass' is no longer larger than the one of the crystal and the system undergoes an **entropy crisis**. Of course experiments cannot be performed in equilibrium below T_g and, in principle, the extrapolation is just a theoretical construction. Having said this, the mean-field models we shall discuss later on realize this feature explicitly and put this hypothesis on a firmer analytic ground. If T_K represents a thermodynamic transition it should be reachable in the limit of infinitely slow cooling rate.

Rheological measurements show that the viscosity of a super-cooled liquid, or the resistance of the fluid to being deformed by either shear or tensile stress, also increases by many orders of magnitude when approaching the glass 'transition'. One finds – or alternatively defines – T_g as the temperature at which the viscosity reaches $\eta = 10^2$ Pa s [Pascal s = k m/s^2 s/m^2 = kg/(m s)]. At this temperature a peak in the specific heat at constant pressure is also observed, but no divergence is measured.

Bulk relaxation times are also given in the figure in units of seconds. In the super-cooled liquid phase the relaxation time varies by 10 orders of magnitude, from $\tau_\alpha \simeq 10^{-13}$ at the melting point to $\tau_\alpha \simeq 10^3$ at the glassy arrest. The interval of variation

of the temperature is much narrower; it depends on the sample at hand but one say that it is of the order of 50 K. We note that the relaxation times remain finite all along the super-cooled liquid phase and do not show an explicit divergence within the temperature range in which equilibrium can be ensured. We discuss below how these relaxation times are estimated and the two classes, i.e. temperature dependences, that are found.

The values of T_g depend on the sample. In polymer glasses one finds a variation from, say, -70 C in rubber to 145 C in polycarbonate passing by 80 C in the ubiquitous PVC.

There are many different routes to the glassy state. In the examples above we described cooling experiments but one can also use crunches in which the system is set under increasing pressure or other.

The **structure and dynamics** of liquids and glasses can be studied by investigating the **two-time dependent density-density correlation**:

$$\begin{aligned} g(r;t,t_w) &\equiv \langle\, \delta\rho(\vec{x},t)\delta\rho(\vec{y},t_w)\,\rangle \quad \text{with} \quad r=|\vec{x}-\vec{y}| \\ &= N^{-2}\sum_{i=1}^{N}\sum_{j=1}^{N}\langle\delta(\vec{x}-\vec{r}_i(t))\delta(\vec{y}-\vec{r}_j(t_w))\rangle \end{aligned}$$

$\delta\rho$ is the density variation with respect to the mean N/V. The average over different dynamical histories (simulation/experiment) $\langle\ldots\rangle$ implies isotropy (all directions are equivalent) and invariance under translations of the reference point $\vec{y}$. Its Fourier transform is

$$F(q;t,t_w) = N^{-1}\sum_{i,j=1}^{N}\langle\, e^{i\vec{q}(\vec{r}_i(t)-\vec{r}_j(t_w))}\,\rangle \tag{1.5}$$

The **incoherent intermediate or self** correlation:

$$F_s(q;t,t_w) = N^{-1}\sum_{i=1}^{N}\langle\, e^{i\vec{q}(\vec{r}_i(t)-\vec{r}_i(t_w))}\,\rangle \tag{1.6}$$

can be accessed with (neutron or other) diffraction experiments.

In the main panel of Fig. 10-left the equal-time two-point correlation function of a Lennard-Jones mixture at different times after an infinite rapid quench below the glassy crossover temperature T_g is shown. The data vary very little although a wide range of time-scales is explored. In the inset a zoom over the first peak taken at the same time for different final temperatures, three of them below T_g the reference one at the numerically determined T_g. Again, there is little variation in these curves. One concludes that the structure of the sample in all these cases is roughly the same.

The change is much more pronounced when one studies the dynamics of the sample, that is to say, when one compares the configuration of the system at different times. The curves on the right panel display the relaxation of the correlation function at different temperatures, all above T_g. The relaxation is stationary in all cases, i.e.

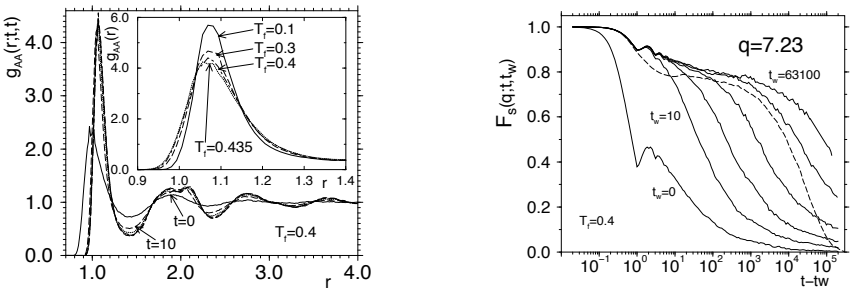

Figure 10: Structure and dynamics of a binary Lennard-Jones mixture. Left: the two-point correlation function of the A atoms at different times (main panel) and at different temperatures (inset). Right: the decay of the Fourier transform of the correlation function at the wave-vector associated to the first peak in $g_{AA}(r)$. Data from Kob & J-L Barrat.

a function of $t - t_w$ only, but it becomes much slower when the working temperature approaches T_g.

In a family if glass formers called **fragile**, in double logarithmic scale used in the plot, a clear plateau develops for decreasing T and may seem to diverge in the $T \to T_g$ limit. In another family of glass formers called **strong** no plateau is seen.

From the analysis of the temperature dependence of the relaxation time, say the time needed for the correlation to decay to half its value at zero time delay[4] one finds two kinds of fitting laws:

$$\tau_\alpha = \begin{cases} \tau_0 \; e^{A/(T-T_0)} & \text{Vogel-Fulcher-Tamann} \\ \tau_0 \; e^{A/T} & \text{Arrhenius} \end{cases} \tag{1.7}$$

In fits T_0 is usually very close to T_K. The former class of systems are the fragile ones while the latter are the strong ones. Note that the first form yields a divergence at a finite T_K while the second one yields a divergence at $T = 0$. Silica belongs to the second class while most polymer glasses belong to the first one. This relaxation time is usually called the **alpha or structural relaxation time**. Recall that in a usual second order phase transition (as realized in an Ising model, for instance) the divergence of the relaxation time close to the critical point is of power law type.

A **real space analysis** of the motion of the particles in atomic, molecules in molecualr, or strings in polymeric glasses (and granular matter as well) demonstrates that the elements move, over short time scales, in cages formed by their neighbors. During this short time span the correlation function decays to the plateau and the mean-square displacement reaches a plateau (in a double logarithmic scale). Note, however, that the particle's displacement is much smaller than the particle radius meaning that the displacement is indeed tiny during this time regime. the second

[4]This is a very naive definition of τ_α, others much more precise are used in the literature.

structural relaxation is the one that take the correlation (displacement) below (above) the plateau.

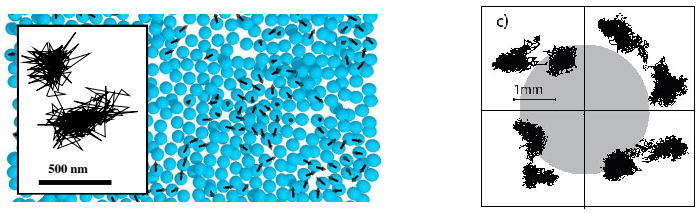

Figure 11: Colloidal suspension (data from E. Weeks group) and granular matter (data from O. Pouliquen's group).

Very recently stress has been put on the analysis of the motion of the elements over longer time-scales. Dynamic heterogeneities [12] were thus uncovered. Dynamic regions with high mobility immersed in larger regions with little mobility were identified. Sometimes stringly motion of particles following each in a periodic path were also observed in confocal microscopy measurements or in molecular dynamics simulations. The length of these strings seem to increase when approaching the crossover temperature T_g. Moreover, dynamic heterogeneities, and a growing length associated to it, were quantified from the analysis of a four-pint correlation function. This function takes different forms depending on the problem at hand but basically searches for spatial correlations in the displacement of particles between different time intervals. Calling $\delta\rho(\vec{r},t) = \rho(\vec{r},t) - \rho_0$ with $\rho_0 = N/V$,

$$\begin{aligned} C_4(r;t,t_w) &= \langle \delta\rho(\vec{x},t_w)\delta\rho(\vec{x},t)\delta\rho(\vec{y},t_w)\delta\rho(\vec{y},t)\rangle \\ &\quad -\langle \delta\rho(\vec{x},t_w)\delta\rho(\vec{x},t)\rangle\langle\delta\rho(\vec{y},t_w)\delta\rho(\vec{y},t)\rangle \ . \end{aligned} \tag{1.8}$$

Terms involving one position only can be extracted from the average since they do not contain information about the spatial correlation. The idea is, roughly, to consider that $\delta\rho(\vec{x},t)\delta\rho(\vec{x},t_w)$ is the **order parameter**. The double spatial integral of this quantity defines a **generalized susceptibility** $\chi_4(t,t_w)$ that has been study in many numerical and laboratory experiments. It shows a peak at the time-delay $t-t_w$ that coincides with the relaxation time τ_α. Assuming a usual kind of scaling with a typical growing length for the four point correlation the characteristic of the appearance of the peak should yield the length of these dynamic heterogeneities. The data can be interpreted as leading to a divergence of the growing length at some temperature but the actual values found are very small, of the order of a few inter-particle distances in the sample.

The defining feature of glasses, i.e., the characterization of their **out of equilibrium relaxation** and **aging phenomena** [13], will be discussed below.

A **summary** of the liquid-super-cooled liquid-glass behavior is given in the table below.

Crytallization at T_m is avoided by cooling fast enough.

Liquid — Supercooled liquid — **Glass**

Exponential relax — Non-exponential relax

Equilibrium — Metastable equilibrium — **Non-equilibrium**

Separation of time-scales &
An exponential number of metastable states!

Stationary — **Aging**

Aging means that correlations and reponses depend on t *and* t_w
ac susceptibilities depend on ω *and* t_w

There might be an **equilibrium transition** to an **ideal glass** at T_s.

1.6 Quenched disorder: still glassiness

In the paragraphs above we characterized the low temperature regime of certain particle models and claimed that their structure is disordered (at least at first sight). Another sense in which the word **disorder** is used is to characterize the **interactions**. Quenched interactions are due to a very sharp separation of time-scales. The traditional example is the one of **spin-glasses** in which the characteristic time for diffusion of magnetic impurities in an inert host is much longer than the characteristic time for magnetic moment change:

$$\tau_d \gg \tau_{exp} \gg \tau_0 \ . \tag{1.9}$$

The position of the magnetic moments are decided at the preparation of the sample. These position are then random and they do not change during experimental times. The interactions between pairs of spins depend on the distance between the magnetic moments via the RKKY formula

$$V_{\rm RKKY}(r_{ij}) = -J \ \frac{\cos(2k_F r_{ij})}{r_{ij}^3} \ s_i s_j \ . \tag{1.10}$$

Therefore quenched competing interactions are fixed in the observational time-scale and they transmit 'contradictory' messages. Typical examples are systems with ferromagnetic and/or antiferromagnetic exchanges that are not organized in a simple way with respect to the geometry and connectivity of the lattice such as spin-glasses [7] (see Fig. 7-right).

Theoretically, this is modeled by random interactions drawn from a probability distribution. For simplicity the spins (magentic moments) are placed on the vertices of a finite dimensional lattice, typically a cubic one. The Edwards-Anderson

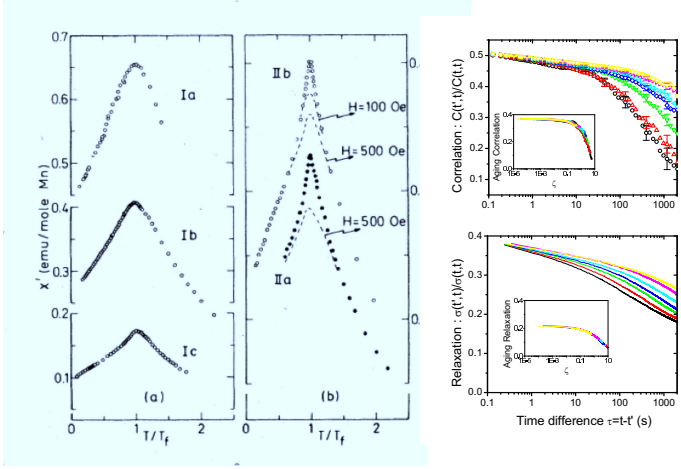

Figure 12: Spin-glasses: Susceptibility data (Mydosh). Aging phenomena (Hérisson and Ocio).

Hamiltonian then reads

$$H_J[\{s_i\}] = \sum_{\langle ij \rangle} J_{ij} s_i s_j \qquad \text{with} \qquad J_{ij} \qquad \text{taken from} \qquad P(J_{ij}) \tag{1.11}$$

Annealed interactions may have a slow time-dependence. Both lead to **disorder**. These can be realized by coupling strengths as in the magnetic example in Fig. 7, but also by magnetic fields, pinning centers, potential energies, *etc.* Disordered interactions usually lead to low-temperature behavior that is similar to the one observed in systems with dynamic competing interactions.

Data showing the cusp in the susceptibility of a spin-glass sample are shown in Fig. 12.

1.7 Static questions

In these lectures we shall only deal with a canonical setting, the microcanonical one being more relevant to quantum systems. Disordered systems (in both senses) are usually in contact with external reservoirs at fixed temperature; their description is done in the canonical (or grand-canonical in particle systems with the possibility of particle exchange with the environment) ensemble.

Many questions arise for the **static properties** of systems with competing interactions. Some of them, that we shall discuss in the rest of the course are:

- Are there equilibrium phase transitions between low-temperature and high temperature phases?
- Is there any kind of order at low temperatures?

- At the phase transition, if there is one, does all the machinery developed for clean systems (scaling, RG) apply?
- Are these phases, and critical phenomena or dynamic crossovers, the same or very different when disorder is quenched or annealed?
- What is the mechanism leading to glassiness?

1.8 Random manifolds

A problem that finds applications in many areas of physics is the dynamics of elastic manifolds under the effect (or not) of quenched random potentials, with (Kardar-Parisi-Zhang) or without (Edwards-Wilkinson, Mullins-Herring) non-linear interactions, with short-range or long-range elastic terms [8, 14].

Under certain circumstances the interfaces **roughen**, that is to say, their asymptotic averaged width depends on their linear size. Take for instance, the local height $h(\vec{r},t)$ of a d dimensional surface (with no overhangs). Its time-dependent width is defined as

$$W_L(t) = L^{-d} \int d^d r \; [h(\vec{r},t) - \langle h(\vec{r},t) \rangle]^2 \tag{1.12}$$

where $\langle \ldots \rangle = L^{-d} \int d^d r \ldots$. This quantity verifies the so-called **Family-Vicsek scaling**. In its simplest form, in which all dependences are power laws, it first increases as a function of time, $W_L(t) \sim t^{2\alpha}$ and independently of L. At a crossover time $t_x \sim L^z$ it crosses over to saturation at a level that grows as $L^{2\zeta}$. α is the growth exponent, z is the dynamic exponent and ζ is the roughness exponent. Consistency implies that they are related by $z\alpha = \zeta$. The values of the exponents are known in a number of cases. For the Edwards-Wilkinson surface one has $\alpha = (2-d)/4$, $z = 2$ and $\zeta = (2-d)/2$ for $d \leq 2$. For the non-linear KPZ line $\alpha = 1/3$, $z = 3/2$ and $\zeta = 1/2$.

In the presence of quenched disorder the dependence of the asymptotic roughness with the length of the line undergoes a crossover. For lines that are shorter than a temperature and disorder strength dependent value L_T the behavior is controlled by thermal fluctuations and relation as the one above holds with $\zeta = \zeta_T$, the thermal roughness exponent. This exponent is the one corresponding to the EW equation. In this thermally dominated scale, the dynamics is expected to be normal in the sense that lengths and times should be thus related by power laws of types with the exponents discussed above. For surfaces such that $L > L_T$ one finds that the same kind of scaling holds but with a roughness exponent that takes a different value. The time dependence and cross-over time are expected, though, not to be power laws and we shall discuss them later.

The relaxation dynamics of such elastic manifolds in the very large limit presents many other interesting phenomena that resemble features observed in more complex glassy systems. Moreover, such elastic surfaces appear in the nucleation and growth

kinetics problems discussed above as the interfaces between equilibrium (sometimes metastable) states.

1.9 Aging

In practice a further complication appears [13]. Usually, disordered phases are prepared with a relatively rapid quench from the high temperature phase. When approaching a characteristic temperature the systems cannot follow the pace of evolution dictated by the environment and **fall out of equilibrium** [2]. Indeed, their key feature is that below some characteristic temperature T_g, or above a critical density ρ_g, the relaxation time goes beyond the experimentally accessible time-scales and the system is next bound to evolve out of equilibrium. Although the mechanism leading to such a slow relaxation is unknown – and might be different in different cases – the out of equilibrium relaxation presents very similar properties. The left panel in Fig. 13 shows one aspect of glassy dynamics, aging, as shown by the two-time relaxation of the self-correlation of a colloidal suspension, that is remarkably similar to the decay of the magnetic correlation in the Ising model shown in the right panel and in Fig. 30.

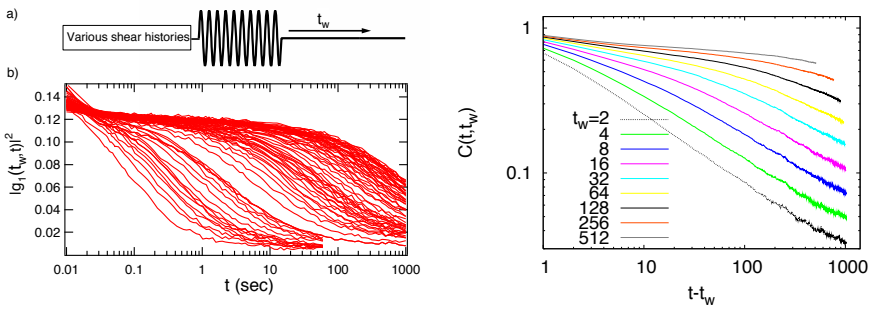

Figure 13: Left: two-time evolution of the self-correlation in a colloidal suspension initialized by applying a shearing rate (data from Viasnoff and Lequeux) The longer the waiting time the slower the decay. Right: two-time evolution in the bi-dimensional Ising model quenched below its phase transition at T_c. A two-scale relaxation with a clear plateau at a special value of the correlation is seen in the double logarithmic scale. Data from Sicilia *et al.* We shall discuss this feature at length in the lectures.

A purely static description, based on the use of the canonical (or grand-canonical) partition function is then not sufficient. One is forced to include the time evolution of the individual agents (spins, particles, molecules) and from it derive the macroscopic *time-dependent* properties of the full system. The microscopic time-evolution is given by a stochastic process. The macroscopic evolution is usually very slow and, in probability terms, it is not a small perturbation around the Gibbs-Boltzmann distri-

bution function but rather something quite different. This gives rise to new interesting phenomena.

The questions that arise in the **non-equilibrium** context are

- How to characterize the non-equilibrium dynamics of glassy systems phenomenologically.
- Which are the minimal models that reproduce the phenomenology.
- Which is the relation between the behavior of these and other non-equilibrium systems, in particular, those kept away from equilibrium by external forces, currents, *etc.*
- Which features are generic to all systems with slow dynamics.
- Whether one could extend the equilibrium statistical mechanics ideas; *e.g.* can one use temperature, entropy and other thermodynamic concepts out of equilibrium?
- Related to the previous item, whether one can construct a non-equilibrium measure that would substitute the Gibbs-Boltzmann one in certain cases.

1.10 Driven systems

An out of equilibrium situation can be externally maintained by applying forces and thus injecting energy into the system and driving it. There are several ways to do this and we explain below two quite typical ones that serve also as theoretical traditional examples.

Rheological measurements are common in soft condensed matter; they consist in driving the systems out of equilibrium by applying an external force that does not derive from a potential (e.g. shear, shaking, etc.). The dynamics of the system under the effect of such a strong perturbation is then monitored.

The effect of shear on domain growth is one of great technological and theoretical importance. The growth of domains is anisotropic and there might be different growing lengths in different directions. Moreover, it is not clear whether shear might interrupt growth altogether giving rise to a non-equilibrium stationary state or whether coarsening might continue for ever. Shear is also commonly used to study the mechanical properties of diverse glasses.

Another setting is to couple the system to **different external reservoirs** all in equilibrium but at different temperature or chemical potential thus inducing a heat or a particle current through the system. This set-up is relevant to quantum situations in which one can couple a system to, say, a number of leads at different chemical potential. The heat transport problem in classical physics also belongs to this class.

A pinned interface at zero temperature can be depinned by pulling it with an external force. The depinning problem that is to say the analysis of the dynamics close to the critical force needed to depin the manifold, and the creep dynamics at non-vanishing temperature have also been the subject of much analysis.

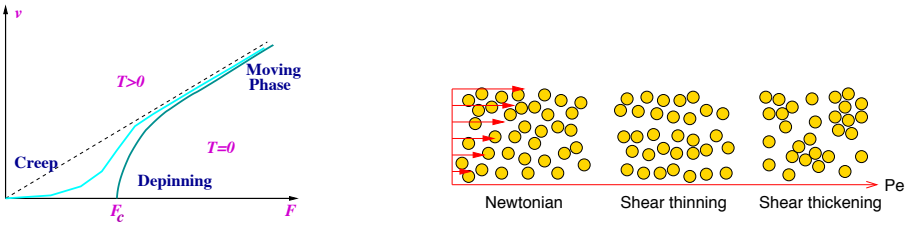

Figure 14: Left: Creep and depinning of elastic objects under quenched randomness. Right: Rheology of complex fluids. Shear thinning: τ decreases or thickening τ increases

1.11 Interdisciplinary aspects

The theory of disordered systems has become quite interdisciplinary in the sense that problems in computer science, biology or even sociology and finance have disorder aspects and can be mimicked with similar models and solved with similar methods to the ones we shall discuss here.

1.11.1 Optimization problems

The most convenient area of application is, most probably, the one of **combinatorial optimization** in computer science [9]. These problems can usually be stated in a form that corresponds to minimizing a cost (energy) function over a large set of variables. Typically these cost functions have a very large number of local minima – an exponential function of the number of variables – separated by barriers that scale with N and finding the truly absolute minimum is hardly non-trivial. Many interesting optimization problems have the great advantage of being defined on random graphs and are then mean-field in nature. The mean-field machinery that we shall discuss at length is then applicable to these problems with minor (or not so minor) modifications due to the finite connectivity of the networks.

Let us illustrate this kind of problems with two examples. The **graph partitioning** problem consists in, given a graph $G(N, E)$ with N vertices and E edges, to partition it into smaller components with given properties. In its simplest realization the uniform graph partitioning problem is how to partition, in the optimal way, a graph with N vertices and E links between them in two (or k) groups of equal size $N/2$ (or N/k) and the minimal the number of edges between them. Many other variations are possible. This problem is encountered, for example, in computer design where one wishes to partition the circuits of a computer between two chips. More recent applications include the identification of clustering and detection of cliques in social, pathological and biological networks.

Another example is **k satisfiability (k-SAT)**. This is the computer science problem of determining whether the variables of a given Boolean formula can be assigned

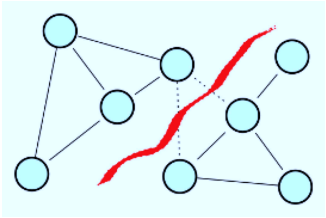

Figure 15: Graph partitioning.

in such a way as to make the formula evaluate to 'true'. Equally important is to determine whether no such assignments exist, which would imply that the function expressed by the formula is identically 'false' for all possible variable assignments. In this latter case, we would say that the function is unsatisfiable; otherwise it is satisfiable. For example, the formula $C_1 : x_1$ OR x_2 made by a single clause C_1 is satisfiable because one can find the values $x_1 =$ true (and x_2 free) or $x_2 =$ true (and x_1 free), which make $C_1 : x_1$ OR x_2 true. This example belongs to the $k = 2$ class of satisfiability problems since the clause is made by two literals (involving different variables) only. Harder to decide formulæ are made of M clauses involving k literals required to take the true value (x) or the false value ($\overline{x}$) each, these taken from a pool of N variables. An example in 3-SAT is

$$\mathrm{F} = \begin{cases} C_1 \ : \ x_1 \ \mathrm{OR} \ \overline{x}_2 \ \mathrm{OR} \ x_3 \\ C_2 \ : \ \overline{x}_5 \ \mathrm{OR} \ \overline{x}_7 \ \mathrm{OR} \ x_9 \\ C_3 \ : \ x_1 \ \mathrm{OR} \ \overline{x}_4 \ \mathrm{OR} \ x_7 \\ C_4 \ : \ x_2 \ \mathrm{OR} \ \overline{x}_5 \ \mathrm{OR} \ x_8 \end{cases} \tag{1.13}$$

All clauses have to be satisfied simultaneously so the formula has to be read F : C_1 AND C_2 AND C_3 AND C_4. It is not hard to believe that when $\alpha \equiv M/N > \alpha_c$ the problems typically become unsolvable while one or more solutions exist on the other side of the phase transition. In **random k-SAT** an instance of the problem, i.e. a formula, is chosen at random with the following procedure: first one takes k variables out of the N available ones. Seconf one decides to require x_i or $\overline{x}_i$ for each of them with probability one half. Third one creates a clause taking the OR of these k literals. Forth one returns the variables to the pool and the outlined three steps are repeated M times. The M resulting clauses form the final formula.

The Boolean character of the variables in the k-SAT problem suggests to transform them into Ising spins, i.e. x_i evaluated to true (false) will correspond to $s_i = 1$ (-1) . The requirement that a formula be evaluated true by an assignment of variables

(i.e. a configuration of spins) will correspond to the ground state of an adequately chosen energy function. In the simplest setting, each clause will contribute zero (when satisfied) or one (when unsatisfied) to this cost function. There are several equivalent ways to reach this goal. For instance C_1 above can be represented by a term $(1-s_1)(1+s_2)(1-s_3)/8$. The fact that the variables are linked together through the clauses suggests to define k-uplet interactions between them. We then choose the interaction matrix to be

$$J_{ai} = \begin{cases} 0 & \text{if neither } x_i \text{ nor } \overline{x}_i \in C_a \\ 1 & \text{if } x_i \in C_a \\ -1 & \text{if } \overline{x}_i \in C_a \end{cases} \tag{1.14}$$

and the energy function as

$$H_J[\{s_i\}] = \sum_{a=1}^{M} \delta(\sum_{i=1}^{N} J_{aj} s_i, -k) \tag{1.15}$$

where $\delta(x, y)$ is a Kronecker-delta. This cost function is easy to understand. The Kronecker delta contributes one to the sum only if all terms in the sum $\sum_{i=1}^{N} J_{ai} s_i$ are equal -1. This can happen when $J_{ai} = 1$ and $s_i = -1$ or when $J_{ai} = -1$ and $s_i = 1$. In both cases the condition on the variable x_i is not satisfied. Since this is required from all the variables in the clause, the clause itself and hence the formula are not satisfied.

These problems are 'solved' numerically, with algorithms that do not necessarily respect physical rules. Thus, one can use non-local moves in which several variables are updated at once – as in cluster algorithms of the Swendsen-Wang type used to beat critical slowing down close to phase transitions or one can introduce a temperature to go beyond cost-function barriers and use dynamic local moves that do not, however, satisfy a detail balance. The problem is that with hard instances of the optimization problem none of these strategies is successful. Indeed, one can expect that glassy aspects, as the proliferation of metastable states separated by barriers that grow very fast with the number of variables, can hinder the resolutions of these problems in polynomial time for *any* algorithm.

Complexity theory in computer science, and the classification of optimization problems in classes of complexity – P for problems solved with algorithms that use a number of operations that grows as a polynomial of the number of variables, *e.g.* as N^2 or even N^{100}, NP for problems for which no polynomial algorithm is known and one needs a number of operations that grow exponentially with N, *etc.* – applies to the worst instance of a problem. Worst instance, in the graph-partitioning example, means the **worst** possible realization of the connections between the nodes. Knowing which one this is is already a very hard problem!

But one can try to study optimization problems on average, meaning that the question is to characterize the **typical** – and not the worst – realization of a problem. The use of techniques developed in the field of disordered physical systems, notably

spin-glasses, have proven extremely useful to tackle typical single randomly generated instances of hard optimization problems.

Note that in statistical mechanics information about averaged macroscopic quantities is most often sufficiently satisfactory to consider a problem solved. In the optimization context one seeks for exact microscopic configurations that correspond to the exact ground state and averaged information is not enough. Nevertheless, knowledge about the averaged behavior can give us qualitative information about the problem that might be helpful to design powerful algorithms to attack single instances.

1.11.2 Biological applications

In the biological context disordered models have been used to describe **neural networks**, *i.e.* an ensemble of many neurons (typically $N \sim 10^9$ in the human brain) with a very elevated connectivity. Indeed, each neuron is connected to $\sim 10^4$ other neurons and receiving and sending messages *via* their axons. Moreover, there is no clear-cut notion of distance in the sense that axons can be very long and connections between neurons that are far away have been detected. Hebb proposed that the memory lies in the connections and the peculiarity of neural networks is that the connectivity must then change in time to incorporate the process of learning.

The simplest neural network models [10] represent neurons with Boolean variables or spins, that either fire or are quiescent. The interactions link pairs of neurons and they are assumed to be symmetric (which is definitely not true). The state of a neuron is decided by an activity function f,

$$\phi_i = f\Big(\sum_{j(\neq i)} J_{ij}\phi_j\Big)\ , \tag{1.16}$$

that in its simplest form is just a theta-function leading to simply two-valued neurons.

Memory of an object, action, *etc.* is associated to a certain pattern of neuronal activity. It is then represented by an N-component vector in which each component corresponds to the activity of each neuron. Finally, sums over products of these patterns constitute the interactions. As in optimization problems, one can study the particular case associated to a number of chosen specific patterns to be stored and later recalled by the network, or one can try to answer questions on average, as how many typical patterns can a network of N neurons store. The models then become fully-connected or dilute models of spins with quenched disorder. The microscopic dynamics cannot be chosen at will in this problem and, in general, will not be as simple as the single spin flip ones used in more conventional physical problems. Still, if the disordered modeling is correct, glassy aspects can render recall very slow due to the presence of metastable states for certain values of the parameters.

Another field of application of disordered system techniques is the description of **hetero-polymers** and, most importantly, protein folding. The question is how to describe the folding of a linear primary structure (just the sequence of different amino-acids along the main backbone chain) into an (almost) unique compact native

Figure 16: Active matter.

structure whose shape is intimately related to the biological function of the protein. In modeling these very complex systems one proposes that the non-random, selected through evolution, macromolecules may be mimicked by random polymers. This assumption is based on the fact that amino-acids along the chain are indeed very different. One then uses monomer-monomer and/or monomer-solvent interactions that are drawn from some probability distribution and are fixed in time (quenched disorder). Still, a long bridge between the theoretical physicists' and the biologists' approaches remain to be crossed. Some of the important missing links are: proteins are mesoscopic objects with of the order of 100 monomers thus far from the thermodynamic limit; interest is in the particular, and not averaged, case in biology, in other words, one would really like to know what is the secondary structure of a particular primary sequence; *etc.* In the protein folding problem it is clear that the time needed to reach the secondary structure from an initially stretched configuration depends strongly on the existence of metastable states that could trap the (hetero) polymer. Glassy aspects have been conjectured to appear in this context too.

The constituents of **active matter**, be them particles, lines or other, absorb energy from their environment or internal fuel tanks and use it to carry out motion. In this new type of soft condensed matter energy is partially transformed into mechanical work and partially dissipated in the form of heat [11]. The units interact directly or through disturbances propagated in the medium. In systems of biological interest, conservative forces (and thermal fluctuations) are complemented by non-conservative forces. Realizations of active matter in biology are thus manifold and exist at different scales. Some of them are: bacterial suspensions, the cytoskeleton in living cells, or even swarms of different animals. Clearly enough, active matter is far from equilibrium and typically kept in a non-equilibrium steady state. The difference between active

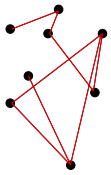

Figure 17: Left: random graph with finite connectivity

matter and other driven systems, such as sheared fluids, vibrated granular matter and driven vortex lattices is that the energy input is located on internal units (e.g. motors) and therefore homogeneously distributed in the sample. In the other driven systems mentioned above, the energy input occurs on the boundaries of the sample. Moreover, the effect of the motors can be dictated by the state of the particle and/or its immediate neighborhood and it is not necessarily fixed by an external field.

The dynamics of active matter presents a number of interesting features that are worth mentioning here. Active matter displays out of equilibrium phase transitions that may be absent in their passive counterparts. The dynamic states display large scale spatio-temporal dynamical patterns and depend upon the energy flux and the interactions between their constituents. Active matter often exhibits unusual mechanical properties, very large responses to small perturbations, and very large fluctuations – not consistent with the central limit theorem. Much theoretical effort has been recently devoted to the description of different aspects of these systems, such as self-organization of living microorganisms, the identification and analysis of states with spatial structure, such as bundles, vortices and asters, the study of the rheological properties of active particle suspensions with the aim of grasping which are the mechanical consequences of biological activity. A rather surprisingly result was obtained with a variational solution to the many-body master equation of the motorized version of the standard hard sphere fluid often used to model colloids: instead of stirring and thus destabilize ordered structures, the motors do, in some circumstances enlarge the range of stability of crystalline and amorphous structures relative to the ones with purely thermal motion.

1.12 Summary

The main steps in the development and application of Statistical Mechanics ideas to macroscopic cooperative systems have been

- The development of the basic ideas (Boltzmann-Gibbs).
- The recognition of collective phenomena and the identification and mean-field description of phase transitions (Curie-Weiss).
- The correct description of critical phenomena with scaling theories and the renormalization group (Kadanoff, Widom, M. Fisher, Wilson) and more recently the development of conformal field theories for two-dimensional systems.

- The study of stochastic processes and time-dependent properties (Langevin, Fokker-Planck, Glauber, *etc.*).

To describe the problems introduced above the same route has been followed. There is no doubt that Equilibrium Statistical Mechanics yields the static properties of these systems. In the case of coarsening problems one understands very well the static phases and phase transitions. In the case of glassy systems this is not so clear. In the case of active matter or other driven systems there are equilibrium phases in the vanishing drive limit only but one can also study the **dynamic phase transitions** with a critical phenomena perspective.

Although the study of equilibrium phases might be a little irrelevant from the practical point of view since, most glassy systems are out of equilibrium in laboratory time-scales, it is certainly a necessary step on which one can try to build a truly dynamic theory. The mean-field study – the second step in the list above – of the equilibrium properties of disordered systems, in particular those with quenched disorder, has revealed an incredibly rich theoretical structure. We still do not know whether it carries through to finite dimensional cases. Even though, it is definitely interesting *per se* and it finds a very promising field of application in combinatorial optimization problems that are defined on random networks, see Fig. 17, with mean-field character. Scaling arguments have been applied to describe finite dimensional disordered systems but they remain – as their parent ones for clean systems – quite phenomenological and difficult to put to sufficiently restrictive numerical or experimental test. The extension of renormalisation group methods to systems with quenched disorder is also under development and still needs quite a lot of work – the third step. As for the out of equilibrium dynamics of these systems, again, it has been solved at the mean-field level but little is known in finite dimensions – apart from numerical simulations or the solution to toy models. As in its static counterpart, the results from the study of dynamic mean-field models have been very rich and they have suggested a number of new phenomena later searched for in numerical simulations and experiments of finite dimensional systems. In this sense, these solutions have been a very important source of inspiration.

2 Modeling

In this section I will revisit certain aspects of statistical physics that are not commonly discussed and that become important for our purposes.

2.1 Fluctuations

There are several possible sources of fluctuations:

- **Classical thermal**: the system is coupled to an environment that ensures fluctuations (noise) and dissipation (the fact that the total energy is not conserved). E.g. coarsening, classical glasses, spin-glasses.
- **Quantum**: the system is coupled to a quantum environment that ensures fluctuations (noise) and dissipation. The temperature of the bath can be zero or not. E.g. quantum coarsening and glasses, quantum spin-glasses.
- **Stochastic motors**: forces that act on the system's particles stochastically. They energy injected in the sample is partially dissipated to the bath and partially used as work. As the system is also coupled to a bath there are also thermal fluctuations in it. E.g. active matter.

Classical and quantum environments are usually modeled as large ensembles of non-interacting variables (oscillators [16], spins [17], fermions) with chosen distributions of coupling constants and energies.

2.2 The classical reduced partition function

We analyze the statistical **static** properties of a **classical canonical system** in equilibrium at inverse temperature β and itself formed by two sub-parts, one that will be treated as an environment (not necessarily of infinite size) and another one that will be the (sub-)system of interest. We study the **partition function** or Gibbs functional, $Z_{\rm TOT}$:

$$Z_{\rm TOT}[\eta] = \sum_{\substack{\rm CONF\ \ ENV \\ \rm CONF\ \ SYST}} \exp(-\beta H_{\rm TOT} - \beta \eta x) \tag{2.1}$$

where the sum represents an integration over the phase space of the full system, i.e. the system's and the environmental ones. η is a source. We take

$$H_{\rm TOT} = H_{\rm SYST} + H_{\rm ENV} + H_{\rm INT} + H_{\rm COUNTER} = H_{\rm SYST} + \tilde{H}_{\rm ENV} \ . \tag{2.2}$$

For simplicity we use a single particle moving in $d = 1$: $H_{\rm SYST}$ is the Hamiltonian of the isolated particle,

$$H_{\rm SYST} = \frac{p^2}{2M} + V(x) \ , \tag{2.3}$$

with p and x its momentum and position. $H_{\rm ENV}$ is the Hamiltonian of a 'thermal bath' that, for simplicity, we take to be an ensemble of N independent harmonic oscillators [15, 16] with masses m_a and frequencies ω_a, $a = 1, \ldots, N$

$$H_{\rm ENV} = \sum_{a=1}^{N} \frac{\pi_a^2}{2m_a} + \frac{m_a \omega_a^2}{2} q_a^2 \tag{2.4}$$

with π_a and q_a their momenta and positions. This is indeed a very usual choice since it may represent phonons. $H_{\rm INT}$ is the coupling between system and environment. We shall restrict the following discussion to a linear interaction in the oscillator coordinates, q_a, and in the particle coordinate,

$$H_{\rm INT} = x \sum_{a=1}^{N} c_a q_a \ , \tag{2.5}$$

with c_a the coupling constants. The counter-term $H_{\rm COUNTER}$ is added to avoid the generation of a negative harmonic potential on the particle due to the coupling to the oscillators (that may render the dynamics unstable). We choose it to be

$$H_{\rm COUNTER} = \frac{1}{2} \sum_{a=1}^{N} \frac{c_a^2}{m_a \omega_a^2} x^2 \ . \tag{2.6}$$

The generalization to more complex systems and/or to more complicated baths and higher dimensions is straightforward. The calculations can also be easily generalized to an interaction of the oscillator coordinate with a more complicated dependence on the system's coordinate, $\mathcal{V}(x)$, that may be dictated by the symmetries of the system. Non-linear functions of the oscillator coordinates cannot be used since they render the problem unsolvable analytically.

Having chosen a quadratic bath and a linear coupling, the integration over the oscillators' coordinates and momenta can be easily performed. This yields the **reduced** Gibbs functional

$$Z_{\rm RED}[\eta] \propto \sum_{\rm CONF\ SYST} \exp\left[-\beta \left(H_{\rm SYST} + H_{\rm COUNTER} + \eta x - \frac{1}{2} \sum_{a=1}^{N} \frac{c_a^2}{m_a \omega_a^2} \, x^2 \right)\right] \ . \tag{2.7}$$

The 'counter-term' $H_{\rm COUNTER}$ is chosen to cancel the last term in the exponential and it avoids the renormalization of the particle's mass (the coefficient of the quadratic term in the potential) due to the coupling to the environment that could have even destabilized the potential by taking negative values. An alternative way of curing this problem would be to take a vanishingly small coupling to the bath in such a way that the last term must vanish by itself (say, all $c_a \to 0$). However, this might be problematic when dealing with the stochastic dynamics since a very weak coupling to the bath implies also a very slow relaxation. It is then conventional to include the counter-term to cancel the mass renormalization. One then finds

$$\boxed{Z_{\rm RED}[\eta] \propto \textstyle\sum_{\rm CONF\ SYST} \exp\left[-\beta \left(H_{\rm SYST} + \eta x\right)\right] = Z_{\rm SYST}[\eta] \ .} \tag{2.8}$$

For a non-linear coupling $H_{\rm INT} = \sum_{a=1}^{N} c_a q_a \mathcal{V}(x)$ the counter-term is $H_{\rm COUNTER} = \frac{1}{2}\sum_{a=1}^{N} \frac{c_a^2}{m_a \omega_a^2}[\mathcal{V}(x)]^2$.

The interaction with the reservoir does not modify the statistical properties of the particle since $Z_{\rm RED} \propto Z_{\rm SYST}$, independently of the choices of c_a, m_a, ω_a and N.

If one is interested in the **dynamics** of a coupled problem, the characteristics of the sub-system that will be considered to be the bath have an influence on the reduced dynamic equations found for the system, that are of generic Langevin kind, as explained in Sect. 2.3.

Quantum mechanically the reduced partition function depends explicitly on the properties of the bath. The interaction with quantum harmonic oscillators introduces non-local interactions (along the Matsubara time direction) and there is no physical way to introduce a counter-term to correct for this feature.

The **dynamics of quantum systems** has all these diffilculties.

2.3 The Langevin equation

Examples of experimental and theoretical interest in condensed matter and biophysics in which quantum fluctuation can be totally neglected are manifold. In this context one usually concentrates on systems in contact with an environment: one selects some relevant degrees of freedom and treats the rest as a bath. It is a canonical view. Among these instances are colloidal suspensions which are particles suspended in a liquid, typically salted water, a 'soft condensed matter' example; spins in ferromagnets coupled to lattice phonons, a 'hard condensed matter' case; and proteins in the cell a 'biophysics' instance. These problems are modeled as stochastic processes with Langevin equations, the Kramers-Fokker-Planck formalism or master equations depending on the continuous or discrete character of the relevant variables and analytic convenience.

The Langevin equation is a stochastic differential equation that describes phenomenologically a large variety of problems. It models the time evolution of a set of slow variables coupled to a much larger set of fast variables that are usually (but not necessarily) assumed to be in thermal equilibrium at a given temperature. We first introduce it in the context of Brownian motion and we derive it in more generality in Sect. 2.3.2.

2.3.1 Langevin's Langevin equation

The Langevin equation[5] for a particle moving in one dimension in contact with a **white-noise** bath reads

$$\boxed{m\dot{v} + \gamma_0 v = F + \xi \,, \qquad v = \dot{x} \,,} \tag{2.9}$$

with x and v the particle's position and velocity. ξ is a Gaussian white noise with zero mean and correlation $\langle \xi(t)\xi(t')\rangle = 2\gamma_0 k_B T \delta(t-t')$ that mimics thermal agitation.

[5] P. Langevin, *Sur la théorie du mouvement brownien*, Comptes-Rendus de l'Académie des Sciences **146**, 530-532 (1908).

$\gamma_0 v$ is a friction force that opposes the motion of the particle. The force F designates all external deterministic forces and depends, in the most common cases, on the position of the particle x only. In cases in which the force derives from a potential, $F = -dV/dx$. The generalization to higher dimensions is straightforward. Note that γ_0 is the parameter that controls the strength of the coupling to the bath (it appears in the friction term as well as in the noise term). In the case $\gamma_0 = 0$ one recovers Newton equation of motion. The relation between the friction term and thermal correlation is non-trivial. Langevin fixed it by requiring $\langle v^2(t)\rangle \to \langle v^2\rangle_{eq}$. We shall give a different argument for it in the next section.

2.3.2 Derivation of the Langevin equation

Let us take a system in contact with an environment. The interacting system+environment ensemble is 'closed' while the system is 'open'. The nature of the environment, *e.g.* whether it can be modeled by a classical or a quantum formalism, depends on the problem under study. We focus here on the classical problem. A derivation of a generalized Langevin equation with memory is very simple starting from Newton dynamics of the full system [15, 18].

We shall then study the coupled system introduced in Sect. .

The generalization to more complex systems and/or to more complicated baths and higher dimensions is straightforward. The calculations can also be easily generalized to an interaction of the oscillator coordinate with a more complicated dependence on the system's coordinate, $\mathcal{V}(x)$, that may be dictated by the symmetries of the system, see Ex. 1.

Hamilton's equations for the particle are

$$\dot{x}(t) = \frac{p(t)}{m} , \qquad \dot{p}(t) = -V'[x(t)] - \sum_{a=1}^{N} c_a q_a(t) - \sum_{a=1}^{N} \frac{c_a^2}{m_a \omega_a^2} x(t) \tag{2.10}$$

(the counter-term yields the last term) while the dynamic equations for each member of the environment read

$$\dot{q}_a(t) = \frac{\pi_a(t)}{m_a} , \qquad \dot{\pi}_a(t) = -m_a \omega_a^2 q_a(t) - c_a x(t) , \tag{2.11}$$

showing that they are all massive harmonic oscillators **forced by the chosen particle**. These equations are readily solved by

$$q_a(t) = q_a(0)\cos(\omega_a t) + \frac{\pi_a(0)}{m_a \omega_a}\sin(\omega_a t) - \frac{c_a}{m_a \omega_a}\int_0^t dt' \sin[\omega_a (t-t')] x(t') \tag{2.12}$$

with $q_a(0)$ and $\pi_a(0)$ the initial coordinate and position at time $t = 0$ when the particle is set in contact with the bath. It is convenient to integrate by parts the last term. The replacement of the resulting expression in the last term in the RHS of eq. (2.10) yields

$$\boxed{\dot{p}(t) = -V'[x(t)] + \xi(t) - \int_0^t dt' \; \Gamma(t-t')\dot{x}(t') ,} \tag{2.13}$$

with the **symmetric and stationary kernel** Γ given by

$$\boxed{\Gamma(t-t') = \sum_{a=1}^{N} \frac{c_a^2}{m_a \omega_a^2} \cos[\omega_a (t-t')] \,,} \tag{2.14}$$

$\Gamma(t-t') = \Gamma(t'-t)$, and the **time-dependent force** ξ given by

$$\boxed{\xi(t) = -\sum_{a=1}^{N} c_a \left[\frac{\pi_a(0)}{m_a \omega_a} \sin(\omega_a t) + \left(q_a(0) + \frac{c_a x(0)}{m_a \omega_a^2} \right) \cos(\omega_a t) \right] \,.} \tag{2.15}$$

This is the equation of motion of the **reduced** system. It is still **deterministic**.

The third term on the RHS of eq. (2.13) represents a rather complicated **friction force**. Its value at time t depends explicitly on the history of the particle at times $0 \leq t' \leq t$ and makes the equation **non-Markovian**. One can rewrite it as an integral running up to a total time $\mathcal{T} > \max(t, t')$ introducing the **retarded friction**:

$$\boxed{\gamma(t-t') = \Gamma(t-t')\theta(t-t') \,.} \tag{2.16}$$

Until this point the dynamics of the system remain deterministic and are completely determined by its initial conditions as well as those of the reservoir variables. The **statistical element** comes into play when one realizes that it is impossible to know the initial configuration of the large number of oscillators with great precision and one proposes that the initial coordinates and momenta of the oscillators have a canonical distribution at an **inverse temperature** β. Then, one chooses $\{\pi_a(0), q_a(0)\}$ to be initially distributed according to a canonical phase space distribution:

$$\boxed{P(\{\pi_a(0), q_a(0)\}, x(0)) = 1/\tilde{\mathcal{Z}}_{\text{ENV}}[x(0)] \; e^{-\beta \tilde{H}_{\text{ENV}}[\{\pi_a(0), q_a(0)\}, x(0)]}} \tag{2.17}$$

with $\tilde{H}_{\text{ENV}} = H_{\text{ENV}} + H_{\text{INT}} + H_{\text{COUNTER}}$, that can be rewritten as

$$\tilde{H}_{\text{ENV}} = \sum_{a=1}^{N} \left[\frac{m_a \omega_a^2}{2} \left(q_a(0) + \frac{c_a}{m_a \omega_a^2} x(0) \right)^2 + \frac{\pi_a^2(0)}{2 m_a} \right] \,. \tag{2.18}$$

The randomness in the initial conditions gives rise to a random force acting on the reduced system. Indeed, ξ is now a **Gaussian random variable**, that is to say a noise, with

$$\langle \xi(t) \rangle = 0 \,, \qquad \langle \xi(t) \xi(t') \rangle = k_B T \, \Gamma(t-t') \,. \tag{2.19}$$

One can easily check that higher-order correlations vanish for an odd number of ξ factors and factorize as products of two time correlations for an even number of ξ factors. In consequence ξ has Gaussian statistics. Defining the inverse of Γ over the interval $[0, t]$, $\int_0^t dt'' \; \Gamma(t-t'')\Gamma^{-1}(t''-t') = \delta(t-t')$, one has the Gaussian pdf:

$$P[\xi] = \mathcal{Z}^{-1} e^{-\frac{1}{2k_B T} \int_0^t dt \int_0^t dt' \; \xi(t) \Gamma^{-1}(t-t') \xi(t')} \,. \tag{2.20}$$

$\mathcal{Z}$ is the normalization. A random force with non-vanishing correlations on a finite support is usually called a **coloured noise**. Equation (2.13) is now a genuine Langevin equation. A multiplicative retarded noise arises from a model in which one couples the coordinates of the oscillators to a generic function of the coordinates of the system, see Ex. 1 and eq. (2.27).

The use of an **equilibrium measure** for the oscillators implies the relation between the friction kernel and the noise-noise correlation, which are proportional, with a constant of proportionality of value $k_B T$. This is a generalized form of the **fluctuation-dissipation relation**, and it applies to the environment.

Different choices of the environment are possible by selecting different ensembles of harmonic oscillators. The simplest one, that leads to an approximate Markovian equation, is to consider that the oscillators are coupled to the particle via coupling constants $c_a = \tilde{c}_a/\sqrt{N}$ with $\tilde{c}_a$ of order one. One defines

$$\boxed{S(\omega) \equiv \frac{1}{N} \sum_{a=1}^{N} \frac{\tilde{c}_a^2}{m_a \omega_a} \, \delta(\omega - \omega_a)} \tag{2.21}$$

a function of ω, of order one with respect to N, and rewrites the kernel Γ as

$$\boxed{\Gamma(t-t') = \int_0^\infty d\omega \, \frac{S(\omega)}{\omega} \, \cos[\omega(t-t')] \; .} \tag{2.22}$$

A common choice is

$$\boxed{\frac{S(\omega)}{\omega} = 2\gamma_0 \left(\frac{|\omega|}{\tilde{\omega}}\right)^{\alpha-1} \, f_c\left(\frac{|\omega|}{\Lambda}\right) \; .} \tag{2.23}$$

The function $f_c(x)$ is a high-frequency cut-off of typical width Λ and is usually chosen to be an exponential. The frequency $\tilde{\omega} \ll \Lambda$ is a reference frequency that allows one to have a coupling strength γ_0 with the dimensions of viscosity. If $\alpha = 1$, the friction is said to be **Ohmic**, $S(\omega)/\omega$ is constant when $|\omega| \ll \Lambda$ as for a white noise. This name is motivated by the electric circuit analog exposed by the end of this Section. When $\alpha > 1$ ($\alpha < 1$) the bath is **superOhmic** (**subOhmic**). The exponent α is taken to be > 0 to avoid divergencies at low frequency. For the exponential cut-off the integral over ω yields

$$\Gamma(t) = 2\gamma_0 \tilde{\omega}^{-\alpha+1} \, \frac{\cos[\alpha \arctan(\Lambda t)]}{[1+(\Lambda t)^2]^{\alpha/2}} \, \Gamma\mathrm{a}(\alpha) \, \Lambda^\alpha \tag{2.24}$$

with $\Gamma\mathrm{a}(x)$ the Gamma-function, that in the Ohmic case $\alpha = 1$ reads

$$\Gamma(t) = 2\gamma_0 \, \frac{\Lambda}{[1+(\Lambda t)^2]} \; , \tag{2.25}$$

and in the $\Lambda \to \infty$ limit becomes a delta-function, $\Gamma(t) \to 2\gamma_0 \delta(t)$. At long times, for any $\alpha > 0$ and different from 1, one has

$$\lim_{\Lambda t \to \infty} \Gamma(t) \quad = \quad 2\gamma_0 \tilde{\omega}^{-\alpha+1} \, \cos(\alpha\pi/2) \Gamma\mathrm{a}(\alpha) \, \Lambda^{-1} \, t^{-\alpha-1} \; , \tag{2.26}$$

a **power law decay**.

Time-dependent, $f(t)$, and constant non-potential forces, $f^{\rm NP}$, as the ones applied to granular matter and in rheological measurements, respectively, are simply included in the right-hand-side (RHS) as part of the deterministic force. When the force derives from a potential, $F(x,t) = -dV/dx$.

In so far we have discussed systems with position and momentum degrees of freedom. Other variables might be of interest to describe the dynamics of different kind of systems. In particular, a continuous Langevin equation for classical spins can also be used if one replaces the hard Ising constraint, $s_i = \pm 1$, by a soft one implemented with a potential term of the form $V(s_i) = u(s_i^2 - 1)^2$ with u a coupling strength (that one eventually takes to infinity to recover a hard constraint). The soft spins are continuous unbounded variables, $s_i \in (-\infty, \infty)$, but the potential energy favors the configurations with s_i close to ± 1. Even simpler models are constructed with spherical spins, that are also continuous unbounded variables globally constrained to satisfy $\sum_{i=1}^{N} s_i^2 = N$. The extension to fields is straightforward and we shall discuss one when dealing with the $O(N)$ model.

Exercise 1. Prove that for a non-linear coupling $H_{\rm INT} = \mathcal{V}[x] \sum_{a=1}^{N} c_a q_a$ there is a choice of counter-term for which the Langevin equation reads

$$\dot{p}(t) = -V'[x(t)] + \xi(t)\mathcal{V}'[x(t)] - \mathcal{V}'[x(t)] \int_0^t dt' \; \Gamma(t-t')\mathcal{V}'[x(t')]\dot{x}(t') \qquad (2.27)$$

with the same Γ as in eq. (2.14) and $\xi(t)$ given by eq. (2.15) with $x(0) \to \mathcal{V}[x(0)]$. The noise appears now **multiplying** a function of the particles' coordinate.

Another derivation of the Langevin equation uses collision theory and admits a generalization to relativistic cases [19].

The electric analog: take an LRC circuit. The resistance is of the usual Ohmic type, that is to say, the potential drop, V_R, across it is given by $V_R = IR$ with I the current and R the resistance. The potential drop, v_L, across the inductor L is given by $V_L = LdI/dt$. Finally, the potential drop across the capacitor is $V_C = -C^{-1}\int Idt$. The balance between these potentials implies a Langevin type equation for the current circulating across the circuit:

$$L\frac{d^2I}{dt^2} + R\frac{dI}{dt} + C^{-1}I = 0 \; . \qquad (2.28)$$

This analogy justifies the Ohmic name given to a dissipative term proportional to the velocity in the general presentation.

2.3.3 Irreversibility and dissipation.

The friction force $-\gamma_0 v$ in eq. (2.9) – or its retarded extension in the non-Markovian case – explicitly breaks time-reversal ($t \to -t$) invariance, a property that has to be

respected by any set of microscopic dynamic equations. Newton equations describing the whole system, the particle and all the molecules of the fluid, are time reversal invariant. However, time-reversal can be broken in the **reduced** equation in which the fluid is treated in an effective statistical form and the fact that it is in equilibrium is assumed from the start.

Even in the case in which all forces derive from a potential, $F = -dV/dx$, the energy of the particle, $mv^2/2 + V$, is not conserved and, in general, flows to the bath leading to **dissipation**. At very long times, however, the particle may reach a stationary regime in which the particle gives and receives energy from the bath at equal rate, on average.

Exercise 2. Prove the time-irreversibility of the Langevin equation and the fact that the symmetry is restored if $\gamma_0 = 0$. Show that $d\langle H_{\rm SYST}\rangle/dt \neq 0$ when $\gamma_0 \neq 0$.

2.3.4 Discretization of stochastic differential equations

The way in which a stochastic differential equation with white noise is to be discretized is a subtle matter that we shall not discuss in these lectures, unless where it will be absolutely necessary. There are basically two schemes, called the Itô and Stratonovich calculus, that are well documented in the literature.

In short, we shall use a prescription in which the pair velocity-position of the particle at time $t + \delta$, with δ an infinitesimal time-step, depends on the pair velocity-position at time t and the value of the noise at time t.

2.3.5 Markov character

In the case of a white noise (delta correlated) the full set of equations defines a **Markov process**, that is a stochastic process that depends on its history only through its very last step.

2.3.6 Generation of memory

The Langevin equation (2.9) is actually a set of two first order differential equations. Notice, however, that the pair of first-order differential equations could also be described by a single second-order differential equation:

$$m\ddot{x} + \gamma_0 \dot{x} = F + \xi \; . \tag{2.29}$$

Having replaced the velocity by its definition in terms of the position $x(t)$ depends now on $x(t-\delta)$ and $x(t-2\delta)$. This is a very general feature: by integrating away some degrees of freedom (the velocity in this case) one generates memory in the evolution. Generalizations of the Langevin equation, such as the one that we have just presented with colored noise, and the ones that will be generated to describe the slow evolution of super-cooled liquids and glasses in terms of correlations and linear responses, do have memory.

2.3.7 Smoluchowski (overdamped) limit

In many situations in which friction is very large, the characteristic time for the relaxation of the velocity degrees of freedom to their Maxwellian distribution, t_r^v, is very short (see the examples in Sect. 2.3). In consequence, observation times are very soon longer than this time-scale, the inertia term $m\dot{v}$ can be dropped, and the Langevin equation becomes

$$\gamma_0 \dot{x} = F + \xi \tag{2.30}$$

(for simplicity we wrote the white-noise case). Indeed, this **overdamped** limit is acceptable whenever the observation times are much longer than the characteristic time for the velocity relaxation. Inversely, the cases in which the friction coefficient γ_0 is small are called **underdamped**.

In the overdamped limit with white-noise the friction coefficient γ_0 can be absorbed in a rescaling of time. One defines the new time τ

$$t = \gamma_0 \tau \tag{2.31}$$

the new position, $\tilde{x}(\tau) = x(\gamma_0 \tau)$, and the new noise $\eta(\tau) = \xi(\gamma_0 \tau)$. In the new variables the Langevin equation reads $\dot{\tilde{x}}(\tau) = F(\tilde{x}, \tau) + \eta(\tau)$ with $\langle \eta(\tau)\eta(\tau') \rangle = 2k_B T \delta(\tau - \tau')$.

2.4 The basic processes

We shall discuss the motion of the particle in some $1d$ representative potentials: under a constant force, in a harmonic potential, in the flat limit of these two (Fig. 18) and the escape from a metastable state and the motion in a double well potential (Fig. 21).

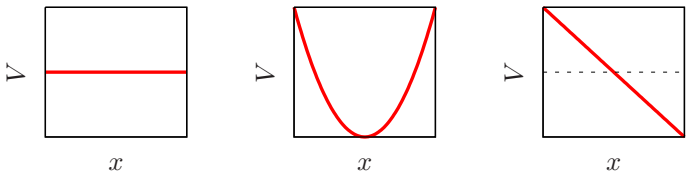

Figure 18: Three representative one-dimensional potentials.

2.4.1 A constant force

Let us first consider the case of a **constant force**, F. The first thing to notice is that the Maxwell-Boltzmann measure

$$P_{\rm GB}(v,x) \propto e^{-\beta\left(\frac{v^2}{2m}+V(x)\right)} \tag{2.32}$$

is not normalizable if the size of the line is infinite, due to the $\exp[-\beta V(x)] = \exp(\beta F x)$ term. Let us then study the evolution of the particle's velocity and position to show how these variables behave and the fact that they do very differently.

The problem to solve is a set of two coupled stochastic first order differential equations on $\{v(t), x(t)\}$, one needs two initial conditions v_0 and x_0.

The velocity

The time-dependent velocity follows from the integration of eq. (2.9) over time

$$v(t) = v_0\ e^{-\frac{\gamma_0}{m}t} + \frac{1}{m}\int_0^t dt'\ e^{-\frac{\gamma_0}{m}(t-t')}\ [\,F + \xi(t')\,]\,, \qquad\qquad v_0 \equiv v(t=0)\ .$$

The velocity is a **Gaussian variable** that inherits its average and correlations from the ones of ξ. Using the fact that the noise has zero average

$$\langle v(t)\rangle = v_0\ e^{-\frac{\gamma_0}{m}t} + \frac{F}{\gamma_0}\left(1 - e^{-\frac{\gamma_0}{m}t}\right)\ .$$

In the short time limit, $t \ll t_r^v = m/\gamma_0$, this expression approaches the Newtonian result ($\gamma_0 = 0$) in which the velocity grows linearly in time $v(t) = v_0 + F/m\ t$. In the opposite long time limit, $t \gg t_r^v = m/\gamma_0$, for all initial conditions v_0 the averaged velocity decays exponentially to the constant value F/γ_0. The saturation when the bath is active ($\gamma_0 \neq 0$) is due to the friction term. The **relaxation time** separating the two regimes is

$$\boxed{t_r^v = \tfrac{m}{\gamma_0}\ .} \tag{2.33}$$

The velocity mean-square displacement is

$$\sigma_v^2(t) \equiv \langle (v(t) - \langle v(t)\rangle)^2\rangle = \frac{k_B T}{m}\left(1 - e^{-2\frac{\gamma_0}{m}t}\right) \tag{2.34}$$

independently of F. This is an example of the **regression theorem** according to which the fluctuations decay in time following the same law as the average value. The short and long time limits yield

$$\sigma_v^2(t) \equiv \langle (v(t) - \langle v(t)\rangle)^2\rangle \simeq \frac{k_B T}{m}\begin{cases} \frac{2\gamma_0}{m}\ t & t \ll t_r^v \\ 1 & t \gg t_r^v \end{cases} \tag{2.35}$$

and the two expressions match at $t \simeq t_r^v/2$. The asymptotic limit is the result expected from equipartition of the velocity mean-square displacement, $\langle (v(t) - \langle v(t)\rangle)^2\rangle \to \langle (v(t) - \langle v\rangle_{\rm STAT})^2\rangle_{\rm STAT}$ that implies for the kinetic energy $\langle K\rangle_{\rm STAT} = k_B T/2$ (only if the

velocity is measured with respect to its average). In the heuristic derivation of the Langevin equation for $F = 0$ the amplitude of the noise-noise correlation, say A, is not fixed. The simplest way to determine this parameter is to require that equipartition for the kinetic energy holds $A/(\gamma_0 m) = T/m$ and hence $A = \gamma_0 T$. This relation is known under the name of **fluctuation–dissipation theorem** (FDT) **of the second kind** in Kubo's nomenclature. It is important to note that this FDT characterizes the surrounding fluid and not the particle, since it relates the noise-noise correlation to the friction coefficient. In the case of the Brownian particle this relation ensures that after a transient of the order of t_r^v, the bath maintains the fluctuations of the velocity, σ_v^2, constant and equal to its equilibrium value.

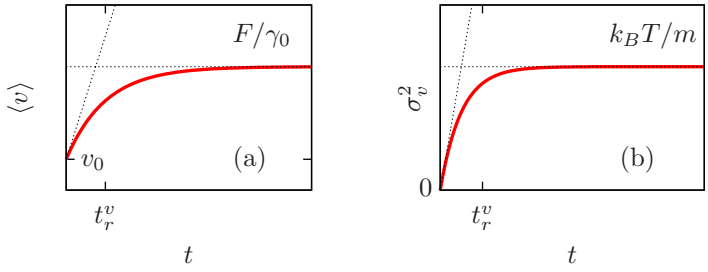

Figure 19: Results for the constant force problem. (a) Mean velocity as a function of time. (b) Velocity mean-square displacement as a function of time. In both cases the linear behavior at short times, $t \ll t_r^v$ and the saturation values are shown.

The velocity **two-time connected correlation** reads

$$\langle [v(t) - \langle v(t) \rangle][v(t') - \langle v(t') \rangle] \rangle = \frac{k_B T}{m} \left[e^{-\frac{\gamma_0}{m}|t-t'|} - e^{-\frac{\gamma_0}{m}(t+t')} \right] .$$

This is sometimes called the **Dirichlet correlator**. This and all other higher-order velocity correlation functions approach a **stationary limit** when the shortest time involved is longer than t_r^v. At $t = t'$ on recovers the mean-square displacement computed in eq. (2.34). When both times are short compared to t_r^v the two-time correlator behaves as $\sim 2k_B T\gamma_0/m^2 \ \max(t, t')$. When at least one of the two times is much longer than t_r^v the second term vanishes and one is left with an exponential decay as a function of time delay:

$$C_{vv}^c(t, t') \equiv \langle [v(t) - \langle v(t) \rangle][v(t') - \langle v(t') \rangle] \rangle \to \frac{k_B T}{m} e^{-\frac{\gamma_0}{m}|t-t'|} \qquad t, t' \gg t_r^v \ . \quad (2.36)$$

The two-time connected correlation falls off to, say, $1/e$ in a **decay time** $t_d^v = m/\gamma_0$. In this simple case $t_r^v = t_d^v$ but this does not happen in more complex cases.

More generally one can show that for times $t_1 \geq t_2 \geq \ldots \geq t_n \geq t_r^v$:

$$\boxed{\langle v(t_1+\Delta)\ldots v(t_n+\Delta)\rangle = \langle v(t_1)\ldots v(t_n)\rangle \quad \text{(TTI)}} \tag{2.37}$$

for all delays Δ. **Time-translation invariance (TTI)** or **stationarity** is one generic property of **equilibrium dynamics**. Another way of stating (2.37) is

$$\langle v(t_1)\ldots v(t_n)\rangle = f(t_1-t_2,\ldots,t_{n-1}-t_n)\ . \tag{2.38}$$

Another interesting object is the linear response of the averaged velocity to a small perturbation applied to the system in the form of $V \to V - fx$, i.e. a change in the slope of the potential in this particular case. One finds

$$R_{vx}(t,t') \equiv \left.\frac{\delta\langle v(t)\rangle_f}{\delta f(t')}\right|_{f=0} = \frac{1}{m}\ e^{-\frac{\gamma_0}{m}(t-t')}\ \theta(t-t') \tag{2.39}$$

$$\simeq \frac{1}{k_B T}\langle [v(t)-\langle v(t)\rangle][v(t')-\langle v(t')\rangle]\rangle\ \theta(t-t') \tag{2.40}$$

the last identity being valid in the limit t or $t' \gg t_r^v$. This is an FDT relation between a linear response, $R_{vx}(t,t')$, and a connected correlation, $C^c_{vv}(t,t')$, that holds for one of the particle variables, its velocity, when this one reaches the stationary state.

$$\boxed{k_B T\ R_{vx}(t,t') = C^c_{vv}(t,t')\ \theta(t-t') \qquad \text{(FDT)}\ .} \tag{2.41}$$

In conclusion, the velocity is a Gaussian variable that after a characteristic time t_r^v verifies 'equilibrium'-like properties: its average converges to a constant (determined by F), its multi-time correlation functions become stationary and a fluctuation-dissipation theorem links its linear response to the connected correlation at two times. More general FDT's are discussed in the exercise proposed below.

The position

The particle's position, $x(t) = x_0 + \int_0^t dt' v(t')$ is still a Gaussian random variable:

$$\begin{aligned} x(t) &= x_0 + v_0\ t_r^v + \frac{F}{\gamma_0}(t-t_r^v) + t_r^v\left(\frac{F}{\gamma_0} - v_0\right) e^{-\frac{\gamma_0}{m}t} \\ &\quad + \frac{1}{m}\int_0^t dt' \int_0^{t'} dt''\ e^{-\frac{\gamma_0}{m}(t'-t'')}\ \xi(t'')\ . \end{aligned} \tag{2.42}$$

Its noise-average behaves as the Newtonian result, **ballistic motion**, $\langle x(t)\rangle = x_0 + v_0 t + F/(2m)\ t^2$ at short times $t \ll t_r^v$ and it crossover to

$$\boxed{\langle x(t)\rangle \to x_0 + v_0\ t_r^v + \tfrac{F}{\gamma_0}(t-t_r^v)} \tag{2.43}$$

for $t \gg t_r^v$. Note the reduction with respect to ballistic motion ($x \propto Ft^2$) due to the friction drag and the fact that this one-time observable does not saturate to a constant.

The position mean-square displacement approaches

$$\boxed{\sigma_x^2(t) \equiv \langle (x(t) - \langle x(t) \rangle)^2 \rangle \to 2D_x t \quad \text{with} \quad D_x \equiv \frac{k_B T}{\gamma_0} \quad \text{(Diffusion)}} \tag{2.44}$$

in the usual $t \gg t_r^v$ limit, that is to say **normal diffusion** with the **diffusion constant** D_x. This expression can be computed using $x(t) - \langle x(t) \rangle$ as obtained from the $v(t) - \langle v(t) \rangle$ above (and it is quite a messy calculation) or one can simply go to the Smoluchowski limit, taking advantage of the knowledge of what we have just discussed on the behavior of velocities, and obtain diffusion in two lines. In contrast to the velocity mean-square displacement this quantity does not saturate at any finite value. Similarly, the particle displacement between two different times t and t' is

$$\Delta_{xx}(t, t') \equiv \langle [x(t) - x(t')]^2 \rangle \to 2D_x |t - t'| \, . \tag{2.45}$$

It is interesting to note that the force dictates the mean position but it does not modify the fluctuations about it (similarly to what it did to the velocity). Δ_{xx} is stationary for time lags longer than t_r^v.

The two-time position-position connected correlation reads

$$C_{xx}^c(t, t') = \langle (x(t) - \langle x(t) \rangle)(x(t') - \langle x(t') \rangle) \rangle = \dots \tag{2.46}$$

Exercise 3: compute it.

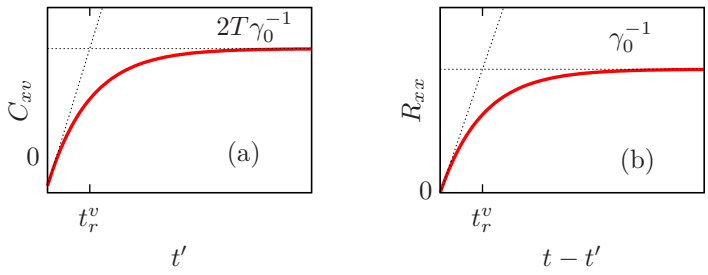

Figure 20: Results for the constant force problem. (a) The correlation between the position and the velocity of the particle measured at different times. (b) The linear response of the position to a kick applied linearly to itself at a previous time. In both cases the linear behavior at short times, $t \ll t_r^v$ and the saturation values are shown.

Another way to measure the diffusion coefficient directly from the velocity that is commonly used in the literature is

$$\boxed{D_x = \lim_{\tau \to \infty} \lim_{t' \to \infty} \int_0^\tau dt' \langle v(\tau + t') v(t') \rangle \, .} \tag{2.47}$$

One can check that it gives the same result.

The linear response of the particle's position to a kick linearly applied to itself at a previous time, in the form $V \to V - fx$ at $t' < t$, is

$$R_{xx}(t,t') \equiv \left.\frac{\delta\langle x(t)\rangle_f}{\delta f(t')}\right|_{f=0} = \frac{1}{\gamma_0}\left[1 - e^{-\frac{\gamma_0}{m}(t-t')}\right]\theta(t-t') \,, \tag{2.48}$$

with the limits

$$R_{xx}(t,t') \to \begin{cases} m^{-1}\,(t-t')\,\theta(t-t') & t-t' \ll t_r^v \,, \\ \gamma_0^{-1}\,\theta(t-t') & t-t' \gg t_r^v \,. \end{cases} \tag{2.49}$$

A simple calculation proves that in the short time-differences limit this is the results for Newton dynamics (**Exercise 4:** show it.)

The correlation between the position and the velocity reads

$$\begin{aligned} \langle (x(t) - \langle x(t)\rangle)(v(t') - \langle v(t')\rangle)\rangle &= \frac{2k_BT}{m}\left[\frac{m}{\gamma_0} - \left(1 + \frac{m}{\gamma_0}\right)e^{-\frac{\gamma_0}{m}t'}\right] \\ &\to \frac{2k_BT}{\gamma_0} \end{aligned} \tag{2.50}$$

and it is only a function of t'. One notices that in the asymptotic limit in which both sides of the equation saturate

$$\boxed{2k_BT\; R_{xx}(t,t') = C_{xv}^c(t,t') \quad \text{for } \; t-t' \gg t_r^v \;\text{ and }\; t' \gg t_r^v \,,} \tag{2.51}$$

with a factor of 2 different from the relation in eq. (2.41).

In conclusion, the position is also a Gaussian variable but it is explicitly out of equilibrium. Its average and variance grow linearly in time, the latter as in normal diffusion, and the fluctuation-dissipation relation has an additional factor of 1/2 (or 2, depending on on which side of the equality one writes it) with respect to the form expected in equilibrium.

The energy

The averaged potential energy diverges in the long-time limit since the potential is unbounded in the $x \to \infty$ limit: $\langle V(t)\rangle = -F\langle x(t)\rangle \simeq -F^2/\gamma_0 t$ for $t \gg t_r^v$.

Two kinds of variables

This example shows that even in this very simple problem the velocity and position variables have distinct behavior: the former is in a sense trivial, after the transient t_r^v and for longer times, all one-time functions of $v - F/\gamma_0$ saturate to their equilibrium-like and the correlations are stationary. Instead, the latter remains non-trivial and evolving out of equilibrium. One can loosely ascribe the different behavior to the fact that the velocity feels a confining potential $K = mv^2/2$ while the position feels an unbounded potential $V = -Fx$ in the case in which a force is applied, or a flat

potential $V = 0$ if F is switched off. In none of these cases the potential is able to take the particle to equilibrium with the bath. The particle slides on the slope and its excursions forward and backward from the mean get larger and larger as time increases.

Quite generally, the classical problems we are interested in are such that the friction coefficient γ_0 is large and the inertia term can be neglected, in other words, all times are much longer than the characteristic time t_r^v. We shall do it in the rest of the lectures.

Ergodicity

The ergodic hypothesis states that, in equilibrium, one can exchange ensemble averages by time averages and obtain the same results. Out of equilibrium this hypothesis is not expected to hold and one can already see how dangerous it is to take time-averages in these cases by focusing on the simple velocity variable. Ensemble and time averages coincide if the time-averaging is done over a time-window that lies after t_r^v but it does not if the integration time-interval goes below t_r^v.

Tests of equilibration have to be done very carefully in experiments and simulations. One can be simply mislead by, for instance, looking just at the velocities statistics.

A measure for the time dependent fluctuating position and velocity can be written down, taking advantage of the fact that both variables are Gaussian:

$$P(v,x) \propto \exp\left[-\frac{1}{2}\int dt \int dt' \; \delta y^t(t) A(t,t') \delta y(t')\right] \tag{2.52}$$

with the 2×2 matrix A being the inverse of the matrix of correlations, ${A^{-1}}_{ij}(t,t') = \langle \delta y_i(t) \delta y_j(t')\rangle$ with $i,j = 1,2$, $\delta y^t(t) = (\delta v(t)\ \delta x(t))$ and $\delta v(t) = v(t) - \langle v(t)\rangle$ (similarly for x). The correlations are given above so the dynamic pdf can be easily constructed. There will be elements in the matrix that remain time-dependent for all times.

Exercise 5. Confront

$$\langle v^m(t) x^n(t) x^k(t')\rangle \qquad \text{and} \qquad \langle v^m(t) x^n(t) k x^{k-1}(t') v(t')\rangle \; ; \tag{2.53}$$

conclude.

Effect of a colored bath: anomalous diffusion

The **anomalous diffusion** of a particle governed by the generalized Langevin equation, eq. (2.13), with colored noise characterized by power-law correlations, eq. (2.14), a problem also known as fractional Brownian motion, was studied in detail by N. Pottier [20]. The particle's velocity equilibrates with the environment although it does at a much slower rate than in the Ohmic case: its average and mean-square displacement decay as a power law - instead of exponentially - to their asymptotic values (still satisfying the regression theorem). The particle's mean square displacement is determined by the exponent of the noise-noise correlation, $\langle x^2(t)\rangle \simeq t^\alpha$, i.e. the dynamics is

subdiffusive for $\alpha < 1$, **diffusive** for $\alpha = 1$ and **superdiffusive** for $\alpha > 1$. A time-dependent diffusion coefficient verifies $D_x(t) \equiv 1/2\, d\langle x^2(t)\rangle/dt \propto t^{\alpha-1}$: it is finite and given by eq. (2.45) for normal diffusion, it diverges for superdiffusion and it vanishes for subdiffusion. The ratio between the linear response and the time-derivative of the correlation ratio reads $TR_{xx}(t,t')/\partial_{t'}C_{xx}(t,t') = D_x(t-t')/[D_x(t-t') + D_x(t')]$. It approaches $1/2$ for normal diffusion and the two-time dependent function $1/[1 + (t'/(t-t'))^{\alpha-1}]$ in other cases.

2.4.2 Relaxation in a quadratic potential

Another relevant example is the relaxation of a particle in a harmonic potential, with its minimum at $x^* \neq 0$:

$$V(x) = \frac{k}{2}(x - x^*)^2 \,, \tag{2.54}$$

in contact with a white noise. The potential confines the particle and one can then expect the coordinate to reach an equilibrium distribution.

This problem can be solved exactly keeping inertia for all values of γ_0 but the calculation is slightly tedious. The behavior of the particle velocity has already been clarified in the constant force case. We now focus on the overdamped limit,

$$\gamma_0 \dot{x} = -k(x - x^*) + \xi \,, \tag{2.55}$$

with k the spring constant of the harmonic well, that can be readily solved,

$$x(t) = x_0\, e^{-\frac{k}{\gamma_0}t} + \gamma_0^{-1} \int_0^t dt'\; e^{-\frac{k}{\gamma_0}(t-t')}\, [\xi(t') + kx^*] \,, \qquad x_0 = x(0) \,. \tag{2.56}$$

This problem become formally identical to the velocity dependence in the previous example.

Convergence of one-time quantities

The averaged position is

$$\boxed{\langle x(t) - x^* \rangle = (x_0 - x^*) e^{-\frac{k}{\gamma_0}t} \to 0 \qquad\qquad t_r^x \gg \gamma_0/k \quad \text{(Convergence)}} \tag{2.57}$$

Of course, one-time quantities should approach a constant asymptotically if the system equilibrates with its environment.

Two-time quantities

The two-time connected correlation (where one extracts, basically, the asymptotic position x^*) reads

$$\langle \delta x(t) \delta x(t') \rangle = k_B T\; k^{-1}\; e^{-\frac{k}{\gamma_0}(t+t')} \left[e^{2\frac{k}{\gamma_0}\min(t,t')} - 1 \right] \,. \tag{2.58}$$

Again, the **Dirichlet correlator** ($\delta x(t) = x(t) - \langle x(t)\rangle$). For at least one of the two times going well beyond the position relaxation time $t_r^x = \gamma_0/k$ the memory of the initial condition is lost and the connected correlation becomes **stationary**:

$$C_c(t,t') = \langle \delta x(t)\delta x(t')\rangle \to k_B T\ k^{-1}\ e^{-\frac{k}{\gamma_0}|t-t'|} \qquad \min(t,t') \gg t_r^x\ . \tag{2.59}$$

For time-differences that are longer than $t_d^x = \gamma_0/k$ the correlation decays to $1/e$ and one finds $t_d^x = t_r^x$. Interestingly enough, the relaxation and decay times diverge when $k \to 0$ and the potential becomes flat.

Note that when the time-difference $t - t'$ diverges the average of the product factorizes, in particular, for the correlation one gets

$$\langle x(t)x(t')\rangle \to \langle x(t)\rangle\langle x(t')\rangle \to x^*\langle x(t')\rangle \tag{2.60}$$

for any t', even finite. We shall see this factorization property at work later in more complicated cases.

Fluctuation-dissipation theorem (FDT)

One can also compute the linear response to an infinitesimal perturbation that couples linearly to the position changing the energy of the system as $H \to H - fx$ at a given time t':

$$R(t,t') = \left.\frac{\delta\langle x(t)\rangle_f}{\delta f(t')}\right|_{f=0}\ . \tag{2.61}$$

The explicit calculation yields

$$\begin{aligned} &R(t,t') = \gamma_0^{-1}\ e^{-k\gamma_0^{-1}(t-t')}\ \theta(t-t') \\ &\boxed{R(t,t') = \tfrac{1}{k_B T}\ \tfrac{\partial C_c(t,t')}{\partial t'}\ \theta(t-t') \quad \text{(FDT)}} \end{aligned} \tag{2.62}$$

The last equality holds for times that are longer than t_r^x. It expresses the **fluctuation-dissipation theorem (FDT)**, a model-independent relation between the two-time linear response and correlation function. Similar - though more complicated - relations for higher-order responses and correlations also exist in equilibrium. There are many ways to prove the FDT for stochastic processes. We shall discuss one of them in Sect. 2.3.2 that is especially interesting since it applies easily to problems with correlated noise.

It is instructive to examine the relation between the linear response and the correlation function in the limit of a flat potential ($k \to 0$). The linear response is just $\gamma_0^{-1}\theta(t-t')$. The Dirichlet correlator approaches the diffusive limit:

$$\langle \delta x(t)\delta x(t')\rangle = 2\gamma_0^{-1}k_B T\ \min(t,t') \qquad \text{for} \qquad k \to 0 \tag{2.63}$$

and its derivative reads $\partial_{t'}\langle \delta x(t)\delta x(t')\rangle = 2\gamma_0^{-1}k_B T\ \theta(t-t')$. Thus,

$$\begin{aligned} &R(t,t') = \frac{1}{2k_B T}\ \partial_{t'}\langle \delta x(t)\delta x(t')\rangle\ \theta(t-t') \\ &\boxed{R(t,t') = \tfrac{1}{2k_B T}\ \partial_{t'}C_c(t,t')\ \theta(t-t') \quad \text{(FDR for diffusion)}} \end{aligned} \tag{2.64}$$

A factor 1/2 is now present in the relation between R and C_c. It is another signature of the fact that the coordinate is not in equilibrium with the environment in the absence of a confining potential.

Exercise 6. Evaluate the two members of the FDT, eq. (2.62), in the case of the tilted potential $V(x) = -Fx$.

Reciprocity or Onsager relations

Let us compare the two correlations $\langle x^3(t)x(t')\rangle$ and $\langle x^3(t')x(t)\rangle$ within the harmonic example. One finds $\langle x^3(t)x(t')\rangle =$
$3\langle x^2(t)\rangle\langle x(t)x(t')\rangle$ and $\langle x^3(t')x(t)\rangle = 3\langle x^2(t')\rangle\langle x(t')x(t)\rangle$. Given that $\langle x^2(t)\rangle = \langle x^2(t')\rangle \to \langle x^2\rangle_{eq}$ and the fact that the two-time self-correlation is symmetric,

$$\langle x^3(t)x(t')\rangle = \langle x^3(t')x(t)\rangle \ . \tag{2.65}$$

With a similar argument one shows that for any functions A and B of x:

$$\begin{aligned} &\langle A(t)B(t')\rangle = \langle A(t')B(t)\rangle \\ &\boxed{C_{AB}(t,t') = C_{AB}(t',t) \quad \text{(Reciprocity)}} \end{aligned} \tag{2.66}$$

This equation is known as **Onsager relation** and applies to A and B that are even under time-reversal (e.g. they depend on the coordinates but not on the velocities or they have an even number of verlocities).

All these results remain unaltered if one adds a linear potential $-Fx$ and works with connected correlation functions.

2.4.3 Thermally activated processes

The phenomenological **Arrhenius law**[6] yields the typical time needed to escape from a potential well as an exponential of the ratio between the height of the barrier and the thermal energy scale k_BT, (with prefactors that can be calculated explicitly, see below). This exponential is of crucial importance for understanding slow (glassy) phenomena, since a mere barrier of $30k_BT$ is enough to transform a microscopic time of 10^{-12}s into a macroscopic time scale. See Fig. 21-right for a numerical study of the Coulomb glass that demonstrates the existence of an Arrhenius time-scale in this problem. In the glassy literature such systems are called **strong** glass formers as opposed to **weak** ones in which the characteristic time-scale depends on temperature in a different way.

In 1940 Kramers estimated the **escape rate** from a potential well as the one shown in Fig. 21-center due to thermal fluctuations that give sufficient energy to the particle to allow it to surpass the barrier[7]. After this seminal paper this problem has

[6] S. A. Arrhenius, *On the reaction velocity of the inversion of cane sugar by acids*, Zeitschrift für Physikalische Chemie **4**, 226 (1889).

[7] H. A. Kramers, *Brownian motion in a field of force and the diffusion model of chemical reactions*, Physica **7**, 284 (1940).

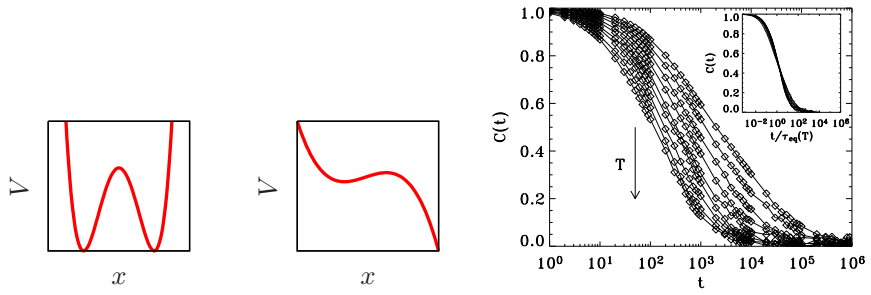

Figure 21: Left: sketch of a double-well potential. Center: sketch of a potential with a local minimum. Right: correlation function decay in a classical model of the $3d$ Coulomb glass at nine temperatures ranging from $T = 0.1$ to $T = 0.05$ in steps of 0.05 and all above T_g. In the inset the scaling plot $C(t) \sim f(t/t_A)$ with a characteristic time-scale, t_A, that follows the Arrhenius activated law, $t_A \simeq 0.45/T$. Figure due to Kolton, Domínguez and Grempel [21].

been studied in great detail [19] given that it is of paramount importance in many areas of physics and chemistry. An example is the problem of the dissociation of a molecule where x represents an effective one-dimensional **reaction coordinate** and the potential energy barrier is, actually, a **free-energy barrier**.

Kramers assumed that the reaction coordinate is coupled to an equilibrated environment with no memory and used the probability formalism in which the particle motion is described in terms of the time-dependent probability density $P(x, v, t)$ (that for such a stochastic process follows the Kramers partial differential equation).

If the thermal energy is at least of the order of the barrier height, $k_B T \sim \Delta V$, the reaction coordinate, x, moves freely from the vicinity of one well to the vicinity of the other.

The treatment we discuss applies to the opposite weak noise limit in which the thermal energy is much smaller than the barrier height, $k_B T \ll \Delta V$, the random force acts as a small perturbation, and the particle current over the top of the barrier is very small. Most of the time x relaxes towards the minimum of the potential well where it is located. Eventually, the random force drives it over the barrier and it escapes to infinity if the potential has the form in Fig. 21-center, or it remains in the neighbourhood of the second well, see Fig. 21-left.

The treatment is simplified if a constant current can be imposed by injecting particles within the metastable well and removing them somewhere to the right of it. In these conditions Kramers proposed a very crude approximation whereby P takes the stationary canonical form

$$P_{\rm ST}(x, v) = \mathcal{N} e^{-\beta \frac{v^2}{2} - \beta V(x)} \ . \tag{2.67}$$

If there is a sink to the right of the maximum, the normalization constant $\mathcal{N}$ is fixed by further assuming that $P_{\rm ST}(x,v) \sim 0$ for $x \geq \tilde{x} > x_{\rm MAX}$. The resulting integral over the coordinate can be computed with a saddle-point approximation justified in the large β limit. After expanding the potential about the minimum and keeping the quadratic fluctuations one finds

$$\mathcal{N}^{-1} = \frac{2\pi}{\beta\sqrt{V''(x_{\rm MIN})}}\, e^{-\beta V(x_{\rm MIN})} \ .$$

The escape rate, r, over the top of the barrier can now be readily computed by calculating the outward flow across the top of the barrier:

$$r \equiv \frac{1}{t_A} \equiv \int_0^\infty dv\ vP(x_{\rm MAX},v) = \frac{\sqrt{V''(x_{\rm MIN})}}{2\pi}\, e^{-\beta(V(x_{\rm MAX})-V(x_{\rm MIN}))} \ . \tag{2.68}$$

Note that we here assumed that no particle comes back from the right of the barrier. This assumption is justified if the potential quickly decreases on the right side of the barrier.

The crudeness of the approximation (2.67) can be grasped by noting that the equilibrium form is justified only near the bottom of the well. Kramers estimated an improved $P_{\rm ST}(x,v)$ that leads to

$$r = \frac{\left(\frac{\gamma^2}{4} + V''(x_{\rm MAX})\right)^{1/2} - \frac{\gamma}{2}}{\sqrt{V''(x_{\rm MAX})}}\ \frac{\sqrt{V''(x_{\rm MIN})}}{2\pi}\, e^{-\beta(V(x_{\rm MAX})-V(x_{\rm MIN}))} \ . \tag{2.69}$$

This expression approaches (2.68) when $\gamma \ll V''(x_{\rm MAX})$, *i.e.* close to the underdamped limit, and

$$r = \frac{\sqrt{V''(x_{\rm MAX})V''(x_{\rm MIN})}}{2\pi\gamma}\, e^{-\beta(V(x_{\rm MAX})-V(x_{\rm MIN}))} \tag{2.70}$$

when $\gamma \gg V''(x_{\rm MAX})$, *i.e.* in the overdamped limit (see Sect. 2.3.7 for the definition of these limits).

The inverse of (2.69), t_A, is called the **Arrhenius time** needed for **thermal activation** over a barrier $\Delta V \equiv V(x_{\rm MAX}) - V(x_{\rm MIN})$. The prefactor that characterises the well and barrier in the harmonic approximation is the **attempt frequency** with which the particles tend to jump over the barrier. In short,

$$\boxed{t_A \simeq \tau\ e^{\beta|\Delta V|} \qquad \text{(Arrhenius time)}} \tag{2.71}$$

The one-dimensional reaction coordinate can be more or less easily identified in problems such as the dissociation of a molecule. In contrast, such a single variable is much harder to visualize in an interacting problem with many degrees of freedom. The Kramers problem in higher dimensions is highly non-trivial and, in the infinite-dimensional **phase-space**, is completely out of reach.

The Arrhenius time can be derived within the path-integral formalism that we will discuss later [23, 22].

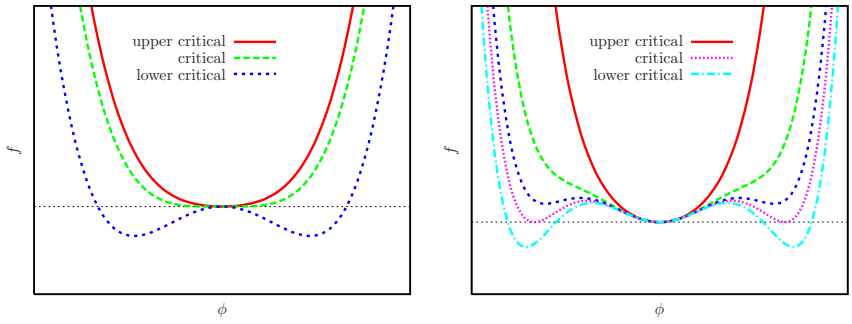

Figure 22: Left: second-order phase transition. Right: first order phase transition.

3 Dynamics at or through a phase transition

Take a piece of material in contact with an external reservoir. The material will be characterized by certain observables, energy density, magnetization density, *etc.* The external environment will be characterized by some parameters, like the temperature, magnetic field, pressure, *etc.* In principle, one is able to tune the latter and study the variation of the former. Note that we are using a **canonical setting** in the sense that the system under study is not isolated but open.

Sharp changes in the behavior of macroscopic systems at critical points (or lines) in parameter space have been observed experimentally. These correspond to **equilibrium phase transitions**, a non-trivial collective phenomenon appearing in the thermodynamic limit. We shall assume that the main features of, and analytic approaches used to study, phase transitions are known.

Imagine now that one changes an external parameter instantaneously or with a finite rate going from one phase to another in the (equilibrium) phase diagram. The kind of internal system interactions are not changed. In the statistical physics language the first kind of procedure is called a **quench** and the second one an **annealing** and these terms belong to the metalurgy terminology. We shall investigate how the system evolves by trying to accomodate to the new conditions and equilibrate with its environment. We shall first focus on the dynamics at the critical point or going through phase transitions between well-known phases (in the sense that one knows the order parameter, the structure, and all thermodynamic properties on both sides of the transition). Later we shall comment on cases in which one does not know all characteristics of one of the phases and sometimes one does not even know whether

there is a phase transition.

The evolution of the **free-energy landscape** (as a function of an order parameter) with the control parameter driving a phase transition is a guideline to grasp the dynamics following a quench or annealing from, typically, a disordered phase to the phase transition or into the ordered phase. See Fig. 22 for a sketch. We shall discuss quenches to the phase transition and below it. In the former case, the system can get to a critical point (Fig. 22-left) in which the free-energy is metastable in the sense that its second derivative vanishes (second order phase transition cases) or to a first-order phase transition (Fig. 22-right) in which various minima are degenerate. In the latter case the initial state becomes **unstable**, that is to say a maximum, and the phase transition is of second-order (see Fig. 22-left) or **metastable**, that is to say a local minimum, and the phase transition is of first order (see Fig. 22-right) in the final externally imposed conditions.[8] In the former case the **ordering process** occurs **throughout the material**, and not just at **nucleation sites**. Two typical examples are spinodal decomposition, *i.e.* the method whereby a mixture of two or more materials can separate into distinct regions with different material concentrations, or magnetic domain growth in ferromagnetic materials. Instead, in the latter case, the stable phase conquers the system through the **nucleation of a critical localized bubble** via thermal activation and its further growth.

Having described the dependence of the free-energy landscape on the external parameters we now need to choose the microscopic dynamics of the order parameter. Typically, one distinguishes two classes: one in which the order parameter is locally conserved and another one in which it is not. **Conserved** order parameter dynamics are found for example in phase separation in magnetic alloys or inmiscible liquids. Ferromagnetic domain growth is an exemple of the **non-conserved** case.

3.1 Time-dependent Ginzburg-Landau description

The kinetics of systems undergoing critical dynamics or an ordering process is an important problem for material science but also for our generic understanding of pattern formation in non-equilibrium systems. The late stage dynamics is believed to be governed by a few properties of the systems whereas material details should be irrelevant. Among these relevant properties one may expect to find the number of degenerate ground states, the nature of the conservation laws and the hardness or softness of the domain walls that is intimately related to the dimension of the order parameter. Thus, classes akin to the universality ones of critical phenomena have been identified. These systems constitute a first example of a problem with **slow dynamics**. Whether all systems with slow dynamics, in particular structural and spin glasses, undergo some kind of simple though slow domain growth is an open question.

Take a magnetic system, such as the ubiquitous Ising model with ferromagnetic uniform interactions, and quench it to its Curie point or into the low temperature

[8] Strictly speaking metastable states with infinite life-time exist only in the mean-field limit.

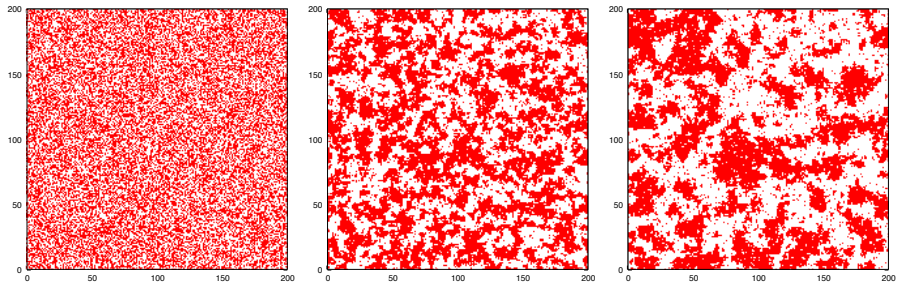

Figure 23: Monte Carlo simulations of a $2d$ Ising model. Three snapshots at $t = 1,\ 3 \times 10^5,\ 3 \times 10^6$ MCs after a quench to T_c.

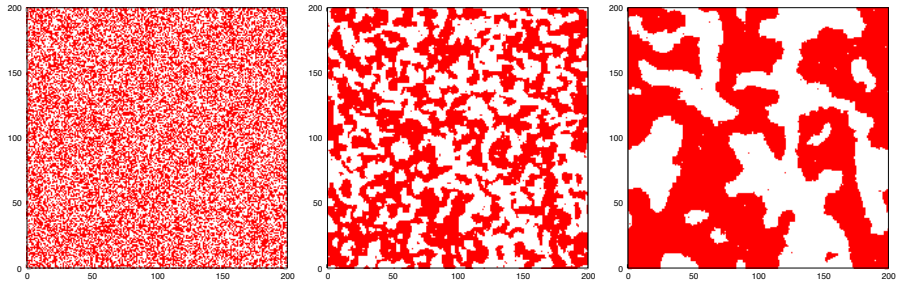

Figure 24: Monte Carlo simulations of a $2d$ Ising model. Three snapshots at $t = 1,\ 3 \times 10^5,\ 3 \times 10^6$ MCs after a quench to $0.5\ T_c$. Thermal fluctuations within the domains are visible.

phase starting from a random initial condition. Classically, the spins do not have an intrinsic dynamics; it is defined via a stochastic rule of Glauber, Metropolis or similar type with or without locally conserved magnetization. For the purpose of the following discussion it is sufficient to focus on non-conserved local microscopic dynamics. Three snapshots taken after times 1, 3×10^5 and 3×10^6 MCs in a critical and two sub-critical quenches are shown in Figs. 23, 24, and 25.

Time-dependent macroscopic observables are then expressed in terms of the values of the spins at each time-step. For instance, the magnetization density and its two-time self correlation function are defined as

$$m(t) \equiv N^{-1} \sum_{i=1}^{N} \langle\, s_i(t) \,\rangle \ , \qquad C(t,t') \equiv N^{-1} \sum_{i=1}^{N} \langle\, s_i(t) s_i(t') \,\rangle \ , \tag{3.1}$$

where the angular brackets indicate an average over many independent runs (i.e. random numbers) starting from identical initial conditions and/or averages over different

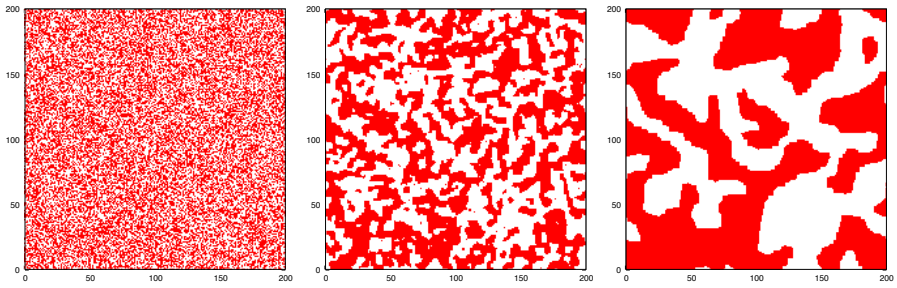

Figure 25: Monte Carlo simulations. Three snapshots at $t = 1,\ 3 \times 10^5, 3 \times 10^6$ MCs after a quench to 0.01 T_c. There is almost perfect order within the domains ($m_{eq} \simeq 1$).

initial configurations.

In **critical quenches**, patches with equilibrium critical fluctuations grow in time but their linear extent never reaches the equilibrium correlation length that diverges. Clusters of neighbouring spins pointing the same direction of many sizes are visible in the figures and the structure is quite intricate with clusters within clusters and so on and so forth. The interfaces look pretty rough too.

In **quenches into the ordered phase through a second order phase transition** the ferromagnetic interactions tend to align the neighbouring spins in parallel direction and in the course of time domains of the two ordered phases form and grow, see Fig. 26. At any finite time the configuration is such that both types of domains exist. If one examines the configurations in more detail one reckons that there are some spins reversed within the domains. These 'errors' are due to thermal fluctuations and are responsible of the fact that the magnetization of a given configuration within the domains is smaller than one and close to the equilibrium value at the working temperature (apart from fluctuations due to the finite size of the domains). The total magnetization, computed over the full system, is zero (up to fluctuating time-dependent corrections that scale with the square root of the inverse system size). The thermal averaged spin, $\langle s_i(t) \rangle$ vanishes for all i and all finite t, see below for a more detailed discussion of the time-dependence. As time passes the typical size of the domains increases and the interfaces get flatter in a way that we shall also discuss below.

Quenches across first order phase transitions will be discussed separately below.

In order to treat phase-transitions and the coarsening process analytically it is preferable to introduce a coarse-grained description in terms of a continuous coarse-grained field,

$$\phi(\vec{x}, t) \equiv \frac{1}{V} \sum_{i \in V_{\vec{x}}} s_i(t) \ , \tag{3.2}$$

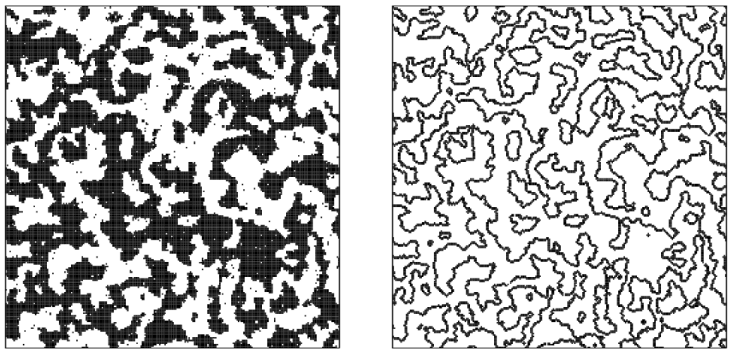

Figure 26: Snapshot of the $2d$ Ising model at a number of Monte Carlo steps after a quench from infinite to a subcritical temperature. Left: the up and down spins on the square lattice are represented with black and white sites. Right: the domain walls are shown in black.

the fluctuating magnetization density. In a first approximation a Landau-Ginzburg free-energy functional is introduced

$$F[\phi] = \int d^d x \, \left\{ \frac{c}{2} \left[\nabla \phi(\vec{x}, t) \right]^2 + V[\phi(\vec{x}, t)] \right\} \, . \tag{3.3}$$

With the choice of the potential one distinguishes between a second order and a first order phase transition. In the former case, the typical form is the ϕ^4 form:

$$V(\phi) = a\phi^4 + b(g)\phi^2 \, . \tag{3.4}$$

The first term in eq. (3.3) represents the energy cost to create a domain wall or the elasticity of an interface. The second term depends on a parameter, g, and changes sign from positive at $g > g_c$ to negative at $g < g_c$. Above the critical point determined by $b(g_c) = 0$ it has a single minimum at $\phi = 0$, at g_c it is flat at $\phi = 0$ and below g_c it has a double well structure with two minima, $\phi = \pm[-b(g)/(2a)]^{1/2} = \langle \phi \rangle_{eq}(g)$, that correspond to the equilibrium states in the ordered phase. Equation (3.3) is exact for a fully connected Ising model where $V(\phi)$ arises from the multiplicity of spin configurations that contribute to the same $\phi(\vec{x}) = m$. The order-parameter dependent free-energy density reads $f(m) = -Jm^2 - hm + k_B T\{(1+m)/2 \ln[(1+m)/2] + (1-m)/2 \ln[(1-m)/2]$ that close to the critical point where $m \simeq 0$ becomes $f(m) \simeq (k_B T - 2J)/2 \; m^2 - hm + k_B T/12 \; m^4$ demonstrating the passage from a harmonic form at $k_B T > k_B T_c = 2J$, to a quartic well at $T = T_c$, and finally to a double-well structure at $T < T_c$.

Exercise. Prove the above.

With a six-order potential one can mimic the situation in the right panel of Fig. 22.

When discussing dynamics one should write down the stochastic evolution of the individual spins and compute time-dependent averaged quantities as the ones in (3.1). This is the procedure used in numerical simulations. Analytically it is more convenient to work with a field-theory and an evolution equation of Langevin-type. This is the motivation for the introduction of continuous field equations that regulate the time-evolution of the coarse-grained order parameter. Ideally these equations should be derived from the spin stochastic dynamics but in practice they are introduced phenomenologically. In the magnetic case as well as in many cases of interest, the domain wall and interface dynamics can be argued to be **overdamped** (i.e. $t \gg t_r^{\dot{\phi}}$).

Two very similar approaches are used. Assuming T is only relevant to determine the equilibrium coarse-grained field one uses the phenomenological **zero-temperature time-dependent Ginzburg-Landau** equation or **model A** in the classification of Hohenberg-Halperin deterministic equation

$$\frac{\partial \phi(\vec{x},t)}{\partial t} = -\frac{\delta F[\phi]}{\delta \phi(\vec{x},t)} \tag{3.5}$$

(the friction coefficient has been absorbed in a redefinition of time). Initial conditions are usually chosen to be random with short-range correlations

$$[\,\phi(\vec{x},0)\phi(\vec{x}',0)\,]_{ic} = \Delta\delta(\vec{x}-\vec{x}') \tag{3.6}$$

thus mimicking the high-temperature configuration ($[\ldots]_{ic}$ represent the average over its probability distribution). The numeric solution to this equation with the quartic potential and $b < 0$ shows that such a random initial condition evolves into a field configuration with patches of ordered region in which the field takes one of the two values $[-b/(2a)]^{1/2}$ separated by sharp walls. It ignores temperature fluctuations within the domains meaning that the field is fully saturated within the domains and, consequently, one has access to the aging part of the correlations only, see *e.g.* eq. (3.23). The phase transition is controlled by the parameter b in the potential.

Another, similar approach, is to add a thermal noise to the former

$$\frac{\partial \phi(\vec{x},t)}{\partial t} = -\frac{\delta F[\phi]}{\delta \phi(\vec{x},t)} + \xi(\vec{x},t)\ . \tag{3.7}$$

This is the field-theoretical extension of the Langevin equation in which the potential is replaced by the order-parameter-dependent funcitonal free-energy in eq. (3.3) with a potential form with fixed parameters (independent of T). ξ is a noise taken to be Gaussian distributed with zero mean and correlations

$$\langle \xi(\vec{x},t)\xi(\vec{x}',t')\rangle = 2k_B T\delta^d(\vec{x}-\vec{x}')\delta(t-t')\ . \tag{3.8}$$

The friction coefficient has been absorbed in a redefinition of time. For a quartic potential a dynamic phase transition arises at a critical T_c; above T_c the system freely

moves above the two minima and basically ignores the double well structure while below T_c this is important. Within the growing domains the field ϕ fluctuates about its mean also given by $[-b/(2a)]^{1/2}$ and the fluctuations are determined by T. One can describe the rapid relaxation at ties such that the domain walls do not move with this approach. This formulation is better suited to treat critical and sub-critical dynamics in the same field-theoretical framework.

These equations do not conserve the order parameter neither locally nor globally. Extensions for cases in which it is conserved exist (model B). Cases with vectorial or even tensorial order parameters can be treated similarly and are also of experimental relevance, notably for vectorial magnets or liquid crystals.

3.2 Relaxation and equilibration time

We wish to distinguish the **relaxation time**, t_r, defined as the time needed for a given initial condition to reach equilibrium in one of the (possibly many equivalent) phases, from the **decorrelation time**, t_d, defined as the time needed for a given configuration to decorrelate from itself. To lighten the notation we do not signal out the variable that we use to study these typical times (as we did with the velocity and position in the examples of Sect. 2.4). We further define the **reversal time**, t_R, as the time needed to go from one to another of the equivalent equilibrium phases. We focus on second-order phase transitions here.

3.2.1 Quench from $T \gg T_c$ to $T > T_c$

If one quenches the system to $T > T_c$ the relaxation time, t_r, needed to reach configurations sampled by the Boltzmann measure depends on the system's parameters but not on its size. Hence it is finite even for an infinite-size system. Once a short transient overcome, the average of a local spin approaches the limit given by the Boltzmann measure, $\langle s_i(t)\rangle \to \langle s_i\rangle_{eq} = m = 0$, for all i and all other more complex observables satisfy equilibrium laws. The relaxation time is estimated to behave as $|T-T_c|^{-\nu z_{eq}}$ close to T_c, with ν the critical exponent characterizing the divergence of the equilibrium correlation length, $\xi \sim (T-T_c)^{-\nu}$, and z_{eq} the equilibrium exponent that links times and lengths, $\xi \sim t^{1/z_{eq}}$.

The relaxation of the two-time self-correlation at $T > T_c$, when the time t' is chosen to be longer than t_r, decays exponentially

$$\lim_{t' \gg t_r} \langle s_i(t) s_i(t')\rangle \simeq e^{-(t-t')/t_d} \tag{3.9}$$

with a decorrelation time that increases with decreasing temperature and close to (but still above) T_c diverges as the power law, $t_d \sim (T-T_c)^{-\nu z_{eq}}$. The divergence of t_d is the manifestation of **critical slowing down**. The asympotic value verifies

$$\lim_{t-t' \gg t' \gg t_r} \langle s_i(t) s_i(t')\rangle = \lim_{t \gg t_r} \langle s_i(t)\rangle \lim_{t' \gg t_r} \langle s_i(t')\rangle = \langle s_i\rangle_{eq} \langle s_i\rangle_{eq} = m^2 = 0 \,, \tag{3.10}$$

cfr. eq. (2.60).

3.2.2 Quench from $T \gg T_c$ to $T \leq T_c$

At or below T_c, coarsening from an initial condition that is **not correlated with the equilibrium state** and with no bias field does not take the system to equilibrium in finite times with respect to a function of the system's linear size, L. More explicitly, if the growth law is a power law [see eq. (3.31)] one needs times of the order of $L^{z_{eq}}$ (critical) or L^{z_d} (subcrititcal) to grow a domain of the size of the system. This gives a rough idea of the time needed to take the system to one of the two equilibrium states. For any shorter time, domains of the two types exist and the system is **out of equilibrium**.

The self-correlation of such an initial state evolving at $T \leq T_c$ involves power laws or logarithms and although one cannot associate to it a decay time as one does to an exponential, one can still define a characteristic time that, quite generally, turns out to be related to the age of the system, $t_d \simeq t_w$ [see eq. (3.29)].

In contrast, the relaxation time of an **equilibrium** magnetized configuration at temperature T vanishes since the system is already equilibrated while the decorrelation time t_d is a finite function of T.

The relaxation of the two-time self-correlation at $T < T_c$, when the time t' is chosen to be longer than t_r, that is to say, once the system has thermalized in one of the two equilibrium states, decays exponentially

$$\langle s_i(t) s_i(t') \rangle \simeq e^{-(t-t')/t_d} \tag{3.11}$$

with a decorrelation time that decreases with decreasing temperature and close to T_c (but below it) also diverges as a power law, $t_d \sim (T - T_c)^{-\nu z_{eq}}$. The asympotic value verifies

$$\lim_{t-t' \gg t' \gg t_r} \langle s_i(t) s_i(t') \rangle = \lim_{t \gg t_r} \langle s_i(t) \rangle \lim_{t' \gg t_r} \langle s_i(t') \rangle = \langle s_i \rangle_{eq} \langle s_i \rangle_{eq} = m^2 \geq 0 \ , \tag{3.12}$$

cfr. eqs. (2.60) and (3.10), depending on $T = T_c$ or $T > T_c$.

3.2.3 Summary

The lesson to learn from this comparison is that the relaxation time and the decorrelation time not only depend upon the working temperature but they also depend upon the initial condition. Moreover, in all critical or low-temperature cases we shall study the relaxation time depends on (L, T) – and diverges in the infinite size limit – while the decorrelation time depends on (T, t_w). For a random initial condition and an infinite system one has

$$t_r^{\phi} \simeq \begin{cases} \text{finite} & T > T_c \ , \\ |T - T_c|^{-\nu z_{eq}} & T \gtrsim T_c \ , \\ \infty & T \leq T_c \end{cases}$$

while for a finite system

$$t_r^\phi \simeq \begin{cases} L^{z_{eq}} & T = T_c \ , \\ L^{z_d} & T < T_c \ . \end{cases}$$

Still another time scale is given by the time needed to reverse an equilibrium configuration in the low-T phase. This one is expected to be given by an Arrhenius law, with the height of the barrier being determined by the extensive free-energy barrier between the two minima, i.e. $\Delta F \simeq L^d f$, therefore,

$$\boxed{t_R^\phi \simeq e^{\beta L^d f} \qquad \text{Reversal time-scale .}} \tag{3.13}$$

The Ginzburg-Landau description allows for a pictorial interpretation of these results. The dynamics of the full system is visualized as the motion of its representative point in the Ginzburg-Landau potential. At high T the potential is harmonic in the deterministic Allen-Cahn equation, or the double-well structure in the time-dependent stochastic Ginzburg-Landau equation is completely ignored. The relaxation is similar to the one of a particle in a harmonic potential studied in Sect. 2.4.2. At low T, the initial position in the double-well potential depends on the type of initial condition $\phi(\vec{x}, 0) = 0$ or $\phi(\vec{x}, 0) \neq 0$. In the first case, the point sits on top of the central barrier and it does not detach from it in finite times with respect to a function of L. In the second case, the point starts from within one well and it simply rolls to the bottom of the well. This relaxation is similar to the one in the harmonic case. To reverse the configuration from, say, positive to negative magnetization the point needs to jump over the barrier in the double well potential and it does via thermal activation ruled by the Arrhenius law.

Note however that the phase-space of the system is actually N-dimensional while the description that is given here is projected onto one single coordinate, the one of the order-parameter. This reduction might lead to some misunderstandings and one should be very careful with it.

3.3 Short-time dynamics

Take an initial configuration $\phi(\vec{x}, 0) = 0$ on average with small fluctuations, as in equilibrium at very high temperature, and quench the system. At very short time one can expand the non-linear potential and the Ginzburg-Landau equation (3.5), for the Fourier components, $\phi(\vec{k}, t) = L^{-d/2} \int d^d x \ \phi(\vec{x}, t) e^{-i\vec{k}\vec{x}}$ with $\vec{k} = 2\pi/L \ (n_1, \ldots, n_d)$ and n_k integer, reads

$$\frac{\partial \phi(\vec{k}, t)}{\partial t} = [-k^2 - V''(0)]\phi(\vec{k}, t) + \xi(\vec{k}, t) \ . \tag{3.14}$$

If $V''(0) > 0$ all modes decay exponentially and no order develops. If $V''(0) < 0$ instead modes with $-k^2 - V''(0) > 0$ are unstable and grow exponentially until a time $t^* \simeq -1/V''(0)$ when the small ϕ expansion ceases to be justified. The instability of

the small wave-vector modes indicates that the system tends to order. To go beyond this analysis one needs to consider the full non-linear equation.

3.4 Growing length and dynamic scaling

In usual coarsening systems the averaged space-time correlation function

$$\boxed{NC(r,t) = \sum_{ij/|\vec{r}_i - \vec{r}_j| = r} \langle s_i(t) s_j(t) \rangle}$$

allows for the identification of a growing length from, for example,

$$R_{\rm a}(T,t) \equiv \int d^d r \; r^{{\rm a}+1} C(r,t) / \int d^d r \; r^{\rm a} C(r,t) \tag{3.15}$$

(a is a parameter chosen to weight preferentially short or long distances; the time-dependence of $R_{\rm a}(t)$ should not depend on a.) Here and in the following $\langle \ldots \rangle$ stands for an average over different realizations of thermal histories at heat-bath temperature T and/or initial conditions. In presence of quenched disorder one adds an average over it and denotes it $[\ldots]$. The stochastic time-dependent function $N^{-1} \sum_{ij/|\vec{r}_i - \vec{r}_j| = r} s_i(t) s_j(t)$ after a quench from a random initial condition does not fluctuate in the thermodynamic limit. Therefore, the averages are not really necessary but they are usually written down. In spin-glasses and glasses this observable does not yield information on the existence of any growing length as we shall discuss below.

The spherically averaged structure factor $S(k,t)$ – the Fourier transform of $C(r,t)$ – can be measured experimentally with small-angle scattering of neutrons, x-rays or light and from it $R_{\rm a}(T,t)$ can be extracted.

The ordering process is characterized by the growth of a **typical length**, $R(T,t)$. The growth regimes are summarized in the following equation and in Fig. 27:

$$\left\{ \begin{array}{lll} R_c(t) \to \xi(T) < +\infty & T > T_c & \text{saturation,} \\ R_c(t) \to \xi(T) \to \infty & T = T_c & \text{critical coarsening,} \\ R_c(t) \to \xi(T) < R(T,t) \to L & T < T_c & \text{sub-critical coarsening.} \end{array} \right. \tag{3.16}$$

After a quench to the high temperature phase $T > T_c$ the system first grows equilibrium regions until reaching the correlation length ξ and next relaxes in equilibrium as explained in the previous section. The correlation length could be very short and the transient non-equilibrium regime be quite irrelevant ($T \gg T_c$). In the critical region, instead, the correlation length grows and it becomes important. In a critical quench the system never orders sufficiently and $R(T_c,t) < \xi$ for all finite times. Finally, a quench into the subcritical region is characterized by two growth regimes: a first one in which the critical point dominates and the growth is as in a critical quench; a second one in which the proper sub-critical ordering is at work. The time-dependence of the growth law is different in these two regimes as we shall see below. (Note that

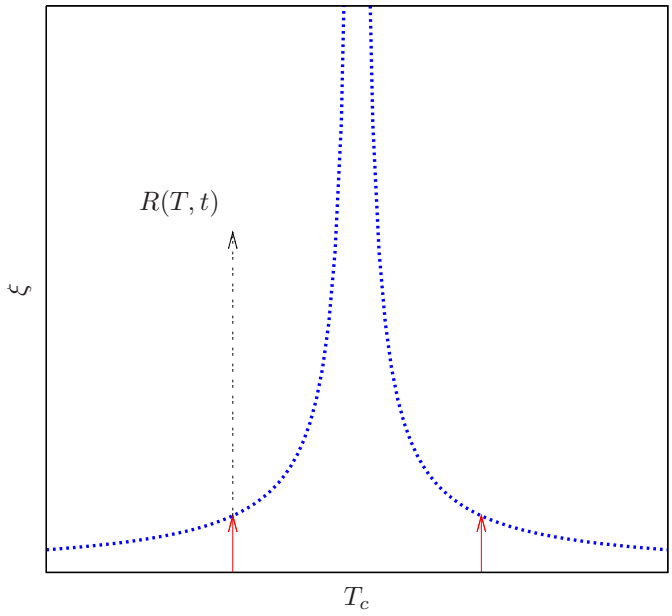

Figure 27: Sketch of the growth process in a second-order phase transition. The thick line is the equilibrium correlation length $\xi \simeq |T - T_c|^{-\nu}$. The thin solid (red) arrows indicate the growing length R_c in the critical coarsening regime and the dashed (black) arrow the sub-critical growing length R in the coarsening regime.

below T_c ξ does not measure the size of ordered regions but the typical distance until which a fluctuation has an effect.)

In the asymptotic time domain, when $R(T,t)$ has grown much larger than any microscopic length in the system, a **dynamic scaling symmetry** sets in, similarly to the usual scaling symmetry observed in equilibrium critical phenomena. According to this hypothesis, the growth of $R(T,t)$ is the only relevant process and the whole time-dependence enters only through $R(T,t)$.

3.5 Critical coarsening

The scaling behavior of binary systems quenched to the critical point is quite well understood. It can be addressed with scaling arguments and renormalization group approaches [5] which give explicit expressions for many of the quantities of interest up to two loops order. Numerical simulations confirm the analytic results and probe exponents and scaling functions beyond the available perturbative orders. In this case

the system builds correlated critical Fortuin-Kasteleyn clusters with fractal dimension $D_{FK} = (d+2-\eta)/2$, where η is the usual static critical exponent, in regions growing algebraically as $R_c(T_c, t) \equiv R_c(t) \sim t^{1/z_{eq}}$; henceforth we simplify the notation and avoid writing T_c within R. [As an example, for the bidimensional critical Ising class $\eta = 1/4$ and $D_{FK} = (2+2-1/4)/2 = 15/8$.]

In the asymptotic time regime the space-time correlation function has the scaling form

$$\begin{aligned} C(r,t) &= C_{st}(r)\ f\left(\frac{r}{R_c(t)}\right) \\ &= r^{-2(d-D_{FK})}\ f\left(\frac{r}{R_c(t)}\right) \end{aligned} \tag{3.17}$$

$$\boxed{C(r,t) = r^{2-d-\eta}\ f\left(\frac{r}{R_c(t)}\right) \quad \text{Multiplicative separation.}}$$

The pre-factor $r^{2(d-D_{FK})}$ takes into account that the growing domains have a **fractal nature** (hence their *density* decreases as their size grows) and the dependence on $r/R_c(t)$ in $f(x)$ expresses the similarity of configurations at different times once lengths are measured in units of $R_c(t)$. At distances and times such that $r/R_c(t) \ll 1$ the equilibrium power-law decay, $C_{eq}(r) \simeq r^{2-d-\eta}$, should be recovered, thus $f(x) \simeq$ ct at $x \to 0$. $f(x)$ falls off rapidly for $x \gg 1$ to ensure that spins are uncorrelated at distances larger than $R_c(t)$. [More precisely, correlated as in the initial condition that, in the case of a quench from infinite temperature, means indeed uncorrelated.]

For two-time quantities, when t' is sufficiently large one has

$$C(t,t') = C_{st}(t-t')\ f_{\rm C}\left(\frac{R_c(t)}{R_c(t')}\right) \tag{3.18}$$

$$\boxed{C(t,t') = R_c(t-t')^{2-d-\eta}\ f_{\rm C}\left(\frac{R_c(t)}{R_c(t')}\right) \text{ Multiplicative separation.}}$$

Here $C_{st}(t-t') \simeq R_c(t-t')^{-2(d-D_{FK})} = R_c(t-t')^{2-d-\eta}$. The scaling function $f_{\rm C}(x)$ describes the non-equilibrium behavior. It satisfies $f_c(1) = 1$ and $f_c(x \to \infty) = 0$, see the sketch in Fig. 28 (a). In the scaling forms the equilibrium and non-equilibrium contributions enter in a **multiplicative** structure. Non-equilibrium effects are taken into account by taking ratios between the sizes of the correlated domains at the observation times t' and t in the scaling functions. Note that the reason why the equilibrium results are recovered for $t \simeq t'$ is that for very similar times one does not let the system realize that it is out of equilibrium.

In the case of non-conserved scalar order-parameter dynamics the growing length behaves as

$$\boxed{R_c(t) \sim t^{1/z_{eq}}} \tag{3.19}$$

with z_{eq} the equilibrium dynamics exponent (note that z_{eq} is different from z_d). We shall not discuss critical dynamics in detail; this problem is treated analytically with

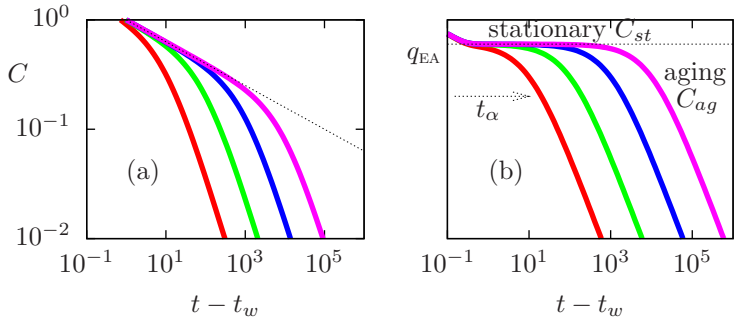

Figure 28: Sketch of the decay of the two-time correlation at T_c (a) and $T < T_c$ (b) for different values of the waiting-time, increasing from left to right.

dynamic renormalization group techniques and it is very well discussed in the literature [5]. In short, the exponent z_{eq} is given by [24]

$$z_{eq} = 2 + \frac{N+2}{(N+8)^2}\left[3\ln\frac{4}{3} - \frac{1}{2}\right]\epsilon^2 + O(\epsilon^3) \tag{3.20}$$

where N is the dimension of the possibly vector field, $N = 1$ for a scalar one, and $\epsilon = 4 - d$ with d the dimension of space. Note that z_{eq} is larger than 2 for all finite N and it approaches 2 in the large N limit (at least up to this order in perturbation theory). In particular, one finds

$$z_{eq} \simeq \begin{cases} 2.0538 & d = 2 \\ 2.0134 & d = 3 \\ 2 & d = 4 \end{cases} \tag{3.21}$$

for $N = 1$. Numerical simulations indicate $z_{eq} \simeq 2.13$ in $d = 2$. These results are valid for white noise dynamics. The effect of colored noise is to change the value of the exponent z_{eq} when it is sufficiently long-range correlated (sub-Ohmic noise with a power-law decay with an exponent smaller than a critical value that depends on the dimension of space).

3.6 Sub-critical coarsening

3.6.1 Dynamic scaling hypothesis

The **dynamic scaling hypothesis** states that at late times and in the scaling limit

$$r \gg \xi(g)\,, \qquad R(g,t) \gg \xi(g)\,, \qquad r/R(g,t) \ \text{ arbitrary}\,, \tag{3.22}$$

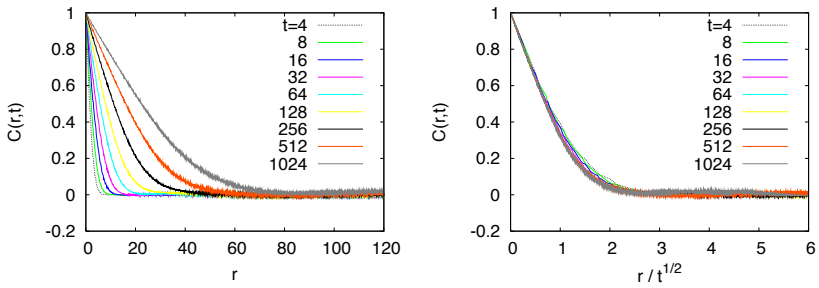

Figure 29: The equal-time correlation as a function of distance in the $2d$IM quenched below T_c. Raw (left) and scaled (right) data. These numerical simulations were performed by A. Sicilia.

where r is the distance between two points in the sample, $r \equiv |\vec{x} - \vec{x}'|$, and $\xi(g)$ is the equilibrium correlation length that depends on all parameters (T and possibly others) collected in g, there exists a **single characteristic length**, $R(g,t)$, such that the domain structure is, in statistical sense, independent of time when lengths are scaled by $R(g,t)$. Time, denoted by t, is typically measured from the instant when the critical point is crossed. In the following we ease the notation and write only the time-dependence in R. This hypothesis has been proved analytically in very simple models only, such as the one dimensional Ising chain with Glauber dynamics or the Langevin dynamics of the d-dimensional $O(N)$ model in the large N limit (see Sect. 3.8).

The late stage of phase-ordering in binary systems is characterized by a patchwork of large domains the interior of which is basically thermalized in one of the two equilibrium phases while their boundaries are slowly moving. This picture suggests the splitting of the degrees of freedom (spins) into two categories, providing statistically independent contributions to observables such as correlation or response functions. More precisely, a quasi-equilibrium stationary contribution arises as due to bulk spins, while boundaries account for the non-equilibrium part. Then asymptotically one has

$$\boxed{C(r,t) \simeq C_{st}(r) + C_{ag}(r,t) \qquad \text{Additive separation.}} \tag{3.23}$$

The first term describes the equilibrium fluctuations in the low temperature broken symmetry pure states

$$C_{st}(r) = (1 - \langle s_i \rangle_{eq}^2)\; g\left(\frac{r}{\xi}\right), \tag{3.24}$$

where $\langle s_i \rangle_{eq}$ is the equilibrium expectation value of the local spin in one of the two symmetry breaking states, $\langle s_i \rangle_{eq} = m$, and $g(x)$ is a function with the limiting values $g(0) = 1$, $\lim_{x\to\infty} g(x) = 0$. The second term takes into account the motion of the

domain walls through

$$C_{ag}(r,t) = \langle s_i \rangle_{eq}^2 \; f\left(\frac{r}{R(t)}\right), \tag{3.25}$$

with $f(1) = 1$ and $\lim_{x\to\infty} f(x) = 0$. Both C_{st} and C_{ag} obey (separately) scaling forms with respect to the equilibrium and the non-equilibrium lengths ξ, $R(t)$. In particular, eq. (3.25) expresses the fact that system configurations at different times are statistically similar provided that lengths are measured in units of $R(t)$, namely the very essence of dynamical scaling.

Monte Carlo simulations of the Ising model and other systems quenched below criticality and undergoing domain growth demonstrate that in the long waiting-time limit $t' \gg t_0$, the spin self-correlation $\langle s_i(t) s_i(t') \rangle$ separates into two additive terms

$$\boxed{C(t,t') \sim C_{st}(t-t') + C_{ag}(t,t') \quad \text{Additive separation}} \tag{3.26}$$

see Fig. 30, with the first one describing equilibrium thermal fluctuations within the domains,

$$C_{st}(t-t') \;\; = \;\; \left\{ \begin{array}{ll} 1 - \langle s_i \rangle_{eq}^2 = 1 - m^2 \; , & t - t' = 0 \; , \\ 0 \; , & t - t' \to \infty \; , \end{array} \right. \tag{3.27}$$

and the second one describing the motion of the domain walls

$$C_{ag}(t,t') \;\; = \;\; \langle s_i \rangle_{eq}^2 \; f_c\left(\frac{R(t)}{R(t')}\right) = \left\{ \begin{array}{ll} \langle s_i \rangle_{eq}^2 \; , & t' \to t^- \; , \\ 0 \; , & t - t' \to \infty \; . \end{array} \right. \tag{3.28}$$

To ease the notation we have not written the explicit T-dependence in R that, as we shall see below, is less relevant than t. Note that by adding the two contributions one recovers $C(t,t) = 1$ as expected and $C(t,t') \to 0$ when $t \gg t'$. The first term is identical to the one of a system in equilibrium in one of the two ordered states, see eq. (3.12) for its asymptotic $t - t' \gg t'$ limit; the second one is inherent to the out of equilibrium situation and existence and motion of domain walls. They vary in completely different two-time scales. The first one changes when the second one is fixed to $\langle s_i \rangle_{eq}^2$, at times such that $R(t)/R(t') \simeq 1$. The second one varies when the first one decayed to zero. The mere existence of the second term is the essence of the aging phenomenon with older systems (longer t') having a slower relaxation than younger ones (shorter t'). The scaling of the second term as the ratio between 'two lengths' is a first manifestation of **dynamic scaling**.

A decorrelation time can also be defined in this case by expandind the argument of the scaling function around $t' \simeq t$. Indeed, calling $\Delta t \equiv t - t'$ one has $R(t)/R(t') \simeq R(t'+\Delta t)/R(t') \simeq [R(t') + R'(t')\Delta t]/R(t') \simeq 1 + \Delta t/[d \ln R(t')/dt']^{-1}$ and one identifies a **t'-dependent decorrelation time**

$$\boxed{t_d \simeq [d \ln R(t')/dt']^{-1} \quad \text{decorrelation time}} \tag{3.29}$$

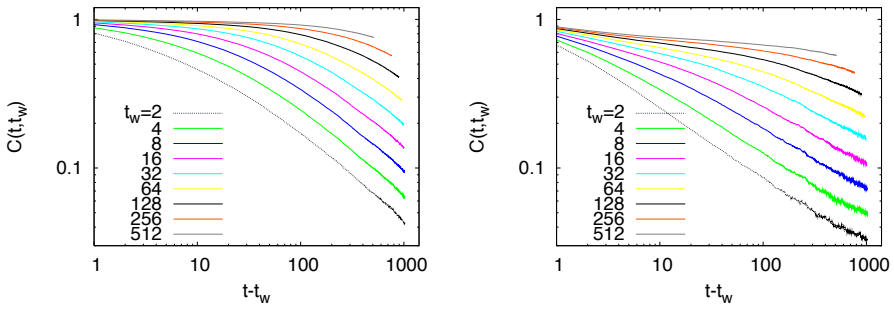

Figure 30: The two-time self-correlation in the $2d$IM with non-conserved order parameter dynamics at several waiting-times given in the key at temperature $T = 0.5$ (left) and $T = 2$ (right). Data obtained with Monte Carlo simulations. Note that the plateau is located at a lower level in the figure on the right consistently with the fact that $\langle \phi \rangle_{eq}$ decreases with increasing temperature. Data from A. Sicilia et al.

which is, in general, a growing function of t'.

In order to fully characterise the correlation functions one then has to determine the typical growing length, R, and the scaling functions, g, f, f_c, *etc.* It turns out that the former can be determined with semi-analytic arguments and the predictions are well verified numerically – at least for clean system. The latter, instead, are harder to obtain. We shall give a very brief state of the art report in Sect. 3.6.9. For a much more detailed discussion of these methods see the review articles in [4].

The time-dependent typical domain length, $R(t)$, is determined numerically by using several indirect criteria or analytically within certain approximations. The most common ways of measuring R are with numerical simulations of lattice models or the numerical integration of the continuous partial differential equation for the evolution of the order parameter. In both cases one

– Computes the 'inverse perimeter density' $R(t) = -\langle H \rangle_{eq} / [\langle H(t) \rangle - \langle H \rangle_{eq}]$ with $\langle H(t) \rangle$ the time-dependent averaged energy and $\langle H \rangle_{eq}$ the equilibrium energy both measured at the working temperature T.

– Puts the dynamic scaling hypothesis to the test and extracts R from the analysis.

3.6.2 $R(t)$ in clean one dimensional cases with non-conserved order parameter

In one dimension, a space-time graph allows one to view coarsening as the diffusion and annhilitation upon collision of point-like particles that represent the domain walls. In the Glauber Ising chain with non-conserved dynamics one finds that the typical domain length grows as $t^{1/2}$ while in the continuous case the growth is only logarithmic, $\ln t$.

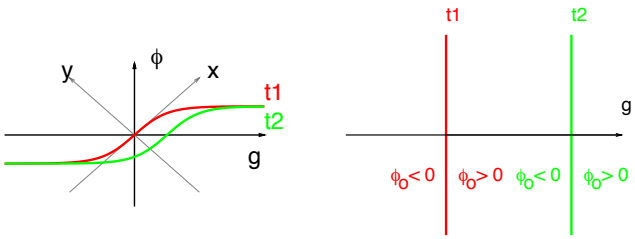

Figure 31: Left: domain wall profile. Right: view from the top. (g is n.)

3.6.3 $R(t)$ in non-conserved order parameter curvature driven dynamics ($d > 2$)

The time-dependent Ginzburg-Landau model allows us to gain some insight on the mechanism driving the domain growth and the direct computation of the averaged domain length. In clean systems temperature does not play a very important role in the domain-growth process, it just adds some thermal fluctuations within the domains, as long as it is smaller than T_c. In dirty cases instead temperature triggers thermal activation.

We focus first on the clean cases at $T = 0$ and only later we discuss thermal effects. Equation (3.5) for $T = 0$ is just a gradient descent in the energy landscape F. Two terms contribute to F: the bulk-energy term that is minimized by $\phi = \pm\phi_0$ and the elastic energy $(\nabla\phi)^2$ which is minimized by flat walls if present. As a consequence the minimization process implies that regions of constant field, $\phi(\vec{x}, t) = \pm\phi_0$, grow and they separated by flatter and flatter walls.

Take a **flat domain wall** separating regions where the configuration is the one of the two equilibrium states, $\phi(\vec{x}, t) = \pm\phi_0 + \delta\phi(\vec{x}, t)$. Linearizing eq. (3.5) around $\pm\phi_0$ and looking for static configurations, *i.e.* $\delta\phi(\vec{x}, t) = \delta\phi(\vec{x}) = \delta\phi(n)$ where n is the distance from the wall along the normal direction one finds $d^2\delta\phi(n)/dn^2 = -V''(\phi_0)\delta\phi(n)$. This equation has the solution $\delta\phi(n) \sim e^{-\sqrt{V''(\phi_0)}n}$ where n is the perpendicular distance to the wall. The order parameter approaches $\pm\phi_0$ on both sides of the wall very rapidly. This means that the free-energy of a configuration with an interface (sum of the elastic and potential terms) is concentrated in a very narrow region close to it. In consequence, the domain-wall curvature is the driving force for domain growth.

Allen and Cahn showed that the local wall velocity is proportional to the local curvature working with the Ginzburg-Landau equation at $T = 0$. The proof goes as follows. Take the Ginzburg-Landau equation and trasform the derivatives to apply in

the direction normal to the wall:

$$\frac{\partial\phi(\vec{x},t)}{\partial t} = -\left.\frac{\partial\phi(\vec{x},t)}{\partial n}\right|_t \left.\frac{\partial n}{\partial t}\right|_\phi , \qquad \vec{\nabla}\phi(\vec{x},t) = \left.\frac{\partial\phi(\vec{x},t)}{\partial n}\right|_t \hat{n} ,$$
$$\nabla^2\phi(\vec{x},t) = \left.\frac{\partial^2\phi(\vec{x},t)}{\partial n^2}\right|_t + \left.\frac{\partial\phi(\vec{x},t)}{\partial n}\right|_t \vec{\nabla}\cdot\hat{n}$$

where the subscripts mean that the derivatives are taken at t or ϕ fixed. Using now $\frac{\partial^2\phi(\vec{x},t)}{\partial n^2}|_t = V'(\phi)$ (note that the derivative is taken at fixed t) in the GL equation one finds the Allen-Cahn result

$$v \equiv \partial_t n|_\phi = -\vec{\nabla}\cdot\hat{n} \equiv -\kappa \tag{3.30}$$

valid in all d with κ the geodesic curvature.

Equation (3.30) allows one to get an intuition about the typical growth law in such processes. Take a spherical wall in any dimension. The local curvature is constant and $\kappa = (d-1)/R$ where R is the radius of the sphere within the hull. Equation (3.30) is recast as $dR/dt = -(d-1)/R$ that implies $R^2(t) = R^2(0) - 2(d-1)t$.

A closer look at the $2d$ equation allows one to go beyond and prove, in this case, that all areas enclosed by domain walls irrespective of their being other structures within (the so-called hull-enclosed areas) tend to diminish at constant rate $dA/dt = -\lambda$. This, of course, does not mean that all domains reduce their area since a domain can gain area from the disappearance of an internal domain of the opposite sign, for instance. The proof is simple and just uses the Gauss-Bonnet theorem: $\frac{dA}{dt} = \oint \vec{v}\wedge d\vec{\ell} = \oint v d\ell$. The local wall-velocity, $\vec{v}$, is proportional to the local geodesic curvature, κ, and the Gauss-Bonnet theorem implies $\oint \kappa d\ell = 2\pi$ for a planar $2d$ manifold with no holes. Therefore, the hull-enclosed area decreases with constant velocity for any geometry.

Therefore the local velocity points in the direction of the local centre of curvature. The effect is to reduce the wall roughness by rendering them smoother.

There are a number of ways to find the growth law

$$\boxed{R(t) = \lambda\, t^{1/z_d}} \tag{3.31}$$

with z_d the **dynamic exponent**, in **pure and isotropic** systems (see [4]). The effects of temperature enter only in the parameter λ and, for clean systems, growth is slowed down by an increasing temperature since thermal fluctuation tend to roughen the interfaces thus opposing the curvature driven mechanism. We estimate the T dependence of λ in Sect. 3.6.5.

In curvature driven Ising or Potts cases with non-conserved order parameter the domains are sharp and $z_d = 2$ with λ a weakly T-dependent coefficient. For systems with continuous variables such as rotors or XY models and the same type of dynamics, a number of computer simulations have shown that domain walls are thicker and $z_d = 4$.

3.6.4 $R(t)$ in conserved order parameter dynamics and the role of bulk diffusion

A different type of dynamics occurs in the case of phase separation (the water and oil mixture ignoring hydrodynamic interactions or a binary allow). In this case, the material is locally conserved, *i.e.* water does not transform into oil but they just separate. The main mechanism for the evolution is diffusion of material through the bulk of the opposite phase. After some discussion, it was established, as late as in the early 90s, that for scalar systems with **conserved order parameter** $z_d = 3$.

3.6.5 Crossover between critical and sub-critical coarsening

Matching critical coarsening with sub-critical one allows one to find the T-dependent prefactor λ [28]. The argument goes as follows. The out of equilibrium growth at criticality and in the ordered phase are given by

$$R(t) \sim \begin{cases} t^{1/z_{eq}} & \text{at} \quad T = T_c \ , \\ (\lambda(T)t)^{1/z_d} & \text{at} \quad T < T_c \ . \end{cases} \tag{3.32}$$

z_{eq} is the equilibrium dynamic critical exponent and z_d the out of equilibrium growth exponent. Close but below criticality one should have an interpolating expression of the kind

$$R(t) \sim \xi^{-a} t^{1/z_d} f\left(\frac{t}{\xi^{z_{eq}}}\right) \qquad \text{at} \qquad T = T_c - \epsilon \tag{3.33}$$

with ξ the T-dependent equilibrium correlation length, $\xi(T) \sim (T_c - T)^{-\nu}$. The last factor tends to one, $f(x \to \infty) \to 1$, when $R(t) \gg \xi$, that is to say when the argument diverges and the system enters the sub-critical coarsening regime. It is however non-trivial when $R(t) \sim \xi$, the argument is finite and critical coarsening must be described. In particular, we determine its behavior for $x = O(1)$ by requiring that eq. (3.33) matches the subcritical growing length which is achieved by (i) recovering the correct t dependence, (ii) cancelling the ξ factor. (i) implies

$$f(x) \sim x^{-1/z_d + 1/z_{eq}} \qquad \text{for} \qquad x = O(1) \ . \tag{3.34}$$

Then eq. (3.33) becomes

$$R(t) \sim \xi^{-a + z_{eq}/z_d - 1} t^{1/z_{eq}} \tag{3.35}$$

and to eliminate ξ we need

$$a = z_{eq}/z_d - 1 \ . \tag{3.36}$$

Comparing now the subcritical growing length and (3.33) in the very long times limit such that $R(t) \gg \xi$ and $f(x \to \infty) \to 1$:

$$[\lambda(T)]^{1/z_d} \sim \xi^{-a} \sim (T_c - T)^{\nu(z_{eq} - z_d)/z_d} \ . \tag{3.37}$$

Note that quite generally one finds $z_{eq} > z_d$ and $\lambda(T)$ vanishes at T_c.

3.6.6 The $2d$ XY model

The XY model in $d = 2$ is quite special since it is critical at all temperatures below $T_{\rm KT}$. It is then worth analyzing this special case in detail. Moreover, it has topological defects and the rate of approach to the equilibrium state is affected by them.

The model is fully solvable in the spin-wave approximation in which the field is supposed to vary smoothly in space and, hence, vortices are neglected. The functional Langevin equation acting on the angle between the local spins and a chosen axis is linear in Fourier space and it can be readily solved. The angle correlation functions in equilibrium are

$$\langle (\theta(r) - \theta(0))^2 \rangle = \frac{k_B T}{\pi J} \ln r/a \tag{3.38}$$

leading to

$$C(r) = \langle \mathbf{s}(r)\mathbf{s}(0) \rangle = \left(\frac{a}{r}\right)^{k_B T/\pi J} = \left(\frac{a}{r}\right)^{\eta(T)} \tag{3.39}$$

The equilibrium correlation length is $\xi(T) = a/\ln(k_B T/\pi J)$ that tends to zero only at $T \to \infty$ and diverges at $T \to 0$.

Spin-waves are non-local and extensive while vortices are local and intensive. The latter cannot be eliminated by simple perturbations but they annihilate.

The global correlation and linear response, $C(t,t') = V^{-1} \int d^2x \, \langle \, \mathbf{s}(\vec{x},t) \cdot \mathbf{s}(\vec{x},t') \, \rangle$ and $R(t,t') = V^{-1} \int d^2x \, \left. \frac{\delta \langle \, \mathbf{s}(\vec{x},t) \, \rangle}{\delta \mathbf{h}(\vec{x},t')} \right|_{\mathbf{h}=0}$ take the following scaling forms in the limit $t - t' \gg \Lambda^{-2}$:

$$C(t,t') \quad \sim \quad \frac{1}{(t-t')^{\eta(T)/2}} \, \Phi\left(\frac{R_c(t)}{R_c(t')}\right) \tag{3.40}$$

$$R(t,t') \quad \sim \quad \frac{1}{4\pi\rho(T)(t-t')^{1+\eta(T)/2}} \, \Phi\left(\frac{R_c(t)}{R_c(t')}\right) \tag{3.41}$$

with Φ a scaling function and $R_c(t)$ the growing correlation length (that should not be confused with the linear response). The first remarkable property of these functions is that they are both decomposed in the product of a function of the time-difference $t-t'$ and a function of the ratio $\lambda \equiv R_c(t')/R_c(t)$, like in the general critical coarsening case. When $t - t' \ll R_c(t')$ and $\lambda \sim 1$, the decay is stationary

$$C(t,t') \sim (t-t')^{-\eta(T)/2} \, , \quad R(t,t') \sim (t-t')^{-1-\eta(T)/2}$$

and the FDR equals one. This limit defines a quasi-equilibrium regime. When the time difference increases and λ becomes smaller than one the relaxation enters an aging regime in which the decay of the correlation and response depends on the waiting-time t'. The behavior in the aging regime depends on the initial conditions as discussed below.

Uniform initial conditions.

The uniform initial condition contains no free vortices and none are generated by thermal fluctuations at any $T < T_{\rm KT}$. The evolution is well captured by the simple spin-wave approximation and after a simple calculation one finds

$$\Phi\left(\frac{\xi(t)}{\xi(t')}\right) = \left[\frac{(1+\lambda)}{4\lambda}\right]^{\eta(T)/4} , \qquad R_c(t) = t^{1/2} . \tag{3.42}$$

Beyond the crossover time $t-t' \sim t'$, when $C(2t',t') \sim t'^{-\eta(T)/2}$ and λ becomes smaller than one, the correlation and response decay to zero as power laws of the waiting-time t'. There is no clear-cut separation of time-scales characterised by the correlation reaching a constant value independently of the waiting-times but only a t' dependent pseudo-plateau where the behavior of the two-time correlation changes. This is to be confronted to the behavior of ferromagnetic coarsening systems quenched to the low-temperature phase for which the crossover occurs at $C(2t',t') = m^2_{\rm EQ}$. Above this plateau, the relaxation corresponds to the equilibrium fluctuations of short wave-length while below the plateau the decorrelation is due to the domain-wall motion that manifests into a scaling in terms of $\lambda = t'/t$ only. In the 2d XY case the order parameter vanishes and there is no plateau at any finite value of C.

In the aging regime the fluctuation – dissipation ratio is larger than one. This *a priori* surprising result can be understood when interpreted in terms of the effective – temperature. The completely order configuration is the equilibrium state at zero temperature. The evolution of this initial state at finite temperature can be thought of as representing a sudden inverse quench of the system from $T = 0$ to $T > 0$. If the FDR is related to a remembrance of the temperature of the initial condition, in this case this is lower than the working temperature T and thus, the effective temperature also turns out to be lower than T.

Random initial conditions.

When random initial conditions with only short-ranged spatial correlations are considered, free vortices and antivortices are present initially. The relaxation occurs vis the annihilation of vortex-antivortex pairs and this coarsening process is much slower than the relaxation of spin-waves. The simple Gaussian theory is no more suited to describe this dynamics and a full analytic treatment is too hard to implement. With scaling and numeric analysis the dynamic correlation length has been estimated to be [4]

$$\boxed{R_c(t) \sim (t/\ln t)^{1/2} .}$$

The numerical simulations of Berthier, Holdsworth and Sellitto have proven that the two-time correlation and response are correctly described by the scaling form (3.40) and (3.41) with this length scale and the full decay looks like the one shown in the sketch above. The FDR is rather different from the one following the evolution of a uniform initial condition. The non-equilibrium susceptibility is now smaller than the equilibrium value, and in terms of the effective temperature this means that the fluctuations of the wave-lengths longer than $R_c(t)$ occur at a $T_{\rm EFF} > T$ and hence keep a memory of the initial temperature $T = \infty$.

3.6.7 Role of weak disorder: thermal activation

The situation becomes much less clear when there is weak quenched disorder in the form of non-magnetic impurities in a magnetic sample, lattice dislocations, residual stress, *etc.* These are assumed not to modify the nature of the equilibrium states with respect to the ones of the clean system. Qualitatively, the dynamics are expected to be slower than in the pure cases since disorder pins the interfaces. In general, based on an argument due to Larkin (and in different form to Imry-Ma) one expects that in $d < 4$ the late epochs and large scale evolution is no longer curvature driven but controlled by disorder. Indeed, within a phase space view disorder generates metastable states that trap the system and thus slow down the relaxation.

A hand-waving argument to estimate the growth law in dirty systems is the following. Take a system in one equilibrium state with a domain of linear size R of the opposite equilibrium state within it. This configuration could be the one of an excited state with respect to the fully ordered one with absolute minimum free-energy. Call $\Delta F(R)$ the free-energy barrier between the excited and equilibrium states. The thermal activation argument (see Sect. 2.3) yields the activation time scale for the decay of the excited state (*i.e.* erasing the domain wall)

$$t_A \sim \tau \; e^{\Delta F(R)/(k_B T)} \; . \tag{3.43}$$

For a barrier growing as a power of R, $\Delta F(R) \sim \Upsilon(T, J) R^{\psi}$ (where J represents the disorder) one inverts (3.43) to find the linear size of the domains still existing at time t, that is to say, the growth law

$$\boxed{R(t) \sim \left(\frac{k_B T}{\Upsilon(T)} \; \ln \frac{t}{\tau} \right)^{1/\psi} \; .} \tag{3.44}$$

All smaller fluctuation would have disappeared at t while typically one would find objects of this size. The exponent ψ is expected to depend on the dimensionality of space but not on temperature. In 'normal' systems it is expected to be just $d-1$ – the surface of the domain – but in spin-glass problems, it might be smaller than $d-1$ due to the presumed fractal nature of the walls. The prefactor Υ is expected to be weakly temperature dependent.

One assumes that the same argument applies out of equilibrium to the reconformations of a portion of any domain wall or interface where R is the observation scale.

However, already for the (relatively easy) random ferromagnet there is no consensus about the actual growth law. In these problems there is a competition between the 'pure' part of the Hamiltonian, that tries to minimize the total $(d-1)$ dimensional area of the domain wall, and the 'impurity' part that makes the wall deviate from flatness and pass through the locations of lowest local energy (think of $J_{ij} = J + \delta J_{ij}$ with J and δJ_{ij} contributing to the pure and impurity parts of the Hamiltonian, respectively). The activation argument in eq. (3.43) together with the

power-law growth of barriers in $\Delta F(R) \sim \Upsilon(T,J)R^{\psi}$ imply a logarithmic growth of $R(t)$. Simulations, instead, suggest a power law with a temperature dependent exponent. Whether the latter is a pre-asymptotic result and the trully asymptotic one is hidden by the premature pinning of domain walls or it is a genuine behavior invalidating $\Delta F(R) \sim \Upsilon(T,J)R^{\psi}$ or even eq. (3.43) is still an open problem. See the discussion below for a plausible explanation of the numerical data that does not invalidate the theoretical expectations.

In the $3d$ RFIM the curvature-driven growth mechanism that leads to (3.31) is impeded by the random field roughening of the domain walls. The dependence on the parameters T and h has been estimated. In the early stages of growth, one expects the zero-field result to hold with a reduction in the amplitude $R(t) \sim (A - Bh^2)\, t^{1/2}$. The time-window over which this law is observed numerically decreases with increasing field strength. In the late time regime, where pinning is effective Villain deduced a logarithmic growth $R(t) \sim (T/h^2)\, \ln t/t_0$ by estimating the maximum barrier height encountered by the domain wall and using the Arrhenius law to derive the associated time-scale.

In the case of spin-glasses, if the mean-field picture with a large number of equilibrium states is realized in finite dimensional models, the dynamics would be one in which all these states grow in competition. If, instead, the phenomenological droplet model applies, there would be two types of domains growing and $R(t) \sim (\ln t)^{1/\psi}$ with the exponent ψ satisfying $0 \leq \psi \leq d-1$. Some refined arguments that we shall not discuss here indicate that the dimension of the bulk of these domains should be compact but their surface should be rough with fractal dimension $D_s > d-1$.

3.6.8 Temperature-dependent effective exponents

The fact that numerical simulations of dirty systems tend to indicate that the growing length is a power law with a T-dependent exponent can be explained as due to the effect of a T-dependent cross-over length L_T. Indeed, if below $L_T \sim T^{\phi}$ the growth process is as in the clean limit while above L_T quenched disorder is felt and the dynamics is thermally activated:

$$R(t) \quad \sim \quad \begin{cases} t^{1/z_d} & \text{for} \quad R(t) \ll L_T \,, \\ (\ln t)^{1/\psi} & \text{for} \quad R(t) \gg L_T \,. \end{cases} \tag{3.45}$$

These growth-laws can be first inverted to get the time needed to grow a given length and then combined into a single expression that interpolates between the two regimes:

$$t(R) \sim e^{(R/L_T)^{\psi}} R^{z_d} \tag{3.46}$$

where the relevant T-dependent length-scale L_T has been introduced.

Now, by simply setting $t(R) \sim R^{\overline{z}(T)}$ one finds $\overline{z}(T) \sim z_d + \frac{1}{\ln R(t)} \left(\frac{R^{\psi}(t)}{L_T^{\psi}} \right)$ that replacing $R \sim t^{1/\overline{z}(T)}$ becomes $\overline{z}(T) \sim z_d + \frac{\overline{z}(T)}{\ln t} \left(\frac{t^{\psi/\overline{z}(T)}}{L_T^{\psi}} \right)$. Using now $\overline{z}(T) \simeq z_d$ in

the correction term and focusing on times such that $t^{\psi/z_d}/\ln t$ is almost constant and equal to c one finds $\overline{z}(T) - z_d \simeq \mathrm{c}\ z_d/L_T^{\psi}$. Similarly, by equating $t(R) \sim \exp(R^{\overline{\psi}(T)}/T)$ one finds that $\overline{\psi}(T)$ is a decreasing function of T approaching ψ at high T.

3.6.9 Scaling functions for subcritical coarsening

Even though the qualitative behavior of the solution to eq. (3.5) is easy to grasp, it is still too difficult to solve analytically and not much is known exactly on the scaling functions. A number of approximations have been developed but none of them is fully satisfactorily (see [4] for a critical review of this problem).

The **super-universality hypothesis** states that in cases in which temperature and quenched disorder are 'irrelevant' in the sense that they do not modify the nature of the low-temperature phase (*i.e.* it remains ferromagnetic in the case of ferromagnetic Ising models) the scaling functions are not modified. Only the growing length changes from the, say, curvature driven $t^{1/2}$ law to a logarithmic one. This hypothesis has been verified in a number of two and three dimensional models including the RBIM and the RFIM.

3.6.10 Breakdown of dynamic scaling

Some special cases in which dynamic scaling does not apply have also been exhibited. Their common feature is the existence of two (or more) growing lengths associated to different ordering mechanisms. An example is given by the Heisenberg model at $T \to 0$ in which the two mechanisms are related to the vectorial ordering within domains separated by couples of parallel spins that annhilate in a way that is similar to domain-wall annihilation in the Ising chain.

3.7 Annealing: crossover from critical to subcritical coarsening

There has been recent interest in understanding how a finite rate cooling affects the defect density found right after the quench. A scaling form involving equilibrium critical exponents was proposed by Zurek following work by Kibble. The interest is triggered by the similarity with the problem of quantum quenches in atomic gases, for instance. An interplay between critical coarsening (the dynamics that occurs close in the critical region) that is usually ignored (!) and sub-critical coarsening (once the critical region is left) is the mechanism determining the density of defects right after the end of the cooling procedure.

The growing length satisfies a scaling law

$$
\begin{array}{rcll}
R(t,\epsilon(t)) & \sim & \epsilon^{-\nu}(t)\ f[t\epsilon^{z_{eq}\nu}(t)] & \epsilon(t) = |T(t) - T_c| \\
f(x) & \to & \left\{ \begin{array}{ll} \mathrm{ct} & x \ll -1 \\ \sqrt{x} & x \gg 1 \end{array} \right. & \begin{array}{l} \text{Equilibrium at high } T \\ \text{Coarsening at low } T \end{array}
\end{array}
$$

with t measured from the instant when the critical point is crossed and $x \in (-1,1)$ is the critical region. A careful analysis of this problem can be found in Biroli, LFC, Sicilia (2010).

3.8 An instructive case: the large N approximation

A very useful approximation is to upgrade the scalar field to a vectorial one with N components

$$\phi(\vec{x},t) \to \vec{\phi}(\vec{x},t) = (\phi_1(\vec{x},t),\ldots,\phi_N(\vec{x},t)) \;, \tag{3.47}$$

and modify the free-energy

$$F = \int d^dx \left[\frac{1}{2}(\nabla\vec{\phi})^2 + \frac{N}{4}(\phi_0^2 - N^{-1}\phi^2)^2\right] \;, \tag{3.48}$$

with $\phi^2 = \sum_{\alpha=1}^N \phi_\alpha^2$ and ϕ_0 finite. The $T=0$ dynamic equation then becomes

$$\partial_t\phi_\alpha(\vec{x},t) = \nabla^2\phi_\alpha(\vec{x},t) - 4\phi_\alpha(\vec{x},t)\,[\phi_0^2 - N^{-1}\phi^2(\vec{x},t)] \tag{3.49}$$

and it is clearly **isotropic** in the N dimensional space implying

$$C_{\alpha\beta}(\vec{x},t;\vec{x}',t') = \delta_{\alpha\beta}C(\vec{x},t;\vec{x}',t') \tag{3.50}$$

In the limit $N\to\infty$ while keeping the dimension of real space fixed to d, the cubic term in the right-hand-side can be replaced by

$$-\phi_\alpha(\vec{x},t)N^{-1}\phi^2(\vec{x},t) \to -\phi_\alpha(\vec{x},t)N^{-1}[\,\phi^2(\vec{x},t)\,]_{ic} \equiv -\phi_\alpha(\vec{x},t)\,a(t) \tag{3.51}$$

since $N^{-1}\phi^2(\vec{x},t)$ does not fluctuate, it is equal to its average over the initial conditions and it is therefore not expected to depend on the spatial position if the initial conditions are chosen from a distribution that is statistically translational invariant. For the scalar field theory the replacement (3.51) is just the **Hartree approximation**. The dynamic equation is now **linear** in the field $\phi_\alpha(\vec{x},t)$ that we rename $\phi(\vec{x},t)$ (and it is now order 1):

$$\partial_t\phi(\vec{x},t) = [\nabla^2 + a(t)]\phi(\vec{x},t) \;, \tag{3.52}$$

where the time-dependent harmonic constant $a(t) = \phi_0^2 - [\phi^2(\vec{x},t)]_{ic} = \phi_0^2 - [\phi^2(\vec{0},t)]_{ic}$ has to be determined self-consistently. Equation (3.52) can be Fourier transformed

$$\partial_t\phi(\vec{k},t) = [-k^2 + a(t)]\phi(\vec{k},t) \;, \tag{3.53}$$

and it takes now the form of almost independent oscillators under different time-dependent harmonic potentials coupled only through the self-consistent condition on $a(t)$. The stability properties of the oscillators depend on the sign of the prefactor in the RHS. The solution is

$$\phi(\vec{k},t) = \phi(\vec{k},0)\; e^{-k^2t + \int_0^t dt'\; a(t')} \tag{3.54}$$

and the equation on $a(t)$ reads:

$$a(t) \quad = \quad \phi_0^2 - \Delta \; e^{2\int_0^t dt' a(t')} \left(\frac{2\pi}{4t}\right)^{d/2} \quad , \tag{3.55}$$

where one used $[\phi^2(\vec{x},t)]_{ic} = [\phi^2(\vec{0},t)]_{ic}$ and a delta-correlated Gaussian distribution of initial conditions with strength Δ. The self-consistency equation is not singular at $t = 0$ since there is an underlying cut-off in the integration over k corresponding to the inverse of the lattice spacing, this implies that times should be translated as $t \to t + 1/\Lambda^2$ with $\Lambda = 1/a$ the lattice spacing.

Without giving all the details of the calculation, eq. (3.55), generalized to the finite T case, can be solved at all temperatures [33]. One finds that there exists a finite $T_c(d)$ and

Upper-critical quench

$$a(t) \to -\xi^{-2} \tag{3.56}$$

with ξ the equilibrium correlation length, and the 'mass' (in field theoretical terms) or the harmonic constant saturates to a finite value: $-k^2 + a(t) \to -k^2 - \xi^{-2}$.

Critical quench

$$a(t) \to -w/(2t) \quad \text{with} \quad w = 0 \;\; \text{for} \;\; d > 4 \;\; \text{and} \;\; w = (d-4)/2 \;\; \text{for} \;\; d < 4 \; . \tag{3.57}$$

The dynamics is trivial for $d > 4$ but there is critical coarsening in $d < 4$. z_{eq} equals 2 in agreement with the result from the ϵ expansion once evaluated at $N \to \infty$.

Sub-critical coarsening

In the long times limit in which the system tends to decrease its elastic and potential energies $[\,\phi^2(\vec{x},t)\,]_{ic}$ must converge to $\phi_0^2 \neq 0$ **below criticality** and this imposes $2\int_0^t dt'\, a(t') \simeq \frac{d}{2}\;\ln(t/t_0)$ with $t_0 = \pi/2\;(\Delta/\phi_0^2)^{2/d}$ at large times, *i.e.*

$$a(t) \simeq \frac{d}{4t} \qquad \text{for} \qquad t \gg t_0 \tag{3.58}$$

and the time-dependent contribution to the spring constant vanishes asymptotically. Knowing the long-time behavior of $a(t)$ implies that each mode $[\phi(\vec{k},t)]_{ic}$ with $\vec{k} \neq 0$ vanishes asymptotically but the $\vec{k} = 0$ mode grows as $t^{d/4}$. The growth of the $\vec{k} = 0$ reflects the domain growth process whereby all modulations tend to disappear and the configuration gets more and more uniform as time passes.

We focus now on two interesting cases: quenches to T_c and $T < T_c$. The asymptotic behavior of the space-time correlation function in the aging regime is

$$[\,\phi(\vec{x},t)\phi(\vec{x}',t')\,]_{ic} = \phi_0^2 \left[\frac{4tt'}{(t+t')^2}\right]^{d/4} \exp\left[-\frac{(\vec{x}-\vec{x}')^2}{4(t+t')}\right] \; , \tag{3.59}$$

for $t \geq t'$ for a quench to $T < T_c$ and

$$[\,\phi(\vec{x},t)\phi(\vec{x}',t')\,]_{ic} = \phi_0^2\, t'^{1-d/2} f(t/t')\ \exp\left[-\frac{(\vec{x}-\vec{x}')^2}{4(t+t')}\right]\ , \tag{3.60}$$

for a quench to T_c. We focus on $d < 4$. These expressions capture the main features of the domain growth process:

- In Fourier space all $k \neq 0$ modes have an exponential decay while the $k = 0$ one is fully massless asympotically and diffuses.
- In sub-critical quenches, for any finite and fixed $(\vec{x}-\vec{x}')$, in the long times limit the exponential factor approaches one and one obtaines a function of t'/t only.
- In critical quenches the two-time dependent prefactor is of the form expected from dynamic scaling.
- Due to the exponential factor, for fixed but very large time t and t' the correlation falls off to zero over a distance $|\vec{x}-\vec{x}'| \propto \sqrt{t+t'}$. This means that, at time t, the typical size of the regions in the states $\pm\phi_0$ is $R(t) \propto t^{1/2}$. This holds for critical and sub-critical quenches as well and it is a peculiar property of the large N $O(N)$ model that has $z_{eq} = z_d$.
- For fixed $|\vec{x}-\vec{x}'|$, the correlation always falls to zero over a time separation $t-t'$ *which is larger than* t'. This means that the time it takes to the system to decorrelate from its configuration at time t' is of the order of t' itself, $t_d \simeq t'$. The age of the system is the characteristic time-scale for the dynamical evolution: the older is the system, the slower is its dynamics. After a time of the order of the age of the system any point $\vec{x}$ will be swept by different domain walls and the correlation will be lost.
- In a critical quench the correlation always decays to zero due to the prefactor that goes as $t^{(2-d)/2}$ and vanishes in all $d > 2$. The aging curves have an envelope that approaches zero as a power law.
- In a sub-critical quench, for any finite and fixed $(\vec{x}-\vec{x}')$, in the long t' and t limit such that $t'/t \to 1$ the time dependence disappears and the correlation between two points converges to ϕ_0^2. This means that, typically, if one looks at a finite spatial region on a finite time-scale this region will be in one of the two states $\pm\phi_0$, i.e. within a domain.

Note that we have obtained the field and then computed correlations from the time-dependent configuration. We have not needed to compute the linear response. We shall see later that in other more complex glassy systems one cannot follow this simple route and one needs to know how the linear response behave. We refer to the reviews in [41] for detailed accounts on the behavior of the linear response in critical dynamics.

3.9 Nucleation and growth

In a **first-order** phase transition the equilibrium state of the system changes abruptly. Right at the transition the free-energies of the two states involved are identical and the transition is driven by lowering the free-energy as the new phase forms, see Fig. 22. The original phase remains meta-stable close to the transition. The nucleation of a sufficiently large bubble of the trully stable phase into the metastable one needs to be thermally activated to trigger the growth process [3]. The rate of the process can be very low or very fast depending on the height of the free-energy barrier between the two states and the ambient temperature.

Two types of nucleation are usually distinguished: homogeneous (occurying at the bulk of the meta-stable phase) and heterogeneous (driven by impurities or at the surface). The more intuitive examples of the former, on which we focus here, are the condensation of liquid droplets from vapour and the crystallization of a solid from the melt.

The **classical theory of nucleation** applies to cases in which the identification of the nucleous is easy. It is based on a number of assumptions that we now list. First, one associates a number of particles to the nucleous (although in some interesting cases this is not possible and a different approach is needed). Second, one assumes that there is no memory for the evolution of the number densities of clusters of a given size in time (concretely, a Markov master equation is used). Third, one assumes that clusters grow or shrink by attachment or loss of a single particle, that is to say, coallescence and fission of clusters are neglected. Thus, the length-scale over which the slow part of the dynamics takes place is the one of the critical droplet size, the first one to nucleate. Fourth, the transition rates satisfy detail balance and are independent of the droplet form. They just depend on the free-energy of the droplet with two terms: a contribution proportional to the droplet volume and the chemical potential difference between the stable and the metastable states, Δf, and a contribution proportional to the bubble surface that is equal to the surface area times the surface tension, σ, that is assumed to be the one of coexisting states in equilibrium - that is to say the energy of a flat domain wall induced by twisted boundary conditions. Fift, the bubble is taken to be spherical and thus dependent of a single parameter, the radius. Thus

$$\Delta F[R] = \sigma \; \Omega_{d-1} \; R^{d-1} - |\Delta f| \; \Omega_d \; R^d \tag{3.61}$$

for $d > 1$. Ω_d is the volume of the unit sphere in d dimensions. For small radii the surface term dominates and it is preferable to make the droplet disappear. In contrast, for large radii the bulk term dominates and the growth of the bubble is favoured by a decreasing free-energy. Thus the free-energy difference has a maximum at

$$\boxed{R^* = \frac{(d-1) \; \Omega_{d-1} \; \sigma}{d \; \Omega_d \; |\Delta f|} \propto \sigma |\Delta f|^{-1}} \tag{3.62}$$

and the system has to thermally surmount the barrier $\Delta F^* \equiv \Delta F[R^*]$. The Kramers escape theory, see Sect. 2.3, implies that the nucleation rate or the average number

of nucleations per unit of volume and time is suppressed by the Arrhenius factor

$$\boxed{r_A = t_A^{-1} \sim e^{-\beta \Delta F^*} \qquad \text{with} \qquad \Delta F^* = \frac{(d-1)^{d-1}}{d^d} \, \frac{\Omega_{d-1}^d}{\Omega_d^{d-1}} \, \frac{\sigma^d}{|\Delta f|^{d-1}}} \tag{3.63}$$

As expected, ΔF^* increases with increasing σ and/or $|\Delta f|^{-1}$ and r^{-1} vanishes for $T \to 0$ when thermal agitation is switched off. The implicit assumption is that the time to create randomly the critical droplet is much longer than the time involved in the subsequent growth. The relaxation of the entire system is thus expected to be given by the inverse probability of escape from the metastable well. The determination of the prefactor [that is ignored in eq. (3.63)] is a hard task.

3.10 Summary

In the table below we summarize the results describe above.

In short, critical and sub-critical coarsening occurs in models with conventional second order phase transitions (or for systems with first order phase transitions when one quenches well below the region of metastability). Close to the critical point the dynamics is characterized by **critical slowing down** with the relaxation time diverging as a power law of the distance to criticality. Growth of order is characterized by a growing length that depends on time as a power law at criticality and with a different power below the transition (in the absence of disorder). The dynamic mechanisms are well understood but quantitative results are hard to obtain since the equation to solve are highly non-linear and there is no small parameter to expand around.

In structural glasses the slowing down is not of power law type so such a simple coarsening description seems to be excluded for these systems.

For spin-glasses this modeling has been pushed by Bray, Moore, Fisher and Huse. It is not clear whether it is correct as no clearcut experimental evidence for the coarsening type of scaling has been presented yet.

	g_c	$g < g_c$
Order param.	0	$\neq 0$
Growing length	$R_c(t) \simeq \begin{array}{ll} t^{1/z_{eq}} & \text{clean} \\ \frac{t^{\frac{1}{2}}}{\ln^{\frac{1}{2}} \frac{t}{t_0}} & 2d \text{ xy} \\ ? & \text{disordered} \end{array}$	$R(t) \simeq \begin{array}{ll} t^{1/2} & \text{sc. NCOP} \\ t^{1/3} & \text{sc. COP} \\ \left(\ln \frac{t}{t_0}\right)^{\frac{1}{\psi}} & \text{dis.} \end{array}$
$V \simeq R^{D_F^V}(t)$	$D_F^V < D$	$D_F^V = D$
$S \simeq R^{D_F^S}(t)$	$D_F^S < D-1$	$D_F^S = D-1$
$C(r,t)$	$r^{2-d-\eta}\ f\left(\frac{r}{R_c(t)}\right)$	$C_{st}(r) + \ C_{ag}\left(\frac{r}{R_c(t)}\right)$
$C(t,t')$	$R_c^{2-d-\eta}(t-t')\ g\left(\frac{R_c(t')}{R_c(t)}\right)$	$C_{st}(t-t') + C_{ag}\left(\frac{R_c(t')}{R_c(t)}\right)$

Table 1: This table summarizes the behavior of growing structures and correlation functions in critical and sub-critical quenches. Interesting information is also contained in the behavior of the linear response function but we shall discuss it later.

4 Disordered systems: statics

No material is perfectly homogeneous: impurities of different kinds are distributed randomly throughout the samples.

A natural effect of disorder should be to lower the critical temperature. Much attention has been payed to the effect of **weak** disorder on phase transitions, that is to say, situations in which the nature of the ordered and disordered phases is not modified by the impurities but the critical phenomenon is. On the one hand, the critical exponents of second order phase transitions might be modified by disorder, on the other hand, disorder may smooth out the discontinuities of first order phase transitions rendering them of second order. **Strong** disorder instead changes the nature of the low-temperature phase and before discussing the critical phenomenon one needs to understand how to characterize the new ordered 'glassy' phase.

In this Section we shall discuss several types of *quenched* disorder and models that account for it. We shall also overview some of the theoretical methods used to deal with the static properties of models with quenched disorder, namely, scaling arguments and the droplet theory, mean-field equations, and the replica method.

4.1 Quenched and annealed disorder

First, one has to distinguish between **quenched** and **annealed** disorder. Imagine that one mixes some random impurities in a melt and then very slowly cools it down in such a way that the impurities and the host remain in thermal equilibrium. If one wants to study the statistical properties of the full system one has to compute the full partition function, summing over all configurations of original components and impurities. This is called annealed disorder. In the opposite case in which upon cooling the host and impurities do not equilibrate but the impurities remain blocked in random fixed positions, one talks about quenched disorder. Basically, the relaxation time associated with the diffusion of the impurities in the sample is so long that these remain trapped:

$$\tau_o \sim 10^{-12} - 10^{-15}\text{sec} \ll t_{obs} \sim 10^{4}\text{sec} \ll t_{\text{DIFF}} \ , \tag{4.1}$$

where τ_o is the microscopic time associated to the typical scale needed to reverse a spin.

The former case is easier to treat analytically but is less physically relevant. The latter is the one that leads to new phenomena and ideas that we shall discuss next.

4.2 Bond disorder: the case of spin-glasses

Spin-glasses are alloys in which magnetic impurities substitute the original atoms in positions randomly selected during the chemical preparation of the sample. The

interactions between the impurities are of RKKY type:

$$V_{\text{RKKY}} = -J \, \frac{\cos(2k_F r_{ij})}{r_{ij}^3} \, s_i s_j \tag{4.2}$$

with $r_{ij} = |\vec{r}_i - \vec{r}_j|$ the distance between them and s_i a spin variable that represents their magnetic moment. Clearly, the location of the impurities varies from sample to sample. The time-scale for diffusion of the magnetic impurities is much longer than the time-scale for spin flips. Thus, for all practical purposes the positions $\vec{r}_i$ can be associated to quenched random variables distributed according to a uniform probability distribution that in turn implies a probability distribution of the exchanges. This is **quenched disorder**.

4.2.1 Lack of homogeneity

It is clear that the presence of quench disorder, in the form of random interactions, fields, dilution, *etc.* **breaks spatial homogeneity** and renders single samples **heterogenous**. Homogeneity is recovered though, if one performs an average over all possible realizations of disorder, each weighted with its own probability.

4.2.2 Frustration

Depending on the value of the distance r_{ij} the numerator in eq. (4.2) can be positive or negative implying that both ferromagnetic and antiferromagnetic interactions exist. This leads to **frustration**, which means that some two-body interactions cannot be satisfied by any spin configuration. An example with four sites and four links is shown in Fig. 32-left, where we took three positive exchanges and one negative one all, for simplicity, with the same absolute value, J. Four configurations minimize the energy, $E_f = -2J$, but none of them satisfies the lower link. One can easily check that any closed loop such that the product of the interactions takes a negative sign is frustrated. Frustration naturally leads to a **higher energy** and a **larger degeneracy** of the number of ground states. This is again easy to grasp by comparing the number of ground states of the frustrated plaquette in Fig. 32-left to its unfrustrated counterpart shown on the central panel. Indeed, the energy and degeneracy of the ground state of the unfrustrated plaquette are $E_u = -4J$ and $n_u = 2$, respectively.

Frustration may also be due to pure geometrical constraints. The canonical example is an anti-ferromagnet on a triangular lattice in which each plaquette is frustrated, see Fig. 32-right. This is generically called **geometric frustration**.

In short, frustration arises when the geometry of the lattice and/or the nature of the interactions make impossible to simultaneously minimize the energy of all pair couplings between the spins. Any loop of connected spins is said to be frustrated if the product of the signs of connecting bonds is negative. In general, energy and entropy of the ground states increase due to frustration.

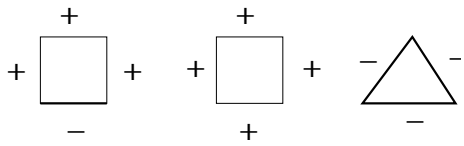

Figure 32: A frustrated (left) and an unfrustrated (center) square plaquette. A frustrated triangular plaquette (right).

4.2.3 Gauge invariance

The **gauge** transformation

$$s'_i = \tau_i s_i \ , \qquad J'_{ij} = \tau_i J_{ij} \tau_j \ , \qquad \text{with} \qquad \tau_i = \pm 1 \tag{4.3}$$

leaves the energy and the partition function of an Ising spin model with two-body interactions invariant:

$$E_J[\{s\}] = E_{J'}[\{s'\}] \qquad Z_J = Z_{J'} \ . \tag{4.4}$$

This invariance means that all thermodynamic quantities are independent of the particular choice of the quenched disordered interactions.

Whenever it exists a set of τ_is such that frustration can be eliminated from all loops in the model, the effects of disorder are less strong than in trully frustrated cases, see the example of the Mattis model in Sect. .

4.2.4 Self-averageness

If each sample is characterized by its own realization of the exchanges, should one expect a totally different behavior from sample to sample? Fortunately, many generic static and dynamic properties of spin-glasses (and other systems with quenched disorder) do not depend on the specific realization of the random couplings and are **self-averaging**. This means that the typical value is equal to the average over the disorder:

$$A_J^{typ} = [\, A_J \,] \tag{4.5}$$

in the thermodynamic limit. More precisely, in self-averaging quantities sample-to-sample fluctuations with respect to the mean value are expected to be $\mathrm{O}(N^{-a})$ with $a > 0$. Roughly, observables that involve summing over the entire volume of the system are expected to be self-averaging. In particular, the free-energy density of models with short-ranged interactions is expected to be self-averaging in this limit.

An example: the disordered Ising chain

The meaning of this property can be grasped from the solution of the random bond Ising chain defined by the energy function $E = -\sum_i J_i s_i s_{i+1}$ with spin variables

$s_i = \pm$, for $i = 1, \ldots, N$ and random bonds J_i independently taken from a probability distribution $P(J_i)$. For simplicity, we consider periodic boundary conditions. The disorder-dependent partition function reads

$$Z_J = \sum_{\{s_i = \pm 1\}} e^{\beta \sum_i J_i s_i s_{i+1}} \tag{4.6}$$

and this can be readily computed introducing the change of variables $\sigma_i \equiv s_i s_{i+1}$. One finds.

$$Z_J = \prod_i 2\cosh(\beta J_i) \qquad \Rightarrow \qquad -\beta F_J = \sum_i \ln\cosh(\beta J_i) + N \ln 2 \,. \tag{4.7}$$

The partition function is a *product* of *i.i.d.* random variables and it is itself a random variable with a log-normal distribution. The free-energy density instead is a *sum* of *i.i.d.* random variables and, using the central limit theorem, in the large N limit becomes a Gaussian random variable narrowly peaked at its maximum. The typical value, given by the maximum of the Gaussian distribution, coincides with the average, $\lim_{N\to\infty} f_J^{typ} - [\, f_J \,] = 0$.

General argument

A simple argument justifies the self-averageness of the free-energy density in generic finite dimensional systems with short-range interactions. Let us divide a, say, cubic system of volume $V = L^d$ in n subsystems, say also cubes, of volume $v = \ell^d$ with $V = nv$. If the interactions are short-ranged, the total free-energy is the sum of two terms, a contribution from the bulk of the subsystems and a contribution from the interfaces between the subsystems: $-\beta F_J = \ln Z_J = \ln \sum_{conf} e^{-\beta E_J(conf)} = \ln \sum_{conf} e^{-\beta E_J(bulk) - \beta E_J(surf)} \approx \ln \sum_{bulk} e^{-\beta E_J(bulk)} + \ln \sum_{surf} e^{-\beta E_J(surf)} = -\beta F_J^{bulk} - \beta F_J^{surf}$ (we neglected the contributions from the interaction between surface and bulk). If the interaction extends over a short distance σ and the linear size of the boxes is $\ell \gg \sigma$, the surface energy is negligible with respect to the bulk one and $-\beta F_J \approx \ln \sum_{bulk} e^{-\beta E_J(bulk)}$. In the thermodynamic limit, the disorder dependent free-energy is then a sum of $n = (L/\ell)^d$ random numbers, each one being the disorder dependent free-energy of the bulk of each subsystem: $-\beta F_J \approx \sum_{k=1}^{n} \ln \sum_{bulk_k} e^{-\beta E_J(bulk_k)}$. In the limit of a very large number of subsystems ($L \gg \ell$ or $n \gg 1$) the central limit theorem implies that the total free-energy is Gaussian distributed with the maximum reached at a value F_J^{typ} that coincides with the average over all realizations of the randomness $[\, F_J \,]$. Morever, the dispersion about the typical value vanishes in the large n limit, $\sigma_{F_J} / [\, F_J \,] \propto \sqrt{n}/n = n^{-1/2} \to 0$ in the large n limit. Similarly, $\sigma_{f_J}/[f_J] \sim O(n^{-1/2})$ where $f_J = F_J/N$ is the intensive free-energy. In a sufficiently large system the typical F_J is then very close to the averaged $[\, F_J \,]$ and one can compute the latter to understand the static properties of typical systems.

Lack of self-averageness in the correlation functions

Once one has $[F_J]$, one derives all disordered average thermal averages by taking derivatives of the disordered averaged free-energy with respect to sources introduced in the partition function. For example,

$$[\langle s_i \rangle] = -\left.\frac{\partial [F_J]}{\partial h_i}\right|_{h_i=0} , \tag{4.8}$$

$$[\langle s_i s_j \rangle - \langle s_i \rangle \langle s_j \rangle] = T \left.\frac{\partial [F_J]}{\partial h_i h_j}\right|_{h_i=0} , \tag{4.9}$$

with $E \to E - \sum_i h_i s_i$. Connected correlation functions, though, *are not* self-averaging quantities. This can be seen, again, studying the random bond Ising chain:

$$\langle s_i s_j \rangle_J - \langle s_i \rangle_J \langle s_j \rangle_J = Z_J^{-1} \frac{\partial}{\partial \beta J_i} \ldots \frac{\partial}{\partial \beta J_j} Z_J = \tanh(\beta J_i) \ldots \tanh(\beta J_j) , \tag{4.10}$$

where we used $\langle s_i \rangle = 0$ (valid for a distribution of random bonds with zero mean) and the dots indicate all sites on the chain between the ending points i and j. The last expression is a product of random variables and it is not equal to its average (4.9) – not even in the large separation limit $|\vec{r}_i - \vec{r}_j| \to \infty$.

Quenched vs. annealed averages

Take a case in which the partition function equals

$$Z = \begin{cases} e^{-\beta N} & p = 1/N \\ e^{-2\beta N} & p = (1 - 1/N) \end{cases} \tag{4.11}$$

The **annealed free-energy density**, f_a is

$$\begin{aligned} f_a &= (-\beta N)^{-1} \ln[\, Z \,] = (-\beta N)^{-1} \ln \left(N^{-1} e^{-\beta N} + (1 - N^{-1}) e^{-2\beta N} \right) \\ &= \lim_{N \gg 1} (-\beta N)^{-1} \ln N^{-1} e^{-\beta N} = 1 \end{aligned}$$

The **quenched free-energy density**, f_q, is

$$\begin{aligned} f_q &= (-\beta N)^{-1} [\, \ln Z \,] = (-\beta N)^{-1} \left(N^{-1} (-\beta N) + (1 - N^{-1})(-2\beta N) \right) \\ &= \lim_{N \gg 1} (-\beta N)^{-1} (-2\beta N) = 2 \end{aligned}$$

As the logarithm is a concave function, $[\, \ln Z \,] < \ln[\, Z \,]$ and then $f_a < f_q$.

4.3 Models with quenched disorder

4.3.1 Spin-glass models

In the early 70s Edwards and Anderson proposed a rather simple model that should capture the main features of spin-glasses. The interactions (4.2) decay with a

cubic power of the distance and hence they are relatively short-ranged. This suggests to put the spins on a regular cubic lattice model and to trade the randomness in the positions into random nearest neighbor exchanges taken from a Gaussian probability distribution:

$$E_{\rm EA} = -\sum_{\langle ij \rangle} J_{ij} s_i s_j \qquad \text{with} \qquad P(J_{ij}) = (2\pi\sigma^2)^{-\frac{1}{2}}\, e^{-\frac{J_{ij}^2}{2\sigma^2}} \; . \tag{4.12}$$

The precise form of the probability distribution of the exchanges is suppose not to be important, though some authors claim that there might be non-universality with respect to it.

A natural extension of the **EA model** in which all spins interact has been proposed by Sherrington and Kirkpatrick

$$E = -\sum_{i \neq j} J_{ij} s_i s_j - \sum_i h_i s_i \tag{4.13}$$

and it is called the **SK model**. The interaction strengths J_{ij} are taken from a Gaussian pdf and they scale with N in such a way that the thermodynamic is non-trivial:

$$P(J_{ij}) = (2\pi\sigma_N^2)^{-\frac{1}{2}}\, e^{-\frac{J_{ij}^2}{2\sigma_N^2}} \qquad \sigma_N^2 = \sigma^2 N \; . \tag{4.14}$$

The first two-moments of the exchange distribution are $[J_{ij}] = 0$ and $[J_{ij}^2] = J^2/(2N)$. This is a case for which a mean-field theory is expected to be exact.

A further extension of the EA model is called the *p* **spin model**

$$E = -\sum_{i_1 < \ldots < i_p} J_{i_1 \ldots i_p} s_{i_1} \ldots s_{i_p} - \sum_i h_i s_i \tag{4.15}$$

with $p \geq 3$. The sum can also be written as $\sum_{i_1 < i_2 < \ldots < i_p} = 1/p! \sum_{i_1 \neq i_2 \neq i_p}$. The exchanges are now taken from a Gaussian probability distribution

$$P(J_{ij}) = (2\pi\sigma_N^2)^{-\frac{1}{2}}\, e^{-\frac{J_{ij}^2}{2\sigma_N^2}} \qquad \sigma_N^2 = J^2 p!/(2N^{p-1}) \; . \tag{4.16}$$

with $[J_{i_1 \ldots i_p}] = 0$ and $[J_{i_1 \ldots i_p}^2] = \frac{J^2 p!}{2N^{p-1}}$. Indeed, an extensive free-energy is achieved by scaling $J_{i_1 \ldots i_p}$ with $N^{-(p-1)/2}$. This scaling can be justified as follows. The **local field** $h_i = 1/(p-1)! \sum_{i i_2 \neq i_p} J_{i i_2 \ldots i_p} m_{i_2} \ldots m_{i_p}$ should be of order one. At low temperatures the m_i's take plus and minus signs. In particular, we estimate the order of magnitude of this term by working at $T = 0$ and taking $m_i = \pm 1$ with probability $\frac{1}{2}$. In order to keep the discussion simple, let us take $p = 2$. In this case, if the strengths J_{ij}, are of order one, h_i is a sum of N *i.i.d.* random variables, with zero mean and unit variance[9], and h_i has zero mean and variance equal to N. Therefore,

[9] The calculation goes as follow: $\langle F_i \rangle = \sum_j J_{ij} \langle m_j \rangle = 0$ and $\langle F_i^2 \rangle = \sum_{jk} J_{ij} J_{ik} \langle m_j m_k \rangle = \sum_j J_{ij}^2$

one can argue that h_i is of order $\sqrt{N}$. To make it finite we then chose J_{ij} to be of order $1/\sqrt{N}$ or, in other words, we impose $[\, J_{ij}^2 \,] = J^2/(2N)$. The generalization to $p \geq 2$ is straightforward.

Cases that find an application in computer science are defined on random graphs with fixed or fluctuating finite connectivity. In the latter case one places the spins on the vertices of a graph with links between couples or groups of p spins chosen with a probability c. These are called **dilute spin-glasses**.

Exercise 7. Study the statics of the fully connected p-spin ferromagnet in which all coupling exchanges are equal to J. Distinguish the cases $p = 2$ from $p > 2$. What are the order of the phase transitions?

4.3.2 Random ferromagnets

Let us now discuss some, *a priori* simpler cases. An example is the Mattis random magnet in which the interaction strengths are given by

$$J_{i_1 \dots i_p} = \xi_{i_1} \dots \xi_{i_p} \qquad \text{with} \qquad \xi_j = \pm \quad \text{with} \quad p = 1/2 \,. \tag{4.17}$$

In this case a simple *gauge transformation*, $\eta_i \equiv \xi_i s_i$, allows one to transform the disordered model in a ferromagnet, showing that there was no true frustration in the system.

Random bond ferromagnets (RBFMs) are systems in which the strengths of the interactions are not all identical but their sign is always positive. One can imagine such a exchange as the sum of two terms:

$$J_{ij} = J + \delta J_{ij} \,, \qquad \text{with} \qquad \delta J_{ij} \qquad \text{small and random} \,. \tag{4.18}$$

There is no frustration in these systems either.

Models with site or link dilution are also interesting:

$$E_{\text{SITE DIL}} = -J \textstyle\sum_{\langle ij \rangle} s_i s_j \epsilon_i \epsilon_j \,, \qquad E_{\text{LINK DIL}} = -J \textstyle\sum_{\langle ij \rangle} s_i s_j \epsilon_{ij} \,, \qquad . \tag{4.19}$$

with $P(\epsilon_i = 0, 1) = p, 1-p$ in the first case and $P(\epsilon_{ij} = 0, 1) = p, 1-p$ in the second.

Link randomness is not the only type of disorder encountered experimentally. Random fields, that couple linearly to the magnetic moments, are also quite common; the classical model is the *ferromagnetic random field Ising model* (RFIM):

$$E_{\text{RFIM}} = -J \sum_{\langle ij \rangle} s_i s_j - \sum_i s_i h_i \qquad \text{with} \qquad P(h_i) = (2\pi\sigma^2)^{-\frac{1}{2}} \, e^{-\frac{h_i^2}{2\sigma^2}} \,. \tag{4.20}$$

The *dilute antiferromagnet in a uniform magnetic field* is believed to behave similarly to the ferromagnetic random field Ising model. Experimental realizations of the former are common and measurements have been performed in samples like $Rb_2Co_{0.7}Mg_{0.3}F_4$.

Note that the up-down Ising symmetry is preserved in models in which the impurities (the J_{ij}'s) couple to the local energy (and there is no applied external field) while it is not in models in which they couple to the local order parameter (as the RFIM).

The random fields give rise to many metastable states that modify the equilibrium and non-equilibrium behavior of the RFIM. In one dimension the RFIM does not order at all, in $d = 2$ there is strong evidence that the model is disordered even at zero temperature, in $d = 3$ it there is a finite temperature transition towards a ferromagnetic state. Whether there is a glassy phase near zero temperture and close to the critical point is still and open problem.

The RFIM at zero temperature has been proposed to yield a generic description of material cracking through a series of avalaches. In this problem one cracking domain triggers others, of which size, depends on the quenched disorder in the samples. In a random magnetic system this phenomenon corresponds to the variation of the magnetization in discrete steps as the external field is adiabatically increased (the time scale for an avalanche to take place is much shorter than the time-scale to modify the field) and it is accessed using Barkhausen noise experiments. Disorder is responsible for the jerky motion of the domain walls. The distribution of sizes and duration of the avalanches is found to decay with a power law tail cut-off at a given size. The value of the cut-off size depends on the strength of the random field and it moves to infinity at the critical point.

4.3.3 Random manifolds

Once again, disorder is not only present in magnetic systems. An example that has received much attention is the so-called **random manifold**. This is a d dimensional **directed** elastic manifold moving in an embedding $N + d$ dimensional space under the effect of a quenched random potential. The simplest case with $d = 0$ corresponds to a particle moving in an embedding space with N dimensions. If, for instance $N = 1$, the particle moves on a line, if $N = 2$ it moves on a plane and so on and so forth. If $d = 1$ one has a line that can represent a domain wall, a polymer, a vortex line, *etc.* The fact that the line is directed means it has a preferred direction, in particular, it does not have overhangs. If the line moves in a plane, the embedding space has $(N = 1) + (d = 1)$ dimensions. One usually describes the system with an N-dimensional coordinate, $\vec{\phi}$, that locates in the transverse space each point on the manifold, represented by the internal d-dimensional coordinate $\vec{x}$,

The elastic energy is $E_{elas} = \gamma \int d^d x \, \sqrt{1 + (\nabla \phi(\vec{x}))^2}$ with γ the deformation cost of a unit surface. Assuming the deformaiton is small one can linearize this expression and get, upto an additive constant, $E_{elas} = \frac{\gamma}{2} \int d^d x \, (\nabla \phi(\vec{x}))^2$.

Disorder is introduced in the form of a random potential energy at each point in the $N + d$ dimensional space. The manifold feels, then a potential $V(\vec{\phi}(\vec{x}), \vec{x})$ characterized by its pdf. If the random potential is the result of a large number of impurities, the central limit theorem implies that its probability density is Gaussian.

Just by shifting the energy scale one can set its average to zero, $[\,V\,]=0$. As for its correlations, one typically assumes, for simplicity, that they exist in the transverse direction only:

$$[\,V(\vec{\phi}(\vec{x}),\vec{x})V(\vec{\phi}'(\vec{x}'),\vec{x}')\,]=\delta^d(\vec{x}-\vec{x}')\mathcal{V}(\vec{\phi},\vec{\phi}')\;. \tag{4.21}$$

If one further assumes that there is a statistical isotropy and translational invariance of the correlations, $\mathcal{V}(\vec{\phi},\vec{\phi}')=W/\Delta^2\;\mathcal{V}(|\vec{\phi}-\vec{\phi}'|/\Delta)$ with Δ a correlation length and $(W\Delta^{d-2})^{1/2}$ the strength of the disorder. The disorder can now be of two types: short-ranged if $\mathcal{V}$ falls to zero at infinity sufficiently rapidly and long-range if it either grows with distance or has a slow decay to zero. An example involving both cases is given by the power law $\mathcal{V}(z)=(\theta+z)^{-\gamma}$ where θ is a short distance cut-off and γ controls the range of the correlations with $\gamma>1$ being short-ranged and $\gamma<1$ being long-ranged.

The random manifold model is then

$$H=\int d^dx\left[\frac{\gamma}{2}\left(\nabla\phi(\vec{x})\right)^2+V(\vec{\phi}(\vec{x}),\vec{x})\right]\;. \tag{4.22}$$

This model also describes directed domain walls in random systems. One can derive it in the long length-scales limit by taking the continuum limit of the pure Ising part (that leads to the elastic term) and the random part (that leads to the second disordered potential). In the pure Ising model the second term is a constant that can be set to zero while the first one implies that the ground state is a perfectly flat wall, as expected. In cases with quenched disorder, the long-ranged and short-ranged random potentials mimic cases in which the interfaces are attracted by pinning centers ('random field' type) or the phases are attracted by disorder ('random bond' type), respectively. For instance, random bond disorder is typically described by a Gaussian pdf with zero mean and delta-correlated $[V(\vec{\phi}(\vec{x}),\vec{x}),V(\vec{\phi}'(\vec{x}'),\vec{x}')]=W\Delta^{d-2}\;\delta^d(\vec{x}-\vec{x}')\delta(\vec{\phi}-\vec{\phi}')$.

4.4 The spin-glass transition

Let us now discuss a problem in which disorder is so strong as to modify the nature of the low temperature phase. If this is so, one needs to define a new order parameter, capable of identifying order in this phase.

4.4.1 The simplest order parameter

The spin-glass equilibrium phase is one in which spins "freeze" in randomly-looking configurations. In finite dimensions these configurations are spatially irregular. A snapshot looks statistical identical to a high temperature paramagnetic configuration in which spins point in both directions. However, while at high temperatures the spins flip rapidly and another snapshot taken immediately after would look completely

different from the previous one, at low temperatures two snapshots taken at close times are highly correlated.

In a spin-glass state the local magnetization is expected to take a non-zero value, $m_i = \langle\, s_i \,\rangle \neq 0$, where the average is interpreted in the restricted sense introduced in the discussion of ferromagnets, that we shall call here within a **pure state** (the notion of a pure state will be made more precise below). Instead, the total magnetization density, $m = N^{-1} \sum_{i=1}^{N} m_i$, vanishes since one expects to have as many averaged local magnetization pointing up ($m_i > 0$) as spins pointing down ($m_i < 0$) with each possible value of $|m_i|$. Thus, the *total magnetization*, m, of a spin-glass vanishes at all temperatures and it is not a good order parameter.

The spin-glass transition is characterized by a finite peak in the linear magnetic susceptibility and a diverging non-linear magnetic susceptibility. Let us discuss the former first and show how it yields evidence for the freezing of the local magnetic moments. For a generic magnetic model such that the magnetic field couples linearly to the Ising spin, $E \to E - \sum_i h_i s_i$, the linear susceptibility is related, via the static *fluctuation-dissipation theorem* to the correlations of the fluctuations of the magnetization:

$$\chi_{ij} \equiv \left. \frac{\partial \langle\, s_i \,\rangle_h}{\partial h_j} \right|_{h=0} = \beta \, \langle \, (s_i - \langle\, s_i \,\rangle)(s_j - \langle\, s_j \,\rangle) \, \rangle \; . \tag{4.23}$$

The averages in the rhs are taken without perturbing field. This relation is proven by using the definition of $\langle\, s_i \,\rangle_h$ and simply computing the derivative with respect to h_j. In particular,

$$\chi_{ii} = \beta \, \langle \, (s_i - \langle\, s_i \,\rangle)^2 \, \rangle = \beta \left(1 - m_i^2\right) \geq 0 \; , \tag{4.24}$$

with $m_i = \langle\, s_i \,\rangle$. The total susceptibility measured experimentally is $\chi \equiv N^{-1} \sum_{ij} \chi_{ij}$. On the experimental side we do not expect to see $O(1)$ sample-to-sample fluctuations in this global quantity. On the analytical side one can use a similar argument to the one presented in Sect. to argue that χ should be self-averaging (it is a sum over the entire volume of site-dependent terms). Thus, the experimentally observed susceptibility of sufficiently large samples should be given by

$$\chi = [\, \chi \,] = N^{-1} \sum_{ij} [\, \chi_{ij} \,] \approx N^{-1} \sum_{i} [\, \chi_{ii} \,] = N^{-1} \sum_{i} \beta \left(1 - [\, m_i^2 \,]\right) \; , \tag{4.25}$$

since we can expect that cross-terms will be subleading in the large N limit under the disorder average (note that χ_{ij} can take negative values). The fall of χ at low temperatures with respect to its value at T_c, *i.e.* the *cusp* observed experimentally, signals the freezing of the *local magnetizations*, m_i, in the non-zero values that are more favourable thermodynamically. Note that this argument is based on the assumption that the measurement is done in equilibrium.

Thus, the natural and simpler **global order parameter** that characterizes the spin-glass transition is

$$q \equiv N^{-1} \sum_{i} [\, m_i^2 \,] \tag{4.26}$$

as proposed in the seminal 1975 Edwards-Anderson paper. q vanishes in the high temperature phase since all m_i are zero but it does not in the low temperature phase since the square power takes care of the different signs. Averaging over disorder eliminates the site dependence. Thus, q is also given by

$$q = [\, m_i^2 \,] \,. \tag{4.27}$$

These definitions, natural as they seem at a first glance, hide a subtle distinction that we discuss below.

4.4.2 Pure states and more subtle order parameters

Let us *keep disorder fixed* and imagine that there remain more than two pure or equilibrium states in the selected sample. A factor of two takes into account the spin reversal symmetry. Later we shall consider half the phase space, getting rid of this 'trivial' symmetry. Consider the disorder-dependent quantity

$$q_J = N^{-1} \sum_i m_i^2 \tag{4.28}$$

where the m_i depend upon the realization of the exchanges. Then, two possibilities for the statistical average in $m_i = \langle s_i \rangle$ have to be distinguished:

Restricted averages

If we interpret the statistical average in the same restricted sense as the one discussed in the paramagnetic - ferromagnetic transition of the usual Ising model, *i.e.* under a pinning field that selects *one* chosen pure state, in (4.28) we define a disorder and pure state dependent **Edwards-Anderson parameter**,

$$q^\alpha_{J\,ea} = N^{-1} \sum_i^N (m_i^\alpha)^2 \,, \tag{4.29}$$

where we label α the selected pure state. Although $q^\alpha_{J\,ea}$ could depend on α it turns out that in all known cases it does not and the α label is superfluos.

In addition, $q^\alpha_{J\,ea}$ could fluctuate from sample to sample since the individual m_i do. It turns out that in the thermodynamic limit $q_{J\,ea}$ does not fluctuate. With this in mind we shall later use

$$q_{ea} = q^\alpha_{ea} = q_J{}^\alpha_{ea} \tag{4.30}$$

for the **intra-state average**. This is the interpretation of the order parameter proposed by Edwards-Anderson who did not take into account the possibility that is discussed next.

In the clean Ising model, had we taken into account all the phase space, $\alpha = 1, 2$ and $m_i^\alpha = \langle s_i \rangle_\alpha$ with $m_i^{(1)} = -m_i^{(2)} = m > 0$. If we kept only half phase space $\alpha = 1$ and $m_i = m > 0$, say. The dependence on J does not exist in this case from the

very definition of the model. In the RBIM the J and i-dependences remain but there are still only two states to be considered. In the Potts model with q equilibrium FM states there are q possible values for α and consequently m_i^α.

Full statistical averages

If, instead, the statistical average in m_i runs over *all* possible equilibrium states (and we imagine there are more than one even if we consider only half the phase space, that is to say, if we eliminate spin-reversal) the quantity (4.28) has non-trivial contributions from overlaps between different states.

Imagine each state has a probability weight w_α^J. Then

$$m_i = \sum_\alpha w_J^\alpha m_i^\alpha \tag{4.31}$$

and

$$q_J = \frac{1}{N}\sum_i m_i^2 = \frac{1}{N}\sum_{i=1}^N \left(\sum_\alpha w_\alpha^J m_i^\alpha\right)^2 = \sum_{\alpha\beta} w_\alpha^J w_\beta^J \frac{1}{N}\sum_{i=1}^N m_i^\alpha m_i^\beta \,. \tag{4.32}$$

A number of examples will clarify what we mean here. In the ferromagnetic phase of the clean or dirty Ising models one has only two pure states with $w_1 = w_2 = 1/2$ and the fully averaged m_i is $m_i = 1/2\ \langle s_i\rangle_1 + 1/2\ \langle s_i\rangle_2 = 0$. If one considers half the phase space, where spin-reversal is not allowed, then $w_1 = 1$, $m_i = \langle s_i\rangle$ and one does not see any difference between the intra-state and the fully averaged m_i. As for the q parameters, considering the full phase space $q_{ea}^{(1)} = q_{ea}^{(2)} = m^2$, while $q = 0$. Instead, taking into account half the phase space $q = q_{ea} = m^2$, and q_{ea} and q are identical order parameters in this case. In the Potts model with more than two equilibrium states the intra-state and fully averaged local magnetizations are not identical.

In the ferromagnetic modes discussed in the previous paragraph the Edwards-Anderson order parameter takes the same value in each equilibrium state. This is also the case in spin-glass models, $q_J{}_{ea}^\alpha$ independently of there being only two (as in the usual ferromagnetic phase) or more (as we shall see appearing in fully-connected spin-glass models). Therefore it does not allow us to distinguish between the two-state and the many-state scenarii. Instead, q_J does.

Having defined a disorder-dependent order parameter, q_J, and its disorder average, q, that explains the decay of the susceptibility below T_c, we still have to study whether this order parameter characterises the low temperature phase completely. It will turn out that the knowledge of q is not enough, at least in fully-connected and dilute spin-glass models. Indeed, one needs to consider the probability distribution of the fluctuating q_J quantity, $P(q_J)$. The more pertinent definition of an order parameter as being given by such a probability distribution allows one to distinguish between the simple, two-state, and the many-state scenarii.

In practice, a way to compute the **probability distribution of the order parameter** is by using an **overlap** – or correlation – between two spin configurations,

say $\{s_i\}$ and $\{\sigma_i\}$, defined as

$$q^J_{s\sigma} = N^{-1} \sum_i \langle\ s_i \sigma_i\ \rangle \tag{4.33}$$

where $\langle\ \ldots\ \rangle$ is an unrestricted thermal average. $q^J_{s\sigma}$ takes values between -1 and 1. It equals one if $\{s_i\}$ and $\{\sigma_i\}$ differ in a number of spins that is smaller than $O(N)$, it equals -1 when the two configurations are totally anticorrelated – with the same proviso concerning a number of spins that is not $O(N)$ – and it equals zero when $\{s_i\}$ and $\{\sigma_i\}$ are completely uncorrelated. Note that the *self-overlap* of a configuration with itself is identically one for Ising spins. Other values are also possible. A related definition is the one of the **Hamming distance**:

$$d^J_{s\sigma} = N^{-1} \sum_{i=1}^{N} \langle\ (s_i - \sigma_i)^2\ \rangle = 2(1 - q^J_{s\sigma})\ . \tag{4.34}$$

The overlap can be computed by running a Monte Carlo simulation, equilibrating a sample and recording many equilibrium configurations. With them one computes the overlap and should find a histogram with two peaks at q_{ea} and $-q_{ea}$ (the values of the overlap when the two configurations fall in the same pure state or in the sign reversed ones) and, in cases with many different pure states, other peaks at other values of $q^J_{s\sigma}$. This is observed in the SK model. Note that $q^J_{s\sigma}$ is related to the q definition above.

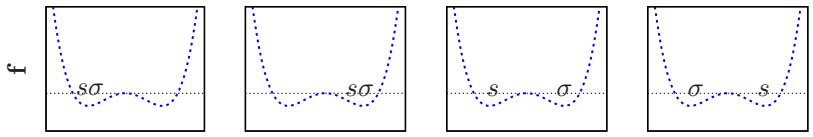

Figure 33: The overlap between two equilibrium configurations in a FM system.

4.4.3 Pinning fields

In the discussion of the ferromagnetic phase transition one establishes that one of the two equilibrium states, related by spin reversal symmetry, is chosen by a small pinning field that is taken to zero after the thermodynamic limit, $\lim_{h\to 0} \lim_{N\to\infty}$.

In a problem with quenched disorder it is no longer feasible to choose and apply a magnetic field that is correlated to the statistical averaged local magnetization in a single pure state since this configuration is not known! Moreover, the remanent

magnetic field that might be left in any experience will certainly not be correlated with any special pure state of the system at hand.

Which is then the statistical average relevant to describe experiments? We shall come back to this point below.

4.4.4 Divergent susceptibility

In a pure magnetic system with a second-order phase transition the susceptibility of the order parameter to a field that couples linearly to it diverges when approaching the transition from both sides. In a paramagnet, one induces a local magnetization with a local field

$$m_i = \langle\, s_i \,\rangle = \sum_{j=1}^{N} \chi_{ij} h_j \tag{4.35}$$

with χ_{ij} the linear susceptibilities, the magnetic energy given by $E = E_0 - \sum_i s_i h_i$, and the field set to zero at the end of the calculation. Using this expression, the order parameter in the high temperature phase becomes

$$q = q_{ea} = \frac{1}{N} \sum_{i=1}^{N} [\, m_i^2 \,] = \frac{1}{N} \sum_{i=1}^{N} \sum_{j=1}^{N} \sum_{k=1}^{N} [\, \chi_{ij} \chi_{ik} h_j h_k \,] \tag{4.36}$$

If the applied fields are random and taken from a probability distribution such that $\overline{h_j h_k} = \sigma^2 \delta_{jk}$ one can replace $h_j h_k$ by $\sigma^2 \delta_{jk}$ and obtain

$$q = \frac{1}{N} \sum_{i=1}^{N} [\, m_i^2 \,] = \frac{1}{N} \sum_{i=1}^{N} \sum_{j=1}^{N} [\, \chi_{ij}^2 \,]\, \sigma^2 \equiv \chi_{SG}\, \sigma^2 \,. \tag{4.37}$$

σ^2 acts as a field conjugated to the order parameter. (One can also argue that a uniform field looks random to a spin-glass sample and therefore the same result holds. It is more natural though to use a trully random field since a uniform one induces a net magnetization in the sample.) The **spin-glass susceptibility** is then defined as

$$\chi_{SG} \equiv \frac{1}{N} \sum_{ij} [\, \chi_{ij}^2 \,] = \frac{\beta^2}{N} \sum_{ij} [\, (\langle\, s_i s_j \,\rangle - \langle\, s_i \,\rangle \langle\, s_j \,\rangle)^2 \,] = \frac{\beta^2}{N} \sum_{ij} [\, \langle\, s_i s_j \,\rangle^2 \,]$$

in the high T phase and one finds that it diverges as $T \to T_c^+$ as expected in a second-order phase transition. (Note that there is no cancelation of crossed terms because of the square.) Indeed, the divergence of χ_{SG} is related to the divergence of the non-linear magnetic susceptibility that is measurable experimentally and numerically. An expansion of the total mangnetization in powers of a uniform field h acting as $E \to E - h \sum_i s_i$ is

$$M_h = \chi h - \frac{\chi^{(3)}}{6} h^3 + \dots \,, \tag{4.38}$$

and the first non-linear susceptibility is then given by

$$-\chi^{(3)} \equiv \left.\frac{\partial^3 M_h}{\partial h^3}\right|_{h=0} = -\beta^{-1} \left.\frac{\partial^4 \ln Z_h}{\partial h^4}\right|_{h=0} = -\frac{\beta^3 N}{3} \left\langle \left(\sum_i s_i\right)^4 \right\rangle_c \tag{4.39}$$

with the subindex c indicating that the quartic correlation function is connected. Above T_c, $m_i = 0$ at zero field,

$$\chi^{(3)} = \beta^3 \sum_{ijkl} \left(\langle\, s_i s_j s_k s_l \,\rangle - 3\langle\, s_i s_j \,\rangle\langle\, s_k s_l \,\rangle\right) = \frac{\beta^3}{N} 3 \left(4N - 6\sum_{ij} \langle\, s_i s_j \,\rangle^2\right) ,$$

and one can identify χ_{SG} when $i = k$ and $j = l$ plus many other terms that we assume are finite. Then,

$$\chi^{(3)} = \beta(\chi_{SG} - \frac{2}{3}\beta^2) \, . \tag{4.40}$$

This quantity can be accessed experimentally. A careful experimental measurement of $\chi^{(3)}$, $\chi^{(5)}$ and $\chi^{(7)}$ done by L. Lévy demonstrated that all these susceptibilities diverge at T_c.

4.4.5 Calorimetry

No cusp in the specific heat of spin-glasses is seen experimentally. Since one expects a second order phase transition this means that the divergence of this quantity must be very weak.

4.4.6 Critical scaling

Having identified an order parameter, the linear and the non-linear susceptibility one can now check whether there is a static phase transition and, if it is of second order, whether the usual scaling laws apply. Many experiments have been devoted to this task. It is by now quite accepted that Ising spin-glasses in $3d$ have a conventional second order phase transition. Still, the exponents are difficult to obtain and there is no real consensus about their values. There are two main reasons for this: one is that as T_c is approached the dynamics becomes so slow that equilibrium measurements cannot really be done. Critical data are thus restricted to $T > T_c$. The other reason is that the actual value of T_c is difficult to determine and the value used has an important influence on the critical exponents. Possibly, the most used technique to determine the exponents is *via* the scaling relation for the non-linear susceptibility:

$$\chi_{nl} = t^\beta f\left(\frac{h^2}{t^{\gamma+\beta}}\right) \tag{4.41}$$

d	β	γ	δ	α	ν	η
∞	1	1	2	-1	$\frac{1}{2}$	0
3	0.5	4	9			

Table 2: Critical exponents in the Ising spin-glass transitions.

with $t = |T - T_c|/T_c$ and one finds, approximately, the values given in Table 2.

4.5 The TAP approach

Disordered models have quenched random interactions. Due to the fluctuating values of the exchanges, one expects that the equilibrium configurations be such that *in each equilibrium state* the spins freeze in different directions. The local averaged magnetizations need not be identical, on the contrary one expects $\langle\, s_i \,\rangle = m_i$ and, if many states exist, each of them can be identified by the vector $(m_1, \ldots, m_N)$.

One may try to use the naive mean-field equations (5.2) to characterize the low temperature properties of these models at *fixed quenched disorder* and determine then the different $(m_1, \ldots, m_N)$ values. It has been shown by Thouless-Anderson-Palmer (TAP) [**?**, **?**] that these equations are not completely correct even in the fully-connected disordered case: a term which is called the Onsager reaction term is missing. This term represents the reaction of the spin i: the magnetization of the spin i produces a field $h'_j = J_{ji}m_i = J_{ij}m_i$ on spin j; this field induces a magnetization $m_j = \chi_{jj}h'_j = \chi_{jj}J_{ij}m_i$ on the spin j and this in turn produces a mean-field $h'_i = J_{ij}m_j = J_{ij}\chi_{jj}J_{ij}m_i = \chi_{jj}J_{ij}^2 m_i$ on the site i. The equilibrium fluctuatio-dissipation relation between susceptibilities and connected correlations implies $\chi_{jj} = \beta\, \langle\, (s_j - \langle\, s_j \,\rangle)^2 \,\rangle = \beta(1 - m_j^2)$ and one then has $h_i = \beta(1 - m_j^2)J_{ij}^2 m_i$. The idea of Onsager – or *cavity method* – is that one has to study the ordering of the spin i in the absence of its own effect on the rest of the system. Thus, the field h'_i has to be subtracted from the mean-field created by the other spins in the sample, *i.e.* $h_i^{corr} = \sum_j J_{ij}m_j + h_i - \beta m_i \sum_j J_{ij}^2(1 - m_j^2)$ where h_i is the external field.

The generalization of this argument to p spin interactions is not so straightforward. The TAP equations for p-spin fully connected models read

$$m_i = \tanh\left[\beta\left(\sum_{i_2\neq\ldots\neq i_p} \frac{1}{(p-1)!} J_{ii_2\ldots i_p} m_{i_2}\ldots m_{i_p} + \beta m_i J_{ii_2\ldots i_p}^2 (1 - m_{i_2}^2)\ldots(1 - m_{i_p}^2) + h_i\right)\right] . \tag{4.42}$$

the first contribution to the internal field is proportional to $J_{i1_2\ldots i_p} \sim N^{-(p-1)/2}$

and once the $p-1$ sums performed it is of order one. The reaction term instead is proportional to $J^2_{ii_2\ldots i_p}$ and, again, a simple power counting shows that it is $O(1)$. Thus, In disordered systems the reaction term is of the same order of the usual mean-field; a correct mean-field description has to include it. In the ferromagnetic case this term can be neglected since it is subleading in N. Using the fact that there is a sum over a very large number of elements, $J^2_{i_1\ldots i_p}$ can be replaced by its site-independent variance $[J^2_{i_1\ldots i_p}] = p!J^2/(2N^{p-1})$ in the last term in (4.42). Introducing the Edwards-Anderson parameter $q_{ea} = N^{-1}\sum_{i=1} m_i^2$ (note that we study the system in one pure state) the TAP equations follow:

$$m_i = \tanh\left(\frac{\beta}{(p-1)!}\sum_{i_2\neq\ldots\neq i_p} J_{ii_2\ldots i_p} m_{i_2}\ldots m_{i_p} + \beta h_i - \frac{\beta^2 J^2 p}{2} m_i (1-q_{ea})^{p-1}\right) . \tag{4.43}$$

The argument leading to the Onsager reaction term can be generalized to include the combined effect of the magnetization of spin i on a sequence of spins in the sample, *i.e.* the effect on i on j and then on k that comes back to i. These higher order terms are indeed negligible only if the series of all higher order effects does not diverge. The ensuing condition is $1 > \beta^2\left(1 - 2q_{ea} + N^{-1}\sum_i m_i^4\right)$.

The importance of the reaction term becomes clear from the analysis of the linearized equations, expected to describe the second order critical behavior for the SK model ($p = 2$) in the absence of an applied field. The TAP equations become $m_i \sim \beta(\sum_j J_{ij} m_j - \beta J^2 m_i + h_i)$. A change of basis to the one in which the J_{ij} matrix is diagonal leads to $m_\lambda \sim \beta(\lambda - \beta J^2)m_\lambda + \beta h_\lambda$. The staggered susceptibility then reads

$$\chi_\lambda \equiv \left.\frac{\partial m_\lambda}{\partial h_\lambda}\right|_{h=0} = \beta\ \left(1 - 2\beta J_\lambda + (\beta J)^2\right)^{-1} . \tag{4.44}$$

The staggered susceptibility for the largest eigenvalue of an interaction matrix in the Gaussian ensemble, $J_\lambda^{max} = 2J$, diverges at $\beta_c J = 1$. Note that without the reaction term the divergence appears at the inexact value $T^* = 2T_c$ (see Sect. for the replica solution of the SK model).

The TAP equations are the extremization conditions on the TAP free-energy density:

$$\begin{aligned} f(\{m_i\}) \;=\; & -\frac{1}{p!}\sum_{i_1\neq\ldots\neq i_p} J_{i_1\ldots i_p} m_{i_1}\ldots m_{i_p} \\ & -\frac{\beta}{4p}\sum_{i_1\neq\ldots\neq i_p} J^2_{i_1\ldots i_p}(1-m^2_{i_1})\ldots(1-m^2_{i_p}) \\ & -\sum_i h_i m_i + T\sum_{i=1}^N\left[\frac{1+m_i}{2}\ln\frac{1+m_i}{2} + \frac{1-m_i}{2}\ln\frac{1-m_i}{2}\right] . \end{aligned} \tag{4.45}$$

The free-energy density as a function of the local magnetizations m_i defines what is usually called *the free-energy landscape*. Note that this function depends on $N \gg 1$

variables, m_i, and these are not necessarily identical in the disordered case in which the interactions between different groups of spins are different. The stability properties of each extreme $\{m_l^*\}$ are given by the eigenvalues of the Hessian matrix

$$\mathcal{H}_{ij} \equiv \left. \frac{\partial f(\{m_k\})}{\partial m_i \partial m_j} \right|_{\{m_l^*\}} . \tag{4.46}$$

The number of positive, negative and vanishing eigenvalues determine then the number of directions in which the extreme is a minimum, a maximum or marginal. The sets $\{m_l^*\}$ for which $f(\{m_l^*\})$ is the absolute minima yield a first definition of equilibrium or pure states.

The TAP equations apply to $\{m_i\}$ and not to the configurations $\{s_i\}$. The values of the $\{m_i\}$ are determined as minima of the TAP free-energy density, $f(\{m_i\})$, and they not need to be the same as those of the energy, $H(\{s_i\})$, a confusion sometimes encountered in the glassy literature. The coincidence of the two can only occur at $T \to 0$.

4.5.1 The complexity or configurational entropy

There are a number of interesting questions about the extreme of the TAP free-energy landscape, or even its simpler version in which the Onsager term is neglected, that help us understanding the static behavior of disordered systems:

- For a given temperature, T, how many solutions to the mean-field equations exist? The number of solutions can be calculated using

$$\mathcal{N}_J = \prod_i \int_{-1}^{1} dm_i \, \delta(m_i - m_i^*) = \prod_i \int_{-1}^{1} dm_i \, \delta(\mathrm{eq}_i) \left| \det \frac{\partial \mathrm{eq}_i}{\partial m_j} \right| . \tag{4.47}$$

  $\{m_i^*\}$ are the solutions to the TAP equations that we write as $\{\mathrm{eq}_i = 0\}$. The last factor is the normalization of the delta function after the change of variables, it ensures that we count one each time the integration variables touch a solution to the TAP equations independently of its stability properties.
  We define the *complexity* or the *configurational entropy* as the logarithm of the number of solutions at temperature T divided by N:

$$\Sigma_J(T) \equiv N^{-1} \ln \mathcal{N}_J(T) . \tag{4.48}$$

  The normalization with N suggests that the number of solutions is actually an exponential of N. We shall come back to this very important point below.
- Does $\mathcal{N}_J(T)$ dependend on T and does it change abruptly at particular values of T that may or may not coincide with static and dynamic phase transitions?
- One can define a free-energy level dependent complexity

$$\Sigma_J(f, T) \equiv N^{-1} \ln \mathcal{N}_J(f, T) \tag{4.49}$$

where $\mathcal{N}_J(f,T)$ is the number solutions in the interval $[f, f+df]$ at temperature T.

- From these solutions, one can identify the minima as well as all saddles of different type, *i.e.* with different indeces K. These are different kinds to metastable states. Geometry constrains the number of metastable states to satisfy Morse theorem that states $\sum_{l=1}^{\mathcal{N}}(-1)^{\kappa_l}=1$, where κ_l is the number of negative eigenvalues of the Hessian evaluated at the solution l, for any continuous and well-behaved function diverging at infinity in all directions.
  One can then count the number of solutions to the TAP equations of each index, $\mathcal{N}_J(K,T)$, and define the corresponding complexity

$$\Sigma_J(K,T) \equiv N^{-1}\ln \mathcal{N}_J(K,T)\;, \tag{4.50}$$

  or even work at fixed free-energy density

$$\Sigma_J(K,f,T) \equiv N^{-1}\ln \mathcal{N}_J(K,f,T)\;. \tag{4.51}$$

  Even more interestingly, one can analyse how are the free-energy densities of different saddles are organized. For instance, one can check whether all maxima are much higher in free-energy density than minima, *etc.*
- What is the barrier, $\Delta f = f_1 - f_0$, between ground states and first excited states? How does this barrier scale with the actual free-energy difference, Δf between these states? The answer to this question is necessary to estimate the nucleation radius for the reversal of a droplet under an applied field, for instance.

The definitions of complexity given above are disorder-dependent. One might then expect that the complexity will show sample-to-sample fluctuations and be characterized by a probability distribution. The *quenched complexity*, $\Sigma^{quenched}$, is then the most likely value of Σ_J, it is defined through $\max P(\Sigma_J) = P(\Sigma^{quenched})$. In practice, this is very difficult to compute. Most analytic results concern the *annealed* complexity

$$\Sigma_{ann} \equiv N^{-1}\ln\left[\,\mathcal{N}_J\,\right] = N^{-1}\ln[\,e^{N\Sigma_J}\,]\;. \tag{4.52}$$

One can show that the annealed complexity is smaller or equal than the quenched one.

4.5.2 Weighted averages

Having identified many solutions to the TAP equations in the low-T phase one needs to determine now how to compute statistical averages. A natural proposal is to give a probability weight to each solution, w_α, and to use it to average the value the observable of interest:

$$\langle\, O\,\rangle = \sum_\alpha\; w_\alpha^J\; O_\alpha \tag{4.53}$$

where α labels the TAP solutions, $O_\alpha = O(\{m_i^\alpha\})$ is the value that the observable O takes in the TAP solution α, and w_α^J are their statistical weights, satisfying the normalization condition $\sum_\alpha w_\alpha^J = 1$. Two examples can illustrate the meaning of this average. In a spin-glass problem, if $O = s_i$, then $O_\alpha = m_i^\alpha$. In an Ising model in its ferromagnetic phase, if $O = s_i$, then $O_\alpha = m_i^\alpha = \pm m$ and $w_\alpha = 1/2$. Within the TAP approach one proposes

$$w_\alpha^J = \frac{e^{-\beta F_\alpha^J}}{\sum_\gamma e^{-\beta F_\gamma^J}} \tag{4.54}$$

with F_α^J the total free-energy of the α-solution to the TAP equations. The discrete sum can be transformed into an integral over free-energy densities, introducing the degeneracy of solutions quantified by the free-energy density dependent complexity:

$$\langle O \rangle = \frac{1}{Z} \int df\, e^{-N\beta f} \mathcal{N}_J(f,T) O(f) = \frac{1}{Z} \int df\, e^{-N(\beta f - \Sigma_J(f,T))}\, O(f)\,. \tag{4.55}$$

The normalization is the 'partition function'

$$Z = \int df e^{-N\beta f} \mathcal{N}_J(f,T) = \int df\, e^{-N(\beta f - \Sigma_J(f,T))}\,. \tag{4.56}$$

We assumed that the labelling by α can be traded by a labelling by f that implies that at the same free-energy density level f the observable O takes the same value. In the $N \to \infty$ limit these integrals can be evaluated by saddle-point, provided the parenthesis is positive. The disorder-dependent complexity is generally approximated with the annealed value introduced in eq. (4.52).

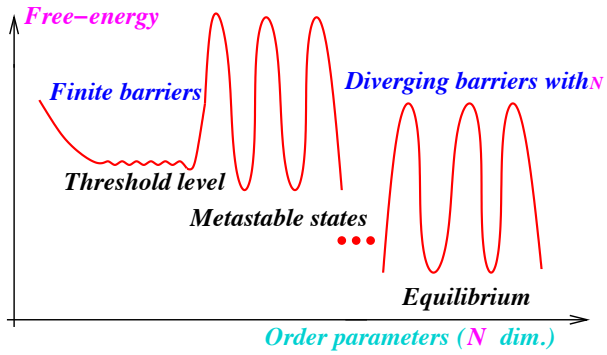

Figure 34: Sketch of the free-energy landscape in the p-spin model.

The equilibrium free-energy

The total equilibrium free-energy density, using the saddle-point method to evaluate the partition function Z in eq. (4.56), reads

$$-\beta f_{eq} = N^{-1} \ln Z = \min_f \left[f - T\Sigma_J(f,T) \right] \equiv \min_f \Phi_J(f,T) \tag{4.57}$$

It is clear that $\Phi_J(f,T)$ is the Landau free-energy density of the problem with f playing the rôle of the energy and Σ_J of the entropy. If we use $f = (E - TS)/N = e - Ts$ with E the actual energy and S the microscopic entropy one has

$$\Phi_J(f,T) = e - T\left(s + \Sigma_J(f,T)\right) \ . \tag{4.58}$$

Thus, Σ_J is an extra contribution to the total entropy that is due to the exponentially large number of metastable states. Note that we do not distninguish here their stability.

Note that Σ_J is subtracted from the total free-energy. Thus, it is possible that in some cases states with a *higher* free-energy density but *very numerous* have a *lower* total free-energy density than lower lying states that are less numerous. Collectively, higher states dominate the equilibrium measure in these cases.

The order parameter

The Edwards-Anderson parameter is understood as a property of a single state. Within the TAP formalism on then has

$$q_J{}^{\alpha}_{ea} = N^{-1} \sum_i (m_i^{\alpha})^2 \ . \tag{4.59}$$

An average over pure states yields $\sum_\alpha w_\alpha^J (m_i^\alpha)^2$.

Instead, the statistical *equilibrium* magnetization, $m_i = \langle s_i \rangle = \sum_\alpha w_\alpha^J m_i^\alpha$, squared is

$$q_J \equiv \langle\, s_i \,\rangle^2 = m_i^2 = \left(\sum_\alpha w_\alpha^J m_i^\alpha \right)^2 = \sum_{\alpha\beta} w_\alpha^J w_\beta^J \ m_i^\alpha m_i^\beta \ . \tag{4.60}$$

If there are multiple phases, the latter sum has crossed contributions from terms with $\alpha \neq \beta$. These sums, as in a usual paramagnetic-ferromagnetic transition have to be taken over half space-space, otherwise global up-down reversal would imply the cancellation of all cross-terms.

This discussion is totally equivalent to the one we developed when we introduced q_J and q_{ea}.

4.6 Metastable states in two families of models

In this subsection we summarize the structure of metastable states found in two families of models, the ones in the SK and the ones in the p-spin class.

4.6.1 High temperatures

For all models, at high temperatures $f(m_i)$ is characterized by a single stable absolute minimum in which all local magnetizations vanish, as expected; this is the paramagnetic state.

In models of the p-spin class the $m_i = 0$ for all i minimum continues to exist at all temperatures. However, even if it is still a minimum of f the TAP free-energy density, $f(\{m_i\})$,it becomes unstable thermodynamically at a given temperature, and it is substituted as the equilibrium state, by other non-trivial configurations with $m_i \neq 0$ that are the absolute minima of Φ. Note the difference with the ferromagnetic problem for which the paramagnetic solution is no longer a minimum below T_c.

4.6.2 Low temperatures

At low temperature many equilibrium states appear (and not just two as in an Ising ferromagnetic model) and they are not related by symmetry (as spin reversal in the Ising ferromagnet or a rotational symmetry in the Heisenberg ferromagnet). These are characterized by non-zero values of the local magnetizations m_i^α that are different in different states.

At low-temperatures both the naive mean-field equations and the TAP equations have an **exponential in N number of solutions** and still an exponential in N number of them correspond to absolute minima of the m_i-dependent free-energy density. This means that $\Sigma_J(T)$ and even $\Sigma_J(0, f_0, T)$ are quantities $O(1)$. These minima can be identified as **different states** that could be accessed by applying the corresponding site-dependent pinning fields.

The derivation and understanding of the structure of the TAP free-energy landscape is quite subtle and goes beyond the scope of these Lectures. Still, we shall briefly present their structure for the SK and p-spin models to give a flavor of their complexity.

The SK model

The first calculation of the complexity in the SK model appeared in 1980. After 25 years of research the structure of the free-energy landscape in this system is still a matter of discussion. At present, the picture that emerges is the following. The temperature-dependent annealed complexity is a decreasing function of temperature that vanishes only at T_c but takes a very small value already at $\sim 0.6T_c$. Surprisingly enough, at finite but large N the TAP solutions come in pairs of minima and saddles of type one, that is to say, extrema with only one unstable direction. These states are connected by a mode that is softer the larger the number of spins: they coalesce and become marginally stable in the limit $N \to \infty$. Numerical simulations show that starting from the saddle-point and following the 'left' direction along the soft mode one falls into the minimum; instead, following the 'right' direction along the same mode one falls into the paramagnetic solution. See Fig. 35 for a sketch of these results. The free-energy difference between the minimum and saddle decreases for increasing N and

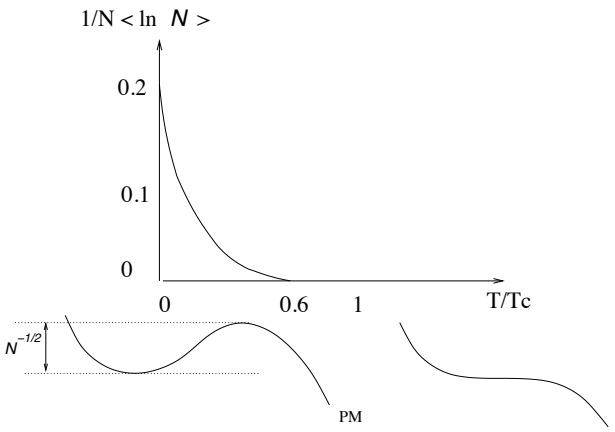

Figure 35: Left: sketch of the temperature dependent complexity, $\Sigma(T)$, of the SK. It actually vanishes only at T_c but it takes a very small value already at $\sim 0.6T_c$. Right: pairs of extrema in the SK model with N large and $N \to \infty$ limit.

one finds, numerically, an averaged $\Delta f \sim N^{-1.4}$. The extensive complexity of minima and type-one saddles is identical in the large N limit, $\Sigma(0,T) = \Sigma(1,T) + O(N^{-1})$ [Aspelmeier, Bray, Moore (06)] in such a way that the Morse theorem is respected. The free-energy dependent annealed complexity is a smooth function of f with support on a finite interval $[f_0, f_1]$ and maximum at f_{max}. The Bray and Moore annealed calculation (with supersymmetry breaking) yields $f_{max} = -0.654$, $\Sigma_{max} = 0.052$, $\Sigma''(f_{max}) = 8.9$. The probability of finding a solution with free-energy density f can be expressed as

$$p(f,T) = \frac{\mathcal{N}(f,T)}{\mathcal{N}(T)} = \frac{e^{N\Sigma(f,T)}}{\mathcal{N}(T)} \sim \sqrt{\frac{N\Sigma''(f_{max})}{2\pi}}\, e^{-\frac{N}{2}|\Sigma''(f_{max})|(f-f_{max})^2}\ , \qquad (4.61)$$

where we evaluated the total number of solutions, $\mathcal{N}(T) = \int df e^{N\Sigma(f,T)}$, by steepest descent The complexity vanishes linearly close to f_0: $\Sigma(f,T) \sim \lambda(f - f_0)$ with $\lambda < \beta$.

Only the lowest lying TAP solutions contribute to the statistical weight. The complexity does not contribute to Φ in the large N limit:

$$\begin{aligned} \Phi &= \beta f - \Sigma_{ann}(f,T) \simeq \beta f - (f - f_0)\lambda \\ \frac{\partial \Phi}{\partial f} &\simeq \beta - \lambda > 0 \qquad \text{iff} \qquad \beta > \lambda \end{aligned} \qquad (4.62)$$

and $\Phi_{min} \simeq \beta f_{min} = \beta f_0$. See Fig. 36. The 'total' free-energy density in the expo-

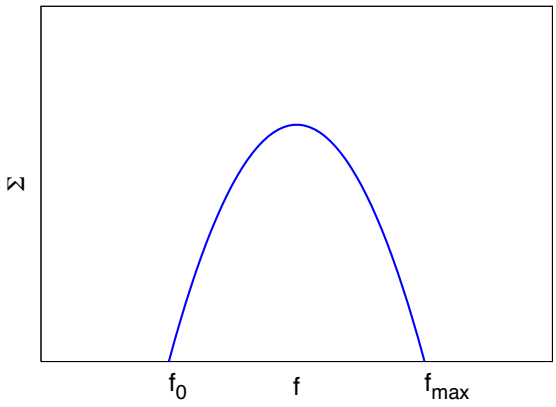

Figure 36: The complexity as a function of f for the SK model.

nential is just the free-energy density of each low-lying solution.

The (spherical) p-spin model

The number and structure of saddle-points is particularly interesting in the $p \geq 3$ cases and it is indeed the reason why these models, with a random first order transition, have been proposed to mimic the structural glass arrest. The $p \geq 3$ model has been studied in great detail in the spherical case, that is to say, when spins are not Ising variables but satisfy the global constraint, $\sum_{i=1}^{N} s_i^2 = N$.

Although in general the minima of the mean-field free energy do not coincide with the minima of the Hamiltonian, they do in the spherical p-spin model. Their positions in the phase space does not depend on temperature, while their self-overlap does. At $T = 0$ a state (stable or metastable) is just a minimum (absolute or local) of the energy. For increasing T energy minima get dressed up by thermal fluctuations, and become states. Thus, the states can be labeled by their zero-temperature energy E^0.

The complexity is given by

$$\Sigma(E) = \frac{1}{2}\left[-\ln\frac{pz^2}{2} + \frac{p-1}{2}z^2 - \frac{2}{p^2 z^2} + \frac{2-p}{p}\right] , \tag{4.63}$$

where z is

$$z = \left[-E^0 - \sqrt{E^{0\,2} - E_c^2}\right] / (p-1) . \tag{4.64}$$

The complexity vanishes at

$$E^0 = E_{min} = f(p) , \tag{4.65}$$

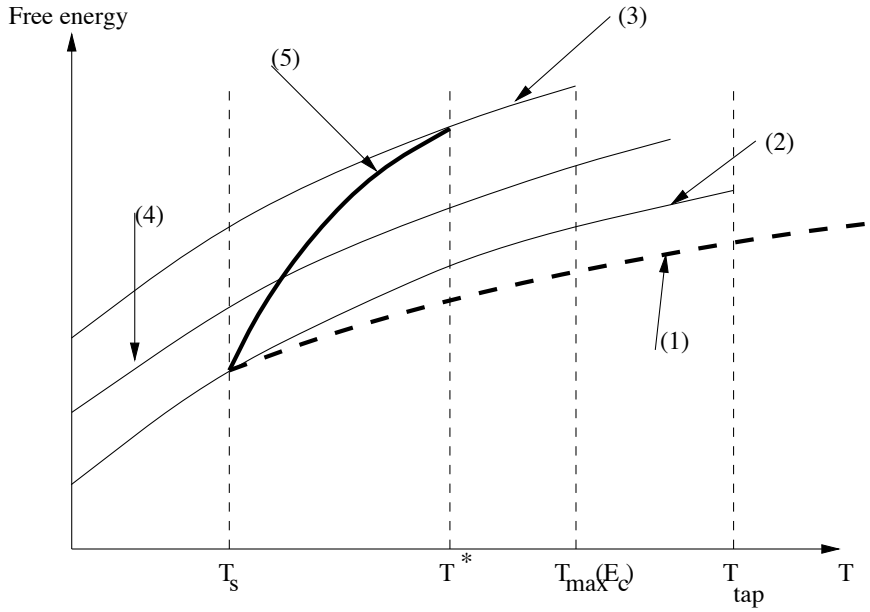

Figure 37: The TAP free-energy as a function of T in the spherical p-spin model. (1) : free energy of the paramagnetic solution for $T > T^*$, F_{tot} for $T < T^*$; (2) : free energy of the lowest TAP states, with zero temperature energy E_{min}; (3) : free energy of the highest TAP states, corresponding to E_c; (4) : an intermediate value of E_0 leads to an intermediate value of f at any temperature; (5) : $f_{eq}(T)$; the difference between curves (5) and (1) gives the complexity $TS_c(f_{eq}(T), T)$.

the ground state of the system, and it is real for zero-temperature energies $E < E_{th}$ with

$$E_{th} = -\sqrt{\frac{2(p-1)}{p}} \,. \tag{4.66}$$

E_{min} is the zero-T energy one finds with the replica calculation using a 1-step RSB *Ansatz* as we shall see below. The finite-T energy of a state α is

$$E_\alpha = q_\alpha^{\frac{p}{2}} E_\alpha^0 - \frac{1}{2T}\left[(p-1)q_\alpha^p - pq_\alpha^{p-1} + 1\right] \,. \tag{4.67}$$

This means that:
- There can be only a finite number of states with $E < E_0$.
- It can be shown that below E_{th} minima dominate on average.
- Above E_{th} one can show that there are states but these are unstable.

Each zero-temperature state is characterized by unit N-vector s_i^α and it gives rise to a finite-T state characterized by $m_i^\alpha = \sqrt{q(E,T)}s_i^\alpha$ with $q(E,T)$ given by

$$q^{p-2}(1-q)^2 = T^2\,\frac{(E+\sqrt{E^2-E_{th}^2})^2}{(p-1)^2} \,. \tag{4.68}$$

($q(E, T = 0) = 1$ and at finite T the solution with q closest to 1 has to be chosen.) The self-overlap at the threshold energy, $E - E_{th}$, is then

$$q_{th}^{p-2}(1-q_{th})^2 = T^2\,\frac{2}{p(p-1)} \,. \tag{4.69}$$

Another way for the q equation to stop having solution, is by increasing the temperature, $T > T_{max}(E^0)$, at fixed bare energy E^0. This means that, even though minima of the energy do not depend on the temperature, states, i.e. minima of the free energy do. When the temperature becomes too large, the paramagnetic states becomes the only pure ergodic states, even though the energy landscape is broken up in many basins of the energy minima. This is just one particularly evident demonstration of the fundamental different between pure states and energy minima. $T_{max}(E^0)$ is obtained as the limiting temperature for which eq. (4.68) admits a solution. It is given by

$$T_{max}(E^0) = \left(\frac{2}{p}\right)\left(\frac{p-1}{-E^0-\sqrt{E^{0\,2}-E_{th}^2}}\right)\left(\frac{p-2}{p}\right)^{\frac{p-2}{2}} \,. \tag{4.70}$$

T_{max} is a decreasing function of E^0. The last states to disappear then are the ones with minimum energu E_{min}, ceasing to exist at $T_{TAP} \equiv= T_{max}(E_{min})$.

Below a temperature T_d, an exponential (in N) number of metastable states contribute to the thermodynamics in such a non-trivial way that their combined contribution to the observables makes them those of a paramagnet. Even if each of these

states is non-trivial (the m_i's are different from zero) the statistical average over all of them yields results that are identical to those of a paramagnet, that is to say, the free-energy density is $-1/(4T)$ as in the $m_i = 0$ paramagnetic solution. One finds

$$T_d = \sqrt{\frac{p(p-2)^{p-2}}{2(p-1)^{p-1}}} \, . \tag{4.71}$$

At a lower temperature T_s ($T_s < T_d$) there is an entropy crisis, less than an exponential number of metastable states survive, and there is a *static phase transition* to a glassy state.

In the p-spin models there is a range of temperatures in which high lying states dominate this sum since they are sufficiently numerous so as to have a complexity that renders the cimbined term $\beta f - \Sigma_J(f, T)$ smaller (in actual calculations the disorder dependent complexity is approximated by its annealed value). In short:

- Above T_d the (unique) paramagnetic solution dominates, $q = 0$ and $\Phi = f = -1/(4T)$.
- In the interval $T \in [T_s, T_d]$ an exponentially large number of states (with $q \neq 0$ given by the solution to $pq^{p-2}(1-q) = 2T^2$) dominate the partition sum. $\Phi = -1/(4T)$ appearing as the continuation of the paramagnetic solution.
- At $T < T_s$ the lowest TAP states with $E^0 = E_{min}$ control the partition sum. Their total free-energy Φ is different from $-1/(4T)$.

This picture is confirmed with other studies that include the use of pinning fields adapted to the disordered situation, the effective portential for two coupled real replicas, and the dynamic approach.

Low temperatures, entropy crisis

The interval of definition of $\Phi(E, T)$ is the same as $\Sigma(E)$, that is $E \in [E_{min} : E_{th}]$. Assuming that at a given temperature T the energy $E_{eq}(T)$ minimizing Φ lies in this interval, what happens if we lower the temperature? Remember that the complexity is an increasing function of E, as of course is $f(E, T)$. When T decreases we favor states with lower free energy and lower complexity, and therefore E_{eq} decreases. As a result, it must exist a temperature T_s, such that, $E_{eq}(T_s) = E_{min}$ and thus, $\Sigma(E_{eq}(T)) = \Sigma(E_{min}) = 0$. Below T_s the bare energy E_{eq} cannot decrease any further: there are no other states below the ground states E_{min}. Thus, $E_{eq}(T) = E_{min}$ for each temperature $T \leq T_s$. As a result, if we plot the complexity of equilibrium states $\Sigma(E_{eq}(T))$ as a function of the temperature, we find a discontinuity of the first derivative at T_s, where the complexity vanishes. A thermodynamic transition takes place at T_s: below this temperature equilibrium is no longer dominated by metastable states, but by the lowest lying states, which have zero complexity and lowest free energy density.

We shall show that T_s is the transition temperature found with a replica calculation. The temperature where equilibrium is given for the first time by the lowest

energy states, is equal to the static transition temperature. Above T_s the partition function is dominated by an exponentially large number of states, each with high free energy and thus low statistical weight, such that they are not captured by the overlap distribution $P(q)$. At T_s the number of these states becomes sub-exponential and their weight nonzero, such that the $P(q)$ develops a secondary peak at $q_s \neq 0$.

The threshold

The stability analysis of the TAP solutions on the threshold level demonstrates that these are only marginally stable, with a large number of flat directions.

Hierarchy of metastable states

The ordering of TAP solutions with different stability properties according to their free-energy density has also been studied in great detail. The exact scaling with N of the height of the barriers separating these solutions is harder to obtain. All these are accepted to be exponential on the number of spins in the sample.

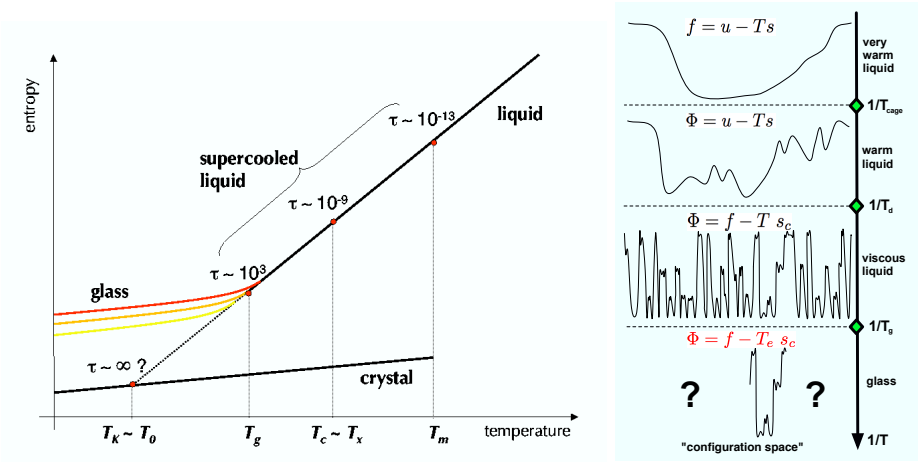

Figure 38: Sketch for the Random first order transition (RFPT) scenario. Left: the experimental observation. Right: its interpretation in terms of metastable states.

Finite dimensions

In finite-dimensional systems, only equilibrium states can break the ergodicity, i.e. states with the lowest free energy density. In other words, the system cannot remain trapped for an infinite time in a metastable state, because in finite dimension free energy barriers surrounding metastable states are always finite.

The extra free energy of a droplet of size r of equilibrium phase in a background metastable phase has a positive interface contribution which grows as r^{d-1}, and a

negative volume contribution which grows as r^d,

$$\Delta f = \sigma r^{d-1} - \delta f \; r^d \tag{4.72}$$

where here σ is the surface tension and δf is the bulk free energy difference between the two phases. This function has always a maximum, whose finite height gives the free energy barrier to nucleation of the equilibrium phase (note that at coexistence $\delta f = 0$ and the barrier is infinite). Therefore, if initially in a metastable states the system will, sooner or later, collapse in the stable state with lower free energy density. For this reason, in finite dimension we cannot decompose the Gibbs measure in metastable components. When this is done, it is always understood that the decomposition is only valid for finite times, i.e times much smaller than the time needed for the stable equilibrium state to take over. On the other hand, in mean-field systems (infinite dimension), barriers between metastable states may be infinite in the thermodynamic limit, and it is therefore possible to call pure states also metastable states, and to assign them a Gibbs weight w_α^J. We will analyze a mean-field spin-glass model, so that we will be allowed to perform the decomposition above even for metastable states.

Comments

There is a close relationship between the topological properties of the model and its dynamical behavior. In particular, the slowing down of the dynamics above but close to T_d is connected to the presence of saddles, whose instability decreases with decreasing energy. In fact, we have seen that the threshold energy level E_{th} separating saddles from minima, can be associated to the temperature $T_{th} = T_d$, marking the passage from ergodicity to ergodicity breaking. In this context the dynamical transition can be seen as a topological transition. The plateau of the dynamical correlation function, which has an interpretation in terms of cage effect in liquids, may be reinterpreted as a pseudo-thermalization inside a saddle with a very small number of unstable modes.

4.7 The replica method

A picture that is consistent with the one arising from the naive mean-field approximation but contradicts the initial assumption of the droplet model arises from the *exact* solution of fully-connected spin-glass models. These results are obtained using a method which is called the *replica trick* and that we shall briefly present below.

In Sect. we argued that the typical properties of a disordered system can be computed from the disorder averaged free-energy

$$[\, F_J \,] \equiv \int dJ P(J) F_J \; . \tag{4.73}$$

One then needs to average the logarithm of the partition funtion. In the annealed approximation one exchanges the ln with the average over disorder and, basically,

considers the interactions equilibrated at the same temperature T as the spins:

$$[\ln Z_J] \sim \ln[Z_J]\ . \tag{4.74}$$

This approximation turns out to be correct at high temperatures but incorrect at low ones.

The replica method allows one to compute $[F_J]$ for fully-connected models. It is based on the smart use of the identity

$$\ln Z_J = \lim_{n\to 0} \frac{Z_J^n - 1}{n}\ . \tag{4.75}$$

The idea is to compute the right-hand-side for finite and integer $n = 1, 2, \ldots$ and then perform the analytic continuation to $n \to 0$. Care should be taken in this step: for some models the analytic continuation may be not unique. It turns out that this is indeed the case for the emblematic Sherrington-Kirkpatrick model, as discussed by Palmer and van Hemmen in 1979 though it has also been recently shown that the free-energy $f(T)$ obtained by Parisi with the replica trick is exact!

The disorder averaged free-energy is given by

$$-\beta[F_J] = -\int dJ P(J) \ln Z_J = -\lim_{n\to 0} \frac{1}{n}\left(\int dJ P(J) Z_J^n - 1\right)\ , \tag{4.76}$$

where we have exchanged the limit $n \to 0$ with the integration over the exchanges. For *integer* n the *replicated* partition function, Z_J^n, reads

$$Z_J^n = \sum_{\{s_i^a\}} e^{-\beta[E_J(\{s_i^1\})+\ldots+E_J(\{s_i^n\})]}\ . \tag{4.77}$$

Here $\sum_{\{s_i^a\}} \equiv \sum_{\{s_i^1=\pm 1\}} \cdots \sum_{\{s_i^n=\pm 1\}}$. Z_J^n corresponds to n identical copies of the original system, that is to say, all of them with the same realization of the disorder. Each copy is characterized by an ensemble of N spins, $\{s_i^a\}$. We label the copies with a replica index $a = 1, \ldots, n$. For p-spin disordered spin models Z_J^n takes the form

$$Z_J^n = \sum_{\{s_i^a\}} e^{\beta \sum_{a=1}^n \left[\sum_{i_1\neq\ldots\neq i_p} J_{i_1\ldots i_p} s_{i_1}^a \ldots s_{i_p}^a + \sum_i h_i s_i^a \right]}\ . \tag{4.78}$$

The average over disorder amounts to computing a Gaussian integral for each set of spin indices $i_1, \ldots i_p$. One finds

$$[Z_J^n] = \sum_{\{s_i^a\}} e^{\frac{\beta^2 J^2}{2N^{p-1}} \sum_{i_1\neq\ldots\neq i_p} (\sum_a s_{i_1}^a \ldots s_{i_p}^a)^2 + \beta \sum_a \sum_i h_i s_i^a} \equiv \sum_{\{s_i^a\}} e^{-\beta F(\{s_i^a\})}\ . \tag{4.79}$$

The function $\beta F(\{s_i^a\})$ is not random. It depends on the spin variables only but it includes terms that couple different replica indices:

$$\beta F(\{s_i^a\}) \approx -\frac{N\beta^2 J^2}{2}\left[\sum_{a\neq b}\left(\frac{1}{N}\sum_i s_i^a s_i^b\right)^p + n\right] - \beta \sum_a \sum_i h_i s_i^a\ . \tag{4.80}$$

In writing the last expression we have dropped terms that are subleading in N (in complete analogy with what we have done for the pure p spin ferromagnet). The constant term $-Nn\beta^2 J^2/2$ originates in the terms with $a = b$, for which $(s_i^a)^2 = 1$.

To summarize, we started with an interacting spin model. Next, we enlarged the number of variables from N spins to $N \times n$ replicated spins by introducing n non-interacting copies of the system. By integrating out the disorder we decoupled the sites but we payed the price of coupling the replicas. Hitherto the replica indices act as a formal tool introduced to compute the average over the bond distribution. Nothing distinguishes one replica from another and, in consequence, the "free-energy" $F(\{s_i^a\})$ is invariant under permutations of the replica indices.

The next step to follow is to identify the order parameters and transform the free-energy into an order-parameter dependent expression to be rendered extremal at their equilibrium values. In a spin-glass problem we already know that the order parameter is not the global magnetization as in a pure magnetic system but the parameter q – or more generally the overlap between states. Within the replica calculation an *overlap between replicas*

$$q_{ab} \equiv N^{-1} \sum_i s_i^a s_i^b \tag{4.81}$$

naturally appeared in eq. (4.80). The idea is to write the free-energy density as a function of the order parameter q_{ab} and look for their extreme in complete analogy with what has been done for the fully-connected ferromagnet. This is, of course, a tricky business, since the order parameter is here a matrix with number of elements n going to zero! A recipe for identifying the form of the order parameter (or the correct saddle-point solution) has been proposed by G. Parisi in the late 70s and early 80s. This solution has been recently proven to be exact for mean-field models by two mathematical physics, F. Guerra and M. Talagrand. Whether the very rich physical structure that derives from this rather formal solution survives in finite dimensional systems remains a subject of debate.

Introducing the Gaussian integral

$$\int dq_{ab}\; e^{\beta J q_{ab} \sum_i s_i^a s_i^b - \frac{N}{2} q_{ab}^2} = e^{\frac{N}{2}\left(\frac{1}{N}\beta J \sum_i s_i^a s_i^b\right)^2} \tag{4.82}$$

for each pair of replica indices $a \neq b$, one decouples the site indeces, i, and the averaged replicated partition function can be rewritten as

$$[Z_J^n] = \int \prod_{a \neq b} dq_{ab}\; e^{-\beta F(q_{ab})} \tag{4.83}$$

and

$$\beta F(q_{ab}) = -\frac{N\beta^2 J^2}{2} \left[-\sum_{a \neq b} q_{ab}^p + n \right] - N \ln \zeta(q_{ab}) \;, \tag{4.84}$$

$$\zeta(q_{ab}) = \sum_{s_a} e^{-\beta H(q_{ab}, s_a)} \;, \qquad H(q_{ab}, s_a) = -J \sum_{ab} q_{ab} s_a s_b - h \sum_a s_a \tag{4.85}$$

where for simplicity we set $h_i = h$. The factor N in front of $\ln \zeta$ comes from the decoupling of the site indeces. Note that the transformation (4.82) serves to uncouple the sites and to obtain then the very useful factor N in front of the exponential. The partition function $Z(q_{ab})$ is the one of a fully-connected Ising model with interaction matrix q_{ab}.

We next summarize the saddle-point method used to evaluate the partition sum and free-energy and we enumerate and briefly discuss the *Ansatze* used to characterize the Q matrix and the phases they represent.

4.8 Saddle-point evaluation

Having extracted a factor N in the exponential suggests to evaluate the integral over q_{ab} with the saddle-point method. This, of course, involves the *a priori* dangerous exchange of limits $N \to \infty$ and $n \to 0$. The replica theory relies on this assumption. One then writes

$$\lim_{N\to\infty} -[\, f_J \,] \to -\lim_{n\to 0} \frac{1}{n} f(q_{ab}^{sp}) \tag{4.86}$$

and searches for the solutions to the $n(n-1)/2$ extremization equations

$$\left. \frac{\delta f(q_{ab})}{\delta q_{cd}} \right|_{q_{ef}^{sp}} = 0 \; . \tag{4.87}$$

In usual saddle-point evaluations the saddle-point one should use is (are) the one(s) that correspond to absolute minima of the free-energy density. In the replica calculation the number of variables is $n(n-1)/2$ that becomes negative! when $n < 1$ and makes the saddle-point evaluation tricky. In order to avoid unphysical complex results one needs to focus on the saddle-points with positive (or at least semi-positive) definite Hessian

$$\mathcal{H} \equiv \left. \frac{\partial f(q_{ab})}{\partial q_{cd} \partial q_{ef}} \right|_{q_{ab}^{sp}} \; , \tag{4.88}$$

and these sometimes corresponds to *maxima* (instead of minima) of the free-energy density.

The saddle-point equations are also self-consistency equations

$$q_{ab}^{sp} = \langle s_a s_b \rangle_{H(q_{ab},\{s_a\})} = [\, \langle s_a s_b \rangle \,] \tag{4.89}$$

where the second member means that the average is performed with the *single site Hamiltonian* $H(q_{ab}, s_a)$ and the third member is just one of the averages we would like to compute.

The partition function in eq. (4.85) cannot be computed for generic q_{ab} since there is no large n limit to exploit on the contrary, $n \to 0$. Thus, one usually looks for solutions to eqs. (4.87) within a certain family of matrices q_{ab}. We discuss below the relevant parametrizations.

4.8.1 Replica symmetry (RS)

In principle, nothing distinguishes one replica from another one. This is the reason why Sherrington and Kirkpatrick looked for solutions that preserve replica symmetry:

$$q_{ab} = q \ , \qquad \text{for all } a \neq b \ . \tag{4.90}$$

Inserting this *Ansatz* in (4.84) and (4.85) and taking $n \to 0$ one finds

$$q = \int_{-\infty}^{\infty} \frac{dz}{\sqrt{2\pi}} \, e^{-z^2/2} \, \tanh^2 \left(\beta \sqrt{\frac{pq^{p-1}}{2}} z + \beta h \right) \ . \tag{4.91}$$

This equation resembles strongly the one for the magnetization density of the p-spin ferromagnet, eq. (5.7).

Let us first discuss the case $p = 2$, *i.e.* the SK model. In the absence of a magnetic field, one finds a second order phase transition at $T_s = J$ from a paramagnetic ($q = 0$) to a spin-glass phase with $q \neq 0$. In the presence of a field there is no phase transition. SK soon realized though that there is something wrong with this solution: the entropy at zero temperature is negative, $S(0) = -1/(2\pi)$, and this is impossible for a model with discrete spins, for which S is strictly positive. de Almeida and Thouless later showed that the reason for this failure is that the replica symmetric saddle-point is not stable, since the Hessian (4.88) is not positive definite and has negative eigenvalues. The eigenvalue responsible for the instability of the replica symmetric solution is called the *replicon*.

Comparison with the TAP equations shows that the RS *Ansatz* corresponds to the assumption that the local fields $h_i = \sum_{i_{i_1} \ldots i_{i_p}} J_{i_1 \ldots i_p} m_{i_1} \ldots m_{i_p} + h$ are independent and have a Gaussian distribution with average h and variance $\sigma^2 = J^2 q^{p-1}$. Numerical simulations clearly show that this assumption is invalid.

Interestingly enough, the numerical values for several physical quantities obtained with the replica symmetric solution do not disagree much with numerical results. For instance, the ground state zero-temperature energy density is $E^0 = -0.798$ while with numerical simulations one finds $E^0 \sim -0.76$.

For the $p > 2$ model one finds that the replica symmetric solution is stable at all temperatures. However, the problem of the negative entropy remains and should be solved by another solution. The transition must then have aspects of a first-order one, with another solution appearing at low temperatures and becoming the most convenient one at the transition.

4.8.2 One step replica symmetry breaking (1RSB)

The next challenge is to device a replica symmetry breaking *Ansatz*, in the form of a matrix q_{ab} that is not invariant under permutations of rows or columns. There is

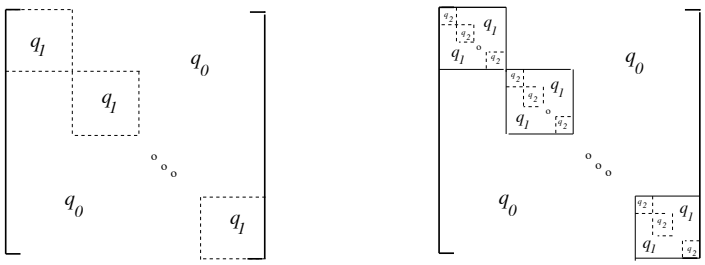

Figure 39: Left: a one-step replica symmetry breaking (1RSB) *Ansatz*. Right: a two-step replica symmetry breaking *Ansatz*. The elements on the main diagonal vanish identically. In the 1RSB case the diagonal blocks have size $m \times m$. In the 2RSB the proceudre is repeated and one has blocks of size $m_1 \times m_1$ with smaller diagonal blocks of size $m_2 \times m_2$.

no first principles way of doing this, instead, the structure of the *Ansatz* is the result of trial and error. Indeed, a kind of minimal way to break the replica symmetry is to propose a structure in blocks as the one shown in Fig. 39-left. The diagonal elements are set to zero as in the RS case. Square blocks of linear size m close to the main diagonal are filled with a paramater q_1. The elements in the rest of the matrix take a different value q_0 and one takes $0 \leq q_0 \leq q_1$. The matrix q_{ab} depends on three parameters $q_0,\ q_1,\ m$ and one has to find the values such that the free-energy density is *maximized*! The conditions for a extreme are

$$\frac{\partial f(q_0, q_1, m)}{\partial q_0} = \frac{\partial f(q_0, q_1, m)}{\partial q_1} = \frac{\partial f(q_0, q_1, m)}{\partial m} = 0 \,. \tag{4.92}$$

In the SK model ($p = 2$) the 1RSB *Ansatz* yields a second order phase transition ($q_0 = q_1 = 0$ and $m = 1$ at criticality) at a critical temperature $T_s = J$, that remains unchanged with respect to the one predicted by the RS *Ansatz*. The 1RSB solution is still unstable below T_s and in all the low temperature phase. One notices, however, that the zero temperature entropy, even if still negative and incorrect, takes a value that is closer to zero, $S(T = 0) \approx -0.01$, the ground state energy is closer to the value obtained numerically, and the replicon eigenvalue even if still negative has an absolute value that is closer to zero. All this suggest that the 1RSB *Ansatz* is closer to the exact solution.

Instead, in all cases with $p \geq 3$ the 1RSB *Ansatz* is stable below the static critical temperature T_s and all the way up to a new characteristic temperature $0 < T_f < T_s$. Moreover, one can prove that in this range of temperatures the model is solved exactly by this *Ansatz*. The critical behavior is quite peculiar: while the order parameters q_0 and q_1 jump at the transition from a vanishing value in the paramagnetic phase to a non-zero value right below T_s, all thermodynamic quantities are continuous since

$m = 1$ at T_s and all q_0 and q_1 dependent terms appear multiplied by $1 - m$. This is a mixed type of transition that has been baptized *random first-order*. Note that disorder weakens the critical behavior in the $p \geq 3$-spin models. In the limit $p \to \infty$ the solutions become $m = T/T_c$, $q_0 = 0$ and $q = 1$.

4.8.3 k-step replica symmetry breaking (kRSB)

The natural way to generalize the 1RSB *Ansatz* is to propose a k-step one. In each step the off-diagonal blocks are left unchanged while the diagonal ones of size m_k are broken as in the first step thus generating smaller square blocks of size m_{k+1}, close to the diagonal. At a generic k-step RSB scheme one has

$$0 \leq q_0 \leq q_1 \leq \ldots \leq q_{k-1} \leq q_k \leq 1 \,, \tag{4.93}$$

$$n = m_0 \geq m_1 \geq \ldots \geq m_k \geq m_{k+1} \,, \tag{4.94}$$

parameters. In the $n \to 0$ limit the ordering of the parameters m is reversed

$$0 = m_0 \leq m_1 \leq \ldots \leq m_k \leq m_{k+1} \,. \tag{4.95}$$

In the SK model one finds that any finite k-step RSB *Ansatz* remains unstable. However, increasing the number of breaking levels the results continue to improve with, in particular, the zero temperature entropy getting closer to zero. In the $p \geq 3$ case instead one finds that the 2RSB *Ansatz* has, as unique solution to the saddle-point equations, one that boils down to the 1RSB case. This suggests that the 1RSB *Ansatz* is stable as can also be checked with the analysis of the Hessian eigenvalues: the replicon is stricly positive for all $p \geq 3$.

4.8.4 Full replica symmetry breaking

In order to construct the full RSB solution the breaking procedure is iterated an infinite number of times. The full RSB *Ansatz* thus obtained generalizes the block structure to an infinite sequence by introducing a function

$$q(x) = q_i \,, \qquad m_{i+1} < x < m_i \tag{4.96}$$

with $0 \leq x \leq 1$. Introducing $q(x)$ sums over replicas are traded by integrals over x; for instance

$$\frac{1}{n} \sum_{a \neq b} q_{ab}^l = \int_0^1 dx \; q^l(x) \,. \tag{4.97}$$

The free-energy density becomes a functional of the function $q(x)$. The extremization condition is then a hard functional equation. A Landau expansion – expected to

be valid close to the assumed second order phase transition – simplifies the task of solving it. For the SK model one finds

$$q(x) = \begin{cases} \frac{x}{2} , & 0 \leq x \leq x_1 = 2q(1) , \\ q_{ea} \equiv q_{max} = q(1) , & x_1 = 2q(1) \leq x \leq 1 , \end{cases} \tag{4.98}$$

at first order in $|T - T_c|$, with $q(1) = |T - T_c|/T_c$ and $x_1 = 2q(1)$. The stability analysis yields a vanishing replicon eigenvalue signalling that the full RSB solution is *marginally stable*.

One can also recover the particular case of the 1RSB using a $q(x)$ with two plateaux, at q_0 and q_1 and the breaking point at $x = m$.

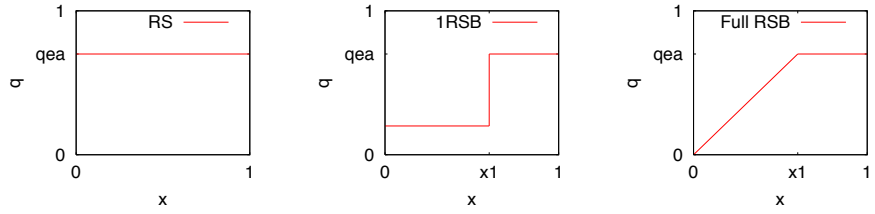

Figure 40: The function $q(x)$ for a replica symmetric (left), one step replica symmetry breaking (center) and full replica symmetry breaking *Ansätze*.

Marginality condition

In the discussion above we chose the extreme that *maximize* the free-energy density since we were interested in studying equilibrium properties. We could, instead, use a different prescription, though *a priori* not justified, and select other solutions. For example, we can impose that the solution is *marginally stable* by requiring that the replicon eigenvalue vanishes. In the $p = 2$ this leads to identical results to the ones obtained with the usual prescription since the full-RSB *Ansatz* is in any case marginally stable. In the p-spin models with $p \geq 3$ instead it turns out that the averaged properties obtained in this way correspond to the asymptotic values derived with the stochastic dynamics starting from random initial conditions. This is quite a remarkable result.

4.8.5 Interpretation of replica results

Let us now discuss the implications of the solution to fully-connected disordered models obtained with the, for the moment, rather abstract replica formalism.

The interpretation uses heavily the identification of *pure states*. Their definition is a tricky matter that we shall not discuss in detail here. We shall just assume it can

be done and use the analogy with the ferromagnetic system – and its two pure states – and the TAP results at fixed disorder. As we already know, which are the pure states, its properties, number, *etc.* can depend on the quenched disorder realization and fluctuate from sample to sample. We shall keep this in mind in the rest of our discussion.

Let us then distinguish the averages computed within a pure state and over all configuration space. In a ferromagnet with no applied magnetic field this is simple to grasp: at high temperatures there is just one state, the paramagnet, while at low temperatures there are two, the states with positive and negative magnetization. If one computes the averaged magnetization restricted to the state of positive (negative) magnetization one finds $m_{eq} > 0$ ($m_{eq} < 0$); instead, summing over all configurations $m_{eq} = 0$ even at low temperatures. Now, if one considers systems with more than just two pure states, and one labels them with Greeks indices, averages within such states are denoted $\langle O \rangle_\alpha$ while averages taken with the full Gibbs measure are expressed as

$$\langle\, O \,\rangle = \sum_\alpha w_\alpha^J \,\langle\, O \,\rangle_\alpha \,. \tag{4.99}$$

w_α^J is the probability of the α state given by

$$w_\alpha^J = \frac{e^{-\beta F_\alpha^J}}{Z_J} \,, \qquad \text{with} \qquad Z_J = \sum_\alpha e^{-\beta F_\alpha^J} \tag{4.100}$$

and thus satisfying the normalization condition $\sum_\alpha w_\alpha^J = 1$. F_α^J can be interpreted as the total free-energy of the state α. These probabilities, as well as the state dependent averages, will show sample-to-sample fluctuations.

One can then define an overlap between states:

$$q_{J\alpha\beta} \equiv N^{-1} \sum_i \langle s_i \rangle_\alpha \langle s_i \rangle_\beta = N^{-1} \sum_i m_i^\alpha m_i^\beta \tag{4.101}$$

and assume rename the self-overlap the 'Edwards-Anderson parameter'

$$q_{J\alpha\alpha} \equiv N^{-1} \sum_i \langle s_i \rangle_\alpha \langle s_i \rangle_\alpha \equiv q_{J ea} \,. \tag{4.102}$$

The statistics of possible overlaps is then characterized by a probability function

$$P_J(q) \equiv \sum_{\alpha\beta} w_\alpha^J w_\beta^J \; \delta(q - q_{\alpha\beta}) \,, \tag{4.103}$$

where we included a subindex J to stress the fact that this is a strongly sample-dependent quantity. Again, a ferromagnetic model serves to illustrate the meaning of $P_J(q)$. First, there is no disorder in this case so the J label is irrelevant. Second, the high-T equilibrium phase is paramagnetic, with $q = 0$. $P(q)$ is then a delta function with weight 1 (see the left panel in Fig. 41). In the low-T phase there are only two

pure states with identical statistical properties and $q_{ea} = m^2$. Thus, $P(q)$ is just the sum of two delta functions with weight 1/2 (central panel in Fig. 41).

Next, one can consider averages over quenched disorder and study

$$[\, P_J(q) \,] \equiv \int dJ\, P(J) \sum_{\alpha\beta} w_\alpha^J w_\beta^J\, \delta(q - q_{\alpha\beta}) \,. \tag{4.104}$$

How can one access $P_J(q)$ or $[\, P_J(q) \,]$? It is natural to reckon that

$$P_J(q) = Z^{-2} \sum_{\sigma s} e^{-\beta E_J(\sigma)} e^{-\beta E_J(s)}\, \delta\left(N^{-1} \sum_i \sigma_i s_i - q \right) \tag{4.105}$$

that is to say, $P_J(q)$ is the probability of finding an overlap q between two *real* replicas of the system with identical disordered interactions in equilibrium at temperature T. This identitiy gives a way to compute $P_J(q)$ and its average in a numerical simulation: one just has to simulate two independent systems with identical disorder in equilibrium and calculate the overlap.

But there is also, as suggested by the notation, a way to relate the pure state structure to the replica matrix q_{ab}. Let us consider the simple case

$$\begin{aligned} [\, m_i \,] &= \left[Z_J^{-1} \sum_{\{s_i\}} s_i\, e^{-\beta E_J(\{s_i\})} \right] = \left[\frac{Z_J^{n-1}}{Z_J^n} \sum_{\{s_i^1\}} s_i^1\, e^{-\beta E_J(\{s_i^1\})} \right] \\ &= \left[\frac{1}{Z_J^n} \sum_{\{s_i^a\}} s_i^1 e^{-\beta \sum_{a=1}^n E_J(\{s_i^a\})} \right] \end{aligned} \tag{4.106}$$

where we singled out the replica index of the spin to average. This relation is valid for all n, in particular for $n \to 0$. In this limit the denominator approaches one and the average over disorder can be simply evaluated

$$[\, m_i \,] = \sum_{\{s_i^a\}} s_i^1 e^{-\beta E^{eff}(\{s_i^a\})} \tag{4.107}$$

and introducing back the normalization factor $Z^n = 1 = \sum_{\{s_i^a\}} e^{-\beta \sum_{a=1}^n E_J(\{s_i^a\})}$ $= [\, \sum_{\{s_i^a\}} e^{-\beta \sum_{a=1}^n E_J(\{s_i^a\})} \,] = e^{-\beta E^{eff}(\{s_i^a\})}$ we have

$$[\, m_i \,] = \langle\, s_i^a \,\rangle_{E_{eff}} \tag{4.108}$$

with a any replica index. The average is taken over the Gibbs measure of a system with effective Hamiltonian E_{eff}. In a replica symmetric problem in which all replicas are identical this result should be independent of the label a. Instead, in a problem with replica symmetry breaking the averages on the right-hand-side need not be identical for all a. This could occur in a normal vectorial theory with dimension n in which

not all components take the same expected value. It is reasonable to assume that the full thermodynamic average is achieved by the sum over all these cases,

$$[\, m_i \,] = \lim_{n\to 0} \frac{1}{n} \sum_{a=1}^{n} \langle\, s_i^a \,\rangle \; . \tag{4.109}$$

Let us now take a less trivial observable and study the spin-glass order parameter q

$$\begin{aligned} q \;\equiv\; [\, \langle\, s_i \,\rangle^2 \,] &= \left[Z_J^{-1} \sum_{\{s_i\}} s_i \; e^{-\beta E_J(\{s_i\})} \; Z_J^{-1} \sum_{\{\sigma_i\}} \sigma_i \; e^{-\beta E_J(\{\sigma_i\})} \right] \\ &= \left[\frac{Z^{n-2}}{Z^n} \sum_{\{s_i\},\{\sigma_i\}} s_i \sigma_i \; e^{-\beta E_J(\{s_i\}) - \beta E_J(\{\sigma_i\})} \right] \\ &= \left[\frac{1}{Z_J^n} \sum_{\{s_i^a\}} s_i^1 s_i^2 \; e^{-\beta \sum_{a=1}^n E_J(\{s_i^a\})} \right] \end{aligned} \tag{4.110}$$

In the $n \to 0$ limit the denominator is equal to one and one can then perform the average over disorder. Introducing back the normalization one then has

$$q = \langle\, s_i^a s_i^b \,\rangle_{E_{eff}(\{s_i^a\})} \tag{4.111}$$

for any arbitrary pair of replicas $a \neq b$ (since $\langle\, s_i^a s_i^a \,\rangle = 1$ for Ising spins). The average is done with an effective theory of n interacting replicas characterized by $E_{eff}(\{s_i^a\})$. Again, if there is replica symmetry breaking the actual thermal average is the sum over all possible pairs of replicas:

$$q = \lim_{n\to 0} \frac{1}{n(n-1)} \sum_{a\neq b} q^{ab} \; . \tag{4.112}$$

A similar argument allows one to write

$$q^{(k)} = [\, \langle\, s_{i_1} \ldots s_{i_k} \,\rangle^2 \,] = \lim_{n\to 0} \frac{1}{n(n-1)} \sum_{a\neq b} q_{ab}^k \; . \tag{4.113}$$

One can also generalize this argument to obtain

$$P(q) = [\, P_J(q) \,] = \lim_{n\to 0} \frac{1}{n(n-1)} \sum_{a\neq b} \delta(q - q^{ab}) \tag{4.114}$$

Thus, the replica matrix q_{ab} can be ascribed to the overlap between pure states.

Note that a small applied field, though uncorrelated with a particular pure state, is necessary to have non-zero local magnetizations and then non-zero q values.

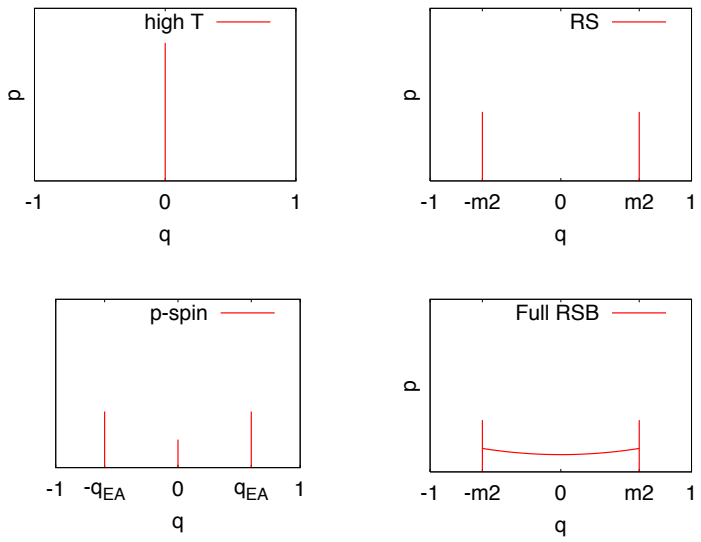

Figure 41: $[\,P_J(q)\,]$ in a paramagnet (top left), in a ferromagnet or a replica symmetric system (top right), in a model with a one step replica symmetry breaking solution (bottom left) and for system with full RSB (bottom right).

The function $P(q)$ then extends the concept of order parameter to a function. In zero field the symmetry with respect to simultaneous reversal of all spins translates into the fact that $P_J(q)$ must be symmetric with respect to $q = 0$. $[\,P_J(q)\,]$ can be used to distinguish between the droplet picture prediction for finite dimensional spin-glasses – two pure states – that simply corresponds to

$$[\,P_J(q)\,] = \frac{1}{2}\delta(q - q_{ea}) + \frac{1}{2}\delta(q + q_{ea}) \tag{4.115}$$

(see the central panel in Fig. 41) and a more complicated situation in which $[\,P_J(q)\,]$ has the two delta functions at $\pm q_{ea}$ plus non-zero values on a finite support (right panel in Fig. 41) as found in mean-field spin-glass models.

The linear susceptibility

Taking into account the multiplicity of pure states, the magnetic susceptibility, eq. (4.25), and using (4.99) becomes

$$T\chi = T[\,\chi_J\,] = 1 - \frac{1}{N}\sum_i [\,\langle\, s_i \,\rangle^2\,] = 1 - \sum_{\alpha\beta} [\,w_\alpha^J w_\beta^J\,]\, q_{\alpha\beta} = \int dq\,(1-q)\,P(q)\;. \tag{4.116}$$

There are then several possible results for the susceptibiliy depending on the level of replica symmetry breaking in the system:

- In a replica symmetric problem or, equivalently, in the droplet model,

$$\chi = \beta(1 - q_{ea}) \; . \tag{4.117}$$

  This is also the susceptibility within a pure state of a system with a higher level of RSB.
- At the one step RSB level, this becomes

$$\chi = \beta \left[1 - (1 - m)q_{ea}\right] \; . \tag{4.118}$$

- For systems with full RSB one needs to know the complete $P(q)$ to compute χ, as in (4.116).

Note that in systems with RSB (one step or full) the susceptibility is larger than $\beta(1 - q_{ea})$.

A system with $q_{ea} = 1$ in the full low-temperature phase (as the REM model or $p \to \infty$ limit of the p spin model, see below) has just one configuration in each state. Systems with $q_{ea} < 1$ below T_c have states formed by a number of different configurations that is exponentially large in N. (Note that $q_{ea} < 1$ means that the two configurations differ in a number of spins that is proportional to N.) The logarithm of this number is usually called the intra-state entropy.

Even if the number of pure states can be very large (exponential in N) only a fraction of them can have a non-negligible weight. This is the case if one finds, for example, $\sum_\alpha w_\alpha^2 < +\infty$

Symmetry and ergodicity breaking

In all $p \geq 2$ spin models there is a phase transition at a finite T_s at which the rather abstract *replica symmetry* is broken. This symmetry breaking is accompanied by ergodicity breaking as in the usual case. Many pure states appear at low temperatures, each one has its reversed $s_i \to -s_i$ counterpart, but not all of them are related by real-space symmetry properties.

The one-step RSB scenario

In this case the transition has first-order and second-order aspects. The order parameters q_0 and q_1 jump at the critical point as in a first-order transition but the thermodynamic quantities are continuous.

The full RSB scenario

Right below T_c an exponential in N number of equilibrium states appear. The transition is continuous, the order parameter approaches zero right below T_c. Lowering further the temperature each ergodic component breaks in many other ones. In this sense, the full spin-glass phase, $T < T_c$, is 'critical' and not only the single point T_c.

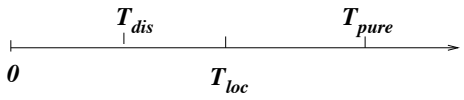

Figure 42: A sketch of critical temperatures.

4.9 Finite dimensional systems

We start now the discussion on the statics of spin-glass models by describing briefly scaling arguments and the droplet theory. Similar arguments can be used to study other models with strong disorder, as a manifold in a random potential.

4.9.1 The Griffiths phase

The effects of quenched disorder show up already in the paramagnetic phase of finite dimensional systems. Below the critical point of the pure case (no disorder) finite regions of the system can order due to fluctuations in the couplings. Take the case of random ferromagnetic interactions. Fluctuations in bonds can be such that in a given region they take higher values than on average. In practice, at the working temperature T that is higher than the transition temperature of the full system, T_c^{dis}, a particular region can behave as if it had have an effective T_c^{loc} that is actually higher than T_c, see Fig. 42. Similarly, fluctuations can make a region more paramagnetic than the average if the J_{ij}'s take smaller values $[\, J_{ij}\,]$. (Note that T_c is typically proportional to J, the strength of the ferromagnetic couplings. In the disordered case we normalize the J_{ij}'s in such a way that $[\, J_{ij}\,] = J_{pure}$. We can then compare the disordered and the pure problems.)

These properties manifest in non-analyticities of the free-energy that appear in a full interval of temperatures above (and below) the critical temperature of the disordered model, as shown by Griffiths. For instance, deviations from Curie-Weiss ($\chi = 1/T$) behavior appear below the Néel temperature of dilute antiferromagnets in a uniform field. These are sometimes described with a Lorentzian distribution of local temperatures with the corresponding Curie-Weiss law at each T. It is clear that Griffiths effects will also affect the relaxation of disordered systems above freezing. We shall not discuss these features in detail here.

4.9.2 Droplets and domain-wall stiffness

Let us now just discuss one simple argument that is at the basis of what is needed to derive the results of the droplet theory without entering into the complications of the calculations.

It is clear the structure of *droplets*, meaning patches in which the spins point in the direction of the opposite state, plays an important role in the thermodynamic behavior of systems undergoing a phase transition. At criticality one observes ordered domains

of the two equilibrium states at all length scales – with *fractal* properties. Right above T_c finite patches of the system are indeed ordered but these do not include a finite fraction of the spins in the sample and the magnetization density vanishes. However, these patches are enough to generate non-trivial thermodynamic properties very close to T_c and the richness of critical phenomena. M. Fisher and others developed a droplet phenomenological theory for critical phenomena in clean systems. Later D. S. Fisher and D. Huse extended these arguments to describe the effects of quenched disorder in spin-glasses and other random systems; this is the so-called *droplet model*.

Critical droplet in a ferromagnet

Let us study the stability properties of an equilibrium ferromagnetic phase under an applied external field that tends to destabilize it. If we set $T = 0$ the free-energy is just the energy. In the ferromagnetic case the free-energy cost of a spherical droplet of radius R of the equilibrium phase parallel to the applied field embedded in the dominant one (see Fig. 43-left) is

$$\Delta F(R) = -2\Omega_d R^d h m_{eq} + \Omega_{d-1} R^{d-1} \sigma_0 \tag{4.119}$$

where σ_0 is the interfacial free-energy density (the energy cost of the domain wall) and Ω_d is the volume of a d-dimensional unit sphere. We assume here that the droplet has a regular surface and volume such that they are proportional to R^{d-1} and R^d, respectively. The excess free-energy reaches a maximum

$$\Delta F_c = \frac{\Omega_d}{d} \frac{\Omega_{d-1}^d}{\Omega_d^d} \left(\frac{d-1}{2dhm_{eq}} \right)^{d-1} \sigma_0^d \tag{4.120}$$

at the critical radius

$$R_c = \frac{(d-1)\Omega_{d-1}\sigma_0}{2d\Omega_d h m_{eq}} , \tag{4.121}$$

see Fig. 43 ($h > 0$ and $m > 0$ here, the signs have already been taken into account). The free-energy difference vanishes at

$$\Delta F(R_0) = 0 \qquad \Rightarrow \qquad R_0 = \frac{\Omega_{d-1}\sigma_0}{2\Omega_d h m_{eq}} . \tag{4.122}$$

Several features are to be stressed:

- The barrier vanishes in $d = 1$; indeed, the free-energy is a linear function of R in this case.
- Both R_c and R_0 have the same dependence on hm_{eq}: they monotonically decrease with increasing hm_{eq} vanishing for $hm_{eq} \to \infty$ and diverging for $hm_{eq} \to 0$.
- In dynamic terms that we shall discuss later, the passage above the barrier is done *via* thermal activation; as soon as the system has reached the height of the barrier it rolls on the right side of 'potential' ΔF and the favorable phase nucleates.

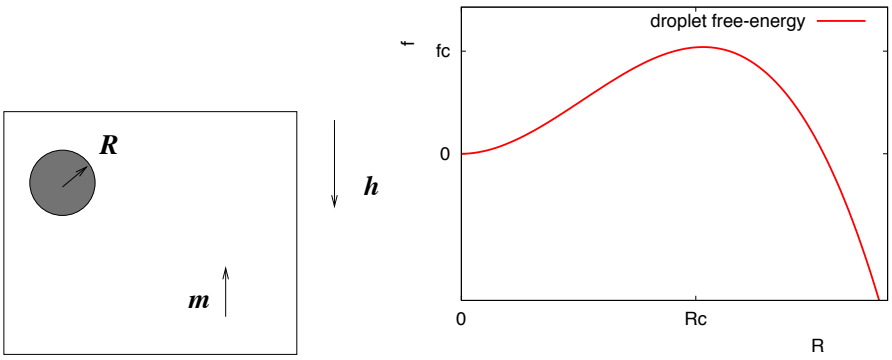

Figure 43: Left: the droplet. Right: the free-energy density $f(R)$ of a spherical droplet with radius R.

- As long as the critical size R_c is not reached the droplet is not favorable and the system remains positively magnetized.

In this example the field drives the system from one state to the other. In studies of phase transitions at zero external field, temperature generates fluctuations of different size and the question is whether these are favourable or not. The study of droplet fluctuations is useful to establish whether an ordered phase can exist at low (but finite) temperatures. One then studies the free-energy cost for creating large droplets with thermal fluctuations that may destabilize the ordered phase, in the way we have done with the simple Ising chain. Indeed, a fundamental difference between an ordered and a disordered phase is their stiffness (or rigidity). In an ordered phase the free-energy cost for changing one part of the system with respect to the other part far away is of the order k_BT and usually diverges as a power law of the system size. In a disordered phase the information about the reversed part propagates only a finite distance (of the order of the correlation length, see below) and the stiffness vanishes.

The calculation of the stiffness is usually done as follows. Antiparallel configurations (or more generally the two ground states) are imposed at the opposite boundaries of the sample. A domain wall is then generated somewhere in the bulk. Its free-energy cost, *i.e.* the difference between the free-energies of the modified configuration and the equilibrium one, is measured and one tests when creating a wall is favourable.

The Imry-Ma argument for the random field Ising model

Take a ferromagnetic Ising model in a random field, defined in eq. (4.20). In zero applied field and low enough temperature, if $d > 1$ there is phase transition between a paramagnetic and a ferromagnetic phase. Under the effect of a random field with very strong typical strength, the spins align with the local external fields and the system

is paramagnetic. It is, however, non-trivial to determine the effect of a relatively weak random field on the ferromagnetic phase at sufficiently low temperature. The long-range ferromagnetic order could be preserved or else the field could be enough to break up the system into large but finite domains of the two ferromagnetic phases.

A qualitative argument to estimate whether the ferromagnetic phase survives or not in presence of the external random field due to Imry and Ma. Let us fix $T = 0$ and switch on a random field. If a domain $\mathcal{D}$ of the opposite order (say down) is created within the bulk of the ordered state (say up) the system pays an energy due to the unsatisfied links lying on the boundary that is

$$\Delta E_{border} \sim 2JL^{d-1} \tag{4.123}$$

where L is the linear length of the border and $d-1$ is the dimension of the border of a domain embedded in d a dimensional volume, assuming it is compact. By creating a domain boundary the system can also gain a magnetic energy in the interior of the domain due to the external field:

$$\Delta E_{rf} \sim -hL^{d/2} \tag{4.124}$$

since there are $N = L^d$ spins inside the domain of linear length L and, using the central limit theorem, $-h\sum_{j\in\mathcal{D}} s_i \sim -h\sqrt{N} = -hL^{d/2}$. The comparison between these two energy scales yields

$$JL_0^{d-1} \sim hL_0^{d/2} \qquad \left(\frac{h}{J}\right)^{\frac{2}{d-2}} \sim L_0 \tag{4.125}$$

In the large L limit ΔE diverges to $+\infty$ with increasing L in $d > 2$. The marginal case $d = 2$ is more subtle and we do not discuss it in detail here. One can also search for an extreme in $\Delta E(L)$ finding

$$L_c \sim \left(\frac{4J(d-1)}{hd}\right)^2 . \tag{4.126}$$

Several comments are in order:

- In $d = 1$ the energy difference is a monotonically decreasing function of L thus suggesting that the creation of droplets is very favorable and there is no barrier to cross to do it.
- In $d > 2$ the energy difference first decreases from $\Delta E(L = 0) = 0$ to reach a nagative minimum at L_c, and then increases back to pass through zero at L_0 and diverge at infinity. This indicates that the creation of domains at zero temperature is not favorable in $d > 2$. Just domains of finite length, upto L_0 can be created. Note that L_0 increases with h/J in $d > 2$ and thus a higher field tends to generate larger droplets and thus disorder the sample.

With this argument one cannot show the existence of a phase transition at h_c nor the nature of it. The argument is such that it suggests that order can be supported by the system at zero temperature and small fields.

An elastic line in a random potential

Let us take an interface model of the type defined in eq. (4.22) with $N = 1$. If one assumes that the interfaces makes an excursion of longitudinal length L and transverse length ϕ the leastic energy cost is

$$E_{elast} = \frac{c}{2}\int d^d x\, (\nabla\phi(\vec{x}))^2 \qquad \Rightarrow \qquad \Delta E_{elast} \sim cL^d (L^{-1}\phi)^2 = cL^{d-2}\phi^2 \quad (4.127)$$

If the excursion is sufficiently large, the interface meets $\phi L^d/\Delta^{d+1}$ impurities (that is to say the volume of the displacement over the typical volume between impurities given by the correlation length of disorder to the power given by the number of dimensions). Each impurity applies a pinning force of the order of $dV/d\phi \sim \sqrt{W/\Delta^d}$ and then the energy gain due to the random potential is

$$\Delta E_{random} \sim \sqrt{W/\Delta^d}\,. \quad (4.128)$$

The balance between the cost of elastic energy and the gain in random energy leads to

$$\phi \sim \Delta (L/\xi)^{(4-d)/3} \quad (4.129)$$

where $\xi = (c^2\Delta^4/W)^{1/(4-d)}$ is the *Larkin length* and $\alpha = (4-d)/3$ is the *Flory exponent* for the roughness of the surface. One then concludes that for $d > 4$ disorder is irrelevant and the interface is flat ($\phi \to 0$ when $L \to \infty$). Since the linearization of the elastic energy [see the discussion leading to eq. (4.22)] holds only if $\phi/L \ll 1$, the result (4.129) may hold only for $d > 1$ where $\alpha < 1$.

The 3d Edwards-Anderson model in a uniform magnetic field

A very similar reasoning is used to argue that there cannot be spin-glass order in an Edwards-Anderson model in an external field. The only difference is that the domain wall energy is here assumed to be proportional to L^y with an *a priori* unknown d-dependent exponent y that is related to the geometry of the domains.

Comments

These arguments are easy to implement when one knows the equilibrium states. They cannot be used in models in which the energy is not a slowly varying function of the domain wall position.

4.9.3 The droplet theory

The droplet theory is a phenomenological model that assumes that the low temperature phase of a spin-glass model has only two equilibrium states related by an

overall spin flip. It is then rather similar to a ferromagnet, only that the nature of the order in the two equilibrium states is not easy to see, it is not just most spins pointing up or most spins pointing down with some thermal fluctuations within. At a glance, one sees a disordered paramagnetic like configuration and a more elaborate order parameter has to be measured to observe the order. The spin-glass phase is then called a *disguised ferromagnet* and a usual spontaneous symmetry breaking (between the two equilibrium states related spin reversal symmetry) leading to usual ergodicity breaking is supposed to take place at T_c.

Once this assumption has been done, renormalization group arguments are used to describe the scaling behavior of several thermodynamic quantities. The results found are then quantitatively different from the ones for a ferromagnet but no *novelties* appear.

5 Formalism: dynamic generating functional and symmetries

In this Section we discuss some static and dynamic aspects of classical statistical systems in the canonical ensemble. In this chapter we introduce the classical path integral formalism. The symmetry arguments follow closely the discussion in [27].

5.1 Classical dynamics: generating functional

In Sect. 2.3 we showed a proof of the (generally non-Markov) Langevin equation based on the integration over a large ensemble of harmonic oscillators that act as a bath with which the system is set in contact.

Observables which are functions of the solution to the Langevin equation can also be computed using a dynamic generating functional that reads [48]

$$Z_{\rm D}[\eta] \equiv \int \mathcal{D}\xi \; dP(t_0) \; e^{-\frac{1}{2k_B T}\int_{t_0}^{\mathcal{T}} dt' \int_{t_0}^{\mathcal{T}} dt'' \, \xi(t')\Gamma^{-1}(t'-t'')\xi(t'') + \int_{t_0}^{\mathcal{T}} dt' \, \eta(t') x_\xi(t')}$$

$x_\xi(t)$ is the solution to the Langevin equation with initial condition $x_0 = x(t_0), \dot{x}_0 = \dot{x}(t_0)$ at the initial time t_0. The factor $dP(t_0)$ is the measure of the initial condition, $dP(t_0) \equiv dx_0 d\dot{x}_0 P_{\rm i}[x_0, \dot{x}_0]$. The Gaussian factor is proportional to $P[\xi]$ the functional probability measure of the noise. The measure is $\mathcal{D}\xi \equiv \prod_{k=0}^{\mathcal{N}} d\xi(t_k)$ with $k = 0, \ldots, \mathcal{N}$, $t_k = t_0 + k(\mathcal{T}t - t_0)/\mathcal{N}$ and $\mathcal{N} \to \infty$ while $(\mathcal{T} - t_0)$ remains finite. The inverse kernel Γ^{-1} is defined within the interval $[t_0, \mathcal{T}]$: $\int_{t_0}^{\mathcal{T}} dt'' \Gamma(t - t'')\Gamma^{-1}(t'' - t') = \delta(t - t')$.

A very useful expression for $Z_{\rm D}[\eta]$, usually called the Martin-Siggia-Rose generating functional (actually derived by Janssen [49]), is obtained by introducing the identity

$$\mathrm{Eq}[x(t)] \equiv m\ddot{x}(t) + \int_{t_0}^{\mathcal{T}} dt' \; \gamma(t - t')\dot{x}(t') + V'[x(t)] = \xi(t) \tag{5.1}$$

valid at each time t, with the delta function

$$1 = \int \mathcal{D}x \;\; \delta\left[\mathrm{Eq}[x(t)] - \xi(t)\right] \left|\det \frac{\delta \mathrm{Eq}[x(t)]}{\delta x(t')}\right| \,, \tag{5.2}$$

with $\mathcal{D}x \equiv \prod_{k=1}^{\mathcal{N}} dx(t_k)$. The factor $|\det \ldots|$ is the determinant of the operator $\delta(t-t')\{m\partial_t^2 + V''[x(t)]\} + \gamma(t-t')\partial_{t'}$ and ensures that the integral equals one.[10] The delta function can be exponentiated with an auxiliary field $i\hat{x}$ (using the Fourier representation of the δ-function). $\mathcal{D}i\hat{x} = \prod_{k=1}^{\mathcal{N}-1} di\hat{x}(t_k)$. The determinant can be exponentiated with time-dependent anticommunting variables – opening the way to the use of super-symmetry [39], a subject that we shall not touch in these notes. However, since it does not yield a relevant contribution to the kind of dynamics we are interested in, we forget it (one can show that the determinant is a constant for Langevin processes with coloured noise and/or inertia and that the discretization of an over-damped Langevin equation with white-noise can also be chosen to set it to one – Itô convention, see App. 4.3). Z_{D} reads

$$\begin{aligned} Z_{\mathrm{D}}[\eta,\hat{\eta}] \equiv & \int \mathcal{D}\xi \mathcal{D}x \mathcal{D}i\hat{x} \; dP(t_0) \\ & \times e^{-\int_{t_0}^{\mathcal{T}} dt' \, i\hat{x}(t') \left[m\ddot{x}(t') + \int_{t_0}^{\mathcal{T}} dt'' \; \gamma(t'-t'')\dot{x}(t'') + V'[x(t')] - \xi(t') \right]} \\ & \times e^{-\frac{1}{2k_B T} \int_{t_0}^{\mathcal{T}} dt' \int_{t_0}^{\mathcal{T}} dt'' \, \xi(t')\Gamma^{-1}(t'-t'')\xi(t'') + \int_{t_0}^{\mathcal{T}} dt' \left[\eta(t')x(t') + \hat{\eta}(t') i\hat{x}(t') \right]} \end{aligned}$$

where we have introduced a new source $\hat{\eta}(t)$, coupled to the auxiliary field $i\hat{x}(t)$. The integration over the noise $\xi(t)$ is Gaussian and it can be readily done; it yields

$$+\frac{k_B T}{2} \int_{t_0}^{\mathcal{T}} dt' \int_{t_0}^{\mathcal{T}} dt'' \; i\hat{x}(t') \, \Gamma(t'-t'') \, i\hat{x}(t'') \tag{5.3}$$

and, for a **coloured bath**, the environment generates a **retarded interaction** in the effective action. In the usual white noise case, this term reduces to, $k_B T \gamma_0 \int_{t_0}^{\mathcal{T}} dt' \, [i\hat{x}(t')]^2$, a local expression. In the end, the generating function and resulting **Martin-Siggia-Rose-Jaenssen-deDominicis** (MSRJD) action reads

$$\begin{aligned} \mathcal{Z}_{\mathrm{D}}[\eta,\hat{\eta}] \equiv & \int \mathcal{D}x \mathcal{D}i\hat{x} \; dP(t_0) \; e^{S[x,i\hat{x},\eta,\hat{\eta}]} \\ S[x,i\hat{x},\eta,\hat{\eta}] = & -\int dt' \, i\hat{x}(t') \left\{ m\ddot{x}(t') + \int dt'' \; \gamma(t'-t'')\dot{x}(t'') + V'[x(t')] \right\} \\ & + \frac{k_B T}{2} \int dt' \int dt'' \, i\hat{x}(t') \Gamma(t'-t'') i\hat{x}(t'') + \text{sources} \,. \end{aligned} \tag{5.4}$$

[10] Its origin is in the change of variables. In the same way as in the one dimensional integral, $\int dx \; \delta[g(x)] = \int dz \; 1/|g'[g^{-1}(z)]| \; \delta(z) = 1/|g'[g^{-1}(0)]|$, to get 1 as a result one includes the inverse of the Jacobian within the integral: $\int dx \; \delta[g(x)] \; |g'(x)| = 1$.

All integrals runs over $[t_0, \mathcal{T}]$. Causality in the integral over t' is ensured by the fact that γ is proportional to θ.

The MSRJD action has two kinds of contributions: the ones that depend on the characteristics of the bath (through Γ) and the ones that do not. The latter also exist in a functional representation of Newton dynamics and we call them S^{DET} (for deterministic) while the former contain all information abour thermal fluctuations and dissipation and we call it S^{DISS} (for dissipation):

$$S[x, i\hat{x}, \eta, i\hat{\eta}] = S^{\text{DISS}}[x, i\hat{x}; \Gamma] + S^{\text{DET}}[x, i\hat{x}, \eta, i\hat{\eta}] \; . \tag{5.5}$$

If the distribution of the initial condition were to be included in the action as an additional term, $\ln P_{\text{i}}[x_0, i\hat{x}_0]$, 6t would be part of S^{DET}.

Interestingly enough, the **dynamic generating functional at zero sources is identical to one** for any model:

$$\mathcal{Z}_{\text{D}}[\eta = 0, \hat{\eta} = 0] = 1 \tag{5.6}$$

as can be concluded from its very first definition. In particular, it does not depend on the coupling constants of the chosen model. This property will be utilized in disordered systems to render the dynamic calculations relatively easier than the static ones.

5.2 Generic correlation and response.

The mean value at time t of a generic observable A is

$$\langle A(t) \rangle = \int \mathcal{D}x\mathcal{D}i\hat{x} \; dP(t_0) \; A[x(t)] \; e^{S[x, i\hat{x}]} \; , \tag{5.7}$$

where $S[x, i\hat{x}]$ is ashort-hand notation for $S[x, i\hat{x}, \eta = 0, \hat{\eta} = 0]$. The self-correlation and linear response of x are given by

$$C(t, t') = \langle x(t) x(t') \rangle = \frac{1}{Z_{\text{D}}[\eta, \hat{\eta}]} \left. \frac{\delta^2 Z_{\text{D}}[\eta, \hat{\eta}]}{\delta\eta(t)\delta\eta(t')} \right|_{\eta=\hat{\eta}=0} = \left. \frac{\delta^2 Z_{\text{D}}[\eta, \hat{\eta}]}{\delta\eta(t)\delta\eta(t')} \right|_{\eta=\hat{\eta}=0} \tag{5.8}$$

$$\begin{aligned} R(t, t') &= \left. \frac{\delta \langle x(t) \rangle}{\delta h(t')} \right|_{h=0} = \langle x(t) \frac{\delta S[x, i\hat{x}; h]}{\delta h(t')} \rangle|_{h=0} = \langle x(t) i\hat{x}(t') \rangle \\ &= \frac{1}{Z_{\text{D}}[\eta, \hat{\eta}]} \left. \frac{\delta^2 Z_{\text{D}}[\eta, \hat{\eta}]}{\delta\eta(t)\delta\hat{\eta}(t')} \right|_{\eta=\hat{\eta}=0} = \left. \frac{\delta^2 Z_{\text{D}}[\eta, \hat{\eta}]}{\delta\eta(t)\delta\hat{\eta}(t')} \right|_{\eta=\hat{\eta}=0} \end{aligned} \tag{5.9}$$

with $h(t')$ a small field applied at time t' that modifies the potential energy according to $V \to V - h(t')x(t')$. The $i\hat{x}$ auxiliary function is sometimes called the **response field** since it allows one to compute the linear response by taking its correlations with x. Similarly, we define the two-time correlation between two generic observables A and B,

$$C_{AB}(t, t') \equiv \int \mathcal{D}x\mathcal{D}i\hat{x} dP(t_0) \, A[x(t)] B[x(t')] \, e^{S[x, i\hat{x}]} = \langle A[x(t)] B[x(t')] \rangle \tag{5.10}$$

and the linear response of A at time t to an infinitesimal perturbation linearly applied to B at time $t' < t$,

$$R_{AB}(t,t') \equiv \left.\frac{\delta\langle A[x(t)]\rangle_{f_B}}{\delta f_B(t')}\right|_{f_B=0}, \tag{5.11}$$

with $V(x) \mapsto V(x) - f_B B(x)$. The function $B(x)$ depends only on x (or on an even number of time derivatives, that is to say, it is even with respect to $t \to -t$). By plugging eq. (5.7) in this definition we get the **classical Kubo formula** for generic observables:

$$R_{AB}(t,t') = \langle A[x(t)]\,\frac{\delta S[x,i\hat{x};f_B]}{\delta f_B(t')}\rangle\Big|_{f_B=0} = \langle A[x(t)]i\hat{x}(t')B'[x(t')]\rangle \tag{5.12}$$

with $B'[x(t')] = \partial_x B[x(t')]$. This relation is also causal and hence proportional to $\theta(t-t')$; it is valid in and out of equilibrium. For $B[x] = x$ it reduces to the correlation between x and $i\hat{x}$.

If the system has **quenched random exchanges** or any kind of **disorder**, one may be interested in calculating the averaged correlations and responses over different realizations of disorder. Surprisingly, this average is very easy to perform in a dynamic calculation [50]. The normalization factors $1/Z_{\rm D}[\eta,\hat{\eta}]$ in (5.8) and (5.9) have to be evaluated at zero external sources in which they are trivially independent of the random interactions. Hence, it is sufficient to average $Z_{\rm D}[\eta,\hat{\eta}]$ over disorder and then take variations with respect to the sources to derive the thermal and disorder averaged two-point functions. This property contrasts with an equilibrium calculation where the expectation values are given by $[\langle A\rangle] = [1/Z\sum_{\rm CONF} A\exp(-\beta H)]$, with $[\cdot]$ denoting the disorder average. In this case, the partition function Z depends explicitly on the random exchanges and one has to introduce **replicas** [40] to deal with the normalization factor and do the averaging.

Having assumed the initial equilibration of the environment ensures that a normal system will eventually equilibrate with it. The interaction with the bath allows the system to dissipate its energy and to relax until thermalization is reached. However, in some interesting cases, as the dyamics across phase transitions and glassy models, the time needed to equilibrate is a fast growing function of N, the number of dynamic degrees of freedom. Thus, the evolution of the system in the thermodynamic limit occurs out of equilibrium. In real systems, a similar situation occurs when the equilibration time crosses over the observation time and falls out of the experimental time-window.

A final interesting remark on the relevance of quenched disorder is the following. When a system with quenched disorder evolves out of equilibrium at finite temperature, the correlation function and the response function do not depend on the realization of disorder if the size of the system is large enough (the realization of disorder has to be a typical one). These quantities are **self-averaging**. This statement is easily checked in a simulation. When times get sufficiently long as to start seeing the approach to equilibrium, dependencies on the realizations of disorder appear.

5.2.1 The linear response as a variable-noise correlation

The correlation between coordinate and a generic colored noise can be obtained from the variation with respect to $\lambda(t,t')$ of the generating functional once the source

$$\int dt''dt'''\ \lambda(t'',t''')\,x(t'')\xi(t''') \tag{5.13}$$

has been added. Integrating over the noise and keeping only the linear terms in λ in the effective action since all others will vanish when setting $\lambda = 0$

$$\begin{aligned}\text{Linear terms} \quad = \quad & \frac{k_BT}{2}\int dt_1dt_2dt_3dt_4\ \left[\lambda(t_1,t_2)x(t_1)\gamma(t_2,t_3)i\hat{x}(t_4)\delta(t_4-t_3)\right.\\ & \left.+i\hat{x}(t_1)\delta(t_1-t_2)\gamma(t_2,t_3)\lambda(t_4,t_3)x(t_4)\right]\ .\end{aligned} \tag{5.14}$$

The variation with respect to $\lambda(t,t')$ yields $(k_BT)/2\int dt''\ [\gamma(t',t'')+\gamma(t'',t')]$ $\langle x(t)i\hat{x}(t'')\rangle = \langle x(t)\xi(t')\rangle$.

5.3 Time-reversal

Since it will be used in the rest of this chapter, we introduce the time-reversed variable $\bar{x}$ by $\bar{x}(t) \equiv x(-t)$ for all t. The time-reversed observable is defined as

$$A_{\rm r}([x],t) \equiv A([\bar{x}],-t). \tag{5.15}$$

It has the effect of changing the sign of all odd time-derivatives in the expression of local observables, *e.g.* if $A[x(t)] = \partial_t x(t)$ then $A_{\rm r}[x(t)] = -\partial_t x(-t)$. As an example for non-local observables, the time-reversed Langevin equation reads

$$\mathrm{EQ}_{\rm r}([x],t) \quad = \quad m\ddot{x}(t) - F_{\rm r}([x],t) - \int_{-\mathcal{T}}^{\mathcal{T}} du\ \gamma(u-t)\dot{x}(u)\ . \tag{5.16}$$

Notice the change of sign in front of the friction term that is no longer dissipative in this new equation.

5.4 An equilibrium symmetry

If the initial time t_0 is set to $t_0 = -\mathcal{T}$ and the system is in equilibrium at this instant, $P_{-\mathcal{T}}$ is given by the Maxwell-Boltzmann measure. One can then check that the zero-source action, $S[x,i\hat{x}]$, is fully invariant under the field transformation $\mathcal{T}_c$ defined as

$$\mathcal{T}_c \equiv \left\{\begin{array}{rcl} x_u & \mapsto & x_{-u}\ , \\ i\hat{x}_u & \mapsto & i\hat{x}_{-u} + \beta d_u x_{-u}\ . \end{array}\right.$$

We introduced the notation $x_t = x(t)$ so as to make the notation more compact. Note that $d_u x_{-u} = -d_{-u}x_{-u}$. This transformation does not involve the kernel Γ and it includes a time-reversal. The invariance is achieved independently by the deterministic

($S^{\rm DET}$) and dissipative ($S^{\rm DISS}$) terms in the action. The former includes the contribution from the initial condition, $\ln P_{-\mathcal{T}}$. Moreover, the path-integral measure is invariant since the Jacobian associated to this transformation is also block triangular with ones on the diagonal. The proof goes as follows.

5.4.1 Invariance of the measure

The Jacobian $\mathcal{J}_{\rm c}$ of the transformation $\mathcal{T}_c$ is the determinant of a triangular matrix:

$$\mathcal{J}_{\rm c} \equiv \det \frac{\delta(x,\hat{x})}{\delta(\mathcal{T}_{\rm c}x,\mathcal{T}_{\rm c}\hat{x})} = \det_{uv}^{-1} \begin{bmatrix} \frac{\delta x_{-u}}{\delta x_v} & 0 \\ \frac{\delta \hat{x}_{-u}}{\delta x_v} & \frac{\delta \hat{x}_{-u}}{\delta \hat{x}_v} \end{bmatrix} = \left(\det_{uv}^{-1}\left[\delta_{u+v}\right]\right)^2 = 1$$

and it is thus identical to one.

5.4.2 Invariance of the integration domain

Before and after the transformation, the functional integration on the field x is performed for values of x_t on the real axis. However, the new domain of integration for the field $\hat{x}$ is complex. For all times, $\hat{x}_t$ is now integrated over the complex line with a constant imaginary part $-i\beta\partial_t x_t$. One can return to an integration over the real axis by closing the contour at both infinities. Indeed the integrand, e^S, goes to zero sufficiently fast at $x_t \to \pm\infty$ for neglecting the vertical ends of the contour thanks to the term $\beta^{-1}\gamma_0(i\hat{x}_t)^2$ (in the white noise limit or the correspondong ones in colored noise cases) in the action. Furthermore the new field is also integrated with the boundary conditions $\hat{x}(-\mathcal{T}) = \hat{x}(\mathcal{T}) = 0$.

5.4.3 Invariance of the action functional

The deterministic contribution satisfies

$$\begin{aligned} S^{\rm det}[\mathcal{T}_{\rm c}x,\mathcal{T}_{\rm c}\hat{x}] &= \ln P_{\rm i}(x_{\mathcal{T}},\dot{x}_{\mathcal{T}}) - \int_u \left[i\hat{x}_{-u} + \beta\partial_u x_{-u}\right]\left[m\partial_u^2 x_{-u} + V'(x_{-u})\right] \\ &= \ln P_{\rm i}(x_{\mathcal{T}},\dot{x}_{\mathcal{T}}) - \int_u i\hat{x}_u\left[m\ddot{x}_u + V'(x_u)\right] + \beta\int_u \dot{x}_u\left[m\ddot{x}_u + V'(x_u)\right] \\ &= \ln P_{\rm i}(x_{\mathcal{T}},\dot{x}_{\mathcal{T}}) - \int_u i\hat{x}_u\left[m\ddot{x}_u + V'(x_u)\right] + \beta\int_u \partial_u \ln P_{\rm i}(x_u,\dot{x}_u) \\ &= S^{\rm det}[x,\hat{x}]\ , \end{aligned}$$

where we used the initial equilibrium measure $\ln P_{\rm i}(x,\dot{x}) = -\beta\left(\frac{1}{2}m\dot{x}^2 + V(x)\right) - \ln\mathcal{Z}$. In the first line we just applied the transformation, in the second line we made the substitution $u \mapsto -u$, in the third line we wrote the last integrand as a total derivative the integral of which cancels the first term and recreates the initial measure at $-\mathcal{T}$.

Secondly, we show that the dissipative contribution is also invariant under $\mathcal{T}_c$. We have

$$\begin{aligned} S^{\rm diss}[\mathcal{T}_c x, \mathcal{T}_c \hat{x}] &= \int_u [i\hat{x}_{-u} + \beta \partial_u x_{-u}] \int_v \beta^{-1}\, \gamma_{u-v}\, i\hat{x}_{-v} \\ &= \int_u [i\hat{x}_u - \beta \dot{x}_u] \int_v \gamma_{v-u} \beta^{-1} i\hat{x}_v \\ &= S^{\rm diss}[x, \hat{x}] \; . \end{aligned}$$

In the first line we just applied the transformation, in the second line we made the substitution $u \mapsto -u$ and $v \mapsto -v$ and in the last step we exchanged u and v.

5.4.4 Invariance of the Jacobian (Grassmann variables)

Finally we show that the Jacobian term in the action is invariant once it is expressed in terms of a Gaussian integral over conjugate Grassmann fields (c and c^*) and provided that the transformation $\mathcal{T}_c$ is extended to act on these as follows[11]

$$\mathcal{T}_c \equiv \left\{ \begin{array}{lcllcl} x_u & \mapsto & x_{-u} \; , & \qquad c_u & \mapsto & c^*_{-u} \; , \\ i\hat{x}_u & \mapsto & i\hat{x}_{-u} + \beta \partial_u x_{-u} \; , & \qquad c^*_u & \mapsto & -c_{-u} \; . \end{array} \right. \tag{5.17}$$

We start from

$$S^{\mathcal{J}}[c, c^*, x] = \int_u \int_v c^*_u \left[m\partial_u^2 \delta_{u-v} + \partial_u \gamma_{u-v} \right] c_v + \int_u c^*_u V''(x_u) c_u \tag{5.18}$$

and we have

$$\begin{aligned} & S^{\mathcal{J}}(\mathcal{T}_c c, \mathcal{T}_c c^*, \mathcal{T}_c x) \\ & \quad = -\int_u \int_v c_{-u} \left[m\partial_u^2 \delta_{u-v} + \partial_u \gamma_{u-v} \right] c^*_{-v} + \int_u c_{-u} \left[-V''(x_{-u}) \right] c^*_{-u} \\ & \quad = \int_u \int_v c^*_v \left[m\partial_u^2 \delta_{v-u} - \partial_u \gamma_{v-u} \right] c_u + \int_u c^*_u V''(x_u) c_u \\ & \quad = S^{\mathcal{J}}(c, c^*, x) \; . \end{aligned}$$

In the first line we just applied the transformation, in the second line we exchanged the anti-commuting Grassmann variables and made the substitutions $u \mapsto -u$ and $v \mapsto -v$, finally in the last step we used $\partial_v \gamma_{v-u} = -\partial_v \gamma_{u-v}$ and we exchanged u and v. Finally the set of boundary conditions [$c(-\mathcal{T}) = \dot{c}(-\mathcal{T}) = c^*(\mathcal{T}) = \dot{c}^*(\mathcal{T})$] is left invariant.

5.5 Consequences of the transformation

We now use the transformation $\mathcal{T}_c$ to derive a number of exact results.

[11] More generally, the transformation on c and c^* is $c_u \mapsto \alpha\, c^*_{-u}$ and $c^*_u \mapsto -\alpha^{-1}\, c_{-u}$ with $\alpha \in C^*$.

5.5.1 The fluctuation-dissipation theorem

This symmetry implies

$$\begin{aligned}\langle x_t i\hat{x}_{t'}\rangle_{S[x,i\hat{x}]} &= \langle \mathcal{T}_c x_t \mathcal{T}_c i\hat{x}_{t'}\rangle_{S[\mathcal{T}_c x,\mathcal{T}_c i\hat{x}]} \\ &= \langle x_{-t} i\hat{x}_{-t'}\rangle_{S[x,i\hat{x}]} + \beta\langle x_{-t} d_{t'} x_{-t'}\rangle_{S[x,i\hat{x}]} \end{aligned} \tag{5.19}$$

that, using time-translational invariance and $\tau \equiv t - t'$, becomes

$$R(\tau) - R(-\tau) = -\beta d_\tau C(-\tau) = -\beta d_\tau C(\tau) \; . \tag{5.20}$$

For generic observables one can similarly apply the $\mathcal{T}_c$ transformation to expression (5.12) of the linear response

$$R_{AB}(\tau) - R_{A_r B_r}(-\tau) = -\beta d_\tau C_{AB}(-\tau) = -\beta d_\tau C_{AB}(\tau) \; . \tag{5.21}$$

where we defined A_r and B_r as

$$A_r([x],t) \equiv A([\bar{x}],-t) \; . \tag{5.22}$$

Take for instance a function $A[x(t),t] = \int du f(x(u))\delta(u-t) + \int du f(\dot{x}(u))\delta(u-t) + \int du f(\ddot{x}(u))\delta(u-t) + \ldots$ then $A_r[x(t),t] = A[x(-t),-t] = \int du f(x(-u))\delta(u+t) + \int du f(\dot{x}(-u))\delta(u+t) + \int du f(\ddot{x}(-u))\delta(u+t) + \ldots$.

Relations between higher order correlation functions evaluated at different times $t_1, t_2, \ldots t_n$ are easy to obtain within this formalism.

5.5.2 Fluctuation theorems

Let us assume that the system is initially prepared in thermal equilibrium with respect to the potential $V(x,\lambda_{-\mathcal{T}})$[12]. The expression for the deterministic part of the MSRJD action functional is

$$\begin{aligned} S^{\rm det}[x,\hat{x};\lambda,\mathrm{f}] &= -\beta\mathcal{H}([x_{-\mathcal{T}}],\lambda_{-\mathcal{T}}) - \ln\mathcal{Z}(\lambda_{-\mathcal{T}}) \\ &\quad - \int_u i\hat{x}_u \left[m\ddot{x}_u + V'(x_u,\lambda_u) - \mathrm{f}_u[x]\right] \; , \end{aligned}$$

where $\mathcal{H}([x_t],\lambda_t) \equiv \frac{1}{2}m\dot{x}_t^2 + V(x_t,\lambda_t)$ and f is a non-conservative force applied on the system. The external work done on the system along a given trajectory between

[12] This is in fact a restriction on the initial velocities, $\dot{x}_{-\mathcal{T}}$, that are to be taken from the Maxwell distribution with temperature β^{-1}, independently of the positions $x_{-\mathcal{T}}$. These latter can be chosen from a generic distribution since the initial potential can be tailored at will through the λ dependence of V.

times $-\mathcal{T}$ and $\mathcal{T}$ is given by

$$\begin{aligned} W[x;\lambda,\mathrm{f}] &\equiv \int_{u_{\lambda_{-\mathcal{T}}}}^{u_{\lambda_{\mathcal{T}}}} dE = \int_{u_{\lambda_{-\mathcal{T}}}}^{u_{\lambda_{\mathcal{T}}}} d_u V = \int_{u_{\lambda_{-\mathcal{T}}}}^{u_{\lambda_{\mathcal{T}}}} \partial_u\lambda_u\ \partial_\lambda V + \int_u \dot{x}_u\ \partial_x V \\ &= \int_{u_{\lambda_{-\mathcal{T}}}}^{u_{\lambda_{\mathcal{T}}}} \partial_{u_{\lambda_{-\mathcal{T}}}}^{u_{\lambda_{\mathcal{T}}}}\lambda_u\ \partial_\lambda V(x_u,\lambda_u) + \int_{u_{\lambda_{-\mathcal{T}}}}^{u_{\lambda_{\mathcal{T}}}} \dot{x}_u\ \mathrm{f}_u[x] \end{aligned} \tag{5.23}$$

where we take into account the time variation of the parameter λ.

Fluctuation Theorem 1.

The transformation $\mathcal{T}_\mathrm{c}$ does not leave S^{det} invariant but yields

$$S^{\mathrm{det}}[x,\hat{x};\lambda,\mathrm{f}] \xmapsto{\mathcal{T}_\mathrm{c}} S^{\mathrm{det}}[x,\hat{x};\bar{\lambda},\mathrm{f}_\mathrm{r}] - \beta\Delta\mathcal{F} - \beta W[x;\bar{\lambda},\mathrm{f}_\mathrm{r}] \tag{5.24}$$

where $S^{\mathrm{det}}[x,\hat{x};\bar{\lambda},\mathrm{f}_\mathrm{r}]$ is the MSRJD action of the system that is prepared (in equilibrium) and evolves under the time-reversed protocol ($\bar{\lambda}(u)\equiv\lambda(-u)$) and external forces ($\mathrm{f}_\mathrm{r}([x],u)\equiv\mathrm{f}([\bar{x}],-u)$). $\Delta\mathcal{F}$ is the change in free energy: $\beta\Delta\mathcal{F}=\ln\mathcal{Z}(\lambda(-\mathcal{T}))-\ln\mathcal{Z}(\lambda(\mathcal{T}))$ between the initial and the final 'virtual' equilibrium states. W is defined above. The dissipative part of the action, S^{diss} does not involve λ and it is still invariant under $\mathcal{T}_c$. This means that, contrary to the external forces, the interaction with the bath is not time-reversed: the friction is still dissipative after the transformation. This immediately yields

$$\langle A[x,\hat{x}]\rangle_{S_\mathrm{c}[x,\hat{x};\lambda,\mathrm{f}]} = e^{-\beta\Delta\mathcal{F}}\langle A[\mathcal{T}_\mathrm{c}x,\mathcal{T}_\mathrm{c}\hat{x}]e^{-\beta W[x;\bar{\lambda},\mathrm{f}_\mathrm{r}]}\rangle_{S_\mathrm{c}[x,\hat{x};\bar{\lambda},\mathrm{f}_\mathrm{r}]} \tag{5.25}$$

for any functional A of x and $\hat{x}$. In particular for a local functional of the field, $A[x(t)]$, it leads to the Crooks relation

$$\langle A[x(t)]\rangle_{S_\mathrm{c}[x,\hat{x};\lambda,\mathrm{f}]} = e^{-\beta\Delta\mathcal{F}}\langle A_\mathrm{r}[x(-t)]e^{-\beta W[x;\bar{\lambda},\mathrm{f}_\mathrm{r}]}\rangle_{S_\mathrm{c}[x,\hat{x};\bar{\lambda},\mathrm{f}_\mathrm{r}]}\ , \tag{5.26}$$

or also

$$\begin{aligned} &\langle A[x(t)]B[x(t')]\rangle_{S_\mathrm{c}[x,\hat{x};\lambda,\mathrm{f}]} \\ &= e^{-\beta\Delta\mathcal{F}}\langle A_\mathrm{r}[x(-t)]B_\mathrm{r}[x(-t')]e^{-\beta W[x;\bar{\lambda},\mathrm{f}_\mathrm{r}]}\rangle_{S_\mathrm{c}[x,\hat{x};\bar{\lambda},\mathrm{f}_\mathrm{r}]}. \end{aligned} \tag{5.27}$$

Setting $A[x,\hat{x}]=1$, we obtain the Jarzynski equality

$$1 = e^{\beta\Delta\mathcal{F}}\langle e^{-\beta W[x;\lambda,\mathrm{f}]}\rangle_{S_\mathrm{c}[x,\hat{x};\lambda,\mathrm{f}]}\ . \tag{5.28}$$

Setting $A[x,\hat{x}]=\delta(W-W[x;\lambda,\mathrm{f}])$ we obtain the transient fluctuation theorem

$$P(W) = P_\mathrm{r}(-W)\ e^{\beta(W-\Delta\mathcal{F})}\ , \tag{5.29}$$

where $P(W)$ is the probability for the external work done between $-\mathcal{T}$ and $\mathcal{T}$ to be W given the protocol $\lambda(t)$ and the non-conservative force $\mathrm{f}([x],t)$. $P_\mathrm{r}(W)$ is the same probability, given the time-reversed protocol $\bar{\lambda}$ and time-reversed force f_r.

Fluctuation Theorem 2.

The result we prove in the following lines is not restricted to Langevin processes with an equilibrium dissipative bath. It applies to generic classical equations of motion, with or without stochastic noise. In short, the proof consists in applying time-reversal on the system and yields an equality between observables and their time-reversed counterparts in a so-called backward (B) process in which the system is prepared in equilibrium with respect to the final conditions of the forward process and is evolved according to the time-reversed equations of motions and protocol. Let us rewrite the action as

$$\begin{aligned} S_{\rm c}[x,\hat{x},\lambda] &= -\beta\mathcal{H}(x_{-\mathcal{T}},\dot{x}_{-\mathcal{T}},\lambda_{-\mathcal{T}}) - \int_u i\hat{x}_u \ {\rm EQ}([x_u],\lambda_u) \\ &\quad + \frac{1}{2}\int_u\int_v i\hat{x}_u \ \beta^{-1}\Gamma_{uv} \ i\hat{x}_v - \ln\mathcal{Z}(\lambda_{-\mathcal{T}}) \ , \end{aligned}$$

and apply the following time-reversal of the fields

$$\mathcal{T}_{\rm tr} \equiv \left\{ \begin{array}{rcl} x_u & \mapsto & x_{-u} \ , \\ i\hat{x}_u & \mapsto & i\hat{x}_{-u} \ . \end{array} \right. \tag{5.30}$$

This yields

$$\begin{aligned} S_{\rm c}[x,\hat{x},\lambda] \ \mapsto \ & -\beta\mathcal{H}([x_{\mathcal{T}}],\bar{\lambda}_{\mathcal{T}}) - \int_u i\hat{x}_u {\rm EQ}_{\rm r}([x_u],\bar{\lambda}_u) \\ & + \frac{1}{2}\int_u\int_v i\hat{x}_u \ \beta^{-1}\Gamma_{uv} \ i\hat{x}_v - \ln\mathcal{Z}(\lambda_{-\mathcal{T}}) \end{aligned}$$

or, by introducing zeroes:

$$\begin{aligned} & -\beta W_{\rm r} - \beta\mathcal{H}([x_{-\mathcal{T}}],\bar{\lambda}_{-\mathcal{T}}) - \int_u i\hat{x}_u {\rm EQ}_{\rm r}([x_u],\bar{\lambda}_u) \\ & + \frac{1}{2}\int_u\int_v i\hat{x}_u \ \beta^{-1}\Gamma_{uv} \ i\hat{x}_v - \beta\Delta\mathcal{F} - \ln\mathcal{Z}(\bar{\lambda}_{-\mathcal{T}}) \ , \end{aligned} \tag{5.31}$$

where $\Delta\mathcal{F} \equiv \mathcal{F}(\lambda_{\mathcal{T}}) - \mathcal{F}(\lambda_{-\mathcal{T}})$ is the free-energy difference between the two 'virtual' equilibrium states corresponding to $\lambda_{\mathcal{T}}$ and $\lambda_{-\mathcal{T}}$. $W_{\rm r} \equiv \mathcal{H}([x_{\mathcal{T}}],\bar{\lambda}_{\mathcal{T}}) - \mathcal{H}([x_{-\mathcal{T}}],\bar{\lambda}_{-\mathcal{T}})$ is the work applied on the system that evolves with the time-reversed equation of motion ${\rm EQ}_{\rm r}$ and under the time-reversed protocol $\bar{\lambda}$. In particular and contrary to the previous paragraph, the friction is no longer dissipative after the transformation. This defines the backward (B) process. Finally, for any observable $A[x,\hat{x}]$ we get the relation

$$\langle A[x,\hat{x}]\rangle_F = e^{-\beta\Delta\mathcal{F}}\langle A[\bar{x},\overline{\hat{x}}]e^{-\beta W_{\rm r}}\rangle_B \ . \tag{5.32}$$

In particular, for two-time correlations, it reads

$$\langle A[x(t)]B[x(t')]\rangle_F = e^{-\beta\Delta\mathcal{F}}\langle A_{\rm r}[x(-t)]B_{\rm r}[x(-t')]e^{-\beta W_{\rm r}}\rangle_B \ . \tag{5.33}$$

Setting $A[x,\hat{x}] = \delta(W - W[x;\lambda,f])$ we obtain the transient fluctuation theorem

$$P_F(W) = P_B(-W)\ e^{\beta(W-\Delta\mathcal{F})}\ , \tag{5.34}$$

where $P_F(W)$ is the probability for the external work done between $-\mathcal{T}$ and $\mathcal{T}$ to be W in the forward process. $P_B(W)$ is the same probability in the backward process.

5.6 Equations on correlations and linear responses

Take any Langevin process in the MSRJD path-integral formalism. From the following four identities

$$\left\langle \frac{\delta i\hat{x}(t)}{\delta i\hat{x}(t')} \right\rangle = \left\langle \frac{\delta x(t)}{\delta x(t')} \right\rangle = \delta(t-t')\ , \qquad \left\langle \frac{\delta x(t)}{\delta i\hat{x}(t')} \right\rangle = \left\langle \frac{\delta i\hat{x}(t)}{\delta x(t')} \right\rangle = 0\ , \tag{5.35}$$

where the angular brackets indicate an average with the MSRJD weight, after an integration by parts, one derives four equations

$$\left\langle x(t)\frac{\delta S}{\delta x(t')} \right\rangle = -\delta(t-t')\ , \qquad \left\langle i\hat{x}(t)\frac{\delta S}{\delta i\hat{x}(t')} \right\rangle = -\delta(t-t')\ , \tag{5.36}$$

$$\left\langle x(t)\frac{\delta S}{\delta i\hat{x}(t')} \right\rangle = 0\ , \qquad \left\langle i\hat{x}(t)\frac{\delta S}{\delta x(t')} \right\rangle = 0\ . \tag{5.37}$$

The second and third one read

$$\begin{aligned} &\left\langle i\hat{x}(t)\left\{m\ddot{x}(t') + \int dt''\ \gamma(t'-t'')\ \dot{x}(t'') + V'[x(t')]\right\}\right\rangle \\ &\qquad\qquad +k_BT\int dt''\ \Gamma(t'-t'')\ \langle i\hat{x}(t)i\hat{x}(t'')\rangle = \delta(t-t')\ , \\ &\left\langle x(t)\left\{m\ddot{x}(t') + \int dt''\ \gamma(t'-t'')\ \dot{x}(t'') + V'[x(t')]\right\}\right\rangle \\ &\qquad\qquad +k_BT\int dt''\ \Gamma(t'-t'')\ \langle x(t)i\hat{x}(t'')\rangle = 0\ , \end{aligned} \tag{5.38}$$

while the other ones, once causality is used (basically $\langle x(t')i\hat{x}(t)\rangle = 0$ for $t > t'$ and $\langle i\hat{x}(t)i\hat{x}(t')\rangle = 0$) do not yield further information. All terms are easily identified with the four types of two-time correlations apart from the ones that involve the potential and are not necessarily quadratic in the fields. The linear terms in two-time functions can be put together after identifying the **free-operator**

$$G_0^{-1}(t',t'') = \delta(t'-t'')m\frac{d^2}{dt''^2} + \gamma(t'-t'')\frac{\partial}{\partial t''} \tag{5.39}$$

The non-linear terms can be approximated in a number of ways: perturbation theory in a small parameter, Gaussian approximation of the MSRJD action, self-consistent

approximations, etc. The choice should be dictated by some knowledge on the system's behavior one wishes to reproduce. In short then

$$
\begin{aligned}
0 &= \int dt'' G_0^{-1}(t',t'')C(t'',t) + \langle x(t)V'[x(t')]\rangle + k_B T \int dt'' \Gamma(t'-t'')R(t,t'') \ , \\
\delta(t-t') &= \int dt'' G_0^{-1}(t',t'')R(t'',t) + \langle i\hat{x}(t)V'[x(t')]\rangle \ . \qquad (5.40)
\end{aligned}
$$

6 Dynamic equations

The generating functionals, with their effective actions, are the adequate starting point to apply perturbation theory (when it is accepted), self-consistent approximations such as the mode-coupling approach, or even more sophisticated techniques as the functional renormalization group. In this section we discuss a number of properties of the generating functional and the ensuing dynamic equations, that we derive in a different ways.

6.1 Connection with the replica formalism

The effective action in a supersymmetric formulation of the generating function has a kinetic minus a potential term $V[\Phi]$. When applying the replica trick to compute the free-energy a replicated effective potential $V[\phi^a]$ appears. A connection between the two formalism, that is based on the similarity between the zero-dimensional replica space and the SUSY one, has been exploited. Roughly speaking, many properties of the replica overlap $Q^{ab} \equiv N^{-1}\sum_{i=1}^{N}\langle s_i^a s_i^b\rangle$ finds a counteraprt in the dynamic SUSY correlator $Q(a,b)$. For instance, a summation over a replica index, $\sum_{a=1}^{n}$ when $n \to 0$, translates into an integration over the supercoordinate $\int da$. For the moment, though, the connection is empirical and a formalization of the relation between the two approaches would be welcome.

6.2 Average over disorder

In general one is interested in the evolution of a model in which the configuration of disorder is typical. One could either attempt to solve the dynamics for one such disorder realization or one can assume that the behavior of a typical system is described by the averaged behavior over all systems, each weighted with its probability. Since the former procedure is more difficult than the latter one usually studies the dynamics averaged over disorder and computes:

$$[\langle A(t)\rangle] = \frac{\int dJP(J)\int \mathcal{D}\phi\mathcal{D}i\hat{\phi}\; A[\phi,i\hat{\phi}]\; e^{-S_{\text{EFF}}[\phi,i\hat{\phi}]}}{\int dJP(J)\int \mathcal{D}\phi\int \mathcal{D}i\hat{\phi}\; e^{-S_{\text{EFF}}[\phi,i\hat{\phi}]}}\,. \tag{6.1}$$

J represents here the random exchanges. Similarly, one can perform an average over a random potential.

One of the advantages of using a dynamic formalism is that when the initial conditions are uncorrelated with disorder there is no need to use the replica trick to average over disorder [50]. Indeed, the classical generating functional is constructed from a path integral that is identical to 1 (and hence independent of disorder) in the absence of sources. The same holds for the quantum Schwinger-Keldysh generating

functional, $\mathrm{Tr}\hat{\rho}_{\mathrm{RED}}(0) = 1$, since we have chosen a diagonal density matrix as the initial condition for the system. Thus,

$$[\langle A(t)\rangle] = \int dJP(J) \int \mathcal{D}\phi\mathcal{D}i\hat{\phi}\; A[\phi, i\hat{\phi}]\; e^{-S_{\mathrm{EFF}}[\phi, i\hat{\phi}]} \tag{6.2}$$

and these averages can be simply computed from $[\mathcal{Z}_J]$.

If the initial condition *is* correlated with the random exchanges or the random potential, the situation is different. One such example is the study of the *equilibrium* dynamics of a disordered model, *i.e.* the study of the evolution of initial conditions taken from P_{GB}. In this case, the use of replicas to average $\ln \mathcal{Z}$ is unavoidable and one is forced to treat replicated dynamic correlators. The initial density operator is a Boltzmann factor that is represented with the Matsubara formalism while the real-time dynamics is written with the Schwinger-Keldysh approach. Mixed correlators and responses intervene in the dynamic equations.

6.3 The equations

We present three derivations of the dynamic equations for the macroscopic order parameters that use the classical or quantum dynamic generating functionals as starting points. Each method is better adapted for different kinds of models.

6.3.1 Supersymmetry and saddle-points

In the white noise limit $\mathcal{Z}$ can be written in a much more compact form if one introduces the super-field formulation of stochastic processes. One first enlarges (space)-time to include two Grassmann coordinates θ and $\overline{\theta}$, *i.e.* $t \to a = (t, \theta, \overline{\theta})$. The dynamic variable $x(t)$ and the auxiliary variable $i\hat{x}(t)$ together with the fermionic ones $\psi(t)$ and $\overline{\psi}(t)$, used to express the Jacobian, are encoded in a super-field,

$$\Phi(a) = x(t) + \overline{\theta}\psi(t) + \overline{\psi}(t)\theta + i\hat{x}(t)\theta\overline{\theta}\;. \tag{6.3}$$

With these definitions,

$$\mathcal{Z}[\eta] = \int d\Phi \exp\left(\frac{1}{2}\int da\; \Phi(a) D_a^{(2)} \Phi(a) - \int da\; V[\Phi(a)] + \int da \Phi(a)\eta(a)\right)$$

with $a = (t, \theta, \overline{\theta})$, $da = dtd\theta d\overline{\theta}$, and the dynamic operator $D_a^{(2)}$ defined as

$$-D_a^{(2)} = 2\gamma k_B T \frac{\partial^2}{\partial\theta\partial\overline{\theta}} + 2\gamma\theta\frac{\partial^2}{\partial\theta\partial t} - \gamma\frac{\partial}{\partial t} - M\theta\frac{\partial^3}{\partial\partial\theta\partial t^2}\;. \tag{6.4}$$

If the model is spherically constrained, $-D_a^{(2)} \to -D_a^{(2)} - \mu(a)$ with $\mu(a)$ a super Lagrange multiplier introduced to enforce the constraint. The delta function $\delta(a-b)$ is defined in Appendix 4.7 and it satisfies $\int db\delta(a-b)f(b) = f(a)$. The super-symmetric notation allows one to encode in the single super correlator $Q(a,b) \equiv \langle\Phi(a)\Phi(b)\rangle$ all

correlators and responses. The generalization to a system with N degrees of freedom is immediate.

Even though the use of the SUSY notation is not necessary to derive the dynamic equations, it is very useful in several aspects. Firstly, it allows to establish contact with the replicated version of the static partition function and the further study of this quantity; secondly, it is very useful as a bookkeeping tool; thirdly, it allows us to develop more sophisticated techniques amenable to derive the dynamic equations of models without fully connected interactions.

Since for classical models the use of white noises is rather generally justified we shall stick to this case. Moreover, we shall drop the inertial contribution to further simplify the presentation. We analyze here models with N variables $\vec{\phi} = (\phi_1, \ldots, \phi_N)$. In SUSY notation we then set the sources to zero and we add a Lagrange multiplier $-D_a^{(2)}$ into $-D_a^{(2)} - \mu_s(a)$ with μ_a a super-field to impose the spherical constraint ($\mu_s(a) = \mu(t) + \text{fermionic} + \hat{\mu}(t)\theta\overline{\theta}$, $\hat{\mu}(t)$ is a Lagrange multiplier that fixes the measure of integration and $\mu(t)$ enters the Langevin equation). Soft spins with their corresponding potential energy can be studied in a similar way though their treatment is slightly more complicated. The potential energy of a rather generic fully connected disordered model can be expressed as a series expansion of the form

$$V[\Phi] = g \sum_{r\geq 0}^{\infty} F_r \sum_{i_1<\ldots<i_{r+1}} J_{i_1\ldots i_{r+1}}\, \Phi_{i_1} \ldots \Phi_{i_{r+1}} \,, \tag{6.5}$$

For each r the sum is taken over all possible groups of $r+1$ spins. The fully-connected character of the model implies that there is no notion of distance or geometry. $J_{i_1\ldots i_{r+1}}$ are random interactions taken from a Gaussian distribution with zero mean and variance $[J^2_{i_1\ldots i_{r+1}}] = (r+1)!/(2N^r)$. Thus (6.5) is a Gaussian random potential with

$$[V(\vec{\Phi}(a))V(\vec{\Phi}(b))] = Ng^2 \sum_{r\geq 0}^{\infty} F_r^2 \left(\frac{\vec{\Phi}(a)\cdot\vec{\Phi}(b)}{N}\right)^{r+1} = N\,\mathcal{V}^{\bullet}\left(\frac{\vec{\Phi}(a)\cdot\vec{\Phi}(b)}{N}\right) . \tag{6.6}$$

The scalar product in the second member is defined as $\vec{\Phi}(a)\cdot\vec{\Phi}(b) = \sum_i \Phi_i(a)\Phi_i(b)$. The bullet means that the powers are taken locally in the super-coordinates a and b and they do not involve an operational product. The term $r = 0$ corresponds to a random field linearly coupled to the spin, the term $r = 1$ is quadratic in the fields while for $r \geq 2$ we obtain higher order interactions. If $F_r = F_p \neq 0, p \geq 2$ and all other $F_r = 0$ one recovers a spherical p spin model. If two parameters are non-zero one obtains a model with two p spin terms. The model of a particle in an infinite dimensional spherical random environment correlated also falls in this category if one can expand the correlator in a power series.

The disordered averaged generating functional reads

$$[\mathcal{Z}] = \int \mathcal{D}\Phi\, e^{-\int da\, \frac{1}{2}\sum_i \Phi_i(a)\,(-D_a^{(2)}-\mu_s(a))\,\Phi_i(a) + \frac{N}{2}\int dadb\, \mathcal{V}^{\bullet}\left(\frac{\vec{\Phi}(a)\cdot\vec{\Phi}(b)}{N}\right)} . \tag{6.7}$$

Introducing the order parameter $Q(a,b) = N^{-1}\sum_{i=1}^{N}\Phi_i(a)\Phi_i(b)$ through

$$1 \propto \int \mathcal{D}Q\mathcal{D}i\tilde{Q}\, e^{-\frac{1}{2}\int da\, db\left(Ni\tilde{Q}(a,b)Q(a,b) - i\tilde{Q}(a,b)\sum_{i=1}^{N}\Phi_i(a)\Phi_i(b)\right)} \tag{6.8}$$

yields

$$[\mathcal{Z}] = \int \mathcal{D}\Phi\mathcal{D}Q\mathcal{D}i\tilde{Q}\ \exp\left[-\frac{1}{2}\int dadb\ \left(Ni\tilde{Q}(a,b)Q(a,b) - N\mathcal{V}^{\bullet}(Q(a,b))\right.\right.$$
$$\left.\left. -\sum_{i=1}^{N}\Phi_i(a)\ (-D_a^{(2)} - \mu_s(a))\ \delta(a-b) - i\tilde{Q}(a,b))\ \Phi_i(b)\right)\right]. \tag{6.9}$$

(Again we omit irrelevant normalization constants.) Note that all terms in the exponent are order N *if* the integrals yield finite contributions. We call the models for which this is true "mean-field" since the saddle-point evaluation of the integral when $N \to \infty$ is exact without including fluctuations.

The saddle-point values for the Landau fields Q are simply related to correlations of the original spins. Indeed, evaluating the generating function in Eq. (6.9) with a saddle-point approximation

$$0 = \left.\frac{\delta S}{\delta i\tilde{Q}(a,b)}\right|_{Q_{\rm SP}} \quad \Rightarrow \quad NQ_{\rm SP}(a,b) = \sum_{i=1}^{N}\langle\Phi_i(a)\Phi_i(b)\rangle_{\tilde{\mathcal{Z}}[Q]}\,, \tag{6.10}$$

where the average on the RHS is taken with the generating functional

$$\tilde{\mathcal{Z}}[Q] \quad \equiv \quad \int \mathcal{D}\Phi\mathcal{D}Q\ e^{\int dadb\,\frac{1}{2}\left[\sum_{i=1}^{N}\Phi_i(a)(-D_a^{(2)}-\mu_s(a))\delta(a-b)\Phi_i(b) + N\mathcal{V}^{\bullet}(Q(a,b))\right]}\,.$$

Opening up the SUSY notation Eq. (6.10) implies, as expected,

$$NC_{\rm SP}(t_1,t_2) = \sum_{i=1}^{N}\langle q_i(t_1)q_i(t_2)\rangle_{\tilde{\mathcal{Z}}[Q]}\,, \quad N\hat{Q}_{\rm SP}(t_1,t_2) = \sum_{i=1}^{N}\langle i\hat{q}_i(t_1)i\hat{q}_i(t_2)\rangle_{\tilde{\mathcal{Z}}[Q]}\,,$$
$$NR_{\rm SP}(t_1,t_2) = \sum_{i=1}^{N}\langle q_i(t_1)i\hat{q}_i(t_2)\rangle_{\tilde{\mathcal{Z}}[Q]}\,, \quad NR^{\dagger}_{\rm SP}(t_1,t_2) = \sum_{i=1}^{N}\langle i\hat{q}_i(t_1)q_i(t_2)\rangle_{\tilde{\mathcal{Z}}[Q]}\,.$$

Going back to Eq. (6.9) we can now shift $i\tilde{Q}$, $\overline{Q} \equiv (-D_a^{(2)} - \mu(t))\ \delta(a-b) - i\tilde{Q}(a,b)$, and integrate over Φ_i

$$[\mathcal{Z}] = \int \mathcal{D}Q\mathcal{D}\overline{Q}\ e^{-\frac{N}{2}\int dadb\,\left[Q(a,b)\overline{Q}(a,b) + (-D_a^{(2)}-\mu(t))\delta(a-b)\ Q(a,b) - \mathcal{V}^{\bullet}(Q(a,b))\right]}$$
$$\times e^{-\frac{N}{2}\mathrm{Tr}\,\mathrm{Ln}\,\overline{Q}}\,.$$

Using a saddle-point evaluation, we eliminate $\overline{Q}$, and we obtain $[\mathcal{Z}] = \int \mathcal{D}Q \, \exp[-N S_{\rm EFF}(Q)]$ with

$$\begin{aligned} 2S_{\rm EFF}(Q) &= \int dadb \left[[-D_a^{(2)} - \mu_s(a)]\delta(a-b)\, Q(a,b) - \mathcal{V}^{\bullet}(Q(a,b)) \right] \\ &\quad -\mathrm{TrLn}\, Q \, . \end{aligned} \tag{6.11}$$

The saddle-point equation over Q, $\delta S_{\rm EFF}/\delta Q = 0$, yields the dynamic equation

$$(D_a^{(2)} + \mu(t))\delta(a-b) + Q^{-1}(a,b) + \mathcal{V}^{\bullet\prime}(Q(a,b)) = 0 \, , \tag{6.12}$$

that takes a more convenient form after multiplying operationally by Q:

$$(D_a^{(2)} + \mu(t))Q(a,b) + \delta(a-b) + \int da' \, \Sigma(a,a')Q(a',b) = 0 \, , \tag{6.13}$$

with the self-energy defined as

$$\Sigma(a,b) \equiv \mathcal{V}^{\bullet\prime}(Q(a,b)) = g^2 \sum_{r\geq 0}^{\infty} F_r^2 (r+1) Q(a,b)^{\bullet\, r} \, . \tag{6.14}$$

We have recasted the saddle-point dynamic equation in the form of a Schwinger-Dyson equation. The dynamic field is here a SUSY correlator that encodes the usual correlation function, the advance and retarded linear responses and the fourth correlator (that vanishes for causal problems):

$$\begin{aligned} &\overline{G}_o^{-1}(t)R(t,t') = \delta(t-t') + 2\gamma\hat{Q}(t,t') + \int dt'' \, [\Sigma(t,t'')R(t'',t') \\ &\quad + D(t,t'')\hat{Q}(t''t,t')] \, , \\ &\overline{G}_o^{-1}(t)C(t,t') = 2\gamma k_B T R(t',t) + \int dt'' \, \Sigma(t,t'')C(t'',t') \\ &\quad + \int dt'' \, + D(t,t'')R(t',t'') \, , \\ &\overline{G}_o^{-1^{\dagger}}(t)R^{\dagger}(t,t') = \delta(t-t') + \int_0^{\infty} dt'' \, \Sigma^{\dagger}(t'',t)R(t',t'') \\ &\quad + \int dt'' \, \hat{\Sigma}(t,t'')C(t'',t') + 2\hat{\mu}(t)C(t,t') \, , \\ &\overline{G}_o^{-1^{\dagger}}(t)\hat{Q}(t,t') = \int dt'' \, \Sigma^{\dagger}(t,t'')\hat{Q}(t'',t') + \int dt'' \, \hat{\Sigma}(t,t'')R(t'',t') \\ &\quad + 2\hat{\mu}(t)R(t,t') \, , \end{aligned}$$

with $\overline{G}_o^{-1}(t) \equiv M\partial_t^2 + \gamma\partial_t + \mu(t)$, $\overline{G}_o^{-1^{\dagger}}(t) \equiv M\partial_t^2 - \gamma\partial_t + \mu(t)$, $\Sigma^{\dagger}(t,t') = \Sigma(t',t)$ and

$$\Sigma(t,t'') = g^2 \sum_{r\geq 0} F_r^2 \, (r+1) r \, C^{r-1}(t,t'')R(t,t'') \tag{6.15}$$

$$D(t,t'') = g^2 \sum_{r\geq 0} F_r^2\,(r+1)\,C^r(t,t'') \tag{6.16}$$

$$\hat{\Sigma}(t,t'') = g^2 \sum_{r\geq 0} F_r^2\,(r+1) r\,C^{r-1}(t,t'')\hat{Q}(t,t'')\;. \tag{6.17}$$

We set to zero all fermionic correlators. We call the above integro-differential equations the Schwinger-Dyson equations for R, C $R^\dagger$ and $\hat{Q}$, respectively.

Causality can be used to simplify the four Schwinger-Dyson equations considerably. For $t' > t$ one has $R(t,t') = 0$ while for $t > t'$ one has $R(t',t) = 0$. Rewriting the equations for R and $R^\dagger$ with these two choices of times one easily sees that $\hat{Q}(t,t') = 0$ for all t and t' (note that $\hat{Q}$ is symmetric in t and t') and $\mu_0(t) = 0$ for all t. Thus, the equation for $\hat{Q}$ vanishes identically when causality holds. In the following we search for causal solutions and we work with their simplified version. We loose in this way the possibility of finding solutions that break causality which are related to instantons. We shall come back to this point later. If we focus on the case $t > t'$ the dynamic equations x(

$$\overline{G}_o^{-1}(t)R(t,t') = \int_{t'}^{t} dt''\;\Sigma(t,t'')R(t'',t')\;, \tag{6.18}$$

$$\overline{G}_o^{-1}(t)C(t,t') = \int_{0}^{t'} dt'' D(t,t'')R(t',t'') + \int_{0}^{t} dt''\Sigma(t,t'')C(t',t'')\;. \tag{6.19}$$

In their integrated form they read

$$R(t,t') = G_o(t,t') + \int_{t'}^{t} dt'' \int_{t'}^{t''} dt'''\; G_o(t,t'')\,\Sigma(t'',t''')\,R(t''',t')\;, \tag{6.20}$$

$$C(t,t') = \int_{0}^{t} dt'' \int_{0}^{t'} dt''' R(t,t'')\,D(t'',t''')\,R(t',t''')\;, \tag{6.21}$$

with the propagator given by $G_o^{-1}(t,t') \equiv \delta(t-t')\overline{G}_o^{-1}(t)$.

The equation for $\mu(t)$ can be derived from the Schwinger-Dyson equation by imposing the spherical constraint through the evaluation at $t = t'$. Multiplying operationally by G_o^{-1} one obtains

$$\begin{aligned}\mu(t) \;=\; & \int_0^t dt''\,[\Sigma(t,t'')C(t,t'') + D(t,t'')R(t,t'')] \\ & + M\int_0^t dt'' \int_0^t dt'''\,(\partial_t R(t,t''))\,D(t'',t''')\,(\partial_t R(t,t''')) \\ & + M^2\left[\partial_t R(t,s)\partial_{st}^2 C(s,t) - \partial_{st}^2 R(t,s)\partial_{t'}C(s,t')\right]\big|_{s\to 0\,t\to t'}\;.\end{aligned} \tag{6.22}$$

The last two terms are a consequence of having a kinetic term with second derivatives. It can be easily identified with minus the second-derivative of the correlation at equal

times by taking the limit $t' \to t^-$ in Eq. (6.19). Thus

$$\mu(t) = \int_0^t dt'' \left[\Sigma(t,t'')C(t,t'') + D(t,t'')R(t,t'')\right] - M \left.\frac{\partial^2}{\partial t^2} C(t,t')\right|_{t'\to t^-} . \quad (6.23)$$

One way of deriving the equation for $\mu(t)$ for a Langevin process with *white noise and no inertia* goes as follows. Considering $t > t'$ in the complete Schwinger-Dyson equation for C and taking $t' \to t^-$, and considering $t < t'$ in the same equation and taking $t' \to t^+$, one finds

$$\lim_{t'\to t^-} \partial_t C(t,t') = \lim_{t'\to t^+} \partial_t C(t,t') - 2k_B T \quad (6.24)$$

where we used $R(t,t' \to t^-) = 1/\gamma$. The derivative of C has a cusp at $t = t'$. The symmetry of the correlation function about $t = t'$ implies $C(t'+\delta,t') = C(t'-\delta,t')$ and an expansion up to first order in δ implies $\lim_{t'\to t^-} \partial_t C(t,t') = -\lim_{t'\to t^+} \partial_t C(t',t)$. From Eq. (6.24) one has $\lim_{t'\to t^-} \partial_t C(t,t') = -k_B T$. Now, one rewrites the complete equation for C exchanging t and t' and adds this equation to the same equation in the limit $t' \to t^-$: $\gamma \lim_{t'\to t^-} [\partial_t C(t,t') + \partial_{t'} C(t,t')] = -2\mu(t) + \lim_{t'\to t^-}$ [rhs eq. for C+rhs eq for $C(t' \leftrightarrow t)$]. From the discussion above the LHS vanishes and the RHS implies

$$\mu(t) = k_B T + \int_0^\infty dt'' \left[\Sigma(t,t'')C(t,t'') + D(t,t'')R(t,t'')\right] . \quad (6.25)$$

For the spherical p spin model $\mu(t)$ is simply related to the energy density $\mathcal{E}(t)$. Indeed, take the Langevin equation evaluated at time t, multiply it by $s_i(t')$, sum over all sites, average over the noise and take the limit $t' \to t$. Repeat this procedure with the Langevin equation evaluated at t' and multiplying by $s_i(t)$. Adding the resulting equations and using $N^{-1}\sum_{i=1}^N \langle s_i(t)\xi_i(t')\rangle = 2\gamma k_B T R(t,t')$ (see Appendix 5.2.1) we have $\mu(t) = -\lim_{t'\to t^-} \left\langle \sum_i \frac{\delta H_J(\vec{s}(t))}{\delta s_i(t)} s_i(t') \right\rangle + k_B T$ that for the spherical p spin model becomes

$$\mu(t) = -p\mathcal{E}(t) + k_B T . \quad (6.26)$$

Thanks to the mean-field character of the model the action is proportional to N and the saddle-point evaluation is exact when $N \to \infty$. For the fully connected models considered in this Section the self-energy is given by a rather simple function of the interactions. For finite dimensional problems none of these procedures are exact. An effective action in terms of *local* order parameters $Q_i(a,b)$ can be written but the evaluation of the generating functional by saddle-point has to include fluctuations.

6.3.2 Field equations

Once we have written the dynamic action in terms of ϕ_i and $i\hat{\phi}_i$ the "field equations" follow from exact properties of the functional integration. Indeed,

$$
\begin{aligned}
0 &= \int \mathcal{D}\phi\mathcal{D}i\hat{\phi}\ \frac{\delta}{\delta i\hat{\phi}_i(t)} e^{-S_{\rm EFF}[\phi_i,i\hat{\phi}_i]+\int_C dt'\left(\eta_i(t')\phi_i(t')+\hat{\eta}_i(t')i\hat{\phi}_i(t')\right)} \\
&= \int \mathcal{D}\phi\mathcal{D}i\hat{\phi}\ \left[-\frac{\delta S_{\rm EFF}(\phi_i,i\hat{\phi}_i)}{\delta i\hat{\phi}_i(t)}+\hat{\eta}_i(t)\right] e^{-S_{\rm EFF}(\phi_i,i\hat{\phi}_i)+\int_C dt'\left(\eta_i(t')\phi_i(t')+\hat{\eta}_i(t')i\hat{\phi}_i(t')\right)} .
\end{aligned}
$$

The subindex C in the integrals stands for "time contour" and it can describe the usual integration from the initial time to infinity for classical models or the close time path for quantum ones. Taking now the variation with respect to the source $i\hat{\eta}_j(t')$ and evaluating at $\eta = i\hat{\eta} = 0$ for all times and components we find

$$
0 \quad = \quad \delta(t-t')\delta_{ij} - \left\langle i\hat{\phi}_j(t')\frac{\delta S_{\rm EFF}(\phi_i,i\hat{\phi}_i)}{\delta i\hat{\phi}_i(t)}\right\rangle \tag{6.27}
$$

where the brackets denote an average with the measure weighted by the dynamic action $S_{\rm EFF}$. If, instead one takes the variation with respect to $\eta_j(t')$ and later evaluates at $\eta = i\hat{\eta} = 0$ one obtains:

$$
\left\langle i\hat{\phi}_i(t)\frac{\delta S}{\delta\phi_j(t')}\right\rangle = 0 . \tag{6.28}
$$

A way to derive dynamic equations for the two-point correlators amounts to use Wick's theorem and rewrite these averages as a sum over all possible factorizations in products of two point-functions. This is of course exact if the action is quadratic but it is only a Gaussian approximation for more general models. This kind of derivation has been mainly used in the study of the dynamics of manifolds in random potentials [32].

6.3.3 The thermodynamic limit and time-scales

It is very important to stress that the dynamic equations derived with the saddle-point approximation hold only when $N \to \infty$ *before* any long-time limit is taken. They describe the dynamics in finite time-scales with respect to N and they cannot capture the crossover from the non-equilibrium relaxation to the equilibrium dynamics reached in time scales that diverge with N [remember that $t_{\rm EQ}(N)$].

Old attempts to study the dynamics of disordered glassy systems assumed that these same equations hold for the equilibrium dynamics when N is finite and time-scales diverge with N [**?**]. This assumption is wrong as shown by several inconsistencies found in the solution at low temperatures: (i) the asymptotic values of one time-quantities do not necessarily coincide with the values calculated with the equilibrium distribution. (ii) the solution exhibited violates the fluctuation - dissipation theorem. These two results are not compatible with equilibrium.

In order to study the equilibrium dynamics of these models one should (i) start from random initial conditions but reach times that grow with N or (ii) impose equilibrium initial conditions. The second route has been implemented – though

without solving the full dynamic problem – by Houghton, Jain and Young. They showed that in this case one is forced to introduce the replica trick to average over disorder.

The dynamic equations here derived are correct when $N \to \infty$ at the outset. Since times are always finite with respect to N, when $t_{\text{EQ}}(N)$ diverges with N the dynamics is not forced to reach equilibrium and there is no contradiction if the solution violates the equilibrium theorems.

6.3.4 Single spin equation

In the limit $N \to \infty$ one can also write the full action S_{EFF} in terms of a *single* variable. This is at the expense of modifying the thermal kernel and the interaction term in a self-consistent way, through the introduction of terms arising from the non-linear interactions (the vertex and self-energy, respectively). For a classical model with white external noise the single variable equation reads

$$M\ddot{\phi}_i(t) + \gamma\,\dot{\phi}_i(t) + \mu(t)\,\phi_i(t) = \int_0^t dt''\,\Sigma(t,t'')\;\phi_i(t'') + \rho_i(t) + \xi_i(t)\;. \tag{6.29}$$

Its generalisation is straightforward. There are two noise sources in this equation: $\xi_i(t)$ is the original white noise while $\rho_i(t)$ is an effective (Gaussian) noise with zero mean and correlations self-consistently given by $\langle \rho_i(t)\rho_j(t')\rangle = \delta_{ij} D(t,t')$. The vertex $D(t,t')$ plays the rôle of the colored noise correlation in a usual Langevin equation. The self-energy $\Sigma(t,t')$ appears here in the place of an 'integrated friction'. A solution of the problem can be attempted numerically using this equation and the self-consistent definitions of Σ and D.

This procedure is not particular useful for the analysis of "polynomial" models since the transformation into a Q dependent effective action can be done exactly. It does however become useful for dealing with models whose single-spin effective action has higher order interaction terms. An example is the quantum SK model.

Interestingly enough a rather flat harmonic oscillator coupled to a bath made of a white and a coloured part at different temperatures acquires two time-scales controlled by the two temperatures involved. We see that a similar structure might appear for the glassy system if the self-energy and vertex self-consistently arrange to act on each degree of freedom as the friction and noise-noise correlator of a complex bath. We shall see that this is indeed what happens to mean-field models.

6.3.5 Diagrammatic techniques

In this Section we first describe the perturbative solution to the Langevin process and how it is used to construct series expansions for the correlations and responses. Self-consistent approximations, such as the *mode coupling* or the *self-consistent screening*, correspond to a selection of a subset of diagrams from the full series. The connection with disordered models is demonstrated. An extension to quantum problems is possible using the generating functional formalism.

Let us focus on a single scalar degree of freedom, q, with potential energy

$$V(x) = \frac{\mu(t)}{2}\, x^2 + \frac{g}{3!}\, x^3 \ , \tag{6.30}$$

and dynamics given by the Langevin in the white noise limit. We take the initial condition $x(t=0) = 0$. $\mu(t)$ is a time-dependent function that we fix at the end of the derivation by requiring $C(t,t) = 1$. In vector models it is the Lagrange multiplier that self-consistently imposes a spherical constraint. Note that this potential is not bounded from below. Setting $G_o(t,t') = [\mu(t) + \gamma\partial_t + M\partial_{t^2}]^{-1}$, a perturbative expansion for $x(t)$ in powers of the noise is easily written as

$$x(t) = (G_o \otimes \xi)(t) - \frac{g}{2}\ (G_o \otimes [G_o \otimes \xi \bullet G_o \otimes \xi])\,(t) + ... \tag{6.31}$$

where $\otimes$ means a time convolution, $(G_o \otimes f)(t) = \int_0^t dt' G_o(t,t') f(t')$, and $\bullet$ is a simple product at equal times. This notation is equivalent to the one used in the SUSY formalism, see Appendix 4.7. Causality implies $G_o(t,t') \propto \theta(t-t')$. If inertia can be neglected $G_o(t,t') = \exp\left(-\int_{t'}^t d\tau\ \mu(\tau)\right)\theta(t-t')$. If one keeps the second-time derivative $G_o(t,t')$ takes a more complicated form. Equation (6.31) can be graphically represented as in Fig. 44. Crosses indicate noise and oriented lines indicate the bare propagator G_o. Each vertex carries a factor $g/2$. Note that the unknown q is evaluated at time t while the noises are evaluated at all previous times.

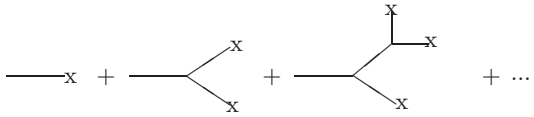

Figure 44: Terms $O(g^0)$, $O(g^1)$ and $O(g^2)$ in the perturbative solution to the Langevin equation.

The expansion for q leads to two expansions for the correlation and response. In simple words, the former corresponds to sandwiching, *i.e.* averaging over the noise, the usual product of two series as the one in Fig. 44 evaluated at different times t and t'. Due to the average over the Gaussian noise noise factors have to be taken by pairs. Let us illustrate this with a few examples.

The first term in the expansion is the result of averaging two $O(g^0)$ terms (first term in Fig. 44):

$$C_o(t,t') = \langle (G_o \otimes \xi)(t) \bullet (G_o \otimes \xi)(t') \rangle = 2\gamma k_B T \int_0^{t'} dt''\, G_o(t,t'') G_o(t',t'') \ ,$$

$t \geq t'$. We depict this term and its contributions to more complicated diagrams with a single crossed line, see the first graph in Fig. 45. The term $O(g)$, as well as all terms which are odd powers of g, vanishes. There are two contributions to the term

$O(g^2)$. One is the result of multiplying a term $O(g^2)$ with a term $O(g^0)$ and it is a tadpole, see the second graph in Fig. 45; we assume this term and all its corrections are included in the contributions from the time-dependent mass and we henceforth ignore them. The other comes from multiplying two $O(g)$ terms, see the third graph in Fig. 45.

Higher order terms are of two types: they either dress the *propagators* or they dress the *vertices*, see the last two diagrams in Fig. 45. These two terms are order $O(g^4)$. The first one follows from averaging two $O(g^2)$ contributions while the second one is the result of averaging an $O(g^3)$ and an $O(g)$ term. The full series yields the *exact perturbative expansion* for C.

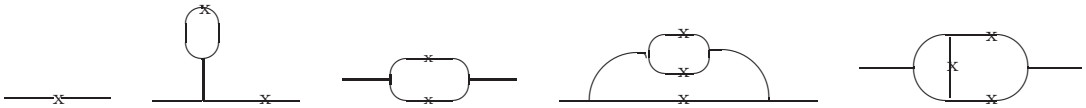

Figure 45: From left to right: $O(g^0)$, two $O(g^2)$ and two $O(g^4)$ terms in the series for C. The next to last diagram dresses the propagator and the last term dresses the vertex. The former is kept in the MCA while the latter is neglected.

The series expansion for the response follows from the relation (**??**) in the white noise limit. In graphical terms we obtain it by multiplying the series in Eq (6.31) and Fig. 44 evaluated at time t by a noise evaluated at time t' and taking the average.

6.4 The mode coupling approximation (MCA)

The diagrammatic expansions for C and R can be represented analytically by introducing the kernels $\Sigma(t,t')$ and $D(t,t')$ through the Schwinger-Dyson equations (6.20) and (6.21) in their integral form. Each of them is a compact notation for a series of diagrams. These equations are exact perturbatively. However, for a generic model one cannot compute the kernels Σ and D exactly.

The mode coupling approach amounts to approximating the kernels $\Sigma(t,t')$ and $D(t,t')$ in the following way. One takes their values at $O(g^2)$ and substitutes in them the bare propagator G_o and the bare correlation C_0 by their dressed values, *i.e.* by R and C themselves. For the model defined in Eq. (6.30) this yields

$$\Sigma(t,t') = g^2\, C(t,t')\, R(t,t')\,, \tag{6.32}$$

$$D(t,t') = 2\gamma k_B T\, \delta(t-t') + \frac{g^2}{2}\, C^2(t,t')\,. \tag{6.33}$$

This approximation neglects "vertex renormalization" in the sense that all diagrams correcting the values of the lines are taken into account while all diagrams correcting the vertices are neglected. For instance, one keeps the fourth diagram in Fig. 45 that represents a line correction, while leaving aside the fifth diagram drawn in the same figure that represents a vertex correction.

The same procedure can be implemented using the SUSY representation of the dynamics. Each line represents the superfield and the super-correlator follows from the sandwich of two series for the super-field evaluated at different super-coordinates a and b.

The Schwinger-Dyson equations can be recast, after multiplying by G_o^{-1}, into the form (6.18) and (6.19) for a random potential (6.5) with only one term $r = p = 3$. Applying the MCA to the trivial (and ill-defined) model (6.30) we derived the dynamic equations for the $p = 3$ spin spherical model! On the one hand, this result is worrying since it shows that the MCA can be rather uncontrolled and it can generate glassy behavior by itself. On the other hand, since the same equations hold in the MCA of a model of interacting particles with realistic interactions, this calculation allows one to understand why the dynamic equations of the MCT for super-cooled liquids coincide with the ones of disordered spin models above T_d. In the next Subsection we show how the diagrams neglected in the MCA vanish in a disordered model with a large number of components.

6.5 MCA and disordered models

The first to notice that the MCA for a "quadratic" dynamic equation corresponds to the exact dynamic equation of a disordered problem with a large number of components was Kraichnan in the context of the Navier-Stokes equation. More recently, Franz and Hertz showed that the "schematic MCT equations of the F_p group" for super-cooled liquids are identical to those arising from a spin model with pseudo-random interactions between groups of three spins. (The schematic MCT focus on a chosen wavevector.)

Indeed, for the example chosen in this Section, one easily demonstrates that the diagrams retained by the MCA are precisely those which survive if one modifies the initial model (6.30) and considers instead the following disordered problem [**?**]. First, let us upgrade q to a vector with N components or "colors" ϕ_i, where $i = 1, 2, ..., N$. Second, let us modify the potential energy (6.30) into

$$V(\vec{\phi}) = g \sum_{i<j<k} J_{ijk}\ \phi_i \phi_j \phi_k \tag{6.34}$$

with couplings J_{ijk} that are independent quenched Gaussian random variables of zero mean and variance $[J_{ijk}^2]_J = 1/N^{p-1} = 1/N^2$. ($p$ is the number of spins in each term in V.) In the large N limit, the noise and disorder averaged correlation and response of this modified model obey Eqs. (6.18) and (6.19) with Σ and D given by Eqs. (6.32) and (6.33), respectively. The fact that these equations are recovered can be seen either directly on the perturbation theory, or using the functional methods given in Section . Since we want to stress that the diagrams neglected in the MCA vanish exactly for this model we use here the first approach.

The bare propagator is diagonal in the color indices, $G_{oij} = G_o \delta_{ij}$. The vertex is now proportional to the random exchanges J_{ijk}. The perturbative solution to the

Langevin equation reads

$$\phi_i(t) = (G_o \otimes \xi_i)(t) - J_{ijk}\, G_o \otimes (G_o \otimes \xi_j \bullet G_o \otimes \xi_k)\,(t) + \dots \ . \tag{6.35}$$

One is interested in computing the self-correlation averaged over the noise and disorder, $N^{-1}\sum_{i=1}^{N}[\langle\phi_i(t)\phi_i(t')\rangle]$. The latter average eliminates all terms with an odd number of couplings. Similarly, since $J_{ijk} \neq 0$ only if all indices i, j, k are different, tadpole contributions as the one in the second graph in Fig. 45 vanish (the noise-noise correlation enforces that two indices in the random exchange must coincide). Finally, one can check that due to the scaling with N of the variance of the disordered interactions, vertex corrections as the one in the last graph in Fig. 45 are sub-leading and vanish when $N \to \infty$. Instead, all line corrections remain finite in the thermodynamic limit. We can check this statement in the two examples shown in Fig. 45 extended to include color indices. The vertex correction has four random exchanges that due to the averaging over the noise are forced to match as, *e.g.* $J_{ijk}J_{jlm}J_{mni}J_{kln}$ leaving 6 free-indices. Averaging over disorder one identifies the indices of two pairs of $J's$, *e.g.* $i = l$ and $k = m$, this yields a factor $(1/N^2)^2$ and, at most, it leaves 4 color indices over which we have to sum from 1 to N (i, j, k, n). We have then an overall factor $1/N^4 \times N^4 = 1$ and this term vanishes when one normalises the correlation by N. Instead, in the line correction, after averaging over the noise, we are left with 6 free indices, *e.g.* $J_{ikj}J_{klm}J_{lmn}J_{inj}$, the average over the noise only imposes $k = n$ in its most convenient contribution, and the overall factor is $1/N^4 \times N^5 = N$. This term contributes to the normalisaed global correlation.

Interestingly enough, the equivalence between the MCA and a disordered system extends to an arbitrary *non-linear* coupling $F(q)$. Expanding F in a power series $F(q) = \sum_{r=2}^{\infty}\frac{F_r}{r!}q^r$ the MCA leads to

$$\Sigma(t,t') \;=\; g^2\sum_{r=2}^{\infty}\frac{F_r^2}{(r-1)!}\,C^{r-1}(t,t')\,R(t,t')\,, \tag{6.36}$$

$$D(t,t') \;=\; 2\gamma k_B T\delta(t-t') + g^2\sum_{r=2}^{\infty}\frac{F_r^2}{r!}\,C^{r}(t,t')\,. \tag{6.37}$$

[Note that for r odd, there appears an additional "tadpole" contribution in Eq. (6.36), which we have assumed again that it has been re-absorbed into the mass term $\mu(t)$.] The dynamic equations can also be obtained as the exact solution of the Langevin dynamics of N continuous spins ϕ_i interacting through the potential

$$V_J[\vec{\phi}] = g\sum_{r\geq 2}^{\infty}F_r\sum_{i_1<\ldots<i_{r+1}}J_{i_1\ldots i_{r+1}}\;\phi_{i_1}\ldots\phi_{i_{r+1}} \tag{6.38}$$

where $J_{\alpha_1,..\alpha_{r+1}}$ are quenched independent Gaussian variables with zero mean and $[(J_{\alpha_1,..\alpha_{r+1}})^2] \propto N^{-r}$. Therefore the MC equations for a single dynamic variable in contact with a heat reservoir and under an arbitrary nonlinear potential $F(q)$ describe

exactly a fully-connected spin-glass problem with arbitrary multi-spin interactions or a particle evolving in an N dimensional space in a quenched random potential $V[\vec{\phi}]$ with a Gaussian distribution with zero mean and variance (6.6) [**?**, 32]. Let us note that in order to be well defined, the model given by V must be supplemented by a constraint preventing the field ϕ_i from exploding in an unstable direction set by the coupling tensor $J_{i_1 \ldots i_{r+1}}$. This problem is cured by imposing the spherical constraint $\sum_{i=1}^{N} \phi_i^2(t) = NC(t,t) \equiv N$.

The extension of the mapping to a space dependent $\phi(\vec{x},t)$ (or to a multicomponent field) is straightforward. Several interesting physical examples involve an equation of the type:

$$\begin{aligned} \frac{\partial \hat{\phi}(\vec{k},t)}{\partial t} &= -(\nu k^2 + \mu)\hat{\phi}(\vec{k},t) - \sum_{r=2}^{\infty} \sum_{\vec{k}_1,..\vec{k}_r} \frac{F_r}{r!} \mathcal{L}_r(\vec{k}|\vec{k}_1,.....\vec{k}_r)\hat{\phi}(\vec{k}_1,t)....\hat{\phi}(\vec{k}_r,t) \\ &\quad +\xi(\vec{k},t) \end{aligned}$$

where $\hat{\phi}(\vec{k},t)$ is the Fourier transform of $\phi(\vec{x},t)$, and $\xi(\vec{k},t)$ a Gaussian noise such that $\langle \xi(\vec{k},t)\xi(\vec{k}',t')\rangle = 2\gamma k_B T \delta(\vec{k}+\vec{k}')\delta(t-t')$. The Kardar-Parisi-Zhang (KPZ) equation corresponds to $r=2$, $\mathcal{L}_2(\vec{k}|\vec{k}_1,\vec{k}_2) = [\vec{k}_1 \cdot \vec{k}_2]\ \delta(\vec{k}_1+\vec{k}_2+\vec{k})$, while domain coarsening in the ϕ^4 theory corresponds to $r=3$, $\mathcal{L}_3(\vec{k}|\vec{k}_1,\vec{k}_2,\vec{k}_3) = \delta(\vec{k}_1+\vec{k}_2+\vec{k}_3+\vec{k})$, with a negative μ [**?**]. The Navier-Stokes equation is similar to the KPZ case with, however, an extra tensorial structure due to the vector character of the velocity field. The correlation and response functions now become $\vec{k}$ dependent, $\delta^d(\vec{k}+\vec{k}')C(\vec{k},t,t') = \langle \tilde{\phi}(\vec{k},t)\tilde{\phi}(\vec{k}',t')\rangle$ and $\delta^d(\vec{k}+\vec{k}')R(\vec{k},t,t') = \langle \partial\tilde{\phi}(\vec{k},t)/\partial\xi(\vec{k}',t')\rangle$. The generalized MC equations then read (assuming that the structure factors are invariant under the permutation of $\vec{k}_1,...,\vec{k}_r$):

$$\begin{aligned} \Sigma(\vec{k},t,t') &= g^2 \sum_{r=2}^{\infty} \frac{F_r^2}{(r-1)!} \sum_{\vec{k}_1,..\vec{k}_r} \mathcal{L}_r(\vec{k}|\vec{k}_1,.....\vec{k}_r)\mathcal{L}_r(\vec{k}_r|\vec{k}_1,.....\vec{k}) \\ &\quad C(\vec{k}_1,t,t')...C(\vec{k}_{r-1},t,t')R(\vec{k}_r,t,t') \qquad (6.39) \\ D(\vec{k},t,t') &= 2\gamma k_B T\ \delta(t-t') + g^2 \sum_{r=2}^{\infty} \frac{F_r^2}{r!} \sum_{\vec{k}_1,..\vec{k}_r} \Big(\mathcal{L}_r(\vec{k}|\vec{k}_1,.....\vec{k}_r)\Big)^2 \\ &\quad C(\vec{k}_1,t,t')...C(\vec{k}_r,t,t') \qquad (6.40) \end{aligned}$$

where $\Sigma(\vec{k},t,t')$ and $D(\vec{k},t,t')$ are defined in analogy with Eqs. (6.36) and (6.37).

6.6 MCA for super-cooled liquids and glasses

In the last 20 years the MCA has been much used in the study of super-cooled liquids. Starting from the realistic interactions between the constituents of a liquid, Götze *et al* used the MCA together with an assumption of equilibrium to derive a dynamic equation for the density-density correlator. This analysis lead to the *schematic*

mode coupling theory (MCT) [**?**] of super-cooled liquids and generalizations (with no reference to wave-vector dependence) and to more sophisticated versions that include a dependence on space. The difference between these models lies on the form of the kernels Σ and D. Kirkpatrick, Thirumalai and Wolynes realized in the late 80s that the schematic mode coupling equation [**?**] is identical to the dynamic equation for the spin-spin correlator in the disordered Potts or p spin model, building a bridge between the study of structural and spin glasses. Why these models and not SK? This will become clear when we present their dynamic and static behavior.

In this Section we explained why the dynamic equation of a disordered model and the one stemming from a MCA of a model with more realistic interactions coïncide: the terms neglected in the latter vanish exactly in the former. The example studied here serves also to signal the danger in using a MCA. One could conclude that a trivial model has a highly non-trivial dynamics, this being generated by the approximation itself.

In the derivation of the dynamic equations presented in this Section no assumption of equilibrium was used. Therefore, these equations hold also in the low temperature phase where equilibrium is lost. It is then natural to propose that the dynamics of the p spin spherical model below T_d schematically describes the dynamics of glasses just as its dynamics above T_d yields the schematic MCT of super-cooled liquids. To go beyond the schematic theory while still keeping a single mode description one simply has to consider $p_1 + p_2$ spherical disordered models. Moreover, the dynamics of a manifold in a random potential is described by dynamic equations with a $\vec{k}$ dependence that goes beyond the single mode MCT.

7 Glassy dynamics: Generic results

Before presenting the explicit solution to the mean-field models we state some generic features of the low-T dynamics that we believe hold in general.

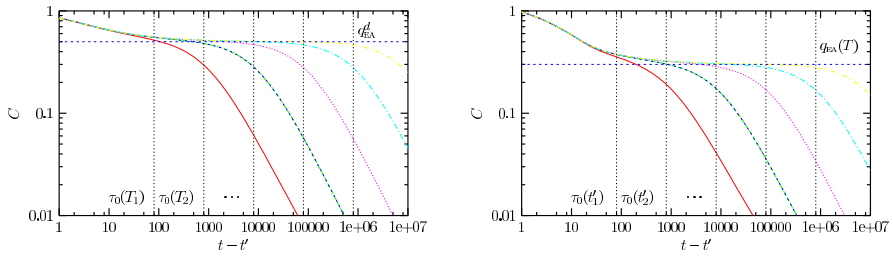

Figure 46: Left: Sketch of the decay of the stationary correlations in the high T phase close to T_d, $T_1 > T_2 > \ldots$. Right: Sketch of the decay of the aging correlations in the low T phase, at fixed $T < T_d$, $t'_1 < t'_2 < \ldots$

7.1 The weak-ergodicity breaking scenario

Figure 46-right shows a sketch of the decay of the correlation as obtained from the numerical solution to the dynamic equations for the mean-field models (see Section). It develops a separation of time scales in the long t' limit. It first approaches a plateau at $q_{\rm EA}$ in a stationary manner and it then decays below this value with an explicit waiting-time dependent form. For each waiting-time there is a sufficiently long t such that the correlation decays to zero. These properties are included in the *weak-ergodicity breaking* (WEB) scenario that states that, for $t \geq t'$, C decays in such a way that

$$\lim_{t'\to\infty} C(t,t') = q_{\rm EA} + C_{\rm ST}(t-t') \tag{7.1}$$

$$\lim_{t-t'\to\infty} C_{\rm ST}(t-t') = 0 \quad \Rightarrow \quad \lim_{t-t'\to\infty}\lim_{t'\to\infty} C(t,t') = q_{\rm EA} \tag{7.2}$$

$$\lim_{t\to\infty} C(t,t') = 0 \quad \text{at fixed } t' \,. \tag{7.3}$$

Equation (7.2) defines the Edwards-Anderson order parameter, $q_{\rm EA}$. For finite t' there is a crossover between two time-scales controlled by a waiting-time dependent characteristic time $\tau_0(t')$ that is a growing function of t' whose precise form depends on the model. For large $t \geq t'$ such that $t - t'$ is small with respect to $\tau_0(t')$, the correlation function first decays from 1 to $q_{\rm EA}$ in a TTI manner. At longer $t-t'$ it goes

further below $q_{\rm EA}$ to eventually reach 0 in a manner that depends both upon t and t' (the aging effect). This behavior suggests the presence of at least two time-sectors in which the dynamics is stationary and non-stationary, respectively. We shall see that the number of time-scales, or more precisely correlation scales, depends on the model.

We write C as the sum of a stationary and an aging contribution:

$$C(t,t') \quad = \quad C_{\rm ST}(t-t') + C_{\rm AG}(t,t') \; . \tag{7.4}$$

The matching conditions at equal times between $C_{\rm ST}$ and $C_{\rm AG}$ are $C(t,t)=1$ implying $C_{\rm ST}(0)+C_{\rm AG}(t,t)=1$ with $C_{\rm ST}(0)=1-q_{\rm EA}$ and $C_{\rm AG}(t,t)=q_{\rm EA}$. Together with Eq. (7.2) they ensure that in the two-time sector in which $C_{\rm ST}$ decays from $1-q_{\rm EA}$ to 0, $C_{\rm AG}$ is just a constant $q_{\rm EA}$. Instead, in the two-time sector in which $C_{\rm AG}$ decays from $q_{\rm EA}$ to 0, $C_{\rm ST}$ vanishes identically.

The name WEB [**?**, **?**] reflects the fact that for short time-differences the system behaves as if it were trapped in some region of phase space of "size" $q_{\rm EA}$ – suggesting ergodicity breaking. However, it is always able to escape this region in a time-scale $\tau_0(t')$ that depends upon its age t'. Hence, trapping is gradual and ergodicity breaking is *weak*. $q_{\rm EA}$ depends on temperature when $T<T_d$.

We have already described, phenomenologically, such a separation of time-scales in the decay of correlation functions when we discussed the domain growth problem and glassy dynamics in Section **??**. The first term describes in this case the fast fluctuations within domains while the second term characterises the domain growth itself. A second example where such a separation of time-scales occurs are the trap models in phase space. The first term corresponds to the dynamics within the traps while the second describes the wandering of the system from trap to trap. In glasses, the first term corresponds to the rapid rattling of each particle within its cage while the second one describes the destruction of the cages and hence the structural relaxation.

In driven models rendered stationary by a weak perturbation we also find a separation of time-scales with τ_0 increasing with weaker strengths of the perturbation. We can also propose that C and R separate in two terms, both being stationary but evolving in different time-scales.

In classical purely relaxational models governed by a Langevin equation with no inertia the correlation functions are monotonic with respect to both times t and t', as it is easily checked numerically. Inertia introduces oscillations and the decay can be non-monotonic. The magnitude of the oscillations depends upon the relative value of the mass M with respect to the other parameters in the problem. However, for a wide choice of parameters the oscillations appear only in the stationary regime, the aging dynamics having a monotonic decay towards zero. This is relevant since it allows one to use the general properties of monotonic correlation functions proven in [**?**] and discussed in Section to find the two-time scaling of $C_{\rm AG}(t,t')$.

7.2 The weak long-term memory scenario

Regarding the response function, we propose a similar separation in two terms:

$$R(t,t') = R_{\rm ST}(t-t') + R_{\rm AG}(t,t') \tag{7.5}$$

with $R_{\rm ST}(t-t') \equiv \lim_{t'\to\infty} R(t,t')$. The matching conditions close to equal times are different for a model with or without inertia. In the former case, $R(t,t)=0$, $R(t,t^-)=1/M$ while in the latter, using the Ito convention, $R(t,t)=0$, $R(t,t^-)=1/\gamma$. In both cases the equal-times condition implies $R_{\rm ST}(0)=0$, $R_{\rm AG}(t,t)=0$ while the next-to-main diagonal values yield $R_{\rm ST}(\delta)=1/M$, $R_{\rm AG}(t,t-\delta)=0$ and $R_{\rm ST}(\delta)=1/\gamma$, $R_{\rm AG}(t,t-\delta)=0$, respectively.

The response tends to zero when times get far apart, and its integral over a *finite* time-interval as well:

$$\lim_{t\to\infty} R(t,t') = 0 \ , \qquad \lim_{t\to\infty} \int_0^{t'} dt''\, R(t,t'') = 0 \qquad \forall \text{ fixed } t' \ . \tag{7.6}$$

These properties imply

$$\lim_{t-t'\to\infty} \lim_{t'\to\infty} R(t,t') = 0 \quad \Rightarrow \quad \lim_{t-t'\to\infty} R_{\rm ST}(t-t') = 0 \ , \ \lim_{t\to\infty} R_{\rm AG}(t,t') = 0 \ . \tag{7.7}$$

However, the contribution of the response to the dynamic equations and to other measurable quantities is not trivial. Examining the integral of the response function over a growing time interval one finds that even if the response vanishes, it yields a contribution to the integration. Figure 49-left shows the integrated linear response (**??**). Using (7.5)

$$\chi(t,t') = \int_{t'}^{t} dt''\ [R_{\rm ST}(t-t'') + R_{\rm AG}(t,t'')] = \chi_{\rm ST}(t-t') + \chi_{\rm AG}(t,t') \ . \tag{7.8}$$

If, for long enough t', the contribution of the second term in (7.8) were negligible, $\chi(t,t')$ should be a stationary quantity. Instead, for all t's studied and for t long enough one clearly sees a waiting-time dependence that can only come from the integration of the second term. This is a *weak long-term memory* (WLTM), the system has an "averaged" memory of its past.

When a system is in equilibrium, the response is simply related to the correlation via FDT. We then assume (and test on the dynamic equations) that the dynamics in the stationary regime satisfies FDT:

$$\begin{aligned} R_{\rm ST}(\tau) &= \frac{1}{k_B T} \frac{dC_{\rm ST}(\tau)}{d\tau} \qquad \tau \geq 0 \ , \\ R_{\rm ST}(\omega) &= -\frac{2}{\hbar} \lim_{\epsilon\to 0^+} \int \frac{d\omega'}{2\pi}\ \frac{1}{\omega-\omega'+i\epsilon}\ \tanh\left(\frac{\beta\hbar\omega'}{2}\right) C_{\rm ST}(\omega') \end{aligned} \tag{7.9}$$

in a classical and quantum problem, respectively. One can formally prove that FDT has to hold for any generic relaxing model fro short time-differences [**?**], see Section . For longer time-differences, when $C_{\rm AG}$ and $R_{\rm AG}$ vary in time while $C_{\rm ST}$ and $R_{\rm ST}$ have decayed to zero, one cannot assume the validity of FDT and, as we shall see, the equations have a solution that explicitly modifies FDT.

7.3 Slow time-reparametrization invariant dynamics

We have already mentioned that the correlations decay monotonically (only below $q_{\rm EA}$ if $M \neq 0$). The final insight coming from the numerical solution to the full equations is that the dynamics becomes slower and slower for fixed waiting-time and as $t-t'$ increases. In the stationary regime $\partial_{t^2}[C(t,t'),R(t,t')]$ and $\partial_{t^2}[C(t,t'),R(t,t')]$ are not negligible with respect to the terms in the RHS of Eqs. (6.18) and (6.19). On the contrary, in the second decay below $q_{\rm EA}$, C and R decay in a much slower manner such that, $\partial_t C(t,t') \ll -\mu(t)C(t,t')$ and $\partial_{t^2} C(t,t') \ll -\mu(t)C(t,t')$ (similarly for R), and the time-derivatives can be neglected.

We choose the following strategy to solve the equations in the long t' limit where a sharp separation of time-scales can be safely assumed. First, we take advantage of the fact that one-time quantities approach a limit, as one can verify numerically, and write the asymptotic form of Eq. (6.25) for μ_∞. The integrals on the RHS are approximated using the separation of C and R in two terms that vary in different time-scales that we assume are well-separated. We detail this calculation below. As regards to the equations for C and R, we proceed in two steps. On the one hand, we choose $t-t'$ short in such a way that $C > q_{\rm EA}$ and we write the dynamic equations for $C_{\rm ST}$ and $R_{\rm ST}$. On the other hand, we take t and t' widely separated so as $C < q_{\rm EA}$ and we write the dynamic equations for $C_{\rm AG}$ and $R_{\rm AG}$. In this way we double the number of unknown functions and equations but we simplify the problem enough as to make it solvable.

Once the time-derivatives are neglected and the integrals are approximated as we explain in Section the aging equations become invariant under reparametrizations of time $t \to h(t)$ that transform the two-point functions as

$$C_{\rm AG}(t,t') \to C_{\rm AG}(h(t),h(t'))\ , \qquad R_{\rm AG}(t,t') \to [d_{t'}h(t')]\ R_{\rm AG}(h(t),h(t'))\ . \tag{7.10}$$

This is not an exact invariance of the dynamic equations. It is only generated when dropping the time-derivatives. This invariance was first noticed by Sompolinsky [**?**] in his study of the equilibrium dynamics (see also [**?**] and it later appeared in the nonequilibrium dynamics [**?**, **?**, **?**, **?**, **?**]. We shall see that this approximation forbids us to solve completely the dynamic equations, in particular, to fix the time scaling (select $h(t)$).

7.4 Correlation scales

Take three ordered times $t_3 \geq t_2 \geq t_1$. The correlations are $C(t_i,t_j) = \frac{1}{N}\sum_k \langle s_k(t_i)s_k(t_j)\rangle \equiv \cos\theta_{ji}$. The monotonicity of the decay of the correlations with respect to the longer time (keeping the shorter time fixed) and the shorter time (keeping the longer time fixed) allows us to derive general properties that strongly constrain the possible scaling forms. Indeed, one can relate any three correlation functions via *triangle relations* [**?**] constructed as follows. Using the fact that the decay is monotonic, one can invert the relation between correlation and times to write, for example, $t_2 = g(C(t_2,t_1),t_1)$ with $g : [0,1]\times[0,\infty] \to [0,\infty]$. This allows us to

rewrite $C(t_3, t_1)$ as

$$C(t_3, t_1) = C(g(C(t_3, t_2), t_2), t_1) = C(g(C(t_3, t_2), g(C(t_2, t_1), t_1), t_1) \ . \tag{7.11}$$

We now define a real function $f(x, y)$, $f : [0, 1] \times [0, 1] \to [0, 1]$, by taking the limit $t_1 \to \infty$ while keeping the intermediate correlations fixed

$$\lim_{\substack{t_1 \to \infty \\ C(t_2,t_1) \text{ and } C(t_3,t_2) \text{ fixed}}} C(t_3, t_1) \quad = \quad f(C(t_3, t_2), C(t_2, t_1)) \ .$$

The fact that the limit exists is a reasonable working assumption. This function completely characterizes the correlations and their scales in the asymptotic limit. (Note that we defined f using the correlation between the longest time and the intermediate as the first argument.)

7.4.1 Properties

The definition of the function f, as well as the properties shown in this Subsection, are model independent. The form taken by f for each model is determined by the dynamic equations.

Time reparametrization invariance The function f is invariant under reparametrizations of time that satisfy (7.10).

Associativity Take now four times $t_4 \geq t_3 \geq t_2 \geq t_1$. The correlation between t_4 and t_1 can be written in two ways

$$\begin{aligned} C(t_4, t_1) &= f(C(t_4, t_2), C(t_2, t_1)) = f(f(C(t_4, t_3), C(t_3, t_2)), C(t_2, t_1)) \ , \\ C(t_4, t_1) &= f(C(t_4, t_3), C(t_3, t_1)) = f(C(t_4, t_3), f(C(t_3, t_2), C(t_2, t_1))) \ . \end{aligned}$$

Thus f satisfies $f(f(x, y), z) = f(x, f(y, z))$, *i.e.* it is an associative function.

Identity. If one takes $t_1 = t_2$

$$C(t_3, t_1) = f(C(t_3, t_2), C(t_2, t_1)) = f(C(t_3, t_1), C(t_1, t_1)) = f(C(t_3, t_1), 1) \ , \tag{7.12}$$

for all $C(t_3, t_1) \in [0, 1]$. Equivalently, if one takes $t_2 = t_3$

$$C(t_3, t_1) = f(C(t_3, t_2), C(t_2, t_1)) = f(C(t_3, t_3), C(t_3, t_1)) = f(1, C(t_3, t_1)) \ , \tag{7.13}$$

for all $C(t_3, t_1) \in [0, 1]$. The correlation at equal times acts as the identity since $x = f(x, 1)$ and $y = f(1, y)$ for all $x, y \in [0, 1]$.

Zero. Taking t_3 and t_2 and much larger than t_1 in such a way that $C(t_2, t_1) \sim 0$ and $C(t_3, t_1) \sim 0$ while $C(t_3, t_2) > 0$,

$$0 \sim C(t_3, t_1) = f(C(t_3, t_2), C(t_2, t_1)) \sim f(C(t_3, t_2), 0) \ . \tag{7.14}$$

Equivalently, taking $t_3 \gg t_2$ and t_1, then $C(t_3, t_2) \sim 0$ and $C(t_3, t_1) \sim 0$ while $C(t_2, t_1) > 0$ and one has

$$0 \sim C(t_3, t_1) = f(C(t_3, t_2), C(t_2, t_1)) \sim f(0, C(t_2, t_1)) \ . \tag{7.15}$$

The minimum correlation acts as a zero of $f(x, y)$ since $0 = f(x, 0)$ and $0 = f(0, y)$ for all $x, y \in [0, 1]$. (This property can be easily generalised if the correlation approaches a non-zero limit.)

Bound. Given that we assume that the system drifts away in phase space, $C(t_2, t_1)$ decays as a function of t_2 for t_1 fixed, and $C(t_2, t_1)$ increases as a function of t_1 for t_2 fixed. This property implies

$$y = f(1, y) \geq f(x, y) \quad \forall y,\ x < 1 \ , \qquad x = f(x, 1) \geq f(x, y) \quad \forall x,\ y < 1 \ . \tag{7.16}$$

Therefore $f(x, y) \leq \min(x, y)$.

Forms for f In [**?**] we proved that

$$f(x, y) = \jmath^{-1}\left(\jmath(x)\jmath(y)\right) \qquad \text{Isomorphic to the product} \tag{7.17}$$

$$f(x, y) = \min(x, y) \qquad \text{Ultrametricity} \tag{7.18}$$

are the only possible forms that satisfy the properties of f shown above. Note that for $\jmath$ equal to the identity the first type of function becomes simply $f(x, y) = xy$, hence the name. It is also possible to prove that the first kind of function (7.17) is only compatible with the time scaling [**?**, **?**]

$$C(t_2, t_1) = \jmath^{-1}\left(\frac{h(t_2)}{h(t_1)}\right) \tag{7.19}$$

with $h(t)$ a monotonically growing function. The actual correlation can have a piecewise form. Here, instead of reproducing the proofs given in [**?**] we explain these statements reviewing the scaling forms found for some physical systems and in the analytic solution to mean-field models.

Examples: domain growth

The correlation decays in two steps, see the right panel in Fig. 46 and for $C > q_{\text{EA}} = m^2_{\text{EQ}}$ the decay is stationary:

$$C_{21} \equiv C(t_2, t_1) = q_{\text{EA}} + C_{\text{ST}}(t_2 - t_1) \ , \tag{7.20}$$

and it can be put in the form (7.19) using $h(t) = \exp(\ln t))$ and $\jmath^{-1}(x) = q_{\text{EA}} + C_{\text{ST}}(x)$. Any three correlation satisfying (7.20) also verify $t_3 - t_1 = C^{-1}_{\text{ST}}(C_{31} - q_{\text{EA}}) = t_3 - t_2 + t_2 - t_1 = C^{-1}_{\text{ST}}(C_{32} - q_{\text{EA}}) + C^{-1}_{\text{ST}}(C_{21} - q_{\text{EA}})$ that implies

$$C_{31} = C_{\text{ST}}[C^{-1}_{\text{ST}}(C_{32} - q_{\text{EA}}) + C^{-1}_{\text{ST}}(C_{21} - q_{\text{EA}})] + q_{\text{EA}} \ . \tag{7.21}$$

This equation is equivalent to (7.17). This means that any three correlations above $q_{\rm EA}$ can be related with an f that is isomorphic to the product, see (7.17), with $\jmath_{\rm ST}^{-1}(x) = C_{\rm ST}(\ln x) + q_{\rm EA}$ and $\jmath_{\rm ST}(x) = \exp(C_{\rm ST}^{-1}(x - q_{\rm EA})$.

When the times are such that the domain walls move, the self-correlation decays below $q_{\rm EA}$ in an aging manner, with

$$C_{21} \equiv C(t_2, t_1) = C_{\rm AG}(t_2, t_1) = \jmath_{\rm AG}^{-1}\left(\frac{\mathcal{R}(t_2)}{\mathcal{R}(t_1)}\right) , \tag{7.22}$$

$\jmath_{\rm AG}^{-1}(1) = q_{\rm EA}$ and $\jmath_{\rm AG}^{-1}(0) = 0$. It is obvious that any three correlations below $q_{\rm EA}$ also satisfy (7.17)

Take now $t_3 = t_2 + \tau_{32}$ with $\tau_{32} < \tau_0(t_2)$ and $C_{32} > q_{\rm EA}$, and t_3 and t_2 sufficiently larger than t_1 ($t_3 = t_1 + \tau_{31}$ with $\tau_{31} > \tau_0(t_1)$ and $t_2 = t_1 + \tau_{21}$ with $\tau_{21} > \tau_0(t_1)$) such that $C_{31} < q_{\rm EA}$ and $C_{32} < q_{\rm EA}$. One has

$$\begin{aligned} C_{31} &= \jmath_{\rm AG}^{-1}\left(\frac{\mathcal{R}(t_3)}{\mathcal{R}(t_1)}\right) = \jmath_{\rm AG}^{-1}\left(\frac{\mathcal{R}(t_3)}{\mathcal{R}(t_2)}(\jmath_{\rm AG} \otimes \jmath_{\rm AG}^{-1})\left(\frac{\mathcal{R}(t_2)}{\mathcal{R}(t_1)}\right)\right) \\ &= \jmath_{\rm AG}^{-1}\left(\frac{\mathcal{R}(t_3)}{\mathcal{R}(t_2)}\jmath_{\rm AG}(C_{21})\right) = C_{21} \ . \end{aligned}$$

The last idendity is a consequence of $\mathcal{R}(t_3)/\mathcal{R}(t_2) \sim 1$ since for a sufficiently small τ_{32}, $\mathcal{R}'(t_2)\tau_{32}/\mathcal{R}(t_2) \ll 1$.

Thus, when the times are such that two correlations, say with values a and b, are both greater than $q_{\rm EA}$ one explores the dynamics in the stationary regime and $f(a, b)$ is isomorphic to the product. When they are both smaller that $q_{\rm EA}$ one explores the dynamics in the aging coarsening regime and again $f(a, b)$ is isomorphic to the product though with a different function $\jmath$. Finally, if $a > q_{\rm EA}$ and $b < q_{\rm EA}$, $f(a, b) = \min(a, b)$ and one finds dynamic ultrametricity.

The structure discussed in the context of the domain growth problem is indeed generic. Some special values of the correlation act as "fixed points" of $f(a, a)$, $f(a, a) = a$. A "correlation scale" spans the values of correlations comprised between two subsequent fixed points. Within a correlation scale f is isomorphic to the product. Any two correlations falling into different correlation scales are related by an ultrametric f. In the domain growth example 1, $q_{\rm EA}$ and 0 are fixed points that are simple to visualize physically. In more abstract models as the SK spin-glass the form of f is more involved, with a stationary scale between 1 and $q_{\rm EA}$ and a dense set fixed points, hence correlation scales, that fill the interval $[0, q_{\rm EA}]$.

Scaling functions

Most solvable models, numerical data and experimental results can be described with only two correlation scales, a stationary and a slow one. Several scaling functions $h(t)$ for the slow decay have been proposed in the literature. In the following

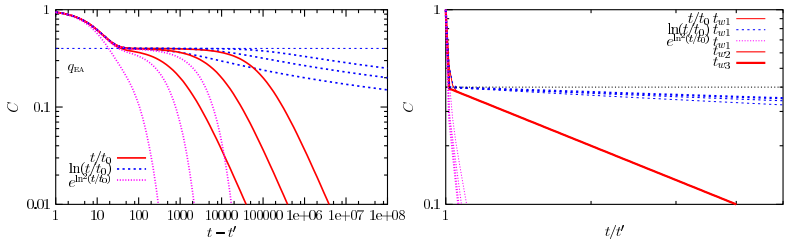

Figure 47: Comparison between three $h(t)$s, power law, enhanced power law and logarithm. Plot of $C(t,t') = (1-q_{\rm EA})\exp(-(t-t')) + q_{\rm EA}h(t)/h(t')$ against the time-difference $t-t'$ (on the left) and against the ratio of times t/t' (on the right) for three waiting times. Note the drift of the curves in the right panel. For the logarithmic law (sub-aging) the curves drift towards the left for increasing waiting-time. Instead, for the enhanced power law (super-aging) the curves drift to the right for increasing waiting-time. For the power law (simple aging) the scaling is perfect. In real systems the decay of the stationary part towards $q_{\rm EA}$ is much slower than exponential (typically power law with a small exponent) and the separation of time-scales is not so neat.

we summarize and discuss the main ones. In Fig. 47 we compare the decay of the correlation from $q_{\rm EA}$ for three of the four laws discussed below.

Power law: $h(t) = at^\alpha$. This is the simplest scaling also called *simple aging*. Ferromagnetic domain growth realizes this form with $\alpha = 1/2$ for non conserved dynamics and $\alpha = 1/3$ for conserved dynamics [**?**]. Several solvable model have simple aging, an example being the classical spherical $p = 2$ model [**?**, **?**]. In [**?**] it was conjectured that a power law also characterized the aging dynamics of the fully connected p spin-model with $p \geq 3$. This was later confirmed with the algorithm of Kim and Latz [**?**] that allows one to reach much longer times. Aging below T_c in the simplest trap model also scales with this law [**?**]. The molecular dynamic simulations of Lennard-Jones mixtures show this type of scaling too. Note that for all α, C scales as a function of t_2/t_1.

Enhanced power law: $h(t) = \exp(\ln^\alpha(t/t_0))$ This law yields the most accurate description of spin-glass experimental data. The exponent α typically takes a possibly T-dependent value about 2 [**?**].

Stretched exponential: $h(t) = \exp[(t/t_0)^\alpha]$ This law has been proposed to describe the slowing down of the full correlation above the critical temperature. As far as we know, no aging model that satisfies a scaling (7.19) with a stretched exponential has been found yet.

Logarithm: $h(t) = \ln^\alpha(t/t_0)$ In the Fisher and Huse droplet model for spin-glasses, activated dynamics is assumed and the domains are found to grow as $\mathcal{R}(t) \sim \ln(t/t_0)$.

This leads to $C(t_2,t_1) \sim g(\ln(t_2/t_0)/\ln(t_1/t_0))$. However, this law does not fit the aging experimental data [**?**].

Dynamic ultrametricity: Even though it seems mysterious at first sight there is a simple graphical construction that allows one to test it. Take two times $t_3 > t_1$ such that $C(t_3,t_1)$ equals some prescribed value, say $C(t_3,t_1) = 0.3 = C_{31}$. Plot now $C(t_3,t_2)$ against $C(t_2,t_1)$ using t_2, $t_1 \le t_2 \le t_3$, as a parameter. Depending on the value of C_{31} with respect to $q_{\rm EA}$ we find two possible plots. If $C(t_3,t_1) > q_{\rm EA}$, for long enough t_1, the function f becomes isomorphic to the product. Plotting then $C(t_3,t_2)$ for longer and longer t_1, the construction approaches a limit in which $C(t_3,t_2) = \jmath^{-1}(\jmath(C_{31})/\jmath(C(t_2,t_1)))$. If, instead, $C_{31} < q_{\rm EA}$, in the long t_1 limit the construction approaches a different curve. We sketch in Fig. 48 two possible outcomes of this construction. On the right, we represent a model with two correlation scales, ultrametricity holds between them and within each of them f is isomorphic to the product. On the left instead we represent a model such that dynamic ultrametricity holds for all correlations below $q_{\rm EA}$. The construction approaches, in the long t_1 limit, the broken curve depicted in the sketch.

The SK spin-glass [**?**] and the dynamics of manifolds in an infinite dimensional embedding space in the presence of a random potential with long-range correlations [**?**, **?**] have ultrametric decays everywhere within the aging regime. This scaling is also found in the trap model at the critical temperature [**?**]. Dynamic ultrametricity in finite dimensional systems has been search numerically. There is some evidence for it in the $4d$EA model. In $3d$ instead the numerical data does not support this scaling [**?**, **?**]. Whether this is due to the short times involved or if the scaling asymptotic is different in $3d$ is still an open question.

7.4.2 Definition of a characteristic time

Expanding the argument in (7.19) for $t_2 = t_1 + \tau$ with $\tau \ll t_1$ one finds, to leading order,

$$\frac{h(t_1)}{h(t_2)} = 1 - \frac{\tau}{t_c(t_1)} \qquad t_c(t_1) \equiv \left(\frac{h'(t_1)}{h(t_1)}\right)^{-1} , \tag{7.23}$$

with $O\left(\tau^2\left(h'^2(t_1)/h^2(t_1) + h''(t_1)/h(t_1)\right)\right)$ corrections. The characteristic time $t_c(t_1)$ is given by

$$t_c(t_1) \quad = \quad \begin{cases} t_1/\alpha & \text{Power law} \\ t_1/[\alpha \ln^{\alpha-1}(t_1/t_0)] & \text{Enhanced power law} \\ t_1\,(t_0/t_1)^{\alpha} & \text{Stretched exponential} \\ t_1\,\ln(t_1/t_0) & \text{Logarithm} \end{cases}$$

Note that $t_c(t_1)$ is defined close to the limit of equal times and (7.23) does not make sense for large τ. Rather often in the literature, the scaling variable $x = \tau/t_1^a$ has been used even for large values of τ. This scaling is incompatible with the general properties of the triangular relations recalled in Section if the exponent a is larger

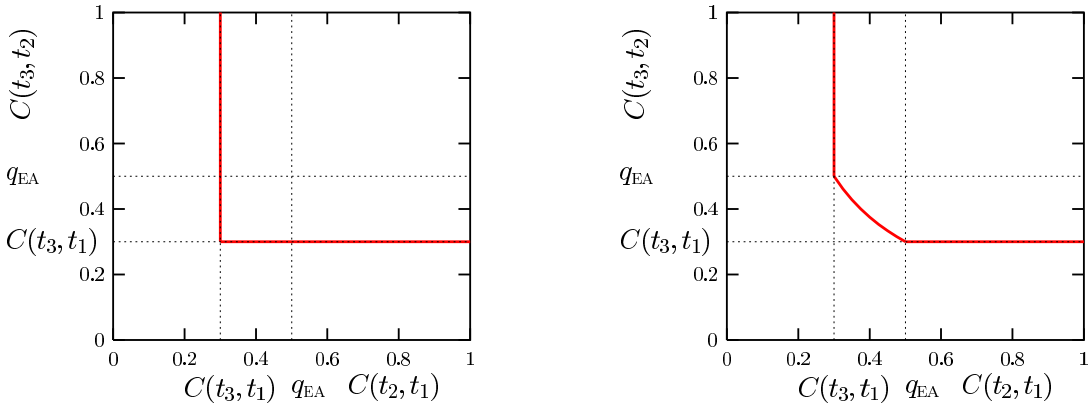

Figure 48: Sketch of a check of ultrametricity using the parametric plot $C(t_3,t_2)$ against $C(t_2,t_1)$ for $C(t_3,t_1) = 0.3 < q_{\rm EA}$ fixed. On the left an ultrametric model, on the right a model with two correlation scales.

than 1 [**?**]. See the right panel in Fig. 47 to see the different trends of these scalings when plotted as functions of t/t'.

For the power law $t_c(t_1)$ scales just as t_1. In the cases of the stretched exponential and the enhanced power law, $t_c(t_1)$ has a slower growth than the linear dependence iff $\alpha > 0$ in the first case and $\alpha > 1$ in the second. This behavior has been called *sub-aging*. For the logarithm $t_c(t_2)$ grows faster than linearly. This function belongs to a different class that we called *super aging* [**?**].

7.5 Modifications of FDT

One of the most important outcomes of the analytic solution to the mean-field glassy models is the need to modify the fluctuation–dissipation relations between linear responses, $R(t,t_w)$, and their partner correlations between spontaneous fluctuations, $C(t,t_w)$, when $T < T_d$. In this Subsection we discuss different ways of presenting the modification of FDT expected in rather generic systems with slow dynamics.

7.5.1 Time domain

The FDT is a linear relation between $\chi(t,t_w)$ and $C(t,t_w)$ for any pair of times (t,t_w), see Eq. (**??**). In early simulations of the $3d$EA model as well as in the analytic solution to fully-connected disordered models a modification of this relation below T_d appeared. Plotting $k_B T\chi(t,t_w)$ and $1-C(t,t_w)$ for t_w fixed as a function of $\ln(t-t_w)$ one typically obtains the pair of curves schematically shown on the left

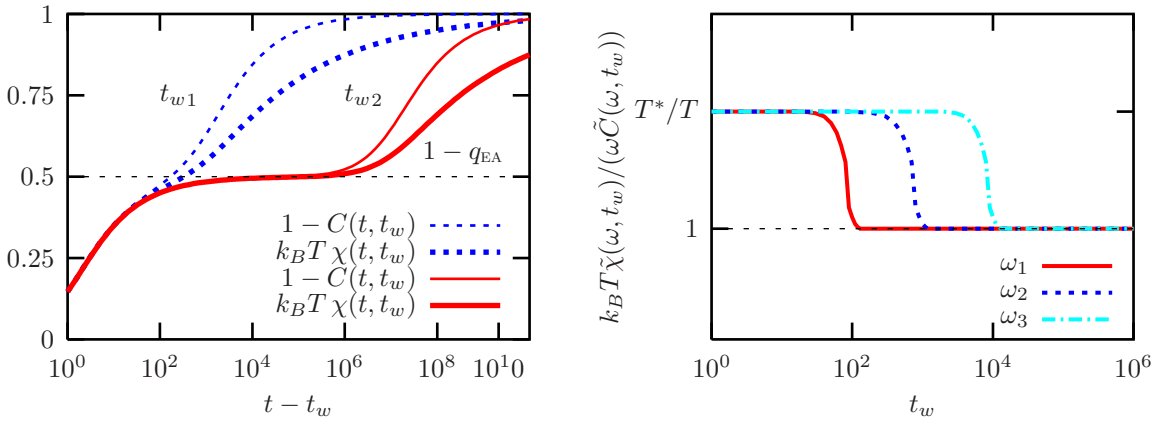

Figure 49: Left: sketch of the modification of FDT in the time-domain. Right: sketch of the modification of FDT in the frequency domain for a glassy system, $\omega_1 > \omega_2 > \omega_3$.

panel of Fig. 49. The two functions go together until $t - t_w$ reaches a characteristic time $\tau_0(t_w)$ and they then depart demonstrating that FDT does not hold beyond this time-scale. The characteristic time $\tau_0(t_w)$ is of the order of the time needed to reach the plateau in the correlation function (this holds for mean-field models but it is not certain in finite dimensional systems). Summarizing

$$t - t_w < \tau_0(t_w) \qquad \text{FDT holds in the fast scale ,} \tag{7.24}$$
$$t - t_w > \tau_0(t_w) \qquad \text{FDT is modified in the slow scale ,} \tag{7.25}$$

with $\tau_0(t_w)$ an increasing function of t_w that depends on the system considered (see Fig. 46).

7.5.2 Frequency domain

Taking a Fourier transform with respect to the time-difference while keeping t_w fixed allows one to work in a mixed frequency-time domain. Since many experimental set-ups are prepared to apply ac-fields it is particularly important to predict the aspect FDT modification have when using these parameters. The condition $t - t_w < \tau_0(t_w)$ to explore the fast relaxation roughly translates into $\omega^{-1} < \tau_0(t_w)$, *i.e.* for a fixed waiting-time high frequencies are required. The longer the waiting time the lower the frequency one has to use to see this scale since $\tau_0(t_w)$ increases with t_w. Instead, when $t - t_w > \tau_0(t_w)$ one has $\omega^{-1} > \tau_0(t_w)$, and very low frequencies are needed to explore the slow scale. These conditions imply

$$\omega\tau_0(t_w) > 1 \qquad \text{FDT holds in the fast scale ,}$$
$$\omega\tau_0(t_w) < 1 \qquad \text{FDT does not hold in the slow scale .} \tag{7.26}$$

Reversing the argument above, if one weakly perturbs the sample with an ac-field of a fixed frequency ω_1 at a chosen time t_w, one can follow the deviation from FDT using t_w as the control parameter. This procedure yields the solid line on the right panel of Fig. 49. Choosing now a lower frequency $\omega_2 (< \omega_1)$ the crossover from the slow to the fast regime occurs at a larger value of t_w. One obtains then the dotted curve on the right panel of Fig. 49. So on and so forth, the smaller the frequency of the applied ac-field the longer the slow regime lasts and the longer one sees deviations from FDT. (Note that the probe does not modify the dynamics.) In the Figure we chose to sketch the behavior of a system with only two-time scales, in which the FDT ratio takes two constant values separated at single breaking point in which the correlation reaches the plateau value $q_{\rm EA}$. This procedure is commonly employed experimentally where we discuss the measurements of Grigera and Israeloff for glycerol.

7.5.3 Time-reparametrization invariant formulation

A more interesting way of displaying the modification of the FDT has been suggested by the analytic solution to the mean-field models discussed in Section . One of its advantages is that it allows one to classify the systems into sort of "universality classes" according to the form the FDT modification takes.

The analytic solution is such that, in the asymptotic limit in which the waiting-time t_w diverges after $N \to \infty$, the integrated linear response approaches the limit

$$\lim_{\substack{t_w \to \infty \\ C(t,t_w) = C}} \chi(t, t_w) = \chi(C) \tag{7.27}$$

when t_w and t diverge while keeping the correlation between them fixed to C [**?**]. Deriving this relation with respect to the waiting time t_w, one finds that the opposite of the inverse of the slope of the curve $\chi(C)$ is a parameter that replaces temperature in the differential form of the FDT. Thus, using Eq. (7.27) one defines

$$k_B T_{\rm EFF}(C) \equiv -(\chi'(C))^{-1} \, , \tag{7.28}$$

that can be a function of the correlation. Under certain circumstances one can show that this quantity has the properties of a temperature [26] in the sense to be described later.

One of the advantages of this formulation is that, just as in the construction of triangle relations, times have been "divided away" and the relation (7.27) is invariant under the reparametrizations of time defined in Eq. (7.10).

Equation (7.27) is easy to understand graphically. Let us take a waiting time t_w, say equal to 10 time units after the preparation of the system (by this we mean that the temperature of the environment has been set to T at the initial time) and trace $\chi(t, t_w)$ against $C(t, t_w)$ using t as a parameter (t varies between t_w and infinity). If we choose to work with a correlation that is normalized to one at equal times, the parametric curve starts at the point $(C(t_w, t_w) = 1, \chi(t_w, t_w) = 0)$ and it arrives at

the point $(C(t \to \infty, t_w) \to \overline{C}, \chi(t \to \infty, t_w) = \overline{\chi})$. Without loss of generality we can assume that the correlation decays to zero, $\overline{C} = 0$. This first curve is traced in red in Figs. 50. Now, let us choose a longer waiting time, say $t_w = 100$ time units, and reproduce this construction. One finds the green curves in Figs. 50. Equation (7.27) states that if one repeats this construction for a sufficiently long waiting time, the parametric curve approaches a limit $\chi(C)$, represented by the blue curves.

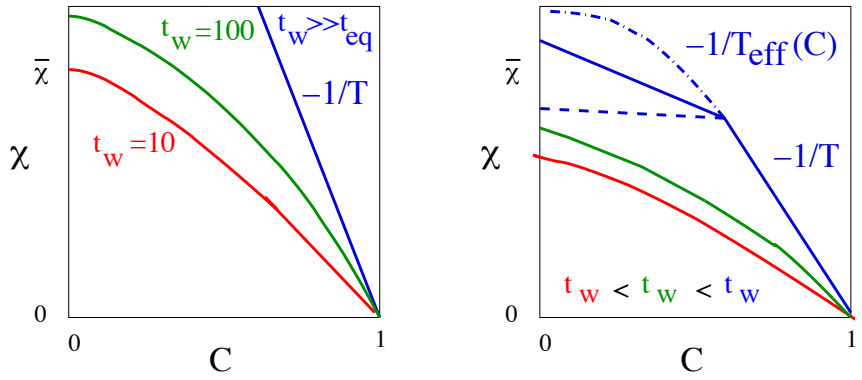

Figure 50: The asymptotic behavior of the integrated linear response against the correlation in a parametric plot, for fixed waiting time and using t as a parameter. Left: behavior in equilibrium. Right: behavior in a slowly relaxing system out of equilibrium. See text for an explanation.

When the system equilibrates with its environment, the construction approaches a straight line with slope $-1/(k_B T)$ as predicted by the FDT. This is the result shown in the left panel of Fig. 50. Instead, for non-equilibrium systems evolving slowly the asymptotic limit is different, it is given by a *curve* $\chi(C)$. For solvable fully-connected models one distinguishes three families, as drawn in the right panel of Fig. 50. They correspond to some systems undergoing domain growth [**?**] (*e.g.* the $O(N)$ model in $d = 3$ when $N \to \infty$), systems behaving like structural glasses (*e.g.* the p-spin model) and spin-glasses (*e.g.* the SK model). Several numerical studies in more realistic models of the three cases tend to confirm this classification. However, two provisos are in order. First, one has to be very cautious about the numerical results given the very short time scales and rather small system sizes accessible in simulations. Second, as shown in Section **??**, at least one system that undergoes domain growth, the ferromagnetic chain, has a non-trivial $\chi(C)$ like the one found for the SK model.

We have already found these asymptotic $\chi(C)$ curves when we discussed the dynamics of a (flat) harmonic oscillator in contact with a complex bath made of subsystems with different characteristic times and temperatures. Here we claim that the same structure arises in a glassy model coupled to a white-bath. Different values of the effective temperature are self-generated in the system.

This plot is invariant under reparametrisations of time $t \to h(t)$ acting on the two-point functions as in Eqs.(7.10). A different choice of the functions h only changes the speed with which the $\chi(C)$ curve is traced but not its form.

7.5.4 FDT part

The Fokker-Planck formalism used to derive the FDT can be also be used to obtain a bound on FDT violations. Indeed, one bounds the difference between response and variation of the correlation with the Cauchy-Schwartz inequality leading to

$$\left|k_B T R(\tau + t_w, t_w) - \partial_s C(\tau + t_w, s)|_{s=t_w}\right| \leq c\sqrt{-d_{t_w}\mathcal{H}(t_w)} \tag{7.29}$$

where c is a constant and $\mathcal{H}(t_w) \equiv \int dq P(q, t_w)(E(q) - k_B T \ln P(q, t_w))$ is a positive definite function that monotonically decreases towards the free-energy when the system eventually equilibrates. One finds a similar bound for Kramers processes and a generalization that includes the power input when time-dependent or non-potential forces are applied. For systems such that $d_{t_w}\mathcal{H}(t_w) \to 0$ sufficiently fast when $t_w \to \infty$ the bound implies that the LHS vanishes in this limit. This can be achieved in two ways: either each term is finite and the difference between them vanishes or each term tends to zero independently. The former possibility is what happens in the fast regime where FDT holds. The latter holds in the slow regime where both the response and the variation of the correlation are very small but the relation between them does not follow FDT. One derives a more useful bound by integrating (7.29) over time:

$$|k_B T \chi(\tau + t_w, t_w) - C(\tau + t_w, t_w) + C(t_w, t_w)| \leq c \int_{t_w}^{\tau + t_w} dt' \, \sqrt{-d_{t'}\mathcal{H}(t')} \, . \tag{7.30}$$

The terms in the LHS are now always finite while the value of the RHS depends on the relation between the time-difference τ and the waiting-time t_w. For sufficiently short τ such that the RHS vanishes FDT has to be satisfied in its integrated form. This result explains the existence of a common straight-line with slope $-1/(k_B T)$ in the nonequilibrium curves in Fig. 50. For sufficiently long τ such that the RHS takes a finite value FDT can be violated. In this second scale a departure from the straight line of slope $-1/(k_B T)$ can occur and it is indeed what happens in systems with slow non-equilibrium dynamics, see the right panel in Fig. 50. One sees how a separation of time-scales in the dynamics influences the FDT violations.

In driven systems the bound depends on the power input and only vanishes in the limit of vanishing applied forces. The FDT is not even enforced in the fast scale and deviations start as soon as C decays from 1. However, as we shall see below, the modification of FDT follow a very similar pattern to the one shown in Fig. 50 with the strength of the applied force playing a similar role to the one of the waiting-time here.

7.5.5 Diffusion

In these Lectures we focus on models with a bounded self-correlation for an observable with zero average that is normalised at equal times. If the averaged observable does not vanish but the equal-time correlation reaches a time-independent limit one can still use the simple self-correlation in the generalisations of FDT. However, in more general diffusive model with an unbounded time-dependent equal-time correlator it is more natural to compare the behaviour of the "displacement" $\Delta(t,t') \equiv C(t,t)+C(t',t')-2C(t,t')$ (that vanishes by definition at equal times) to the linear response. In normal diffusion these are linked by $R(t,t') = 1/(2k_BT)\Delta(t,t')$. In glassy models like the massless manifold in a random potential and others this relation is modified.

8 Solution to mean-field models

In this Section we turn our attention to the solution to the Schwinger-Dyson equations derived in previous Sections. We start by describing the simplest numerical algorithm that solves these equations and we next briefly discuss the asymptotic analytic solution at high temperatures. Next we describe in quite detail the solution at low T.

8.1 Numerical solution

One can attempt a numerical solution to the set of causal integro-differential equations (6.18), (6.19) together with the equation for the Lagrange multiplier $\mu(t)$. One of the questions we would like to explore is whether they encode a non-equilibrium evolution as the one we have already described.

The correlation $C(t,t')$ and response $R(t,t')$ are two-time quantities, that is, they depend on t (which physically corresponds to the time of observation) and t' (which corresponds to the age of the system). In the simplest algorithm one discretises the two-times plane with a *uniform grid*, $t' = j\delta$ and $t = i\delta$. The correlation and response on the diagonal and the next-to-main diagonal of the two-times plane (i,j) are known for all times.

The time-derivatives $\partial_t^2 C(t,t')$ and $\partial_t^2 R(t,t')$ in their discretized form are used to update the two-point functions. Due to causality, to advance one time step, the integrals only need values of C and R that are already known. This algorithm is simple and efficient but it is severely limited by the computer storage capacity. Since one has to store C and R for all previous time steps, the memory used grows as i^2 and this number becomes rather quickly prohibitive. In standard PCs one can use $i_{\rm MAX} \sim 10^4$, get an acceptable precision for $\delta \leq 0.1$ and reach total times of the order of 10^3.

In the quantum case the presence of non local kernels η and ν, that appear convoluted with C and R, renders the numerical solution harder. The larger the cut-off Λ, the smaller the iteration step δ we need to compute these integrals with a good precision. The maximum total time is of the order of 10^2 in this case.

A different starting point for a numerical solution is the single variable equation (6.29). This route was followed by Eissfeller and Opper for spin-glasses [**?**] and it is usually used in the so-called dynamic mean-field theory. Again, this method is limited by the storage capacity.

The knowledge of the qualitative features of the solution helps one devising a more performant algorithm with a *variable two-time grid*. As we shall see from the analytic solution, C and R vary rapidly when times are near the diagonal $j = i$ and decay very slowly far from it. Kim and Latz have exploited this property and wrote such an algorithm for the spherical p spin model reaching total times of the order of 10^8.

Finally, one can think of an iterative search where one starts from a trial form of C and R and uses the dynamic equations to extract the new form. One can expect to obtain the solution by repeating this procedure until the iteration converges to a fixed point. This method would allow one to look for solutions of the full set of Schwinger - Dyson equations that break causality.

The numerical solution for the causal problem, found with the simple uniform grid, has been of great help in deriving the asymptotic analytic solution. In the following we describe how this solution builds up.

8.2 Solution at high temperatures

At high temperature the system equilibrates with its environment since

$$t_{\rm EQ}(N \to \infty, T) = \text{finite} \ . \tag{8.1}$$

The mere existence of an asymptotic limit implies that one-time quantities as, *e.g.*, the energy density, $\mathcal{E}(t)$, or the Lagrange multiplier, $\mu(t)$, have to approach an asymptotic limit, $\lim_{t\to\infty} \mathcal{E}(t) = \mathcal{E}_\infty$ and $\lim_{t\to\infty} \mu(t) = \mu_\infty$. In equilibrium $\mathcal{E}_\infty = \mathcal{E}_{\rm EQ}$ and similarly for all one-time quantities. Two time-quantities, as C and R, depend on times but only through time differences.

To solve the high T dynamics one first assumes that after a transient equilibrium is reached and a solution of the form $\mu(t) \to \mu_\infty$,

$$C(t,t') \to C_{\rm ST}(t-t') \ , \quad R(t,t') \to R_{\rm ST}(t-t') \tag{8.2}$$

with $R_{\rm ST}$ and $C_{|scst}$ related by FDT, for long waiting-times t' and all time-differences $t - t'$, exists. These properties also apply to D and Σ that behave as a correlation and a response, respectively. This *Ansatz* should solve Eqs. (6.18) and (6.19) when $T > T_d$, with T_d the dynamic critical temperature. In order to prove it we take t' long and we assume that we can separate the integrals in Eqs. (6.19) and (6.18) in a *preasymptotic* and an *asymptotic* contribution,

$$\int_0^\infty dt'' \ \cdots \approx \int_0^{t_{\rm EQ}} dt'' \ \cdots + \int_{t_{\rm EQ}}^\infty dt'' \ \cdots \ . \tag{8.3}$$

Next, we assume that the two-point functions decay as fast as to ensure that all preasymptotic contributions vanish, *e.g.* $\int_0^{t_{\rm EQ}} dt'' \ A(t,t'')B(t',t'') \sim 0$ when t' and

$t \geq t'$ are in the asymptotic regime. Using the *Ansatz* (8.2) and this assumption the integrals in the RHS of Eq. (6.19), for a classical problem, read

$$\int_{t_{\rm EQ}}^{t'} dt'' D_{\rm ST}(t-t'') \frac{1}{k_B T} \frac{\partial C_{\rm ST}(t'-t'')}{\partial t''} + \int_{t_{\rm EQ}}^{t} dt'' \frac{1}{k_B T} \frac{\partial D_{\rm ST}(t-t'')}{\partial t''} C_{\rm ST}(|t''-t'|)$$
$$= \frac{1}{k_B T} \int_{t_{\rm EQ}}^{t'} dt'' \frac{\partial}{\partial t''} \left[D_{\rm ST}(t-t'') C_{\rm ST}(t'-t'') \right] + \frac{1}{k_B T} \int_{t'}^{t} dt'' \frac{\partial D_{\rm ST}(t-t'')}{\partial t''} C_{\rm ST}(t''-t')$$

The first integral in the RHS is a total derivative and it can be readily evaluated, it yields $D_{\rm ST}(t-t')C_{\rm ST}(0) - D_{\rm ST}(t-t_{\rm EQ})C_{\rm ST}(t'-t_{\rm EQ}) \approx D_{\rm ST}(\tau)$ where we assumed that t and t' are well in the asymptotic regime in such a way that $C_{\rm ST}(t'-t_{\rm EQ}) \sim 0$, and we defined $\tau \equiv t-t'$. Integrating by parts the last integral in the RHS one finally obtains the high T equation for the correlation

$$G_o^{-1}(\tau) C_{\rm ST}(\tau) = \frac{1}{k_B T} D_{\rm ST}(0) C_{\rm ST}(\tau) - \frac{1}{k_B T} \int_0^{\tau} d\tau' D_{\rm ST}(\tau-\tau') d_{\tau'} C_{\rm ST}(\tau') \qquad (8.4)$$

with $G_o^{-1}(\tau) = M d_{\tau^2} + \gamma d_\tau + \mu_\infty$. One can check that Eq. (6.18) coincides with Eq. (8.4) under the same assumptions. To prove this statement one has to integrate Eq. (6.18) with respect to t' from $t_{\rm EQ}$ to t' taking care of the fact that t' appears in the lower limit of the integral.

Equation (8.4) for the spherical p spin model coincides with the schematic MC equation [**?**, **?**]. This equation has a decaying solution above a sharp critical temperature that we call $T_{\rm MCT} = T_d$ where the assumptions of TTI and FDT are justified. After a short transient (eliminated by the limit $t' \gg t_{\rm EQ}$) the system equilibrates with its environment even if the thermodynamic limit has already been taken. At very high T the decay to zero is very fast and typical of, say, a high-T liquid. Closer to T_d, however, a very interesting structure appears. The solution takes the form sketched in the left panel in Fig. 46. In a logarithmic scale one sees a two step relaxation develop with a first relatively quick decay towards a plateau at a value that we call $q_{\rm EA}$ and next a slower relaxation towards zero. The length of the plateau increases when temperature approaches T_d from above and it diverges at T_d. At T_d the height of the plateau, $q^d_{\rm EA}$, follows from the asymptotic analysis of Eq. (8.4). If one loosely considers $q^d_{\rm EA}$ to be an order parameter, the high temperature analysis yields $q^d_{\rm EA} > 0$ [see Eq. (8.30)] and the transition is *discontinuous*. It is important to stress that, as we shall see below, this does not mean that the model has a first order thermodynamic transition. All susceptibilities are continuous when going across T_d even though $q^d_{\rm EA} > 0$. In the mode-coupling literature these transitions are called type B.

The details of the asymptotic analysis of the schematic MC equation and its relation with the behavior of real systems has been discussed at length in the literature. We shall not develop it here. With the purpose of future comparison with the low-T solution we just recall that the approach and departure from the plateau (*beta* relaxation) occurs with two power laws:

$$C_{\rm ST}(\tau) \sim q^d_{\rm EA} + c_a \tau^{-a} + \dots \qquad C_{\rm ST}(\tau) \sim q^d_{\rm EA} - c_b \tau^{b} + \dots \qquad (8.5)$$

given by

$$\frac{1}{k_B T_d}\frac{\Gamma^2(1+b)}{\Gamma(1+2b)} = \frac{1}{k_B T_d}\frac{\Gamma^2(1-a)}{\Gamma(1-2a)} = \frac{1}{2}\frac{\mathcal{V}'''(q^d_{\rm EA})}{(\mathcal{V}''(q^d_{\rm EA}))^{3/2}} \,. \tag{8.6}$$

A similar analysis can be done for a quantum model.

8.3 Solution at low-T

Three families of mean-field models have been found so far. In this Section we present the solution to the spherical mean-field descriptions of ferromagnetic domain growth and structural glasses in some detail. We use a generic notation that allows us to treat the classical and quantum problem simultaneously. The presentation follows [43]. By the end of this Subsection we discuss the generalisation of these results to models of "spin-glass" type, models with spatial dependence and the effect of different microscopic dynamics.

The numerical solution to the dynamic equations at low T shows no evidence for an arrest in the waiting-time dependence of the decay of C and R. In this regime of temperatures,

$$t_{\rm EQ}(N, T < T_d) \to \infty \tag{8.7}$$

and the equations do not admit the choice of a $t' > t_{\rm EQ}$. In order to consider the crossover towards the equilibration regime one should revisit the derivation of the dynamic equations allowing for N finite. This program has not been pursued in the literature and it remains one of the most interesting open problems in the field.

8.3.1 The Lagrange multiplier

We approximate the integral in Eq. (6.23) by separating its support in three intervals

$$t'' : 0 \to \delta_0 \,, \quad t'' : \delta_0 \to \Delta_t \,, \quad t'' : \Delta_t \to t \,. \tag{8.8}$$

The first time-interval contains only finite times t''. Hence, all correlations and responses of the form $C(t,t'')$ and $R(t,t'')$ vanish due to Eqs. (7.3) and (7.7). In the last time-interval t'' is close to t in the sense that correlations of the kind $C(t,t'')$ are of the form $C_{\rm ST}(t-t'')+q_{\rm EA}$ and similarly for the responses. Finally, in the intermediate time-interval the C and R vary in the aging regime. Of course, we are sloppy in that we do not precise what are the values of δ_0 and Δ_t. The definitions of correlation scales given in Section correct this imprecision exchanging the time limts by limits in the correlation. Within these assumptions the asymptotic value of $\mu(t)$ is given by

$$\begin{aligned} \mu_\infty \;\; = \;\; & A_\infty + q_{\rm EA}\int_0^\infty d\tau' \, \Sigma_{\rm ST}(\tau') + \tilde{D}_{q_{\rm EA}} \int_0^\infty d\tau' R_{\rm ST}(\tau') \\ & + \int_0^\infty d\tau' \, [\, \Sigma_{\rm ST}(\tau') C_{\rm ST}(\tau') + D_{\rm ST}(\tau') R_{\rm ST}(\tau') \,] + {\rm Last} \end{aligned} \tag{8.9}$$

Σ and D are made of two terms, one contribution from the bath and one contribution from the interactions. We called Last a term that equals $-M\ \partial_\tau^2 C_{\rm ST}(\tau)\big|_{\tau\to 0}$ in a model with inertia (classical or quantum) and simply $k_B T$ in classical models without inertia. A_∞ is the aging contribution:

$$A_\infty \;=\; \lim_{t\to\infty}\int_0^t dt''\,[\,\Sigma_{\rm AG}(t,t'')C_{\rm AG}(t,t'')+D_{\rm AG}(t,t'')R_{\rm AG}(t,t'')\,]\ . \qquad (8.10)$$

The bath does not contribute to the integrals in A_∞ when the kernels η and ν decay sufficiently fast to zero as to yield vanishing integrals. This is trivially true for a white noise. It can be a working assumption for colored noises based on a weak limit of the strength of the coupling to the noise. More precisely, we are neglecting terms of the form $\lim_{t\to\infty}\int_0^t dt''\,A(t-t'')B(t,t'')$ where A is either ν or η and B is either $C_{\rm AG}$ or $R_{\rm AG}$. In this case

$$A_\infty \;=\; \lim_{t\to\infty}\int_0^t dt''\,\Big[\,\tilde\Sigma_{\rm AG}(t,t'')C_{\rm AG}(t,t'')+\tilde D_{\rm AG}(t,t'')R_{\rm AG}(t,t'')\,\Big]\ . \qquad (8.11)$$

The second and third terms in Eq. (8.9) come from the constant (non-zero) limit of the first decay of the correlation $q_{\rm EA}\equiv\lim_{t-t'\to\infty}\lim_{t'\to\infty}C(t,t')$ and the vertex $\tilde D_{q_{\rm EA}}\equiv\lim_{t-t'\to\infty}\lim_{t'\to\infty}\tilde D(t,t')$. For the classical spherical p spin model $\tilde D_{q_{\rm EA}}=\frac{p}{2}\,q_{\rm EA}^{p-1}$ and this equation also holds for its quantum extension if we use $\lim_{\tau\to\infty}R_{\rm ST}(\tau)\ll q_{\rm EA}$, a property of the WLTM scenario. The integral over the stationary parts can be simply performed using FDT for classical problems but they cannot in quantum problems.

8.3.2 The stationary regime

If (t,t') are such that $C(t,t')>q_{\rm EA}$, $C(t,t')=q_{\rm EA}+C_{\rm ST}(t-t')$ and $R(t-t')=R_{\rm ST}(t-t')$. The Schwinger-Dyson equation for R in this time sector reads

$$\left(M\partial_\tau^2+\mu_\infty\right)R_{\rm ST}(\tau)=\delta(\tau)+\int_0^\tau d\tau'\,\Sigma_{\rm ST}(\tau-\tau')R_{\rm ST}(\tau') \qquad (8.12)$$

and it keeps the same form as in the high-temperature phase, apart from the fact that the constant μ_∞ has contributions from the aging regime. The Schwinger-Dyson equation for C reads

$$\begin{aligned}\left(M\partial_\tau^2+\mu_\infty\right)\left(q_{\rm EA}+C_{\rm ST}(\tau)\right) &= A_\infty+q_{\rm EA}\int_0^\infty d\tau'\,\Sigma_{\rm ST}(\tau')+\tilde D_{q_{\rm EA}}\int_0^\infty d\tau'\,R_{\rm ST}(\tau')\\ &+\int_{-\infty}^\infty d\tau'\,[\Sigma_{\rm ST}(\tau+\tau')C_{\rm ST}(\tau')+D_{\rm ST}(\tau+\tau')R_{\rm ST}(\tau')]\ . \qquad (8.13)\end{aligned}$$

One can now Fourier-transform both equations

$$\begin{aligned}R_{\rm ST}(\omega) &= \frac{1}{-M\omega^2+\mu_\infty-\Sigma_{\rm ST}(\omega)}\ ,\\ \left(-M\omega^2+\mu_\infty\right)C_{\rm ST}(\omega)+\mu_\infty q_{\rm EA}\delta(\omega) &= \Big(A_\infty+q_{\rm EA}\Sigma_{\rm ST}(\omega)+\tilde D_{q_{\rm EA}}R_{\rm ST}(\omega)\Big)\,\delta(\omega)\\ &\quad+\Sigma_{\rm ST}(\omega)C_{\rm ST}(\omega)+D_{\rm ST}(\omega)R_{\rm ST}(-\omega)\ .\end{aligned}$$

The formal solution to the equation for $C_{\rm ST}$ is

$$C_{\rm ST}(\omega) = \Big(-\mu_\infty q_{\rm EA} + A_\infty + q_{\rm EA}\Sigma_{\rm ST}(\omega) + \tilde{D}_{q_{\rm EA}} R_{\rm ST}(\omega)\Big)\,\delta(\omega) R_{\rm ST}(\omega) + D_{\rm ST}(\omega)|R_{\rm ST}(\omega)|^2 \ .$$

The first term on the RHS has an imaginary and a real part. The imaginary part vanishes identically since, due to FDT, both $\mathrm{Im}R_{\rm ST}(\omega)$ and $\mathrm{Im}\Sigma_{\rm ST}(\omega)$ are proportional to $\tanh(\beta\hbar\omega/2)$ which is zero at $\omega = 0$ for classical and quantum problems. Concerning the real part of this first term, as we have assumed that $C_{\rm ST}(\tau)$ goes to zero for $\tau \to \infty$, we need to impose the self-consistent condition

$$-\mu_\infty q_{\rm EA} + A_\infty + q_{\rm EA}\Sigma_{\rm ST}(\omega = 0) + \tilde{D}_{q_{\rm EA}} R_{\rm ST}(\omega = 0) = 0 \ . \tag{8.14}$$

This is the condition that fixes $q_{\rm EA}$. We shall find it again in the next section as the matching condition between the stationary and aging regimes. The final equation for $C_{\rm ST}(\omega)$ is

$$C_{\rm ST}(\omega) = D_{\rm ST}(\omega)|R_{\rm ST}(\omega)|^2 \ . \tag{8.15}$$

One can check that these calculations are consistent with the results from μ_∞. Actually, the integrals in equation for $\mu(t)$ involving the stationary parts can be evaluated with the help of the equations for $R_{\rm ST}$ and $C_{\rm ST}$, Eqs. (8.14) and (8.15), and yield once again Eq. (8.14).

Similarly to the high-temperature case one can now show that FDT for $\tilde{\Sigma}_{\rm ST}$ and $\tilde{D}_{\rm ST}$ implies FDT for $R_{\rm ST}$ and $C_{\rm ST}$. The remainder of the proof, *i.e.* to show that FDT between $R_{\rm ST}$ and $C_{\rm ST}$ implies FDT between $\tilde{\Sigma}_{\rm ST}$ and $\tilde{D}_{\rm ST}$ depends only upon the form of $\tilde{\Sigma}_{\rm ST}$ and $\tilde{D}_{\rm ST}$ as functions of $R_{\rm ST}$ and $C_{\rm ST}$ and is not modified from the one discussed in Section .

8.3.3 The aging regime

If we now choose the times t, t' to be well-separated so as to have $C(t,t') = C_{\rm AG}(t,t') \leq q_{\rm EA}$ and $R(t,t') = R_{\rm AG}(t,t')$, the WEB and WLTM hypotheses allow us to throw the second time derivatives on the LHS. We assume that their contribution is much weaker than the one of each of the integral terms on the RHS. This is an assumption that we have to verify at the end of the calculation, once the solution for $C_{\rm AG}$ and $R_{\rm AG}$ is known. It corresponds to the over-damped limit.

Using a separation of time-scales in the integrals the equation for R in the aging regime becomes

$$\begin{aligned}\mu_\infty R_{\rm AG}(t,t') = \tilde{\Sigma}_{\rm AG}(t,t') \int_0^\infty d\tau' R_{\rm ST}(\tau') + R_{\rm AG}(t,t') \int_0^\infty d\tau'\, \Sigma_{\rm ST}(\tau') \\ + \int_{t'}^t dt''\, \tilde{\Sigma}_{\rm AG}(t,t'') R_{\rm AG}(t'',t')\end{aligned} \tag{8.16}$$

and we call it the $R_{\rm AG}$-eq. Similarly, the equation for C becomes

$$\mu_\infty C_{\rm AG}(t,t') = C_{\rm AG}(t,t') \int_0^\infty d\tau' \Sigma_{\rm ST}(\tau') + \tilde{D}_{\rm AG}(t,t') \int_0^\infty d\tau' R_{\rm ST}(\tau')$$

$$+\int_0^t dt''\ \tilde{\Sigma}_{\rm AG}(t,t'')C_{\rm AG}(t'',t')+\int_0^{t'} dt''\ \tilde{D}_{\rm AG}(t,t'')R_{\rm AG}(t',t'') \quad (8.17)$$

and we call it the $C_{\rm AG}$-eq. In all integrals over the slow regime we neglected the contributions of the noise kernels η and ν and we approximated $\Sigma_{\rm AG}(t,t') \sim \tilde{\Sigma}_{\rm AG}(t,t')$ and $D_{\rm AG}(t,t') \sim \tilde{D}_{\rm AG}(t,t')$.

8.3.4 The Edwards-Anderson parameter

The Edwards-Anderson parameter, $q_{\rm EA}$, is determined self-consistently from the matching of $\lim_{t\to\infty} C_{\rm AG}(t,t) = \lim_{t-t'\to\infty}\lim_{t'\to\infty} C(t,t') = q_{\rm EA}$. Taking the limit $t' \to t^-$ in the $R_{\rm AG}$-eq and $C_{\rm AG}$-eq one obtains

$$\mu_\infty R_{\rm AG}(t,t) = \tilde{\Sigma}_{\rm AG}(t,t)\int_0^\infty d\tau'\ R_{\rm ST}(\tau') + R_{\rm AG}(t,t)\int_0^\infty d\tau'\ \Sigma_{\rm ST}(\tau')\ , \quad (8.18)$$

$$\mu_\infty q_{\rm EA} = A_\infty + q_{\rm EA}\int_0^\infty d\tau'\ \Sigma_{\rm ST}(\tau') + \tilde{D}_{\rm AG}(t,t)\int_0^\infty d\tau'\ R_{\rm ST}(\tau')\ . \quad (8.19)$$

The first equation admits the solution $R_{\rm AG}(t,t) = 0$ since $\tilde{\Sigma}_{\rm AG}(t,t)$ is proportional to $R_{\rm AG}(t,t)$. This corresponds to the high-temperature solution where there is no aging regime. Here we concentrate on the other possibility. The response becomes smaller and smaller as time passes – though its integral over an infinite interval gives a finite contribution. If we neglect all terms that are proportional to $R_{\rm AG}(t,t)$ with respect to terms that are proportional to $q_{\rm EA}$, only the first term in the power expansions of $\tilde{\Sigma}$ and $\tilde{D}$ survive and

$$\left(\tilde{\Sigma}/R\right)_{q_{\rm EA}} \equiv \lim_{t\to\infty}\frac{\tilde{\Sigma}_{\rm AG}(t,t)}{R_{\rm AG}(t,t)} \qquad \tilde{D}_{q_{\rm EA}} \equiv \lim_{t\to\infty}\tilde{D}_{\rm AG}(t,t) \quad (8.20)$$

that for the p spin model become

$$\left(\tilde{\Sigma}/R\right)_{q_{\rm EA}} = \frac{p(p-1)}{2}\,q_{\rm EA}^{p-2} \qquad \tilde{D}_{q_{\rm EA}} = \frac{p}{2}\,q_{\rm EA}^{p-1}\ , \quad (8.21)$$

in accord with the large τ limit of the stationary values (see Section). Equations (8.18) and (8.19) become

$$\mu_\infty = \left(\tilde{\Sigma}/R\right)_{q_{\rm EA}}\int_0^\infty d\tau'\ R_{\rm ST}(\tau') + \int_0^\infty d\tau'\ \Sigma_{\rm ST}(\tau')\ , \quad (8.22)$$

$$\mu_\infty q_{\rm EA} = A_\infty + q_{\rm EA}\int_0^\infty d\tau'\ \Sigma_{\rm ST}(\tau') + \tilde{D}_{q_{\rm EA}}\int_0^\infty d\tau'\ R_{\rm ST}(\tau')\ . \quad (8.23)$$

The second equation is the same as the one arising from the end of the stationary regime, Eq. (8.14).

From Eqs. (8.14) and (8.15) one derives

$$\int_0^\infty d\tau\ R_{\rm ST}(\tau) = R_{\rm ST}(\omega=0) = \frac{1}{\mu_\infty - \Sigma_{\rm ST}(\omega=0)}\ , \quad (8.24)$$

and

$$1 \quad = \quad \left(\tilde{\Sigma}/R\right)_{q_{\rm EA}} R^2_{\rm ST}(\omega=0) \; . \tag{8.25}$$

We remind that the factor $R^2_{\rm ST}(\omega=0)$ can be written in terms of the stationary correlation function using FDT; therefore this is a closed equation for the correlation that determines $q_{\rm EA}$. In the case of the p-spin model it reads

$$1 \quad = \quad \frac{p(p-1)}{2} q_{\rm EA}^{p-2} \left(\frac{1}{\hbar} \, P \int_{-\infty}^{\infty} \frac{d\omega'}{\omega'} \, \tanh\left(\frac{\beta\hbar\omega'}{2}\right) C_{\rm ST}(\omega') \right)^2 \; . \tag{8.26}$$

In the classical case, the integral can be readily computed and the final equation for $q_{\rm EA}$ is

$$\frac{p(p-1)}{2} \, q_{\rm EA}^{p-2} (1-q_{\rm EA})^2 = (k_B T)^2 \; , \tag{8.27}$$

that coincides with the result for the purely relaxational dynamics. For $p \geq 3$ fixed, $q_{\rm EA}$ is a function of temperature. Equation (8.27) can be solved graphically. The LHS has a bell shape. It vanishes at $q_{\rm EA} = 0, 1$ and it reaches a maximum at $q_{\rm EA}^{\rm MAX} = (p-2)/p$. The equation has two solutions for all temperatures $(k_B T)^2 < (k_B T^{\rm MAX})^2 = p(p-1)/2 \, [(p-2)/p]^{p-2} \, (2/p)^2$, these merge ar $T^{\rm max}$ and disappear for higher T's. The physical solution corresponds to the branch on the right of the maximum, the one that continues the solution $q_{\rm EA} = 1$ at $T = 0$. The minimum value of $q_{\rm EA}$ is reached at the dynamic critical temperature $T_d (< T^{\rm MAX})$, where $q_{\rm EA}^d \equiv q_{\rm EA}(T_d) > q_{\rm EA}^{\rm MAX}$.

8.3.5 Fluctuation - dissipation relation

In order to advance further we have to relate the response to the correlation. If we *assume* that

$$R_{\rm AG}(t,t') = \frac{1}{k_B T^*} \frac{\partial C_{\rm AG}(t,t')}{\partial t'} \; , \tag{8.28}$$

with T^* the value of an effective temperature (see Section **??**) that is determined by Eqs. (8.23) and (8.24) $0 = A_\infty - \frac{q_{\rm EA}}{R_{\rm ST}(\omega=0)} + \tilde{D}_{q_{\rm EA}} \, R_{\rm ST}(\omega=0)$. Using Eq. (8.28) and the equivalent relation between $\tilde{\Sigma}_{\rm AG}$ and $\tilde{D}_{\rm AG}$, we obtain $A_\infty = (k_B T^*)^{-1} \, \lim_{t-t_w \to \infty} \left(\tilde{D}_{\rm AG}(t,t) C_{\rm AG}(t,t) \right) = (k_B T^*)^{-1} \, q_{\rm EA} \tilde{D}_{q_{\rm EA}}$ and

$$\frac{1}{k_B T^*} = \frac{(p-2)}{q_{\rm EA}} R_{\rm ST}(\omega=0) = \sqrt{\frac{2(p-2)^2}{p(p-1)}} \, q_{\rm EA}^{-p/2} \; . \tag{8.29}$$

In the classical limit $T/T^* = (p-2)(1-q_{\rm EA})/q_{\rm EA}$. Note that both in the classical and quantum case, $T^* \to \infty$ if $p = 2$. Since the case $p = 2$ is formally connected to ferromagnetic domain growth in $d = 3$ (in the mean-field approximation) there is no memory neither in the classical nor in the quantum domain growth.

The *Ansatz* in Eq. (8.28) solves classical *and* quantum aging equations. The modification of the FDT in this regime became thus classical even when quantum fluctuations

exist. This is an interesting sort of decoherent effect that will become clearer when we shall discuss the interpretation of this results in terms of effective temperatures.

Using Eq. (8.28) for all values of C below $q_{\rm EA}$ we assumed that there is only one aging correlation scale in the problem. Interestingly enough, one do a more general analysis using the formalism described in Section and find that the dynamic equations force the solution to have only one aging correlation scale.

8.3.6 Discontinuous classical transition

The classical dynamic critical point ($T_d, \hbar = 0$) can arise either when $q_{\rm EA} \to 0$ or when $T^* \to T$. For the p spin model, using Eqs. (8.27) and (8.29) the latter holds and

$$(k_B T_d)^2 = \frac{p\,(p-2)^{p-2}}{2\,(p-1)^{p-1}} \qquad q^d_{\rm EA} = \frac{p-2}{p-1}\,. \tag{8.30}$$

The transition is *discontinuous* since the order parameter $q_{\rm EA}$ jumps at T_d. However, it is still of *second order* thermodynamically since there are no thermodynamic discontinuities, all susceptibilities being continuous across T_d. For instance,

$$\lim_{t \gg t_w} \chi(t, t_w) = \frac{1}{k_B T}(1 - q_{\rm EA}) + \frac{1}{k_B T^*} q_{\rm EA} \to \frac{1}{k_B T} \;\text{ when }\; T \to T^* \;\text{ at }\; T_d\,. \tag{8.31}$$

The dynamic transition occurs at a value T_d that is higher than the static transition temperature T_s. The latter is fixed as the temperature where replica symmetry breaking occurs (using the standard prescription to fix the parameters in the Parisi *Ansatz* to compute the free-energy density). This feature is an explicit realisation of the discussion on T_g and T_0. They are sharp in this model.

8.3.7 The classical threshold level

The asymptotic energy density reads $\mathcal{E}_\infty = -\frac{1}{p}\int_0^\infty dt''[\Sigma(t,t'')C(t,t'') + D(t,t'')R(t,t'')]$ where we used Eq. (6.26). Replacing the solution found above we obtain

$$\mathcal{E}_\infty = -\frac{1}{2}\left[\frac{1}{k_B T}\,(1 - q^p_{\rm EA}) + \frac{1}{k_B T^*} q^p_{\rm EA}\right] \equiv \mathcal{E}_{\rm TH}\,. \tag{8.32}$$

If one compares this expression with the equilibrium energy density, found studying the partition function, one discovers that

$$\mathcal{E}_\infty = \mathcal{E}_{\rm TH} > \mathcal{E}_{\rm EQ}\,. \tag{8.33}$$

Thus, the non-equilibrium dynamics does not approach the equilibrium level asymptotically but it reaches a *threshold* level that is extensively higher than equilibrium (note that the inequality (8.33) holds for the energy density). The name *threshold* is motivated by a similarity with *percolation* (in phase space).

8.3.8 Two p models

In Section we took the limit $t' \to t^-$, or equivalently, $C_{\rm AG} \to q_{\rm EA}^-$ in the equations for the slow part of the response and the correlation and this lead us to Eqs. (8.25) and (8.29) for $q_{\rm EA}$ and T^*. Let us now take subsequent variations of this equation with respect to the correlation and evaluate them in the same limit. It is easy to see that if we neglect the contributions from the integral between t' and t, assuming that the integrands are analytic in this limit, we get new equations linking T^* and $q_{\rm EA}$ that, for generic models, are not compatible. Indeed, as we shall see below, the pure spherical p spin model is the only one for which the solution is given by an analytic function $\jmath^{-1}(x)$ when $x \to 1^-$.

The way out of this contradiction is to propose that the correlation approaches the plateau at $q_{\rm EA}$ with a power law decay and that it departs from it with another non-trivial power law:

$$C_{\rm ST}(t-t') = (1-q_{\rm EA}) + c_a^{(1)}(t-t')^{-a} + c_a^{(2)}(t-t')^{-2a} + \dots\dots \tag{8.34}$$

$$C_{\rm AG}(t,t') = q_{\rm EA} - c_b^{(1)}\left(1-\frac{h(t')}{h(t)}\right)^{b} - c_b^{(2)}\left(1-\frac{h(t')}{h(t)}\right)^{2b} + \dots \tag{8.35}$$

with $c_a^{(i)}$ and $c_b^{(i)}$ constants. If the exponent b is smaller than one, the integrals generated by taking derivatives with respect to $C_{\rm AG}$ do not vanish when $t' \to t^-$. The expansion of the stationary and aging equations around $q_{\rm EA}$ fix the exponents a and b. One finds [32]

$$\frac{1}{k_B T^*}\frac{(\Gamma(1+b))^2}{\Gamma(1+2b)} = \frac{1}{k_B T}\frac{(\Gamma(1-a))^2}{\Gamma(1-2a)} = \frac{1}{2}\frac{\mathcal{V}'''(q_{\rm EA})}{(\mathcal{V}''(q_{\rm EA}))^{3/2}} \tag{8.36}$$

that are to be confronted to Eqs. (8.5) and (8.6) for the high T behavior. We recall that $\mathcal{V}(C)$ is the correlation of the random potential. Importantly enough, the exponents a and b are now T-dependent and they are related via an equation in which T^* enters.

Classical spherical p spin model

Since $\mathcal{V}(C) = C^p/2$ using Eqs. (8.25) and (8.29) to fix T^* and $q_{\rm EA}$ one finds $(\Gamma(1+b))^2/\Gamma(1+2b) = 1/2$ and $b = 1$ for all $T < T_d$. The exponent a interpolates between $a = 1/2$ at $T \to 0$ and $a = 1$ at $T \to T_d$ since $(\Gamma(1-a))^2/\Gamma(1-2a) = T/(2T^*)$.

Classical mixed $p_1 + p_2$ spherical spin model

For adequate choices of the coefficients in $\mathcal{V}(C) = a_1/2C^{p_1} + a_2/2C^{p_2}$ (see below) one finds T-dependent exponents $a(T)$ and $b(T)$.

Ultrametric limit

It is interesting to notice that $(\Gamma(1+b))^2/\Gamma(1+2b)$ is bounded by one. Thus, Eq. (8.36) constrains the random potentials for which a solution with only two correlation scales exists. For a particle in a power-law correlated random potential one sees the transition towards an ultrametric-like solution arrives when the potential goes from short-range to long-range correlated [32]. To our knowledge this has not

been found in a static calculation. An interpretation of the exponents a and b, and this consequence, in terms of the properties of the TAP free-energy landscape is not known either.

8.3.9 SK model and similar

A different family of models, to which the SK model belongs, are solved by an ultrametric *Ansatz*, $C_{31} = f(C_{32}, C_{21})$, for all correlations below $q_{\rm EA}$. The $\chi(C)$ plot yields a non-trivial curve (instead of a straight line) for $C \in [0, q_{\rm EA}]$. The transition is continuous $q^d_{\rm EA} = 0$. These models are called type A in the MCT literature.

Indeed, for a generic disordered model with random potential correlated as in Eq. (6.6), one finds that the solution is ultrametric if and only if [32]

$$\frac{\mathcal{V}'''(C)}{\mathcal{V}'''(q_{\rm EA})} \left(\frac{\mathcal{V}''(q_{\rm EA})}{\mathcal{V}''(C)} \right)^{3/2} < 1 \, . \tag{8.37}$$

This bound constrains, for instance, the values of the coefficients in a polynomial random potential for which the dynamic solution is ultrametric. The FDT is modified with a C dependent factor given by

$$\frac{T}{T_{\rm EFF}(C)} = q_{\rm EA} \mathcal{V}'''(C) \sqrt{\frac{\mathcal{V}''(q_{\rm EA})}{4(\mathcal{V}''(C))^{3/2}}} \, . \tag{8.38}$$

8.3.10 Mode dependence

The models we solved so far have no spatial dependence. The manifold problem has an internal structure that leads to a mode-dependence. This model has been solved for generic potential correlations. We summarize the outcome without presenting its detailed derivation. All modes are slaved to one in the sense that one has to solve for the dynamics of one of them and the mode-dependence follows from an algebraic equation. The value of the effective temperature does not depend on the mode. The mathematical reason for this is the slaved structure of the equations. The physical reason is that all interacting observables evolving in the same time-scale have to partially equilibrate and acquire the same effective temperature. The height of the plateau, $q_{\rm EA}$, is a k dependent quantity. The approach to it and departure from it also depends on k but only via the prefactors; the exponents a and b, see Eqs. (8.34) and (8.35, are the same for all modes.

Mode-couling equations including a wave-vector dependence have been derived by Latz using the Mori-Zwanzig formalism; the structure of the solution to these equations shares the properties just described.

8.3.11 Quantum fluctuations

The simplest effect of quantum fluctuations is to introduce oscillations in the first step of relaxation. These disappear at long enough time-differences and they are totally suppressed from the second decay, that superficially looks classical [43].

The Edwards-Anderson parameter $q_{\rm EA}$ depends upon T *and* $\hbar$. As expected, quantum fluctuations introduce further fluctuations in the stationary regime and they decrease the value of $q_{\rm EA}$, $q_{\rm EA}(T, \hbar \neq 0) < q_{\rm EA}(T, \hbar \to 0)$.

The modification of FDT in the quantum model is of a rather simple kind: $R_{\rm AG}$ and $C_{\rm AG}$ are related as in the classical limit. For the quantum extension of the p spin model there are two correlation scales, one with the temperature of the environment, T, the other with another value of the effective temperature, T^*, that depends on T, $\hbar$ and the characteristics of the environment. This is a kind of decoherent effect.

As regards to the transition from the glassy to the liquid or paramagnetic phase, an interesting effect appears. Keeping all other parameters fixed, the plane $(T, \Gamma \equiv \hbar^2/(JM))$ is separated in these two phases by a line that joins the classical dynamic critical point $(T_d, \Gamma = 0)$ and the quantum dynamic critical point $(T = 0, \Gamma_d)$. Close to the classical dynamic critical point the transition is discontinuous but of second order thermodynamically until it reaches a tricritical point where it changes character to being of first order. This behavior is reminiscent of what has been reported for the quantum spin-glass studied in [**?**].

A still more dramatic effect of quantum mechanics is related to the very strong role played by the quantum environment on the dynamics of a quantum system. Indeed, the location of the transition line depends very strongly on the type of quantum bath considered and on the strength of the coupling between system and environment.

8.3.12 Driven dynamics

The effect of non potential forces can be mimicked with a 'non-symmetric' force with strength α playing an analogue role to the shear stress σ. For strengths that are not too strong, the dynamics presents a separation of time scales with a fast approach to the plateau and a slow escape from it that is now, however, also stationary. Indeed, after a characteristic time $t_{\rm SH}$ the full dynamics becomes stationary though the system is still far from equilibrium. One defines a structural relaxation time, τ_α, as the time needed to reach, say, a correlation equal to a half. One relates the structural relaxation to the viscosity via $\eta \equiv \int dt\, C(t)$. The scaling of η with the shear rate $\dot\gamma \equiv \sigma/\eta$ has been successfully confronted to the behavior in rheological experiments in super-cooled liquids and glasses. In terms of the general scalings discussed in Section , the correlations are characterised by two different functions $\jmath$, one for the fast decay towards the plateau and another for the slow decay from the plateau, while the functions $h(t)$ are simple exponentials.

Interestingly enough, from the study of FDT violations above (though close to) and below T_d, when the forcing is weak, one extracts a still well-defined slope of the $\chi(C)$ plot when C evolves in the slow scale. This means that an effective temperature can also be identified for these systems kept explicitly out of equilibrium (see also [**?**]).

Oscillatory forces, as the ones used to perturb granular matter, have a different effect. Aging is not stopped in a finite region of the phase diagram (T-strength of the force-frequency of the force) [**?**]. An effective temperature can still be defined as

the slope of the $\chi(C)$ plot drawn using stroboscopic time, with a point per oscillatory cycle.

9 Effective temperature measurements

In this Section we discuss measurements of FDT violations and tests of the effective temperature notion in a variety of physical systems out of equilibrium. Since we cannot make the description exhaustive we simply select a number of representative cases that we hope will give a correct idea of the level of development reached in the field. This Section follows closely [**?**] where references to the original papers are given.

9.1 Diffusion

The dynamics of a particle in a potential and subject to a complex environment (colored noise or baths with several time-scales and temperatures) has a pedagogical interest but also admits an experimental realization in the form of Brownian particles immersed in, *e.g.*, colloidal suspensions and controlled by optical tweezers.

A particle coupled to a bath in equilibrium at temperature T with noise-noise correlations of type $\langle \xi(t)\xi(t')\rangle \propto (t-t')^{-a-1}$, $0 < a < 2$, and under no external forces, performs normal or anomalous diffusion depending on a. The fluctuation-dissipation ratio, eq. (**??**), for $t \geq t'$ is

$$X_{xx}(t,t') = \frac{T R_{xx}(t,t')}{\partial_{t'} C_{xx}(t,t')} = \frac{D(t-t')}{D(t-t') + D(t')} \,, \tag{9.1}$$

with the diffusion coefficient $D(t) \equiv 1/2 \; d\langle x^2(t)\rangle/dt \simeq t^a$ for $a \neq 1$ and $D(t) = \mathrm{ct}$ for $a = 1$. In such colored noise cases X_{xx} is a non-trivial function of times and it does not seem to admit a thermodynamic interpretation. Still, for later reference we consider the long times limit:

$$X^\infty = \lim_{t'\to\infty} \lim_{t\to\infty} X_{xx}(t,t') \simeq \begin{cases} 0 & a < 1 \quad \text{subOhmic,} \\ 1/2 & a = 1 \quad \text{Ohmic,} \\ 1 & a > 1 \quad \text{superOhmic.} \end{cases}$$

Another illustrative example is the non-Markovian diffusion of a particle in a harmonic potential and subject to different external baths. As already explained in Sect. **??** this simple system allows one to show how different environments can impose their temperatures on different dynamic regimes felt by the particle. Tests of other definitions of out of equilibrium temperatures in this simple case confirmed that the definition that appears to have the most sensible behaviour is the one stemming from the long-time limit of the relations between induced and spontaneous fluctuations. All other definitions yield results that are more difficult to rationalize: in most cases one simply finds the temperature of the fast bath and in some cases, as with a static limit, one incorrectly mixes different time regimes even when their time-scales are well separated.

9.2 Coarsening

When a system is taken across a second order phase transition into an ordered phase with, say, two equilibrium states related by symmetry, it tends to order locally in each of the two but, globally, it remains disordered. As time elapses the ordered regions grow and the system reaches a scaling regime in which time-dependencies enter only through a typical growing length, $L(t)$. Finite dimensional coarsening systems have been studied in great detail from the effective temperature perspective. In this context, it is imperative to distinguish cases with a finite temperature phase transition and spontaneous symmetry breaking from those with ordered equilibrium at $T = 0$ only. Some representative examples of the former are the clean or dirty $2d$ Ising model with conserved and non-conserved order parameter. An instance of the latter is the Glauber Ising chain and we postpone its discussion to Sect. .

Let us focus on scalar systems with discrete broken symmetry. When time-differences are short with respect to a function – typically algebraic – of the typical growing length $L(t_w)$, domain walls remain basically static and the only variation is due to thermal fluctuations on the walls and, more importantly, within the domains. This regime is stationary, and induced and spontaneous fluctuations are linked by the FDT. At longer time-differences domain walls move and observables display the out of equilibrium character of the system.

The motion of the domain walls in the presence of an external perturbing random field introduced to measure the staggered response is due to two competing factors: on the one hand, the system tends to diminish the curvature of the interfaces due to surface tension, on the other hand the random field tends to pin the domain walls in convenient places.

The correlation and total susceptibility in the $t_w \to \infty$ limit separate in two contributions $C(t, t_w) = C^{\rm ST}(t-t_w)+C^{(1)}(t, t_w)$ and $\chi(t, t_w) = \chi^{\rm ST}(t-t_w)+\chi^{(1)}(t, t_w)$. Numerical studies of $T_{\rm EFF}$ focused on the parametric construction $\chi(C, t_w)$ at fixed and finite t_w where the chosen observable is the spin itself. The resulting plot has a linear piece with slope $-1/T$, as in eq. (**??**), that goes below $C = q_{\rm EA} = m^2$ and, consistently, beyond $\chi = [1 - m^2]/T$. The additional equilibrium contribution is due to the equilibrium response of the domain walls that exist with finite density at any finite t_w. In the truly asymptotic limit their density vanishes and their contribution disappears. Consequently, $\lim_{t_w\to\infty} \chi(C, t_w) = C^{\rm ST} \geq q_{\rm EA}$ satisfies FDT and it is entirely due to fluctuations within the domains. In cases with $L(t) \simeq t^{1/z_d}$, the slow terms take the scaling forms

$$C^{(1)}(t, t_w) \simeq f_C(t/t_w) \, , \qquad \chi^{(1)}(t, t_w) \simeq t_w^{-a_\chi} \, f_\chi(t/t_w) \, . \tag{9.2}$$

It would be natural to assume that $\chi^{(1)}(t, t_w)$ is proportional to the density of defects $\rho_d(t) \simeq L(t)^{-n} \simeq t^{-n/z_d}$ with $n = 1$ for scalar and $n = 2$ for vector order parameter.

Although this seems plausible a_χ is instead d-dependent. Another conjecture is

$$z_d\, a_\chi = \begin{cases} n\ (d-d_L)/(d_U-d_L) & d < d_U\ , \\ n \quad \text{(with ln corrections)} & d = d_U\ , \\ n & d > d_U\ . \end{cases} \tag{9.3}$$

d_L is the dimension at which a_χ vanishes and may coincide with the lower critical dimension. One finds $d_L = 1$ in the Ising model, $d_L = 1$ in the Gaussian approximation of Ohta, Jasnow and Kawasaki, and $d_L = 2$ in the $O(N)$ model in the large N limit. d_U is the dimension at which a_χ becomes d-independent and it does not necessarily coincide with the upper critical dimension. One finds $d_U = 3$ in the Ising model, $d_U = 2$ in the Gaussian approximation, and $d_U = 4$ in the large N $O(N)$ model. It was then suggested that d_U might be the highest d at which interfaces roughen. In all cases in which $a_\chi > 0$, $T_{\rm EFF} \to \infty$. This result was confirmed by studies of second order FDRs in the $2d$ Ising model that showed the existence of stationary contributions verifying the non-linear equilibrium relation and aging terms that satisfy scaling and yield $T_{\rm EFF} \to \infty$ as in the linear case. The approach by Henkel *et al.* based on the conjecture that the response function transforms covariantly under the group of local scale transformations, fixes the form of the scaling function f_χ but not the exponent a_χ and does not make predictions on $T_{\rm EFF}$. The coincidence between statics and dynamics, see Sect. **??**, holds in these cases.

Noise induced spatial fluctuations in the effective temperature of clean coarsening systems were analyzed in the large N $O(N)$ model with $d > 2$ and with numerical simulations. The first study shows that time-reparametrization invariance is not realized and that $T_{\rm EFF}$ is trivially non-fluctuating in this quasi-quadratic model. The second analysis presents a conjecture on the behaviour of the average over local (coarse-grained) susceptibility at fixed local (coarse-grained) correlation that consistently vanishes in coarsening (but is more interesting in critical dynamics as we shall discuss in Sect.).

The results gathered so far and summarized in the conjecture (9.41) imply that the FD ratio vanishes and thus $T_{\rm EFF}$ diverges in quenches into the ordered phase of systems above their lower critical dimension.

9.3 Critical dynamics

The non-equilibrium dynamics following a quench from the disordered state to the critical point consists in the growth of the dynamical correlation length, $\xi(t) \simeq t^{1/z_{eq}}$. This length does not characterize the size of well defined domains but the size of a self-similar structure of domains within domains, typical of equilibrium at the critical point. A continuum of *finite* time-scales associated to different wave-vectors, $\tau^{(k)} \simeq k^{-z_{eq}}$, exists with only the $k \to 0$ diverging. At any finite time t, critical fluctuations of large wave-vectors, $k\xi(t) \gg 1$, are in almost equilibrium, while those with small wave-vectors, $k\xi(t) \ll 1$, retain the non-equilibrium character of the initial condition. This *finite-time* separation, and the fact that the order parameter vanishes, leads to

the *multiplicative* scaling forms

$$C(t,t_w) \simeq \xi(t-t_w)^{-d+2-\eta}\ f_C[\xi(t)/\xi(t_w), \xi_0/\xi(t_w)]\ ,$$
$$\chi(t,t_w) \simeq \beta - \xi(t-t_w)^{-d+2-\eta}\ f_\chi[\xi(t)/\xi(t_w), \xi_0/\xi(t_w)]\ ,$$

with the microscopic length ξ_0 ensuring the normalization of the correlation and the fact that χ vanishes at equal times. These forms imply that beyond the initial equilibrium part, the $\chi(C)$ plot assumes a non-trivial shape that, however, progressively disappears and approaches the equilibrium linear form at all $C > 0$. The limit $C = 0$ is distinct and the limiting parameter X^∞ should be non-trivial and it was conjectured to be universal in the sense of the renormalization group. Whether this one can be interpreted as a temperature is a different issue that has been only partially discussed. For this reason, we keep the notation X^∞ (instead of $T_{\rm EFF}$) in most of this section.

The correct estimation of X^∞ has to take into account that the number of out of equilibrium modes decreases in the course of time (contrary to what happens in the random manifold problem in the large N limit, for example). The best determination of X^∞ is achieved by selecting the $k \to 0$ mode. A thorough review of the properties of X^∞ found with the perturbative field-theoretical approach and some exact solutions to simple models, as well as the comparison to numerical estimates, is given in. At the Gaussian level the X^∞ of local operators (*e.g.* powers of the field, first derivatives of the field, *etc.*) is independent of the chosen pair – but recalls certain features of the initial condition and the correlations of the environment. This is not the case for non-local operators as, *e.g.* the energy or the tensor. Moreover, when fluctuations are taken into account with, *e.g.* a two-loop or first order in $\epsilon = 4 - d$ expansion, the X^∞ of local operators is found to depend upon the observables.

In the scalar model, using the field itself as the observable, one finds the diffusive results, eq. (9.40), at the Gaussian level and corrections when higher orders are taken into account. For example $X^\infty = 0.30(5)$ in $d = 2$, $X^\infty = 0.429(6)$ in $d = 3$ for a quench from a disordered state, white noise and up to second order in $4 - d$. The trend of X^∞ increasing with d was found in other models too. Instead, $X^\infty \simeq 0.78$ ($d = 3$) and $X^\infty = 0.75$ ($d = 2$) if the initial state is magnetized. A larger X^∞ implies a lower $T^\infty_{\rm EFF} = T_c/X^\infty$ and the comparison between these values conforms to the intuitive idea that an ordered initial state leads to a lower effective temperature than a disordered one. X^∞ was found to increase with N in vector models.

A different type of critical phenomena (infinite order) arises in the $2d$ XY model. The magnetic order parameter vanishes at all T but there is a low-T critical phase with quasi long-range order (power-law decaying spatial correlations) that is destroyed at $T_{\rm KT}$ where vortices proliferate and restore a finite correlation length. Out of equilibrium the critical scaling forms apply although with a temperature-dependent exponent, $\eta(T)$, and a growing length scale $\xi(t) \simeq (t/\ln t)^{1/2}$ (the logarithm is due to the effect of vortices). The rôle of the EA order parameter is played by the asymptotically vanishing function $(t_w/\ln t_w)^{-\eta(T)/2}$ and the crossover between equilibrium and out of equilibrium regimes takes place at a t_w-dependent value of the correla-

tion. The $\chi(C, t_w)$ plot at finite t_w is curved, it does not reach a non-trivial master curve for $t_w \to \infty$, but $T_{\rm EFF}(t, t_w) = f_X[\xi(t)/\xi(t_w)]$. Quenches from the disordered phase, $T_0 > T_{\rm KT}$ and heating from a $T_0 = 0$ ground state to $T < T_{\rm KT}$ demonstrate that the slow modes' $T_{\rm EFF}$ depends on the initial state and it is higher (lower) when $T_0 > T$ ($T_0 < T$). We allow ourselves to use the name $T_{\rm EFF}$ in this case since these results point in the direction of justifying its thermodynamic meaning. Similar results were obtained for $1 + 1$ elastic manifolds with and without quenched disorder. As the dynamic-static link is concerned, Berthier *et al.* evinced that the extension to finite-times finite-sizes works, at least at not too high Ts where free vortices inherited from the initial condition are still present.

The exact calculation of the joint probability distribution of the finite-size correlation and linear response in the spherical ferromagnet quenched to its critical temperature was given by Annibale and Sollich. The results prove that these fluctuations are not linked in a manner akin to the relation between the averaged quantities, as proposed by Chamon et al., see Sect. **??**, for glassy dynamics. The analysis of correlation-susceptibility fluctuations in non-disordered finite-dimensional ferromagnets quenched to the critical point showed that the restricted average of the susceptibility, at fixed value of the two-time overlap between system configurations, obeys a scaling form. Within the numerical accuracy of the study the slope of the scaling function yields, in the asymptotic limit of mostly separated times, the value X^∞.

The first experiments testing fluctuation dissipation deviations in a liquid crystal quenched to its critical point appeared recently and the results are consistent with what has been discussed above.

The coexistence of a single time scale in the aging regime together with a smooth and time-dependent $\chi(C, t_w)$ plot arises naturally in a critical regime and it is due to the lack of sharp time-scale separation.

Although many evaluations of X^∞ in a myriad of models tend to confirm that it mostly behaves as a critical property, the thermodynamic nature of this parameter has not been explored in full extent yet. Measurements with thermometers and connections to microcanonical definitions have not been performed at critical points.

9.4 Quenches to the lower critical dimension

The kinetic Glauber-Ising spin chain is the prototype of a dynamic model at its lower critical dimension. Taking advantage of the fact that this is one of the very few exactly solvable models of non-equilibrium statistical mechanics, several issues concerning the effective temperature interpretation have been addressed in this case, notably the observable dependencies.

After a quench from $T_0 \to \infty$ to $T = 0$ the correlation and response vary in a single time-scale with a simple aging scaling (they are both functions of t/t_w) and the $\chi(C)$ relation is a continuous function. The factor $X_s(t, t')$, associated to the spin correlation and susceptibility, is smaller than or equal to one and its value X_s^∞ in the limit $C_s \to 0$ evolves smoothly from $1/2$ (as in models characterized by simple diffusion such as the random walk or the Gaussian model) to 1 (equilibrium) as t/τ_{eq}

grows from 0 to ∞ [$1/\tau_{eq} = 1 - \tanh(2J/T)$ is the smallest eigenvalue of the master equation operator]. Moreover, X_s is an exclusive function of the auto-correlation C_s as in more complex instances of glassy behaviour.

The value for the long-wavelength analogue, the fluctuating magnetization, X_m^∞, is identical to the local value X_s^∞. The physical origin of the local-global correspondence, which can also be obtained by field-theoretic arguments, is that the long wavelength Fourier components dominate the long-time behaviour of both quantities. In contrast, observables that are sensitive to the domain wall motion have $X_d^\infty = 0$, the difference residing on the interplay between criticality and coarsening, a peculiar feature of models with $T_c = 0$.

The dependence on the initial condition is also interesting. A non-zero initial magnetization does not change the value of X_s^∞ at $T = 0$. Instead, demagnetized initial conditions with strong correlations between spins so that only a finite number of domain walls exist in the system, yield $X_s^\infty = 0$ (the same result is found in the spherical ferromagnet). The deviations from non-linear FDTs have not been fully analyzed yet.

The static-dynamics connection sketched in Sect. **??** does not hold in the $1d$ Ising chain and the non-trivial $\chi(C)$ cannot be used to infer the properties of the equilibrium state. Indeed, the aging part of the response is finite asymptotically while the equilibrium $P(q)$ has a double-delta (RS) structure as in higher dimensions. The reason for the failure is that the hypotheses used to derive the connection are not fulfilled.

The large N $O(N)$ model in $d = 2$ shares many common features with the phenomenology described above although it has not been studied in as much detail.

To sum up, a quench to $T = 0$ at the lower critical dimension does not seem to be the dimensional continuation of a line of critical quenches in the (T, d) plane (as often implicitly assumed), but the continuation of a line of $T = 0$ quenches: the system behaves as in the coarsening regime, although $X^\infty \neq 0$ for observables that do not focus on the domain wall dynamics.

9.5 Relaxation in structural glasses

In particle glassy systems a separation of time-scales exists although it is not as sharp as in mean-field models or coarsening systems, at least within simulational and experimental time-scales. In atomic glasses the existence of an FDT part implies that the rapid particle vibrations within the cages occur in equilibrium while the structural relaxation is of a different out of equilibrium kind, and it is not necessarily ruled by the temperature of the bath. Tests of the thermodynamic origin of fluctuation-dissipation violations in the aging regime of these systems were carried through in much greater detail and we summarize them below.

9.5.1 Simulations of microscopic models

Mono-atomic and binary Lennard-Jones mixtures, soft sphere systems, and the BKS potential for silica are standard models for glass forming liquids. Both Monte Carlo and molecular dynamics simulations suggest that the three first cases belong to the RFOT class of systems defined in Sect. **??** with $T_{\rm EFF} = T^{(1)}$ constant in the aging regime. $T^{(1)}$ depends weakly on the bath temperature and systems' parameters but it does not on the preparation protocol as demonstrated by measurements after quenches and crunches or the microscopic dynamics. Tests of partial equilibration between fluctuations at different wave-vector gave positive results. Importantly enough, these models have a well defined equilibrium behaviour and their energy density is naturally bounded. Of special interest is the numerical method devised to compute linear responses in molecular systems with high precision that allowed Berthier to resolve the paradoxical behavior previously reported for silica.

Numerical evidence for a slow decrease in time of the configurational temperature, as defined in eq. (**??**), although with the inherent structure complexity, is in agreement with the idea of the system's representative point penetrating below the threshold in the (free)-energy landscape.

The ratchet effect of an asymmetric intruder in an aging glass was studied numerically by Gradenigo et al. The energy flowing from slow to fast modes is rectified to produce directed motion. The (sub) velocity of the intruder grows monotonically with $T_{\rm EFF}/T$ and this current could be used to measure $T_{\rm EFF}$.

9.5.2 Kinetically constrained models

Kinetically constrained models are toy models of the glassy phenomenon. Their equilibrium measure is just the Boltzmann factor of independent variables and correlations only reflect the hard core constraint. Still, many dynamic properties of glass forming liquids and glasses are captured by these models, due to the sluggishness introduced by the constrained dynamic rules. The literature on kinetically constrained models is vast; a recent review with tests of $T_{\rm EFF}$ was written by Leonard et al. In short, non-monotonic low-temperature response functions were initially taken as evidence against the existence of effective temperatures in these systems. The confusion arosed from the incorrect construction of the $\chi(C)$ plot by using t_w instead of t fixed (see Sect. **??**) that led to the incorrect treatment of the transient regime. Still, even this taken into account, a large number of observables have negative fluctuation-dissipation ratios; this might be related to the fact that these models do not have a proper thermodynamics.

9.5.3 Experiments

Grigera and Israeloff were the first to measure FDT violations in glasses by comparing dielectric susceptibility and polarization noise in glycerol at $T = 179.8$K, *i.e.* relatively close to $T_g \simeq 196$K. At fixed measuring frequency $\omega \simeq 8$Hz, they found an effective temperature that slowly diminishes from $T_{\rm EFF} \simeq 185$K to roughly 180K in 10^5 sec, that is to say in the order of days! This pioneering experiment in such a

traditional glass former has not had a sequel yet.

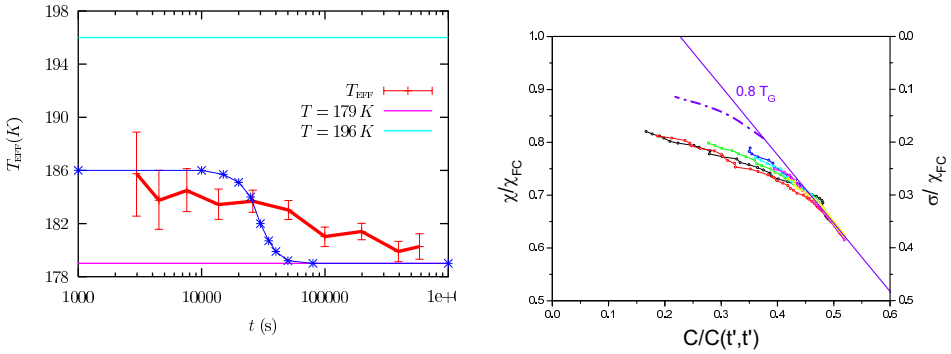

Figure 51: Left: the waiting-time evolution of the effective temperature of glycerol by Grigera and Israeloff. Right: the parametric $\chi(C)$ plot for thiospinel, an insulator spin-glass by Hérisson and Ocio.

Particle tracking experiments in a colloidal suspension of PMMA particles revealed an effective temperature of the order of double the ambient one from the mobility-diffusivity relation.

In the soft matter realm a favorite is an aqueous suspension of clay, Laponite RG, in its colloidal glass phase. During aging, because of electrostatic attraction and repulsion, Laponite particles form a house-of-cards-like structure. After a number of rather confusing reports the status of $T_{\rm EFF}$ in this system can be summarized as follows. The surprisingly high $T_{\rm EFF}$ found with dielectric spectroscopy combined with spontaneous polarization noise measurements was later ascribed to violent and intermittent events possibly linked to the presence of ions in the solution which may be the actual source of FDT violation. For the moment dielectric degrees of freedom are invalidated as a good test ground for $T_{\rm EFF}$ in this sample. Using other methods several groups found that $T_{\rm EFF}$ detaches from the bath temperature. Strachan *et al.* measured the diffusion of immersed probe particles of different sizes via dynamic light scattering and simultaneous rheological experiments and found a slightly higher $T_{\rm EFF}$ than T. With micro-rheology Abou and Gallet observed that $T_{\rm EFF}$ increases in time from T to a maximum and then decreases back to T. Using a passive micro-rheology technique and extracting $T_{\rm EFF}$ from the energy of the probe particle *via* equipartition Greinert *et al.* also observed that $T_{\rm EFF}$ increases in time. In parallel, a series of global mechanical tests, and passive and active micro-rheological measurements that monitor the displacement and mobility of probe Brownian particles were performed by Ciliberto's and D. Bonn's groups, both finding no violation of FDT over a relatively wide frequency range. In a very detailed article Jop *et al.* explain many subtleties in the experimental techniques employed and, especially, the data analysis used to extract $T_{\rm EFF}$ that could have biased the results quoted above. A plausible reason for

the lack of out of equilibrium signal in some experiments using Laponite as well as other colloidal glasses is that the range of frequency-time explored may not enter the aging regime. Moreover, none of these works studied the degrees of freedom of the Laponite disks themselves but, instead, the properties of the solvent molecules or probe particles. More recently, Maggi *et al.* combined dynamic light scattering measurements of the correlation function of the colloid rotations with those of the refringence response and a $\chi(C, t_w)$ plot that is rather constant as a function of C and slowly recovers the equilibrium form as the arrested phase is approached (t_w ranges from 90 to 1200 min and the violations are observed for time differences between 0.1 and 1 ms, *i.e.* frequencies between 10 and 1 kHz). $T_{\rm EFF}$ is at most a factor of 5 larger than T. The actual behaviour of Laponite remains mysterious – and not only in what $T_{\rm EFF}$ is concerned!

Oukris and Israeloff measured local dielectric response and polarization noise in polyvinyl-acetate with electric-force-microscopy. They probed long-lived nano-scale fluctuations just below T_g, achieved a good signal-to-noise ratio down to very low frequencies, constructed a parametric plot by keeping t_w fixed and found a non-trivial asymptotic form with no t_w dependence within the available accuracy. The data combine into the parametric plot $T_{\rm EFF}(C) \simeq TC^{-0.57}$ in the aging regime.

9.6 Relaxation in frustrated magnetic systems

Disordered and frustrated magnets behave collectively at low temperatures and developed ordered phases that although not fully understood are accepted to exist. As macroscopic glassy systems they present a separation of time-scales in their low-temperature dynamics and are good candidates to admit a thermodynamic interpretation of the FDT violations.

9.6.1 Remarks on model systems

The physics of spin-glasses is a controversial subject. Some authors push an Ising domain-growth interpretation of their dynamics – slowed down by domain wall pinning by disorder – a.k.a. the *droplet picture*. If the scheme discussed in Sect. were reproduced under strong disorder, the asymptotic $\chi(C)$ plot would have a linear piece of slope $-1/T$ and a sharp transition at $q_{\rm EA}$ to a flat aging piece. The domain-growth interpretation is not accepted by other authors and more complex *scenarii* based on the static and dynamic solution to the SK model are envisaged, with a non-trivial $\chi(C)$ as a result. Much effort has been put in trying to interpret numerical and experimental data as validating one description at the expense of the other. Unfortunately, it is very difficult to distinguish between the two. A third possibility is that, in a loose sense, the spin-glass be like the low-T phase in the $2d$ XY model, with quasi long-range order. Yet another proposal is that actual spin-glass samples are of Heisenberg-type and that chilarity might be decoupled from spin with a chiral-glass order arriving at a higher critical temperature than the spin-glass ordering.

The trap model was devised to describe slow dynamics in systems with weak ergodicity breaking and it was applied, notably, to describe experiments in spin-glasses. The model shows a glass transition at a T_g below which an equilibrium Boltzmann state cannot exist. The $\chi(C)$ has a slope that varies continuously even though there is a single scaling of relaxation times with age, it depends non-trivially on the observable and one cannot use it to define a meaningful $T_{\rm EFF}$. The reason for this failure seems to be the unbounded nature of the energy and the fact that an equilibrium distribution does not exist below T_g.

9.6.2 Simulations

Monte Carlo simulations of the $3d$ Edwards-Anderson (EA) model were carried out by several groups. One of the hallmarks of the dynamics of the SK model, dynamic ultrametricity, is absent from all numerical and experimental data analyzed so far. Magnetic correlation and susceptibility relax in two scales, the by now usual stationary one for finite time-differences and an aging one in which the data are well described by a simple t/t_w scaling. This aging scaling does not conform with the droplet picture either, which predicts an asymptotic $\ln t/\ln t_w$ form. In all studies so far, the parametric plot was constructed by keeping t_w fixed and the curves drift towards increasing values of χ for longer t_ws as in a transient or critical system. In simple coarsening problems the drift with increasing t_w goes in the opposite direction of rendering the aging part of the curves flatter; this remark suggests to discard a simple droplet picture. The outcome $\chi(C)$ found for the longest t_w reached was interpreted as being non-constant – as in the SK model – although this is, in our opinion, not that clear from the data that could be described by a straight line. The simultaneous t/t_w scaling, the lack of unambiguous evidence for a stable plateau at $q_{\rm EA}$, and a curved $\chi(C)$ in the aging regime is not what would be expected from an analogy with the SK model. Instead, it would be consistent with critical dynamics and the $2d$ XY model similitude. A number of caveats on the numerical analysis should, however, be lifted before reaching a firm conclusion.

The finite-time finite-length relation between static $\aleph(C, \xi(t_w))$ and long-time out of equilibrium dynamic $\chi(C, t_w)$ was put to the test in the $2d$ and $3d$ EA models at finite T. The notable coincidence of the two functions found in the $2d$ case, in which there is no complex equilibrium structure, suggests that the claimed coincidence of $\chi(C)$ and $\aleph(C)$ in $3d$ might also be valid *just* in the transient regime.

Simulations of the $3d$ Heisenberg spin-glass model with weak anisotropy suggest that $T_{\rm EFF}$ associated to the spin degrees of freedom is constant and about twice the critical temperature for spin-glass ordering. As far as we know, chiral degrees of freedom have not been used to estimate $T_{\rm EFF}$.

As regards fluctuations, the two kinds were measured in the $3d$ EA spin-glass. Disordered induced ones, in which one computes strictly local noise-averaged correlations and linear responses, demonstrate the existence of two types of spins in each sample: rapid paramagnetic-like ones and slow ones. The former satisfy FDT while the latter evolve in two time-regimes with a fast one satisfying FDT and a slow one in

which $\chi_i(C_i)$ looks quite flat as in coarsening systems. The simulation suggests that the two ensembles behave independently of each other and are strongly correlated with the backbone of the ground state configurations. The average over all sites (at finite t_w) gives rise to a curve with non-constant slope. These results suggest a still different picture for the spin-glass dynamics in which a rather compact set of spins undergoes coarsening of the backbone equilibrium configurations while the other ones behave paramagnetically. This intriguing idea needs to be put to further test.

The analysis of noise induced fluctuations suggests that eq. (**??**) is valid although better numerical data would be needed to have definitive evidence for this statement. A more detailed discussion can be found in the review by Chamon and Cugliandolo. Very recent studies of non-linear fluctuations that take advantage of FDRs to compute higher order responses point in the direction of the TRI scenario with a finite $T_{\rm EFF}$.

9.6.3 Experiments

On the experimental side the first attempt to quantify FDT violations in spin-glasses was indirect. Simultaneous measurements of global magnetic noise and susceptibility in the thiospinel insulating spin-glass were later performed by Hérisson and Ocio. The data confirm deviations from the FDT with a $\chi(C, t_w)$ plot of relatively curved form although still evolving during the experimental time window. The authors interpreted it as evidence for the full RSB scenario, *via* the association $\chi(C) \leftrightarrow \aleph(C)$. However, as with numerical data, dynamic ultrametricity fails to show off, the asymptotic limit of the parametric construction is still far, and a clear-cut distinction between a curved and a linear $\chi(C)$ is hard to assess.

More recent experiments exploit two novel techniques, Hall-sensor based magnetometer and giant magnetoresistance technology to detect signals from very small samples. The use of these probes opens the way to perform a systematic study of FDT violations in magnetic systems of different kind (spin-glasses, super-spin glasses, disordered ferromagnets...). The first of these measurements appeared recently in a super-spin glass, a system of magnetic nanoparticles suspended in fluid glycerol with a single-domain magnetic structure that behaves as one large spin, the orientation of which is the only degree of freedom. The large magnetic moment facilitates the observation of magnetic noise. For aging times of the order of 1 h, the ratio of $T_{\rm EFF}$ to the bath temperature T grows from 1 to 6.5 when T is lowered from T_g to 0.3 T_g, regardless of the noise frequency.

Artificial spin ice is yet another material in which the $T_{\rm EFF}$ notion has been tested.

9.7 Driven liquids and glasses

Berthier and Barrat used molecular dynamics of a binary Lennard-Jones mixture under a steady and homogeneous shear flow. The deviation from FDT is similar to the one found analytically in disordered spin models of RFOT type with asymmetric couplings that mimic non-conservative forces. Moreover, it does not depend on the observable. The tracer particle experiment was also realized. When the tracers'

Einstein frequency is smaller than the inverse relaxation time of the fluid, a non-equilibrium equipartition theorem holds with $m_{\rm TR} v_z^2 = T_{\rm EFF}$, where v_z is the velocity in the direction transverse to the flow. For increasing $m_{\rm TR}$ the effective temperature very slowly crosses over from T to the slow modes value, in perfect agreement with the notion of a temperature measured by a thermometer sensible to the scale. $T_{\rm EFF}$ also captures the essential phenomenological idea that when a system is sheared more vigorously its effective temperature increases.

O'Hern *et al.* also studied fluctuation-dissipation relations in shear fluids. This group defined an effective temperature through the 'static limit' $\lim_{t\to\infty} \chi(t-t_w)/C(t,t)$, a kind of average of the slope of the $\chi(C)$ plot over the full range of $C(t-t_w)$ that mixes different time scales (in particular, the high and low frequency ones). A more thorough discussion of the comparison between this definition and the one described in this review was given by Ilg and Barrat within a fully solvable model that demonstrates the importance of *not* mixing time-scales to get physically sensible results.

A first study of the fluctuations of entropy production in a Lennard-Jones fluid above and below T_g under a shear flow appeared in and the need to take into account $T_{\rm EFF}$, as obtained from the modification of the FDT below T_g, was signaled in this paper. A more detailed analysis of the time-scale dependent effective temperature would be needed to fully test the proposal in Bonnetto et al.

Another prominent example is the current driven motion of vortices in type II superconductors. Disorder reduces dissipation, is responsible for non-equilibrium transport and magnetic properties. The external force induces two dynamic phase transitions separating plastic flow, smectic flow and a frozen transverse solid. A low-frequencies $T_{\rm EFF}$ that decreases with increasing driving force and reaches the equilibrium melting temperature when the dynamic transverse freezing occurs was computed from the transverse motion in the fluid moving phase.

9.8 Granular matter

Several studies of the effective temperature of granular matter have been pursued theoretically, numerically and experimentally. In the latter front, D'Anna *et al.* immersed a torsion oscillator in a granular system fluidized by strong high frequency external vibrations to realize the 'thermometer' experiment. They found $T_{\rm EFF} \propto \Gamma^2$ with Γ the adimensional measure of vibrational intensity, and quite independently of ω. Wang *et al.* visualized the dynamics of tracer particles embedded in a $3d$ granular ensemble slowly sheared by the rotating inner wall of a Couette cell. $T_{\rm EFF}$, as obtained from the comparison between the tracer's diffusion and mobility perpendicular to the applied rate of strain, is independent of the shear rate used and the tracers properties but does depend on the packing density of the system. Tests of the thermodynamic properties of $T_{\rm EFF}$ have not been carried through in this system yet. The dependence on the direction of the applied stress was studied by Twardos and Dennin in a plastic bead raft close to jamming. As expected, the correlations and linear responses in the direction of flow do not decay slowly and $\chi(C)$ does not have the same properties as in the transverse direction. Gei and Behringer stressed the fact that in a granular

assembly the outcome of a mobility measurement depends on whether one imposes the velocity or the external force.

In the powders literature reference is often made to the 'granular temperature', a measure of the temperature of the fast modes, as given by the kinetic energy of the grains $T_K \equiv \frac{2}{d} E_K \equiv \frac{2}{d}\langle v^2 \rangle$. Importantly enough, T_K is a high frequency measure that does not really access the structural properties of the sample and, in a sense, plays the role of the environmental temperature in thermal systems. T_K is generically smaller than $T_{\rm EFF}$, as in thermal systems where $T_K = T$, the temperature of the bath.

9.9 Activated dynamics

Activated processes often occur in systems that are out of equilibrium, in the sense that their response to an external drive is strongly non-linear or that their phase space distribution is not the Gibbs-Boltzmann one. The question as to whether an Arrhenius law governs the activation rate, possibly with an effective temperature, and how the latter compares to the one defined from the deviations from FDT has been addressed recently. Ilg and Barrat studied the effect of an out of equilibrium flowing environment, a weakly sheared super-cooled liquid, on the activated dynamics between the two stable conformations of dumbbell particles. The transition rate is well described by an Arrhenius law with a temperature that crosses over from the one of the equilibrium bath to a higher value close to the $T_{\rm EFF}$ of the slow modes of the driven fluid. The crossover roughly occurs at the value of the rate that corresponds to the inverse of the α relaxation time of the fluid.

Three related studies are also worth mentioning. An effective temperature, also consistent with the one stemming from fluctuation-dissipation measurements, appears in a phenomenological Arrhenius law that describes transverse jumps between channels in the driven motion of vortex lattices with random pinning. Haxton and Liu showed that in the shear dominated regime the stress of a $2d$ sheared fluid follows an Arrhenius law with the effective temperature. A study of activation and $T_{\rm EFF}$ in a $2d$ granular system close to jamming was performed by Abate and Durian.

9.10 Biological systems

In biologically inspired problems the relevance of $T_{\rm EFF}$ was stressed to reveal the active process in hair bundles and model cells. Morozov *et al.* studied a model of the cytoskeletal network made of semi-flexible polymers subject to thermal and motor-induced fluctuations and found a $T_{\rm EFF}$ that exceeds the environmental temperature T only in the low-frequency domain where motor agitation prevails over thermal fluctuations. Simple gene network models were studied from the $T_{\rm EFF}$ perspective in Lu *et al.* Fluctuation-dissipation ratios were used to quantify the degree of frustration, due to the existence of many metastable disordered states, in the formation of viral capsids and the crystallization of sticky discs, two self-assembly processes. Fluctuations and responses of blood cell membranes for varying ATP concentration were measured very

recently. The measured $T_{\rm EFF}$ approaches the bath temperature at high frequencies and increases at low frequencies reaching 4-10 times the ambient temperature.

Ratchets are simple models of molecular motors, out of equilibrium systems with directed dissipative transport in the absence of any external bias. Harada and Sasa proposed to use the violations of FDT in flashing ratchets as a means to measure the energy input per unit time in molecular motors – an otherwise difficult quantity to access. Kolton showed that the rectified transverse velocity of a driven particle in a geometric ratchet is equivalent to the response of a $1d$ flashing ratchet at a drive-dependent $T_{\rm EFF}$, as defined from the generalized Einstein relation.

Active matter is driven out of equilibrium by internal or external energy sources. Its constituents absorb energy from their environment or from internal fuel tanks and dissipate it by carrying out internal movements that lead to translational or rotational motion. A typical example are self-propelled particle assemblies in bacterial colonies. The role played by $T_{\rm EFF}$ in the stability of dynamic phases of motorized particle systems was stressed by Shen and Wolynes. Multiple measurements of $T_{\rm EFF}$ were carried out with molecular dynamic simulations of motorized spherical as well as linear molecules in interaction. All measurements (from fluctuation-dissipation ratio and using tracers) yield a constant low-frequency $T_{\rm EFF} > T$ when the effect of the motors is not correlated with the structural rearrangements they induce. Instead, $T_{\rm EFF}$ takes a slightly lower value than T when susceptible motors are used, as argued in [**?**]. Such an 'inversion' also occurs in relaxational systems in which the initial configuration is chosen to be one of equilibrium at a lower T than the working one. In the case of uncorrelated motors, $T_{\rm EFF}/T$ was found to follow the empirical law $T_{\rm EFF}/T \simeq 1 + \gamma f^2$ with f the active force relative to the mean potential force and $\gamma \sim 15$ a parameter. Palacci *et al.*. investigated $T_{\rm EFF}$ by following Perrin's analysis of the density profile in the steady state of an active colloidal suspension under gravity. The active particles used – JANUS particles – are chemically powered colloids and the suspension was studied with optical microscopy. The measurements show that the active colloids are hotter than in the passive limit with a $T_{\rm EFF}$ that increases as the square of the parameter that controls activation, the Peclet number, a dependence that is highly reminiscent of the f^2-dependence of the simulations mentioned above.

Joly *et al.* used numerical techniques to study the non-equilibrium steady state dynamics of a heated crystalline nanoparticle suspended in a fluid. This problem models an active colloid that acts as a local heat source and generates a temperature gradient around it. By comparing the mobility to the velocity correlation function, they found that the FDT approximately holds at short-time lags with a temperature value that coincides with the kinetic one. In contrast, at long-time lags data are compatible with the temperature estimated by using the Einstein relation.

Certainly, many more studies of effective temperatures will appear in this very active field of research, essentially out of equilibrium, in the near future.

10 Conclusions

We discussed the behavior of macroscopic classical systems out of equilibrium.

First, we summarized the dynamics of relatively simple problems, the ones that undergo coarsening, that is to say, the progressive ordering into patches of the two (or more) competing equilibrium states. We also recalled, briefly, the nucleation process relevant to describe the dynamics of systems undergoing first order phase transitions.

Next, we entered the realm of the more interesting, and harder to understand, glassy problems. We modeled these with models with quenched random interactions which, surprisingly enough, render their solution simpler. We mentioned that the mean-field solution of these models allows for a classification into models that mimic spin-glass samples and models that are relevant to describe structural glasses, although there is no explicit quenched randomness in these.

In particular, we analyzed in detail a family of disordered models that yield a mean-field description of the glass transition and dynamics of super-cooled liquids and glasses. The relevance of these models to describe structural glasses was signaled and explained by Kirkpatrick, Thirumalai and Wolynes in the 80s. Their non-equilibrium dynamics and hence the connection with other systems far from equilibrium started to develop more recently.

In short, their behaviour is the following. The dynamic transition arises when the partition function starts being dominated by an exponentially large number of metastable states yielding a finite complexity. The static transition instead is due to an entropy crisis, *i.e.* it occurs when the complexity vanishes and the number of states is no longer exponential in N, just as in the Adams-Gibbs-di Marzio scenario. These transitions mimic, in a mean-field way, the crossover to the glassy phase at T_g and the putative static transition at T_K of fragile glasses.

The equilibrium dynamics close and above T_d coincides with the one obtained with the mode-coupling approach. It describes the relaxation of super-cooled liquids and it contains its most distinctive feature of having a two step decorrelation. The first step is ascribed to the motion of particles within the cages made by their neighbors while the second one is the structural relaxation related to the destruction of the cages.

Below T_d the equilibration time diverges with the size of the system and the models do not equilibrate any longer with their environments (unless one considers times that grow with the size of the system). This is very similar to the situation encountered in real systems below T_g. The experimental time-window is restricted and one is not able to equilibrate the samples any longer below T_g. Aging effects are captured. The correlations still decay to zero but they do in a waiting-time dependent manner. Their decay also occurs in two steps separated by a temperature-dependent plateau at a value related to the size of the cages. One can interpret their stiffness as increasing with the age of the system given that the beginning of the structural relaxation is delayed and slowed down for longer waiting-times.

The nonequilibrium dynamics below T_d approaches a threshold level of flat directions in phase space and it never goes below this level in finite times with respect to the size of the system. The aging dynamics corresponds to the slow drift of the point

representing the system in the slightly tilted set of channels that form the threshold. The motion that is transverse to the channels is related to thermal fluctuations and the first stationary step of the relaxation towards $q_{\rm EA}$, that charcaterises then the transverse "size" of the channel. The longitudinal motion along the channels is related to the structural relaxation. The tilt is proportional to the magnitude of the time-derivatives and these become less and less important as time passes. More generally one interprets the long but finite time non-equilibrium dynamics following saddles that are the borders between basins of attraction of more stable states in phase space.

For times that scale with the size of the system, N, the sharp dynamic transition is avoided, the system penetrates below the threshold via activation and it approaches equilibrium in much longer time-scales. Metastable states below the threshold are typically minima (the fact that they are local minima can be checked studying the dynamics with initial conditions set to be in one of them). This structure allows one to describe the cooling rate effects. For large but finite N and sufficiently slow cooling rate, the system penetrates below the threshold via activation when this is facilitated by T, *i.e.* when passing near T_d. To which level it manages to arrive (roughly speaking to which of the curves in the figure) depends on how long it stays close to T_d. The slower the cooling rate the lower level the system reaches with the ideal "equilibrium" glass corresponding to an infinitely slow cooling.

The region of phase space reached asymptotically in the thermodynamic limit is the threshold of flat directions. The replica analysis of the partition function gives an alternative way of determining its statistical properties. Indeed, by evaluating the partition function on a marginally stable saddle-point in replica space one selects the threshold "states". Dynamic information such as the value of $q_{\rm EA}$ is thus obtained with a pseudo-static calculation. Other facts as, for instance, the scaling of the correlation are not accessible in this way.

One of the hallmarks of the glassy non-equilibrium dynamics is the modification of the relation between correlations and responses, namely, the fluctuation-dissipation theorem. In mean-field models for structural glasses one finds that the integrated linear response is in linear relation with the associated correlation with a proportionality constant that takes the equilibrium value $1/(k_B T)$ when the correlation is above the plateau and it takes a different value $1/(k_B T^*)$ when it goes below the plateau. This behavior has been found in a number of finite dimensional glassy models numerically.

The behavior just described corresponds to a family of mean-field disordered models to which the p spin models with $p \geq 3$ and the Potts glass belong. Other two families exist and they are related to ferromagnetic domain growth and spin-glasses. Two representative models are the spherical p spin model with $p = 2$ and the SK model, respectively. They are characterized by different scalings of the correlations in the aging regime and by different forms of the modification of FDT. The classification in families according to the non-equilibrium behavior has a static counterpart given by the structure of replica symmetry breaking in the low-T phase.

The modification of FDT allows one to define an observable and correlation-scale dependent effective temperature. Fast observables like the kinetic energy are equili-

brated with the environment and the effective temperature equals the thermal bath temperature for them. Other observables though show different values of the effective temperature depending on the time-scales on which one investigates them. The effective temperature has a thermodynamical meaning even if defined out of equilibrium. In particular, it can be directly read with a thermometer coupled to the desired observable and a zero-th law holds for interacting observables that evolve in the same time-scale. As one should have expected the effective temperature shares some of the qualitative features of the phenomenological fictive temperatures. For instance, a system that is quenched from high temperatures has effective temperatures that take higher values than the temperature of the bath, etc. At the mean-field level, when $N \to \infty$, it is history independent but one expects it to depend on the preparation of the sample for finite size and finite dimensional systems. (This is in close relation to the discussion above on cooling rate effects.) There is still no precise determination of which are the necessary conditions a nonequilibrium system has to fulfill to ensure the existence of well-behaved effective temperatures. A clear condition are the need to reach a dynamic regime in which the dynamics is slow and heat exchanges are weak.

Once the effective temperature has been identified one interprets the behavior in the low T phase as follows: the system adjusts to a situation in which each observable sees two baths, one is the white external one and the one characterizing the fast motion of the particles, the other is coloured and at a different temperature T^*. The latter is generated by the interactions. In more complex systems – as mean-field spin-glasses – the asymptotic regime might be multi-thermalised with several time-scales each with its own value of the effective temperature. These results, first derived explicitly for p spin fully-connected models actually hold for any resummation of the perturbative approach that keeps an infinite subset of diagrams (the MCA being one such example). The structure of time-scales and values of the effective temperature is related to the breaking of supersymmetry down to a residual group.

The structure of the free-energy landscape can be computed exactly for mean-field models in general, and for the spherical p spin model in particular. We expect its main features to be reproduced – at least in a smoothen way – in real glassy systems. The free-energy landscape at fixed and low T has a structure as the one roughly sketched in Fig. 52. A pictorial image of the aging process can be quite helpful to understand it. Imagine that one fills phase space with water whose level reaches a free-energy density value, say, f. At high levels of the water, *i.e.* for high free-energy densities, the landscape has only some few isolated stationary states. Looking at the landscape from above one only sees some maxima that are represented as islands in the second panel in the figure. Lowering the water level the islands grow in size and some of them merge: land bridges develop. Lowering still the water level, it eventually reaches a threshold, that corresponds to $f = f_{\rm TH}$, where land percolates. One is left with a labyrinthic path of water as drawn schematically in the third panel that represents a top view of the landscape. This level is "marginal" since the bottom of the water channels is almost completely flat. Draining water from the system the "connectivity" of paths is reduced until the water level goes below the threshold, $f < f_{\rm TH}$, where

minima dominate. In the fourth panel we represent them as lakes immersed in land. Lowering the water level one sees the sizes of the lakes diminish and some of them dry. These minima exist until the lowest level, $f = f_{\rm EQ}$. A "gap" in free-energy density separates the threshold and the equilibrium levels.

This picture allows us to give a natural interpretation of the non-equilibrium dynamics following a quench. Initially, the system is in a configuration typical of high-T, thus, its initial "free-energy density" is very high. This corresponds to a high level of water that fills the landscape. As time passes, water abandons the landscape in such a way that the quantity of water progressively diminishes lowering its level. The system's configuration can be associated to a ship and its evolution to the displacements of the ship sailing on the water. Initially, the water level is very high and the ship can move very rapidly far away from its initial position. It only sees some very few isolated islands that it simply avoids along its motion and the dynamics is very fast. As time passes the water level goes down. Roughly speaking we can associate the speed of drainage with the magnitude of the rate of change of the energy-density. When it approaches the threshold the available path becomes a series of rivers forming a very intricate network. The ship can still follow this network without remaining trapped in any confining region. Its motion, however, gets slower and slower. In finite times with respect to N the water level does not go below the threshold. But for longer times that scale with N it does. When such long times are attained the ship remains trapped in lakes. For still longer times the higher lakes dry and, if the ship got trapped in one of them it must be transported through the land to reach other lakes at lower levels. This action represents an activated process. Part of this image was introduced by Sibani and Hoffmann phenomenologically. The p spin-models and the like realize it explicitly. All quantitative features of the landscape here described with words have been, or in principle can be, calculated analytically.

The value taken by the effective temperature is in direct relationship with the structure of the free-energy landscape. Indeed, again for p-spin model and the like, it has been shown analytically that the asymptotic value T^* reached for long but finite times with respect to N is given by $\beta^* = \partial\Sigma(\beta, f)/\partial f|_{f_{\rm TH}}$, with Σ the complexity. For even longer times such that the system penetrates below the threshold one expects the effective temperature to take different values related to the complexity at lower free-energy density levels. The Edwards-Anderson parameter, $q_{\rm EA}$, also changes since $q_{\rm EA}(f)$. In the longest time-scale such that equilibrium is reached and $q_{\rm EA}$ equals the equilibrium value also obtained with a replica calculation using the standard maximization prescription to determine the breaking point parameter x. This result is intimately related to Edwards' flat measure for granular matter and also to the more recent use of a flat measure over inherent structures to describe the non-equilibrium dynamics of glasses. Note that the these, being defined using the *potential energy-density* landscape, are valid only at zero temperature. However, extensive numerical checks recently performed suggest that the approach, even if not obviously correct at finite T, yields a very good approximation.

Within this picture two distinct regimes would appear in the low-T isothermal dynamics of real systems: a mean-field-like one when the system approaches a pseudo-

threshold of flat directions in phase space and a slower activated regime in which the system jumps over barriers to relax its excess energy density and very slowly progress towards equilibrium. How and if the aging properties in the first and second regime resemble is a very interesting open problem.

The existence of a threshold plays a fundamental role in explaining several features of many experimental observations in such diverse systems as driven granular matter, the rheological properties of complex liquids and glasses, etc. Just to cite two examples, trapping and Reynolds dilatancy effects in granular matter as well as the existence of a static yield stress and thixotropic behaviour in some rheological experiments can be interpreted in terms of threshold and sub-threshold states. These features support the claim that this free-energy structure exists in real physical systems. Moreover, maybe not surprisingly, this structure also appears in optimization problems such as XOR-SAT and K-SAT that can be mapped to dilute p-spin models at zero temperature. In this context the control parameter is the number of requirements over the number variables, α, and the static transition, α_s, is related to the sat-unsat transition while the dynamic transition, $\alpha_d < \alpha_s$ corresponds to the value where greedy algorithms fail to find the existing solutions.

All these arguments can be adapted to include quantum fluctuations The statics is studied with the Matsubara replicated partition function, metastability with an extension of the TAP approach and the real-time dynamics with the Schwinger-Keldysh formalism. The picture that arises is very similar to the one above with some intriguing new ingredients as the emergence of truly first order transitions close to the quantum critical point, highly non-trivial effects due to the quantum environments, a waiting-time dependent quantum-to-classical crossover in the dynamic scaling, etc.

The models we studied in these notes have quenched random interactions. Real glassy systems of the structural type do not. One may wonder if this is an important deficiency of the approach or if similar results can be obtained for models with no disorder. A large variety of models of mean-field type, or defined on large d spaces, with no explicit quenched disorder and having the same phenomenology have been introduced in recent years. Finite d models with similar, eventually interrupted, dynamic behavior have also been exhibited. Their existence supports the belief that the scenario here summarized goes beyond simple modelling. Indeed, it is at the basis of several conjectures for the behavior of other non-equilibrium systems with slow dynamics that have been later checked numerically. It has also motivated several experimental investigations in a variety of systems.

A Conventions

1.1 Fourier transform

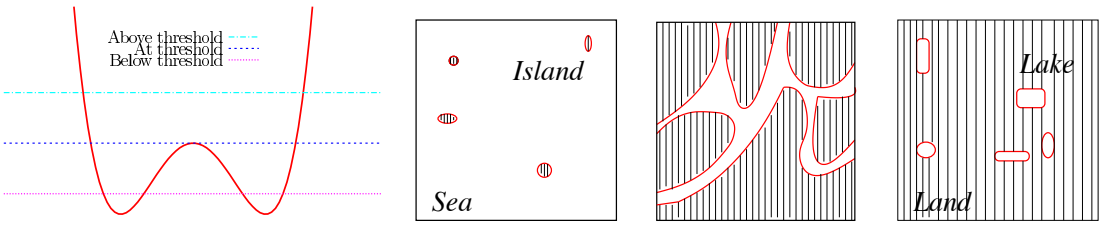

Figure 52: Left: a $1d$ simplified sketch of the free-energy density. Three top views of the free-energy landspcape: above, at and below the threshold.

The convention for the Fourier transform is

$$f(\tau) = \int_{-\infty}^{\infty} \frac{d\omega}{2\pi}\, e^{-i\omega\tau}\, f(\omega)\,, \tag{1.1}$$

$$f(\omega) = \int_{-\infty}^{\infty} d\tau\, e^{+i\omega\tau}\, f(\tau)\,. \tag{1.2}$$

The Fourier transform of the theta function reads

$$\theta(\omega) = i\mathrm{vp}\frac{1}{\omega} + \pi\delta(\omega)\,. \tag{1.3}$$

The convolution is

$$[f\cdot g](\omega) = f\otimes g(\omega) \equiv \int \frac{d\omega'}{2\pi} f(\omega')g(\omega-\omega')\,. \tag{1.4}$$

1.2 Commutation relations

We defined the commutator and anticommutator: $\{A,B\} = (AB+BA)/2$ and $[A,B] = (AB-BA)/2$.

1.3 Time ordering

We define the time odering operator acting on bosons as

$$T\hat{x}(t)\hat{x}(t') \equiv \theta(t,t')\hat{x}(t)\hat{x}(t') + \theta(t',t)\hat{x}(t')\hat{x}(t)\,. \tag{1.5}$$

For fermions, we define the time ordering operator as

$$T\hat{x}(t)\hat{x}(t') \equiv \theta(t,t')\hat{x}(t)\hat{x}(t') - \theta(t',t)\hat{x}(t')\hat{x}(t)\,, \tag{1.6}$$

$$T\hat{x}(t)\hat{x}^\dagger(t') \equiv \theta(t,t')\hat{x}(t)\hat{x}^\dagger(t') - \theta(t',t)\hat{x}^\dagger(t')\hat{x}(t)\,, \tag{1.7}$$

In both cases $\theta(t,t')$ is the Heaviside-function.

We define the time-ordering operator T_C on the Keldysh contour in such a way that times are ordered along it:

$$\begin{aligned} T_C\ x_+(t)x_-(t') &= x_-(t')x_+(t) \qquad T_C\ x_-(t)x_+(t') = x_-(t)x_+(t') \\ T_C x_+(t)x_-(t') &= -x_-(t')x_+(t) \qquad T_C x_-(t)x_+(t') = x_-(t)x_+(t') \end{aligned} \tag{1.8}$$

for all t and t'.

2 Classical statics: the reduced partition function

In order to analyze the statistical static properties of the classical coupled system, we study the partition function or Gibbs functional, $Z_{\rm TOT}$ that reads

$$Z_{\rm TOT}[\eta] = \sum_{\substack{\rm CONF\ OSC \\ \rm CONF\ SYST}} \exp(-\beta H_{\rm TOT} - \beta\eta x) \tag{2.1}$$

where the sum represents an integration over the phase space of the full system, the particle's and the oscillators', and η is a source. Having chosen a quadratic bath and a linear coupling, the integration over the oscillators' coordinates and momenta can be easily performed. This yields the **reduced** Gibbs functional

$$Z_{\rm RED}[\eta] \propto \sum_{\rm CONF\ SYST} \exp\left[-\beta\left(H_{\rm SYST} + H_{\rm COUNTER} + \eta x - \frac{1}{2}\sum_{a=1}^{N_b}\frac{c_a^2}{m_a\omega_a^2}\,x^2\right)\right] . \tag{2.2}$$

The 'counterterm' $H_{\rm COUNTER}$ is chosen to cancel the last term in the exponential and it avoids the renormalization of the particle's mass (the coefficient of the quadratic term in the potential) due to the coupling to the environment that could have even destabilize the potential taking negative values. An alternative way of curing this problem would be to take a vanishingly small coupling to the bath in such a way that the last term must vanish by itself (say, all $c_a \to 0$). However, this might be problematic when dealing with the stochastic dynamics since a very weak coupling to the bath implies also a very slow relaxation. It is then conventional to include the counterterm to cancel the mass renormalization. One then finds

$$Z_{\rm RED}[\eta] \propto \sum_{\rm CONF\ SYST} \exp\left[-\beta\left(H_{\rm SYST} + \eta x\right)\right] = Z_{\rm SYST}[\eta] . \tag{2.3}$$

The interaction with the reservoir does not modify the statistical properties of the particle since $Z_{\rm RED} \propto Z_{\rm SYST}$. This does not necessarily happen quantum mechanically. (For a non-linear coupling $H_{\rm INT} = \sum_\alpha c_\alpha q_\alpha \mathcal{V}(x)$ the counterterm is $H_{\rm COUNTER} = \frac{1}{2}\sum_\alpha \frac{c_\alpha^2}{m_\alpha\omega_\alpha^2}[\mathcal{V}(x)]^2$.)

3 The instanton calculation

The path-integral formalism yields an alternative calculation of the Kramers escape time, the Arrhenius exponential law and its prefactor that, in principle, is easier to generalize to multidimensional cases. For the sake of simplicity let us focus on the overdamped limit in which we neglect inertia. We first rederive the Arrhenius exponential using a simplified saddle-point argument, and then show how Kramers calculation can be recovered by correctly computing the fluctuations around this saddle point. Starting from the following representation of the probability to reach the top of the barrier from the potential well:

$$P(x_{\rm MAX},t|x_{\rm MIN}) = \left\langle \int_{x(0)=x_{\rm MIN}}^{x(t)=x_{\rm MAX}} \mathcal{D}x\ \delta(\xi - {\rm EQ}[x])\ \left|\det\left(\frac{\delta {\rm EQ}[x](t)}{\delta x(t')}\right)\right| \right\rangle_{\xi},$$

and neglecting the determinant (which is justified if one follows the Itô convention), then, for a Gaussian white noise ξ:

$$P(x_{\rm MAX},t|x_{\rm MIN}) = \int_{x(0)=x_{\rm MIN}}^{x(t)=x_{\rm MAX}} \mathcal{D}x\ e^{-\frac{1}{4k_BT}\int_0^t dt'\left(\dot{x}+\frac{dV}{dx}\right)^2}$$

Expanding the square, we find a total derivative contribution to the integral equal to $2[V(x_{\rm MAX})-V(x_{\rm MIN})]$, plus the sum of two squares: $\int_0^t dt'[\dot{x}^2+(V'(x))^2]$. For small T, the path, x^*, contributing most to the transition probability is such that this integral is minimized. Using standard rules of functional derivation one finds

$$\frac{d^2x^*}{dt'^2} = V'(x^*)V''(x^*) \quad \Rightarrow \quad \dot{x}^* = \pm V'(x^*).$$

In order to be compatible with the boundary conditions $x^*(0)=x_{\rm MIN}$ and $x(t)=x_{\rm MAX}$, the + solution must be chosen, corresponding to an overdamped motion in the inverted potential $-V(x)$. The 'action' of this trajectory is

$$\int_0^t dt'\left[\dot{x}^{*2}+(V'(x^*))^2\right] = 2\int_0^t dt'\dot{x}^*V'(x^*) = 2[V(x_{\rm MAX})-V(x_{\rm MIN})],$$

that doubles the contribution of the total derivative above. Hence,

$$P(x_{\rm MAX},t|x_{\rm MIN}) \approx e^{-\beta(V(x_{\rm MAX})-V(x_{\rm MIN}))},$$

independently of t, as in eq. (2.68). This type of calculation can be readily extended to cases in which the noise ξ has temporal correlations, or non Gaussian tails, and to see how these effects change the Arrhenius result. The calculation of the attempt frequency is done using the standard dilute gas instanton approximation developed by several authors but we shall not discuss it here.

The path-integral that we have just computed is a sum over the subset of noise trajectories that lead from the initial condition to a particular final condition that we imposed. Imposing a boundary condition in the future destroys the causal character of the theory.

In a one dimensional problem as the one treated in this Section there is only one possible 'reaction path'. In a multidimensional problem, instead, a system can transit from one state to another following different paths that go through different saddle-points. The lowest saddle-point might not be the most convenient way to go and which is the most favorable path is, in general, difficult to established.

4 Discrete MSRJD for additive noise

4.1 Stratonovich prescription – Mid-point discretization

The Langevin equation is a stochastic differential equation and one can give a rigorous meaning to it by specifying a particular discretization scheme. We adopt the Stratonovitch prescription where the rules of conventional differential calculus can be used. This correponds to a mid-point discretization scheme and is coherent with the convention $\Theta(0) = 1/2$ in the continuum limit.

Let us divide the time interval $[-T, T]$ into $N+1$ infinitesimal slices of width $\epsilon \equiv 2T/(N+1)$. The discretized times are $t_k = -T + k\epsilon$ with $k = 0, ..., N+1$. The discretized version of $x(t)$ is $x_k \equiv x(t_k)$. The continuum limit is achieved by sending N to infinity and keeping $(N+1)\epsilon = 2T$ constant. Given some initial conditions $x_{\rm i}$ and $\dot{x}_{\rm i}$, we set $x_1 = x_{\rm i}$ and $x_0 = x_{\rm i} - \epsilon \dot{x}_{\rm i}$ meaning that the first two times (t_0 and t_1) are reserved for the integration over the initial conditions whereas the N following ones correspond to the stochastic dynamics given by the discretized Langevin equation:

$$\begin{aligned} {\rm EQ}_k \quad \equiv \quad & m\frac{x_{k+2} - 2x_{k+1} + x_k}{\epsilon^2} - F_{k+2}(x_{k+2}, x_{k+1}, ...) \\ & + \sum_{l=1}^{k} \gamma_{kl}(x_{l+2} - x_{l+1}) = \xi_{k+1} \ , \end{aligned} \tag{4.1}$$

defined for $k = 0, ..., N-1$. The notation γ_{kl} stands for $\gamma_{kl} \equiv \epsilon^{-1} \int_{0^-}^{\epsilon} du \gamma(t_k - t_l + u)$ The ξ_k $(k = 1, ..., N)$ are independent Gaussian random variables with variance $\langle \xi_k \xi_l \rangle = \beta^{-1} \Gamma_{kl}$ where $\Gamma_{kl} \equiv \gamma_{kl} + \gamma_{lk}$. Inspecting the equation above, we notice that the value of x_k depends on the realization of the previous noise realisation ξ_{k-1} so that there is no need to specify ξ_0 and ξ_N. In the Markovian limit, one has $\gamma_{kl} = \epsilon^{-1}\gamma_0 \delta_{kl}$, $\langle \xi_k \xi_l \rangle = 2\gamma_0 \beta^{-1} \epsilon^{-1} \delta_{kl}$ where δ is the Kronecker delta, and

$$\begin{aligned} {\rm EQ}_k \quad \equiv \quad & m\frac{x_{k+2} - 2x_{k+1} + x_k}{\epsilon^2} - \overline{F_{k+2}}(x_{k+2}, x_{k+1}, ...) \\ & + \gamma_0 \frac{x_{k+2} - x_{k+1}}{\epsilon} = \xi_{k+1} \ . \end{aligned} \tag{4.2}$$

4.2 Construction of the MSRJD action

The probability density P for a complete field history $(x_0, x_1, ..., x_{N+1})$ is set by the relation

$$P(x_0, x_1, ..., x_{N+1}) dx_0 dx_1 ... dx_{N+1}$$

$$= P_{\rm i}(x_{\rm i},\dot{x}_{\rm i})dx_{\rm i}d\dot{x}_{\rm i}\ P_{\rm n}(\xi_1,\xi_2,...,\xi_N)d\xi_1 d\xi_2...d\xi_N\ . \tag{4.3}$$

$P_{\rm i}$ is the initial probability distribution of the field. The probability for a given noise history to occur between times t_1 and t_N is given by

$$P_{\rm n}(\xi_1,...,\xi_N) \quad = \quad \mathcal{M}_N^{-1}\ e^{-\frac{1}{2}\sum_{k,l=1}^{N}\xi_k\ \beta\Gamma_{kl}^{-1}\ \xi_l} \tag{4.4}$$

with the normalization $\mathcal{M}_N \equiv \left(\frac{(2\pi)^N}{\det_{kl}\beta\Gamma_{kl}^{-1}}\right)^{1/2}$. From eq. (4.3), one gets

$$P(x_0,x_1,...,x_{N+1}) = |\mathcal{J}_N|P_{\rm i}(x_1,\frac{x_1-x_0}{\epsilon})P_{\rm n}({\rm EQ}_0,...,{\rm EQ}_{N-1})\ \ , \tag{4.5}$$

with the Jacobian

$$\mathcal{J}_N \equiv \det\frac{\partial(x_{\rm i},\dot{x}_{\rm i},\xi_1,\ldots,\xi_N)}{\partial(x_0,x_1,\ldots,x_{N+1})} = \det\frac{\partial(x_{\rm i},\dot{x}_{\rm i},{\rm EQ}_0,\ldots,{\rm EQ}_{N-1})}{\partial(x_0,x_1,\ldots,x_{N+1})}\ , \tag{4.6}$$

that will be discusssed in 4.3. The expression (4.4) for the noise history probability reads, after a Hubbard-Stratonovitch transformation that introduces the auxiliary variables $\hat{x}_k$ $(k=1,...,N)$,

$$P_{\rm n}(\xi_1,...,\xi_N) = \mathcal{N}_N^{-1}\ \int d\hat{x}_1...d\hat{x}_N e^{-\sum_k i\hat{x}_k\xi_k+\frac{1}{2}\sum_{kl}i\hat{x}_k\beta^{-1}\Gamma_{kl}i\hat{x}_l}$$

$$= \mathcal{N}_N^{-1}\int d\hat{x}_0...d\hat{x}_{N+1}\delta(\hat{x}_0)\delta(\hat{x}_{N+1})\ e^{-\sum_k i\hat{x}_k{\rm EQ}_{k-1}+\frac{1}{2}\sum_{kl}i\hat{x}_k\beta^{-1}\Gamma_{kl}i\hat{x}_l}\ ,$$

with $\mathcal{N}_N \equiv (2\pi)^N$. In the last step, we replaced ξ_k by ${\rm EQ}_{k-1}$ and we allowed integrations over $\hat{x}_0$ and $\hat{x}_{N+1}$ at the cost of introducing delta functions. Notice that the Hubbard-Stratonovitch transformation allows for some freedom in the choice of the sign in front of $i\hat{x}_k$ in the exponent. Together with eq. (4.5) this gives

$$P(x_0,x_1,...,x_{N+1}) = \mathcal{N}_N^{-1}\,|\mathcal{J}_N|\int d\hat{x}_0...d\hat{x}_{N+1} \tag{4.7}$$

$$\times e^{-\sum_k i\hat{x}_k{\rm EQ}_{k-1}+\frac{1}{2}\sum_{kl}i\hat{x}_k\beta^{-1}\Gamma_{kl}i\hat{x}_l+\ln P_{\rm i}\left(x_1,\frac{x_1-x_0}{\epsilon}\right)}$$

that in the continuum limit becomes

$$P[x] \quad = \quad \mathcal{N}^{-1}e^{\ln P_{\rm i}+\ln|\mathcal{J}[x]|}\int\mathcal{D}[\hat{x}]e^{-\int du\ i\hat{x}(u){\rm EQ}([x],u)+\frac{1}{2}\int duvi\hat{x}(u)\beta^{-1}\Gamma(u-v)i\hat{x}(v)}\ ,$$

with the boundary conditions $\hat{x}(-T)=\hat{x}(T)=0$ and where all the integrals over time run from $-T$ to T. In the following, unless otherwise stated, we shall simply denote them by $\int$. The infinite prefactor $\mathcal{N} \equiv \lim_{N\to\infty}(2\pi)^N$ can be absorbed in the definition of the measure:

$$\mathcal{D}[x,\hat{x}] = \lim_{N\to\infty}\frac{1}{(2\pi)^N}\prod_{k=0}^{N+1}dx_k d\hat{x}_k\ . \tag{4.8}$$

4.3 Evaluation of the Jacobian

In this section we take the continuum limit of the Jacobian defined in eq. (4.6). In the additive noise case, we start from

$$\begin{aligned}
\mathcal{J}_N &= \det \frac{\partial(x_{\rm i}, \dot{x}_{\rm i}, \mathrm{EQ}_0, \ldots, \mathrm{EQ}_{N-1})}{\partial(x_0, x_1, \ldots, x_{N+1})} \\
&= \det \begin{bmatrix}
0 & 1 & 0\ldots & & & \\
-1/\epsilon & 1/\epsilon & 0\ldots & & & \\
\frac{\partial \mathrm{EQ}_0}{\partial x_0} & \frac{\partial \mathrm{EQ}_0}{\partial x_1} & \frac{\partial \mathrm{EQ}_0}{\partial x_2} & 0\ldots & & \\
\frac{\partial \mathrm{EQ}_1}{\partial x_0} & \frac{\partial \mathrm{EQ}_1}{\partial x_1} & \frac{\partial \mathrm{EQ}_1}{\partial x_2} & \frac{\partial \mathrm{EQ}_1}{\partial x_3} & 0\ldots & \\
\ldots & & & & & 0 \\
\frac{\partial \mathrm{EQ}_{N-1}}{\partial x_0} & & \ldots & & & \frac{\partial \mathrm{EQ}_{N-1}}{\partial x_{N+1}}
\end{bmatrix} \\
&= \frac{1}{\epsilon} \det \begin{bmatrix}
\frac{\partial \mathrm{EQ}_0}{\partial x_2} & 0\ldots & & \\
\frac{\partial \mathrm{EQ}_1}{\partial x_2} & \frac{\partial \mathrm{EQ}_1}{\partial x_3} & 0\ldots & \\
\ldots & & & 0 \\
\frac{\partial \mathrm{EQ}_{N-1}}{\partial x_2} & \ldots & & \frac{\partial \mathrm{EQ}_{N-1}}{\partial x_{N+1}}
\end{bmatrix} = \frac{1}{\epsilon} \prod_{k=0}^{N-1} \frac{\partial \mathrm{EQ}_k}{\partial x_{k+2}}
\end{aligned} \tag{4.9}$$

We can safely drop the overall $1/\epsilon$ factor since it can be included in the normalization. Notice that causality manifests itself in the lower triangular structure of the last matrix involved. In the continuous notation, $\lim_{N\to\infty} \mathcal{J}_N$ reads

$$\mathcal{J}[x] = \det_{uv} \left[\frac{\delta \mathrm{EQ}([x], u)}{\delta x(v)} \right] . \tag{4.10}$$

4.4 Markovian case

Let us first consider the Markovian case in which the friction term has no memory and the force F is a local functional of x which can carry a time-dependence. Defining F' as $\delta F_u[x_u]/\delta x_v \equiv F'_u[x_u]\delta(u-v)$, the Jacobian reads

$$\mathcal{J}[x] = \det_{uv} \left[\left(m\partial_u^2 + \gamma_0 \partial_u - F'_u[x_u] \right) \delta_{u-v} \right] . \tag{4.11}$$

Now let us write $\det_{uv} \left[\left(m\partial_u^2 + \gamma_0 \partial_u - F'_u[x_u] \right) \delta_{u-v} \right]$

$$\begin{aligned}
&= \det_{uv} \left[(m\partial_u^2 + \gamma_0 \partial_u) \delta_{u-v} \right] \ \det_{uv} \left[\delta_{u-v} - \int_w G_{u-w} F'_w[x_w] \delta_{w-v} \right] \\
&= \det_{uv} \left[(m\partial_u^2 + \gamma_0 \partial_u) \delta_{u-v} \right] \ \exp \mathrm{Tr}_{uv} \ln \left[\delta_{u-v} - G_{u-v} F'_v[x_v] \right] \\
&= \det_{uv} \left[(m\partial_u^2 + \gamma_0 \partial_u) \delta_{u-v} \right] \ \exp - \sum_{n=1}^{\infty} \frac{1}{n} \int_u \left(\underbrace{M \circ M \circ \ldots \circ M}_{n \text{ times}} \right)_{uu} ,
\end{aligned} \tag{4.12}$$

where we used the matrix notation $M_{uv} \equiv G_{u-v} F'_v[x_v]$ and product $\circ$. G is the retarded Green function solution of

$$\left[m\partial_u^2 + \gamma_0 \partial_u \right] G(u-v) = \delta(u-v) , \tag{4.13}$$

which reads

$$G(t) = \frac{1}{\gamma_0}\left[1 - e^{-\gamma_0 t/m}\right]\Theta(t)\ . \tag{4.14}$$

Since $\Theta(u-v)\Theta(v-u) = 0$, $\forall\ u \neq v$, the $n \geq 2$ terms do not contribute to the sum in eq. (4.12). Furthermore, $G(t=0) = 0$ for finite values of m[13], implying that the $n = 1$ term is zero as well. Therefore we established

$$\mathcal{J}[x] = \det_{uv}\left[m\partial_u^2 + \gamma_0\partial_u\right]\delta(u-v)\ . \tag{4.15}$$

This means that the functional determinant is simply a field independent constant. One can easily generalize this result for time dependent and non potential forces.

4.5 Non Markovian case

Within the Stratonovich prescription (DONNER LES PAPIERS DES JAPONNAIS, OU EXPLIQUER MIEUX OU LAISSER TOMBER), the determinant can be seen as the result of a Gaussian integration over Grassmannian conjugate fields c and c^*. Let us first recall the discretized expression of the Jacobian obtained in eq. (4.9):

$$\mathcal{J}_N = \frac{1}{\epsilon}\det_{kl}\left[\frac{\partial \mathrm{EQ}_k}{\partial x_{l+2}}\right]\ , \tag{4.16}$$

where k and l run from 0 to $N-1$. Introducing ghosts, it can be put in the form

$$\begin{aligned}\mathcal{J}_N &= \frac{1}{\epsilon}\int dc_2 dc_0^* ... dc_{N+1} dc_{N-1}^*\ e^{\sum_{k=0}^{N-1}\sum_{l=2}^{N+1} c_k^*\frac{\partial \mathrm{EQ}_k}{\partial x_l}c_l} \\ &= \frac{1}{\epsilon}\int dc_0 dc_0^* ... dc_{N+1} dc_{N+1}^*\ e^{\sum_{k=0}^{N+1}\sum_{l=0}^{N+1} c_k^*\frac{\partial \mathrm{EQ}_k}{\partial x_l}c_l}\ c_0 c_1 c_N^* c_{N+1}^*\ ,\end{aligned} \tag{4.17}$$

where in the last step, we allowed integration over c_0, c_1, c_N^* and c_{N+1}^* at the cost of introducing delta functions (remember that for a Grassmann number c, the delta function is achieved by c itself). In the continuum limit, dropping the overall $1/\epsilon$ constant (and infinite) factor, this yields

$$\mathcal{J}[x] = \int \mathcal{D}[c, c^*] e^{K[c,c^*,x]} \tag{4.18}$$

with

$$K[c, c^*, x] \equiv \int_{-T}^{T} dduv c^*(u)\,\frac{\delta \mathrm{EQ}([x], u)}{\delta x(v)}\,c(v)\ , \tag{4.19}$$

[13] If we send $m \to 0$ at the end of the calculation, we still get $G(0) = 0$ and a constant Jacobian. However, if m is set to 0 from the begining then $G(t) = \Theta(t)/\gamma_0$ and $G(0) = 1/(2\gamma_0)$ in our conventions. This leads to the so-called Jacobian extra-term in the action: $-1/(2\gamma_0)\int_u F'_u[x_u]$. It is invariant under time-reversal of the field $x_u \mapsto x_{-u}$ as long as F' is itself time-reversal invariant.

and with the extra boundary conditions: $c(-T) = \dot{c}(-T) = c^*(T) = \dot{c}^*(T) = 0$. Plugging the Langevin equation (2.9), we have

$$\frac{\delta \mathrm{EQ}_u[x]}{\delta x_v} = m\partial_u^2 \delta_{u-v} - \frac{\delta F_u[x]}{\delta x_v} + \int_w \gamma_{w-v}\partial_w \delta_{w-v} \ .$$

The kinetic term in $K[c, c^*, x]$ can be re-written

$$\int_u \int_v c_u^* \, \partial_u^2 \delta_{u-v} \, c_v = \int_u c_u^* \, \partial_u^2 c_u + \frac{1}{2}\left[\dot{c}^* c - c^* \dot{c}\right]_{-T}^{T} + \frac{1}{2}\delta_0 \left[c^* c\right]_{-T}^{T} \ .$$

The last two terms in the RHS vanishes by use of the boundary conditions ($c_{-T} = \dot{c}_{-T} = c_T^* = \dot{c}_T^* = 0$). The retarded friction can be re-written

$$\int_u \int_v c_u^* \, \partial_u \gamma_{u-v} \, c_v - \frac{1}{2}\int_u c_u^* \left[\gamma_{u+T} \, c_{-T} - \gamma_{u-T} \, c_T\right] \ ,$$

where the second line vanishes identically for two reasons: the boundary condition ($c_{-T} = 0$) kills the first part and the causality of the friction kernel ($\gamma_u = 0 \ \forall \, u < 0$) suppresses the second one. Notice that if there is a Dirac contribution to γ centered at $u = 0$ like in the Markovian case, the other boundary condition ($c_{-T}^* = 0$) finishes to cancel the second part. Finally we have

$$K[c, c^* x] = \int_u c_u^* \, \partial_u^2 c_u + \int_u \int_v c_u^* \left[\partial_u \gamma_{u-v} - \frac{\delta F_u[x]}{\delta x_v}\right] c_v \ . \tag{4.20}$$

4.6 Discrete MSRJD for multiplicative noise

4.7 Stratonovich prescription – Mid-point discretization

The discretized Langevin equation reads:

$$\begin{aligned} \mathrm{EQ}_k \equiv \ & m\frac{x_{k+2} - 2x_{k+1} + x_k}{\epsilon^2} - F_{k+2}(x_{k+2}, x_{k+1}, ...) \\ & + M'(x_k) \sum_{l=1}^{k} \gamma_{kl} M'(x_l)(x_{l+2} - x_{l+1}) = M'(\tilde{x}_k)\xi_{k+1} \ , \end{aligned} \tag{4.21}$$

with the mid-point $\tilde{x}_k \equiv (x_{k+1} + x_k)/2$. The Jacobian is:

$$\mathcal{J}_N = \frac{1}{\epsilon} \det{}_{kl} \left[\frac{\partial \mathrm{EQ}_k}{\partial x_{l+2}} - \frac{M''(\tilde{x}_k)}{M'(\tilde{x}_k)} \, \mathrm{EQ}_k \, \frac{\delta_{k+1\, l+2} + \delta_{k\, l+2}}{2}\right] \ , \tag{4.22}$$

where k and l run from 0 to $N - 1$. Introducing ghosts, it can be put in the form

$$\mathcal{J}_N = \int dc_0 dc_0^* ... dc_{N+1} dc_{N+1}^* \, c_0 c_1 c_N^* c_{N+1}^* \, e^{K_N} \ ,$$

with

$$K_N \equiv \sum_{k=0}^{N+1}\sum_{l=0}^{N+1} c_k^* \frac{\partial_{\mathrm{EQ}k}}{\partial x_l} c_l - \sum_{k=0}^{N+1} c_k^* \frac{M''(\tilde{x}_k)}{M'(\tilde{x}_k)} \mathrm{EQ}_k \frac{c_{k+1}+c_k}{2} . \quad (4.23)$$

In the continuum limit,

$$K \equiv \lim_{N\to\infty} K_N = \int_u \int_v c_u^* \frac{\delta \mathrm{EQ}_u[x]}{\delta x_v} c_v - \int_u c_u^* \frac{M''(x_u)}{M'(x_u)} \mathrm{EQ}_u[x]\, c_u , \quad (4.24)$$

with the boundary conditions $c(-T) = \dot{c}(-T) = 0$ and $c^*(T) = \dot{c}^*(T) = 0$.

5 Mean-field theory for ferromagnets

In spite of their apparent simplicity, the statics of ferromagnetic Ising models has been solved analytically only in one and two dimensions. The mean-field approximation allows one to solve the Ising model in *any* spatial dimensionality. Even if the qualitative results obtained are correct, the quantitative comparison to experimental and numerical data shows that the approximation fails below an *upper critical dimension* d_u in the sense that it does not capture correctly the behavior of the systems close to the critical point. It is however very instructive to see the mean-field approximation at work.

Naive mean-field approximation

Using the factorization of the joint probability density that defines the mean-field approximation, one finds

$$\begin{aligned} F(\{m_i\}) &= -\sum_{i_1\neq\ldots\neq i_p} J_{i_1\ldots i_p} m_{i_1}\ldots m_{i_p} - \sum_i h_i m_i \\ &\quad + T\sum_{i=1}^{N}\left[\frac{1+m_i}{2}\ln\frac{1+m_i}{2} + \frac{1-m_i}{2}\ln\frac{1-m_i}{2}\right] . \end{aligned} \quad (5.1)$$

Note that a Taylor expansion of the entropic contribution around $m_i = 0$ leads to a polynomial expression that is the starting point in the Landau theory of second order phase transitions (see Sect. **??**).

The local magnetizations, m_i, are then determined by requiring that they minimize the free-energy density, $\partial f(\{m_j\})/\partial m_i = 0$ and a positive definite Hessian, $\partial^2 f(\{m_j\})/\partial m_i \partial m_j$ (*i.e.* with all eigenvalues being positive at the extremal value). This yields

$$m_i = \tanh\left(p\beta \sum_{i_2\neq\ldots\neq i_p} J_{ii_2\ldots i_p} m_{i_2}\ldots m_{i_p} + \beta h_i\right) \quad (5.2)$$

If $J_{i_1 \ldots i_p} = J/(p! N^{p-1})$ for all p uplets and the applied field is uniform, $h_i = h$, one can take $m_i = m$ for all i and these expressions become (5.4) and (5.7) below, respectively. The mean-field approximation is exact for the fully-connected pure Ising ferromagnet, as we shall show below. [Note that the fully-connected limit of the model with pair interactions ($p = 2$) is correctly attained by taking $J \to J/N$ and $2d \to N$ in (**??**) leading to $T_c = J$.]

Exact solution

Let us solve the ferromagnetic model exactly. The sum over spin configurations in the partition function can be traded for a sum over the variable, $x = N^{-1} \sum_{i=1}^{N} s_i$, that takes values $x = -1, -1 + 2/N, -1 + 4/N, \ldots, 1 - 4/N, 1 - 2/N, 1$. Neglecting subdominant terms in N, one then writes

$$Z = \sum_x e^{-N\beta f(x)} \tag{5.3}$$

with the x-parameter dependent 'free-energy density'

$$f(x) = -\frac{J}{p!} x^p - hx + T \left[\frac{1+x}{2} \ln \frac{1+x}{2} + \frac{1-x}{2} \ln \frac{1-x}{2} \right] . \tag{5.4}$$

The first two terms are the energetic contribution while the third one is of entropic origin since $N!/(N(1+x)/2)!(N(1-x)/2)!$ spin configurations have the same magnetization density. The average of the parameter x is simply the averaged magnetization density:

$$\langle\, x \,\rangle = \frac{1}{N} \sum_{i=1}^{N} \langle\, s_i \,\rangle = m \tag{5.5}$$

In the large N limit, the partition function – and all averages of x – can be evaluated in the saddle-point approximation (see Appendix **??**)

$$Z \approx \sum_\alpha e^{-N\beta f(x^\alpha_{sp})} \quad , \tag{5.6}$$

where x^α_{sp} are the absolute minima of $f(x)$ given by the solutions to $\partial f(x)/\partial x|_{x_{sp}} = 0$,

$$x_{sp} = \tanh \left(\frac{\beta J}{(p-1)!} x_{sp}^{p-1} + \beta h \right) , \tag{5.7}$$

together with the conditions $d^2 f(x)/dx^2|_{x^\alpha_{sp}} > 0$. Note that the contributing saddle-points should be degenerate, *i.e.* have the same $f(x^\alpha_{sp})$ for all α, otherwise their contribution is exponentially suppressed. The sum over α then just provides a numerical factor of two in the case $h = 0$. Now, since

$$x_{sp} = -\partial f(x)/\partial h|_{x_{sp}} = \langle\, x \,\rangle = m \, , \tag{5.8}$$

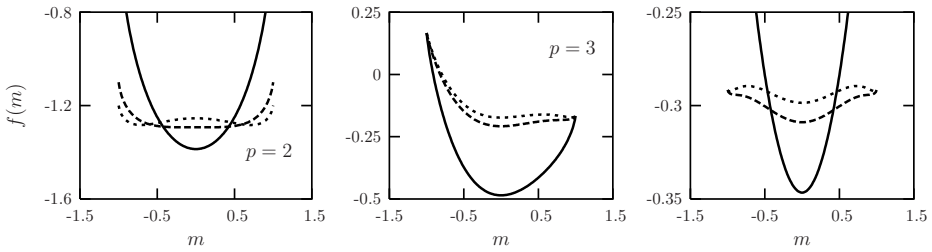

Figure 53: The free-energy density $f(m)$ of the $p = 2$ (left), $p = 3$ (center) and $p = 4$ (right) models at three values of the temperature $T < T_c$ (light dashed line), $T = T_c$ (dark dashed line) and $T > T_c$ (solid line) and with no applied field. (The curves have been translated vertically.)

as we shall show in Eq. (5.9), the solutions to the saddle-point equations determine the order parameter. We shall next describe the phases and phase transition qualitatively and we shall later justify this description analytically.

Model in a finite field

In a finite magnetic field, eq. (5.7) has a unique positive – negative – solution for positive – negative – h at all temperatures. The model is ferromagnetic at all temperatures and there is no phase transition in this parameter.

2nd order transition for $p = 2$

In the absence of a magnetic field this model has a paramagnetic-ferromagnetic phase transition at a finite T_c. The order of the phase transition depends on the value of p. This can be seen from the temperature dependence of the free-energy density (5.4). Figure 53 displays $f(x)$ in the absence of a magnetic field at three values of T for the $p = 2$ (left), $p = 3$ (center) and $p = 4$ (right) models (we call the independent variable m since the stationary points of $f(x)$ are located at the magnetization density of the equilibrium and metastable states, as we shall show below). At high temperature the unique minimum is $m = 0$ in all cases. For $p = 2$, when one reaches T_c, the $m = 0$ minimum splits in two that slowly separate and move towards higher values of $|m|$ when T decreases until reaching $|m| = 1$ at $T = 0$ (see Fig. 53-left). The transition occurs at $T_c = J$ as can be easily seen from a graphical solution to eq. (5.7), see Fig. 54-left. Close but below T_c, the magnetization increases as $m \sim (T_c - T)^{\frac{1}{2}}$. The linear magnetic susceptibility has the usual Curie behavior at very high temperature, $\chi \approx \beta$, and it diverges as $\chi \sim |T - T_c|^{-1}$ on both sides of the critical point. The order parameter is continuous at T_c and the transition is of second-order thermodynamically.

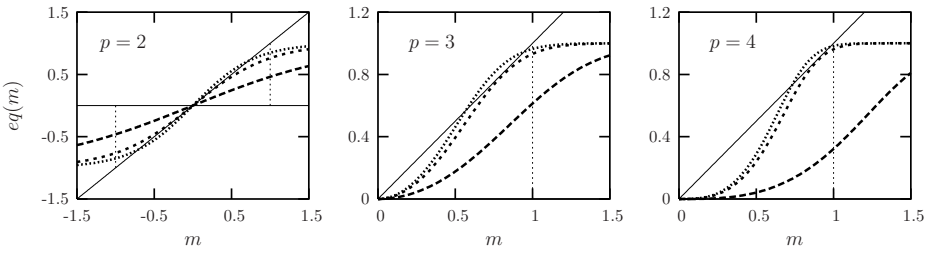

Figure 54: Graphical solution to the equation fixing the order parameter x for $p = 2$ (left), $p = 3$ (center) and $p = 4$ (right) ferromagnetic models at three values of the temperature $T < T^*$, $T = T^*$ and $T > T^*$ and with no applied field. Note that the rhs of this equation is antisymmetric with respect to $m \to -m$ for odd values of p while it is symmetric under the same transformation for even values of p. We show the positive quadrant only to enlarge the figure. T^* is the temperature at which a second minimum appears in the cases $p = 3$ and $p = 4$.

1st order transition for $p > 2$

For $p > 2$ the situation changes. For even values of p, at T^* two minima (and two maxima) at $|m| \neq 0$ appear. These coexist as metastable states with the stable minimum at $m = 0$ until a temperature T_c at which the three free-energy densities coincide, see Fig. 53-right. Below T_c the $m = 0$ minimum continues to exist but the $|m| \neq 0$ ones are favored since they have a lower free-energy density. For odd values of p the free-energy density is not symmetric with respect to $m = 0$. A single minimum at $m^* > 0$ appears at T^* and at T_c it reaches the free-energy density of the paramagnetic one, $f(m^*) = f(0)$, see Fig. 53-center. Below T_c the equilibrium state is the ferromagnetic minimum. For all $p > 2$ the order parameter is discontinuous at T_c, it jumps from zero at T_c^+ to a finite value at T_c^-. The linear magnetic susceptibility also jumps at T_c. While it equals β on the paramagnetic side, it takes a finite value given by eqn. (5.10) evaluated at m^* on the ferromagnetic one. In consequence, the transition is of first-order.

Pinning field, broken ergodicity and spontaneous broken symmetry

The saddle-point equation (5.7) for $p = 2$ [or the mean-field equation (**??**)] admits two equivalent solutions in no field. What do they correspond to? They are the magnetization density of the equilibrium ferromagnetic states with positive and negative value. At $T < T_c$ if one computes $m = N^{-1} \sum_{i=1}^{N} \langle s_i \rangle = \sum_x e^{-\beta N f(x)} x$ summing over the two minima of the free-energy density one finds $m = 0$ as expected by symmetry. Instead, if one computes the averaged magnetization density with the partition sum restricted to the configurations with positive (or negative) x one finds $m = |m_{sp}|$ (or $m = -|m_{sp}|$).

In practice, the restricted sum is performed by applying a small magnetic field, computing the statistical properties in the $N \to \infty$ limit, and then setting the field to zero. In other words,

$$m_\pm \equiv \frac{1}{N}\sum_{i=1}^{N}\langle\, s_i \,\rangle_\pm = \left(\frac{1}{\beta N}\,\frac{\partial \ln Z}{\partial h}\right)\Big|_{h\to 0^\pm} = -\,\frac{\partial f(x_{sp})}{\partial h}\Big|_{h\to 0^\pm} = \pm|x_{sp}|\,. \qquad (5.9)$$

By taking the $N \to \infty$ limit in a field one selects the positive (or negatively) magnetized states.

For all odd values of p the phase transition is not associated to symmetry breaking, since there is only one non-degenerate minimum of the free-energy density that corresponds to the equilibrium state at low temperature. The application of a pinning field is then superfluous.

For any even value of p and at all temperatures the free-energy density in the absence of the field is symmetric with respect to $m \to -m$, see the left and right panels in Fig. 53. The phase transition corresponds to a *spontaneous symmetry breaking* between the states of positive and negative magnetization. One can determine the one that is chosen when going through T_c either by applying a small *pinning field* that is taken to zero only after the thermodynamic limit, or by imposing adequate boundary conditions. Once a system sets into one of the equilibrium states this is completely stable in the $N \to \infty$ limit. In pure static terms this means that one can separate the sum over all spin configurations into independent sums over different sectors of phase space that correspond to each equilibrium state. In dynamic terms it means that temporal and statistical averages (taken over all configurations) in an infinite system do not coincide.

The magnetic linear susceptibility for generic p is a simple generalization of the expression in (**??**) and it is given by

$$\chi \equiv \frac{\partial m}{\partial h}\Big|_{h\to 0^\pm} = \frac{\partial x_{sp}}{\partial h}\Big|_{h\to 0^\pm} = \frac{\beta}{\cosh^2\!\left(\frac{\beta J}{(p-1)!}\,x_{sp}^{p-1}\right) - \frac{\beta J}{(p-2)!}x_{sp}^{p-2}}\,. \qquad (5.10)$$

For $p = 2$, at $T > T_c$, $x_{sp} = 0$ the susceptibility is given by $(T - J)^{-1}$ predicting the second order phase transition with a divergent susceptibility at $T_c = J$. Approaching T_c from below the two magnetized states have the same divergent susceptibility, $\chi \sim (T_c - T)^{-1}$.

For $p > 2$, at $T > T_c$, $x_{sp} = 0$ and the susceptibility takes the Curie form $\chi = \beta$. The Curie law, $\chi = \beta$, jumps to a different value at the critical temperature due to the fact that x_{sp} jumps.

6 Grassmann variables and supersymmetry

Grassmann variables anticommute $\theta^2 = \overline{\theta}^2 = [\theta, \bar{\theta}]_+ = 0$. The integration rules are $\int d\theta = \int d\overline{\theta} = 0$ and $\int d\theta\, \theta = \int d\overline{\theta}\, \overline{\theta} = 1$ while the derivation is such that $\partial_\theta = \int d\theta$ and $\partial_{\overline{\theta}} = \int d\bar{\theta}$.

In the supersymmetric formalism used in Section one enlarges the usual "bosonic" space to include two conjugate Grassmann variables θ and $\overline{\theta}$: $t \to a = (t, \theta, \overline{\theta})$. A "superfield" and its "supercorrelator" are then defined as

$$\Phi(a) \equiv q(t) + \psi(t)\overline{\theta} + \overline{\psi}(t)\theta + i\hat{q}(t)\overline{\theta}\theta \; , \qquad Q(a,b) \equiv \langle \Phi(a)\Phi(b) \rangle \; , \tag{6.1}$$

$b = (t', \theta, \overline{\theta}')$. The latter encodes the usual correlations $\langle x(t)x(t') \rangle$, $\langle x(t)i\hat{x}(t') \rangle$, $\langle i\hat{x}(t)x(t') \rangle$, $\langle i\hat{x}(t)i\hat{x}(t') \rangle$, as well as "fermionic" correlators $\langle x(t)\psi(t') \rangle$, $\langle \overline{\psi}(t)i\hat{x}(t') \rangle$, $\langle \overline{\psi}(t)\psi(t') \rangle$, etc. The solutions we construct and study are such that all correlators that involve only one fermionic variable ψ and $\overline{\psi}$ vanish. We are then left with the usual four correlators purely bosonic correlators and the fermion bilinears. One proves that the latter equal the linear response. If, moreover, we only consider causal solutions, $\hat{Q}(t,t') \equiv \langle i\hat{x}(t)i\hat{x}(t') \rangle = 0$ and

$$Q(a,b) = C(t,t') - (\overline{\theta}' - \overline{\theta}) \left(\theta' R(t,t') - \theta R(t',t) \right) \; . \tag{6.2}$$

Convolutions, or operational products, and Hadamard, or simple products, are defined as

$$\begin{aligned} Q_1(a,b) \otimes Q_2(b,c) &= \int db \, Q_1(a,b) Q_2(b,c) \; , \\ Q_1(a,b) \bullet Q_2(a,b) &= Q_1(a,b) Q_2(a,b) \; , \end{aligned} \tag{6.3}$$

respectively, with $db \equiv dt d\overline{\theta} d\theta$.

For correlators of the causal form (6.2), the convolution and the Hadamard product respect the structure of the correlator. Indeed, the result of the convolution is again of the form (6.2) with

$$\begin{aligned} C_{\rm CONV}(t,t'') &= \int dt' \; \left[C_1(t,t') R_2(t'',t') + R_1(t,t') C_2(t',t'') \right] \; , \\ R_{\rm CONV}(t,t'') &= \int dt' \; R_1(t,t') R_2(t',t'') \; , \end{aligned} \tag{6.4}$$

and the result of the Hadamard product is also of the form (6.2) with

$$\begin{aligned} C_{\rm HAD}(t,t') &= C_1(t,t') C_2(t,t') \; , \\ R_{\rm HAD}(t,t') &= C_1(t,t') R_2(t,t') + C_2(t,t') R_1(t,t') \; . \end{aligned} \tag{6.5}$$

The Dirac delta function is defined as $\delta(a-b) = \delta(t-t')(\overline{\theta} - \overline{\theta}')(\theta - \theta')$.

References

[1] A. Cavagna, *Supercooled liquids for pedestrians*, Phys. Rep. **476**, 51 (2009). L. Berthier & G. Biroli, *A theoretical perspective on the glass transition and nonequilibrium phenomena in disordered materials*, arXiv:1011.2578. Rev. Mod. Phys.

[2] L. F. Cugliandolo, *Dynamics of glassy systems*, in Les Houuches 2002 (Springer, 2003).

[3] D. W. Oxtoby, *Homogeneous nucleation: theory and experiment*, J. Phys.: Condens. Matter **4**, 7626-7650 (1992). K. Binder, *Theory of first-order phase transitions*, Rep. Prog. Phys. **50**, 783-859 (1987).

[4] A. J. Bray, *Thoery of phase ordering kinetics*, Adv. Phys. **43**, 357 (1994). P. Sollich, http://www.mth.kcl.ac.uk/ psollich/

[5] P. C. Hohenberg and B. I. Halperin, Rev. Mod. Phys. **49**, 435 (1977). H. K. Janssen, B. Schaub, and B. Schmittman, Z. Phys. B Cond.Mat. **73**, 539 (1989). P. Calabrese and A. Gambassi, J. Phys. A **38**, R133 (2005).

[6] P. G. Debenedetti, *Metastable liquids* (Princeton Univ. Press, 1997). E. J. Donth, *The glass transition: relaxation dynamics in liquids and disordered materials* (Springer, 2001). K. Binder and W. Kob, *Glassy Materials and Disordered Solids: An Introduction to their Statistical Mechanics* (World Scientific, 2005).

[7] K. H. Fischer and J. A. Hertz, *Spin glasses* (Cambridge Univ. Press, 1991). M. Mézard, G. Parisi, and M. A. Virasoro, *Spin glass theory and beyond* (World Scientific, 1986). N. Kawashima and H. Rieger, *Recent progress in spin glasses* in *Frustrated spin systems*, H. T. Diep ed. (World Scientific, 2004). T. Castellani and A. Cavagna, *Spin-glass theory for pedestrians*, J. Stat. Mech. (2005) P05012. F. Zamponi, *Mean field theory of spin glasses*, arXiv:1008.4844. M. Talagrand, *Spin glasses, a challenge for mathematicians* (Springer-Verlag, 2003).

[8] G. Blatter, M. V. Feigelman, V. B. Geshkenbein, A. I. Larkin, and V. M. Vinokur, Rev. Mod. Phys. **66**, 1125 $\Delta(1994\Theta)$. T. Giamarchi and P. Le Doussal, *Statics and dynamics of disordered elastic systems*, arXiv:cond-mat/9705096. T. Nattermann and S. Scheidl, Adv. Phys. **49**, 607 ($\Delta 2000\Theta$). T. Giamarchi, A. B. Kolton, A. Rosso, *Dynamics of disordered elastic systems*, arXiv:cond-mat/0503437. P. Le Doussal, *Exact results and open questions in first principle functional RG*, arXiv:0809.1192.

[9] O. C. Martin, R. Monasson, R. Zecchina, *Statistical mechanics methods and phase transitions in optimization problems* Theoretical Computer Science **265** (2001) 3-67. M. Mézard and A. Montanari, *Information, Physics, and Computation*, (Oxford Graduate Texts, 2009).

[10] D. J. Amit, *Modeling Brain Function: The World Of Attractor Neural Networks*, (Cambridge Univ. Press, 1992). N. Brunel, *Network models of memory*, in Les Houches 2003 (Elsevier, 2004).

[11] D. A. Fletcher and P. L. Geissler, Annu. Rev. Phys. Chem. **60**, 469 (2009). G. I. Menon, arXiv:1003.2032. S. Ramaswamy, arXiv:1004.1933.

[12] *Dynamical heterogeneities in glasses, colloids, and granular media*, L. Berthier, G. Biroli, J-P Bouchaud, L. Cipelletti and W. van Saarloos eds. (Oxford University Press, Oxford, 2011).

[13] L. C. E. Struick, *Physical Aging in Amorphous Polymers and Other Materials* (Elsevier, Amsterdam, 1978Θ). E. Vincent, J. Hammann, M. Ocio, J-P Bouchaud, L. F. Cugliandolo, *Slow dynamics and aging in spin-glasses*, arXiv:cond-mat/9607224 in Lecture Notes in Physics **492**, 184 (1997).

[14] A.-L. Barabási and H. E. Stanley, *Fractal Concepts in Surface Growth*, (Cambridge University Press, Cambridge, 1995). T. Halpin-Healey and Y.-C. Zhang, Phys. Rep. **254**, 215 Δ(1995)Θ.

[15] R. Zwanzig, J. Stat. Phys. **9**, 215 (1973). S. Nordholm and R. Zwanzig, J. Stat. Phys. **13**, 347-371 (1975). K. Kawasaki, J. Phys. A **6**, 1289-1295 (1973).

[16] R. P. Feynmann and F. L. Vernon, Jr, Ann. Phys. **24**, 114 (1963).

[17] *Theory of the spin bath* N. Prokof'ev and P. Stamp Rep. Prog. Phys. **63**, 669 (2000).

[18] U. Weiss, *Quantum dissipative systems*, Series in modern condensed matter physics vol. 10, World Scientific (1999).

[19] J. Dunkel and P. Hänggi, Phys. Rep. **471**, 1-73 (2009).

[20] N. Pottier, Physica A **317**, 371 (2003).

[21] A. B. Kolton, D. R. Grempel and D. Domínguez, Phys. Rev. B 71, 024206 (2005).

[22] C. Caroli, R. Combescot, P. Nozières and D. Saint-James, J. Phys. C **5**, 21 (1972).

[23] J. S. Langer, *Statistical theory of decay of metastable states* Ann. of Phys. **54**, 258 (1969). C. G. Callan and S. Coleman, Phys. Rev. D **16**, 1762 (1977). B. Caroli, C. Caroli, and B. Roulet, *Diffusion in a bistable potential - systematic WKB treatment* J. Stat. Phys. **21**, 415 (1979). A. M. Polyakov, *Gauge fields and stings* (Harwood Academic Publishers, 1994).

[24] R. Bausch, H. K. Janssen, and H. Wagner, Z. Phys. B **24**, 113 (1976).

[25] J. L. Iguain, S. Bustingorry, A. Kolton, and L. F. Cugliandolo, Growing correlations and aging of an elastic line in a random potential arXiv:0903.4878.

[26] L. F. Cugliandolo, J. Kurchan, and L. Peliti, Phys. Rev. E **55**, 3898 (1997).

[27] C. Aron, G. Biroli, and L. F. Cugliandolo, J. Stat. Mech. (2011).

[28] A. Sicilia, J. J. Arenzon, A. J. Bray, and L. F. Cugliandolo, Phys. Rev. E

[29] see, e.g. R. Chitra, T. Giamarchi and P. Le Doussal, Phys. Rev. B 65, 035312 (2002) and references therein. H. Fukuyama and P. Lee, Phys. Rev. B **18**, 6245 (1978).

[30] C. Aron, G. Biroli, and L. F. Cugliandolo, Phys. Rev. Lett. **102**, 050404 (2009).

[31] M. Mézard and G. Parisi,

[32] L. F. Cugliandolo and P. Le Doussal, Phys. Rev. E L. F. Cugliandolo, J. Kurchan, and P. Le Doussal, Phys. Rev. Lett.

[33] Phys. Rev. E **65**, 046136 (2002).

[34] Grabert Phys. Rep.

[35] Z. Ovadyahu, Phys. Rev. B **73**, 214204 (2006).

[36] R. MacKenzie, *Path integral methods and applications*, VIth Vietnam School of Physics, Vung Tau, Vietnam, 27 Dec. 1999 - 8 Jan. 2000; arXiv:quantum-ph/0004090.

[37] R. P. Feynman and A. R. Hibbs, *Quantum Mechanics and Path Integrals* (New York: McGraw-Hill, 1965). H. Kleinert, *Path Integrals in Quantum Mechanics, Statistics, Polymer Physics, and Financial Markets*, 4th edition (World Scientific, Singapore, 2004) J. Zinn-Justin, *Path Integrals in Quantum Mechanics* (Oxford University Press, 2004), R. J. Rivers, *Path Integrals Methods in Quantum Field Theory* (Cambridge University Press, 1987).

[38] R. P. Feynman, *Statistical mechanics*,

[39] J. Kurchan, *Supersymmetry, replica and dynamic treatments of disordered systems: a parallel presentation* arXiv:cond-mat/0209399.

[40] M. Mézard, G. Parisi, and M. A. Virasoro, *Spin glasses and beyond*, Fischer and J. Hertz,

[41] F. Corberi, E. Lippiello and M. Zannetti J. Stat. Mech. (2007) P07002.

[42] Viasnoff and Lequeux

[43] L. F. Cugliandolo and G. Lozano, Phys. Rev. Lett. 80, 4979 (1998) . Phys. Rev. B59, 915 (1999).

[44] L. F. Cugliandolo, D. R. Grempel, G. Lozano and H. Lozza Phys. Rev. B **70**, 024422 (2004). L. F. Cugliandolo, D. R. Grempel, G. S. Lozano, H. Lozza, C. A. da Silva Santos Phys. Rev. B **66**, 014444 (2002).

[45] R. P. Feynmann and A. R. Hibbs, *Quantum mechanics and path integrals* (Mc Graw-HIll, New York, 1965).

[46] A. J. Leggett, S. Chakravarty, A. T. Dorsey, M. P. A. Fisher, A. Garg, W. Zwerner, Rev. Mod. Phys. **59**, 1 (1987).

[47] A. J. Bray and M. A. Moore, Phys, Rev. Lett. **49**, 1546 (1982).

[48] C. P. Martin, E. Siggia and H. A. Rose, Phys. Rev. **A8**, 423 (1973), H. K. Janssen, Z. Phys. **B23**, 377 (1976) and *Dynamics of critical phenomena and related topics*, Lecture notes in physics **104**, C. P. Enz ed. (Springer Verlag, Berlin, 1979).

[49] H. K. Janssen, in *From Phase Transitions to Chaos—Topics in Modern Statistical Physics*, ed. by G Györgyi et al. (World Scientific, Singapore, 1992).

[50] C. de Dominicis, Phys. Rev. **B18**, 4913 (1978).

[51] J. Schwinger, J. Math. Phys. **2**, 407 (1961). L. V. Keldysh, Zh. Eksp. Teor. Fiz. **47**, 1515 (1964), Sov. Phys. JETP **20** 235 (1965).

[52] A. Kamenev,

[53] G. Parisi, *Statistical Field Theory*, Frontiers in Physics, Lecture Notes Series, Addison-Wesley (1988).

[54] Cugliandolo, Grempel, Lozano, da Silva Santos